The Hydrodynamics of Countercurrent Chromatography in J-type Centrifuges

A thesis submitted for the degree of Doctor of Philosophy

By

Philip Leslie Wood

Department of Biological Sciences, Brunel University

July 2002

Abstract

Countercurrent chromatography (CCC) is an advanced liquid-liquid extraction technique that purifies chemical components from complex mixtures. The Brunel CCC[1] is a J-type centrifuge based upon this technique. This machine can process 5g quantities of sample every 5 hours [Sutherland 1998]. To process 1 tonne of sample per year would require 200 Brunel CCCs, which is not practical as an industrial process. A practical alternative is to use one machine with 200 times the processing capability. To construct such a machine requires a greater understanding of the stationary phase retention inside a coil (column) and the column efficiency (mass transfer between the mobile and stationary phases). This thesis contains research into stationary phase retention. A hypothesis that all J-type centrifuges act as constant pressure drop pumps is proposed. This hypothesis combined with the Hagan-Poiseuille equation for laminar flow produces a theoretical basis for plotting the stationary phase retention against the square root of the mobile phase flow rate as proposed by Du et al [1999]. Supporting experimental evidence is presented showing that the mobile phase flows in a laminar manner and that the pressure drop across a coil is constant for a given set of operating conditions. It is shown that the pressure drop is the same in both normal and reverse phase modes if specific conditions are met. The pressure drop is shown to be independent of tubing bore for helical coils provided that the same helical pitch is used. The experimental results also show how the pressure drop varies with the phase system and rotational speed. Hopefully this is a significant advance in predicting the stationary phase retention of industrial scale J-type centrifuges.

---

[1] Originally the Brunel CCC was called the called the "Quattro".

Table of Contents

Acknowledgements

Firstly I would like to thank my colleagues at the Brunel Institute for Bioengineering for their support and guidance. Special thanks are for Professor Ian A. Sutherland for letting me have the time to conduct my research and being a sounding board for my ideas and being my primary supervisor. Thanks are also due to Dr Christopher Parris as my second supervisor for his advice on writing this thesis and preparing for the viva. I would also like to thank Mr Geoff Bridges, the skilled glass blower, for making stationary phase collectors that have improved the accuracy and ease of the retention measurement.

I would also like to thank my parents for the clutter that they have had in their dinning room for the last three years.

Nomenclature

A_C	cross-sectional area of coil tubing
β–value	ratio r/R
B	gradient of a Du retention characteristic
B_L	gradient of a Du retention characteristic when the lower phase is the mobile phase
B_U	gradient of a Du retention characteristic when the upper phase is the mobile phase
C_M	concentration of solute in the mobile phase
C_S	concentration of solute in the stationary phase
d_C	internal diameter of coil tubing
d_m	equivalent diameter of mean cross-sectional occupied by the mobile phase
F	mobile phase flow rate
g	acceleration due to gravity ($9.81 m/s^2$)
$H_{P=n}$	number of CCD transfers for the until the elution of the P = n peak
K	dimensionless constant of proportionality for the pressure drop across a coil
k'	capacity factor
L	length of tubing used to wind a coil
N	rotational speed measured in revolutions per minute
P	distribution constant $P = C_S/C_M$
ΔP_L	pressure drop across a coil when the lower phase is the mobile phase
ΔP_U	pressure drop across a coil when the upper phase is the mobile phase
ρ	density
ρ_L	density of the lower phase
ρ_m	density of the mobile phase
ρ_U	density of the upper phase
$\Delta\rho$	density difference between the upper and lower phases ie $\Delta\rho = \rho_L - \rho_U$

r	distance from the planetary axis to a given point on a bobbin
r_m	equivalent radius of mean cross-sectional occupied by the mobile phase
R	distance from centre of main rotor to the planetary axis
R_e	Reynolds number
R_S	resolution between two peaks
S_f	retention of stationary phase expressed as a fraction or a percentage
t_A	time from sample injection to elution of the P = A peak minus the chromatographic dead volume time t_{VCd}
t_B	time from sample injection to elution of the P = B peak minus the chromatographic dead volume time t_{VCd}
t_d	time taken for the sample to flow through the retention dead volume
$t_{P=n}$	time between a sample entering the column and the elution of the P = n peak
t_{tn}	time from sample injection to elution of the P = n peak known as the trace time and taken from a chromatogram
t_M	time from sample injection to the solvent front the P = 0 peak minus the dead volume time t_{VCd}
t_{VCd}	time taken for the sample to flow through the chromatographic dead volume
T	interfacial tension
θ	the angular position of a point on a coil
μ_m	dynamic viscosity of the mobile phase
μ_L	dynamic viscosity of the lower phase
μ_U	dynamic viscosity of the upper phase
u	mean flow velocity
u_m	mean flow velocity of the mobile phase
ν	kinematic viscosity
V_C	volume of the coil
V_{Cd}	chromatographic dead volume
V_d	retention dead volume

V_{DT}	volume of delivery tubes
V_E	volume of stationary phase eluted from the system volume
V_{in}	volume of inlet flying lead
V_m	volume of mobile phase in the coil
V_{out}	volume of outlet flying lead
V_S	volume of stationary phase in the coil
V_{SYS}	system volume ie $V_C + V_{in} + V_{out}$
W_P	time width of peak with distribution constant coefficient P
ω	rotational speed measured in radians per second

Indexing

This thesis has up to five levels of subject division or sub-sections. The highest of which is the chapters followed by four levels of sub-sections. Equations, figures and tables have been placed within the appropriate chapter and sub-section and have been given a number that corresponds to the chapter, sub-section and its sequential number as an equation, figure or table in that sub-section. Some equations, figures and tables have the same number but references will be made as equation, figure or table. For example table 4.3.4.17 will be in Chapter 4 section 4.3.4 and will be the 17th table in that section, equation 4.3.4.17 will also be in Chapter 4 section 4.3.4 and will be the 17th equation in that section. To find a particular equation, figure or table remove the last number to determine which chapter and sub-section it is in and then use the Table of Contents on page 3 to find the page number at which the appropriate sub-section begins.

Chapter 1 Introduction and Literature Review

1.1 Scope

The ideal is to be able to predict the resolution of a given separation before it is performed. In CCC there are two scientific hurdles to overcome before the resolution can be predicted, these are:

1. The accurate prediction of the retention of stationary phase for a given mobile phase flow rate.
2. The development of a method for predicting the column efficiency.

Column efficiency is related to the mixing, transfer and settling process that occurs in CCC and is not intended for detailed study in this thesis although it is discussed in the broader outline of the topic.

This thesis contains the research work into the hydrodynamics of CCC in J-type centrifuges. The greater understanding of the relationship between stationary phase retention and the mobile phase flow rate developed in this thesis will allow accurate prediction of stationary phase retention for a J-type centrifuge before the centrifuge has been built. This will allow the 1 tonne per annum machine to be constructed while reducing the technical and financial risks involved.

The title of the research is the Hydrodynamics of Countercurrent Chromatography. This study is confined to J-type planetary centrifuges, as there are many different types of chromatography centrifuges that all have different hydrodynamics. The J-type centrifuge appears to be the most likely form of CCC technology to have a commercial future as it has the potential for high retention of stationary phase and high through put of sample [Sutherland 1998, Marston 1994].

1.2 Aims and Objectives

The aims and objectives of the research are:

1. To determine which phase, upper or lower, is pumped to the head end of a helical coil and compare with the results for spiral coils.
2. To qualitivily understand head and tail distribution of the upper and lower phases in helical coils when there is no external pumping of a mobile phase.
3. To understand and mathematically model the retention of stationary phase in the coil when an externally pumped mobile phase is present. This mathematical model will be developed for both normal and reverse phase modes.

1.3 Basic Chromatography

A basic explanation of chromatography is given in the first sub-section 1.3.1. Countercurrent distribution (CCD) is used to show how separations can occur in liquid-liquid forms of chromatography. In the second sub-section, a simple explanation of the hydrodynamics of CCC in J-type centrifuges is given. A comparison between CCD and the hydrodynamics of J-type centrifuges explains how a separation occurs in CCC. In the third section the measurement of resolution from a separation performed using a J-type centrifuge is explained.

1.3.1 Definition of terms

Chromatography was invented and named early in the 20th century by the Russian botanist Mikhail Tswett [1906]. His inventiveness was not credited until the publication of Kuhn et al's work in the 1930s [1931]. Tswett separated plant pigments, which appeared as coloured bands on the column. This also explains the name, as in Greek, 'chroma' means 'colour' and 'graphein' means 'to write'. The chromatography originally created by Tswett was based on the differential absorption of the chemical components in the plant pigments. There are many different types of chromatography that have been developed since Mikhail Tswett's pioneering work; all of these are based on different chemical phenomena. The main types are gas chromatography and liquid chromatography. Gas chromatography is not covered in this thesis, since CCC is a form of liquid chromatography. Liquid chromatography can be subdivided into the following topics: liquid-liquid chromatography and liquid-solid technologies such as high-performance liquid chromatography (HPLC).

There are a number of terms used in liquid-liquid chromatography that need to be defined before an explanation of the CCC process can be understood. These mainly relate to the description of the liquids used. A phase system consists of two immiscible liquid solvents that

are used in a chromatography device. If a test tube is filled with a mixture of these two phases and they are allowed to settle, the liquid at the bottom of the test tube is called the lower phase and the liquid above it is called the upper phase.

Another method of differentiating between the liquid phases is based upon the chemical properties of a phase. The phase that is mainly water is called the aqueous phase and the other phase that is mostly organic solvent is termed the organic phase. The aqueous phase is usually the densest phase and hence is often the lower phase. The organic phase usually being the least dense is often the upper phase. However this is not always true, in the case of chloroform-water phase systems the organic phase is the lower phase and the upper phase is the aqueous phase, hence care must be taken when assigning labels to phases.

In chromatography one phase remains in the column and is termed the stationary phase. The other phase is pumped through the coil past the stationary phase and is called the mobile phase. A separation is performed by injecting a sample into the flow of mobile phase upstream of the column. As the sample passes through the column its chemical components are partially absorbed into the stationary phase. The amount of partial absorption of each chemical component is different. The differing amounts of partial absorption mean that each component will leave the column at a different time hence each chemical component is separated from the other components.

There are two chromatographic methods in which a separation can be performed. These methods are normal phase mode and reverse phase mode. In normal phase mode the organic phase is the mobile phase and the aqueous is the stationary phase. In reverse phase mode the aqueous phase is the mobile phase and the organic phase is the stationary phase.

In HPLC the mobile phase is a liquid and the stationary phase is chemically bonded to the surface of a solid support. The solid support is mounted inside the column. Chemically the separation process is the same as that for liquid-liquid chromatography. However the sample can react with the bonding agents used to attach the stationary phase to the solid support. These reactions between the bonding agents can cause the sample components to be hydrolysed or non-specifically adsorbed. There is also only a very small amount of stationary phase present in a HPLC column. This is because the stationary phase can only be attached to the surface of the solid support. The majority of the column volume is occupied by solid support. The very small volume of stationary phase means that a HPLC column must have a very high efficiency [Giddings 1965] in order to achieve a baseline resolution separation. CCC

columns can perform the same baseline separation with much lower efficiency due to far greater volumes of stationary phase [Conway 1985, Bousquet 1991, Menet 1992].

A HPLC column cannot perform both normal and reverse phase mode separations. Different columns are required to perform each type of separation; hence a normal phase mode column and reverse phase mode column are required to conduct both types of separations.

1.3.1.1 Countercurrent Distribution

A simple chromatography or separation technique is to partly fill a test tube with a pure solvent, called the stationary phase. A second solvent, named the mobile phase, has the sample dissolved within it. The mobile phase must be immiscible with the stationary phase. The mobile phase is then added to the test tube. If left alone the sample will very slowly diffuse from the mobile phase to the stationary phase and a separation will occur. However the speed of the diffusion process can be increased rapidly by sealing the test tube. The test tube is then shaken causing the phases to mix. During mixing, the interfacial area between the two phases increases and the components in the sample quickly divide between the two solvents, reaching an equilibrium according to the distribution constant P[ii] of each component present, see equation 1.3.1.1.1 [Conway 1990]. When the shaking stops the immiscible phases settle out into two layers. The mobile phase can then be easily decanted into another test tube. The components present in each solvent phase can then be extracted from the phase in which it is dissolved.

Separation has occurred as a result of the different solubility of the components in the two immiscible phases. This effect depends on the distribution constant P[iii]:

$$P = \frac{C_S}{C_M} \qquad (1.3.1.1.1)$$

C_s is the concentration of the sample component in the stationary phase and C_m is the concentration of the component in the mobile phase.

A component of the sample with a high distribution constant will have a higher concentration in the test tube containing the stationary phase than in the test tube partly filled with mobile

---

[ii] The Distribution constant P is known as the partition coefficient k in most of the references given in this thesis.

[iii] Usually in CCD the distribution constant is expressed as $P = C_M/C_S$ but the reciprocal is used here to aid the reader's understanding of CCC.

phase. Another component with a low distribution constant will have a higher concentration in the test tube containing the mobile phase than in the test tube partly filled with stationary phase. If initially both components had the same concentration in the original mobile phase it can be seen that a low purity separation has occurred. This separation has occurred over one partitioning stage.

Countercurrent Distribution (CCD) [Martin 1941] is identical to the process described above except that it uses a greater number of partitioning steps ie a lot more test tubes. CCD is used when the separation of components in a mixture cannot be achieved in a single partition step. This technique works with a number of test tubes, see figure 1.3.1.1.1, which are all partially filled with stationary phase. The mobile phase with the sample in it is inserted into the first tube. Then the first test tube is shaken, which causes the sample components to partition between the phases, as described above. The phases are then allowed to settle and then mobile phase is decanted into the second test tube. The first test tube is also filled with fresh mobile phase and the mixing, settling and transfer process repeats until the last test tube is filled with mobile phase ie the number of mixing, settling and transfer steps equals the number of test tubes minus one. The resulting distribution of sample components can be seen in figure 1.3.1.1.2.

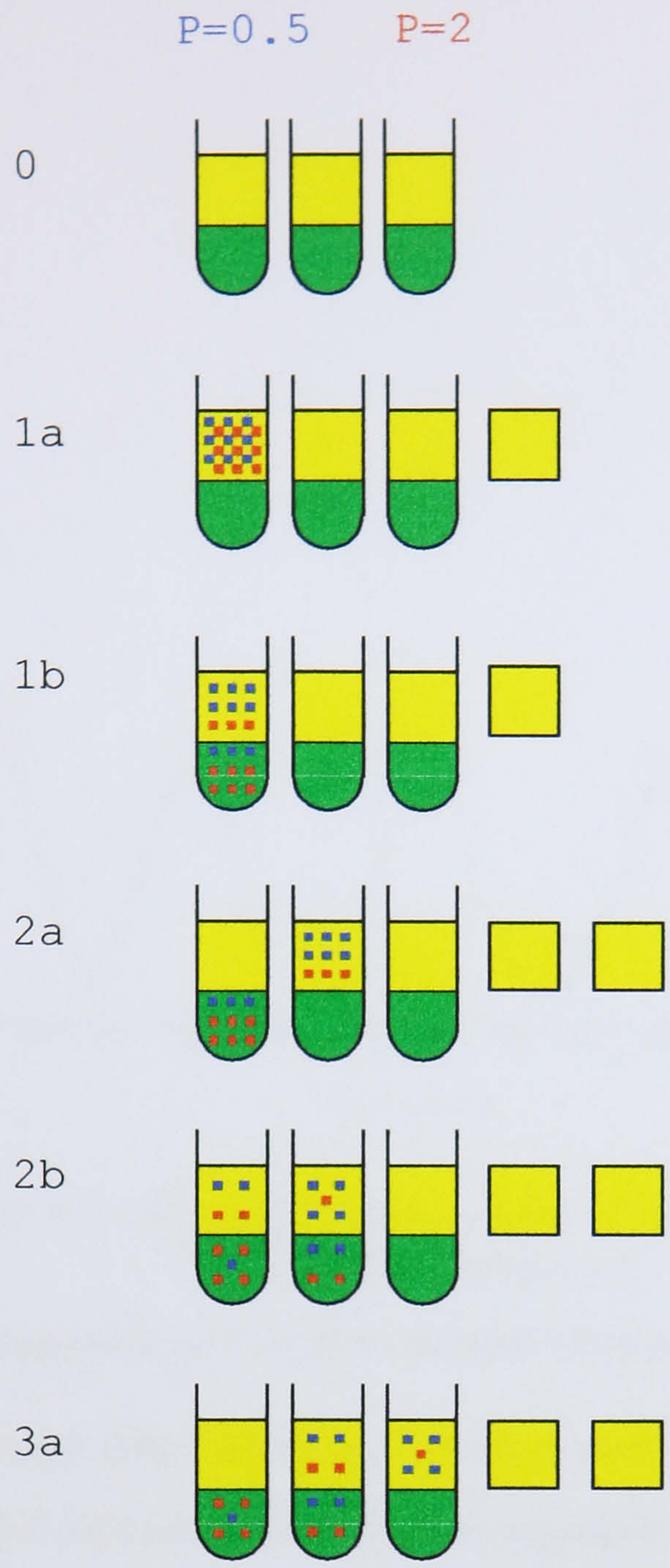

Figure 1.3.1.1.1 Sample component distribution for 2 mixing, settling and transfer steps [Folter 1998]

If the distribution constant (P) from a component equals 0, the concentration in the stationary phase is 0 and hence the component stays in the mobile phase. The peak produced by this P = 0 component will be the first peak to appear from the last test tube. If P equals 1, the component partitions equally between both the mobile and the stationary phases ie the concentration in each phase is equal. The P =1 peak travels through slower than the P = 0 peak and therefore the P = 1 appears from the last test tube after the P = 0 peak. If P equals infinity, the component completely moves into the stationary phase in the first test tube. This component does not partition back into the mobile phase and hence remains in the stationary in the first test tube. Therefore the P = infinity component will not travel along the test tube and hence will never appear as a peak from the last test tube. Hence the distribution constant determines the speed at which components travel along the test tubes and the order in which peaks appear from the last test tube. The higher the distribution constant (P) the slower the

component travel along the test tubes and the later the peak will appear from the last test tube see figure 1.3.1.1.2.

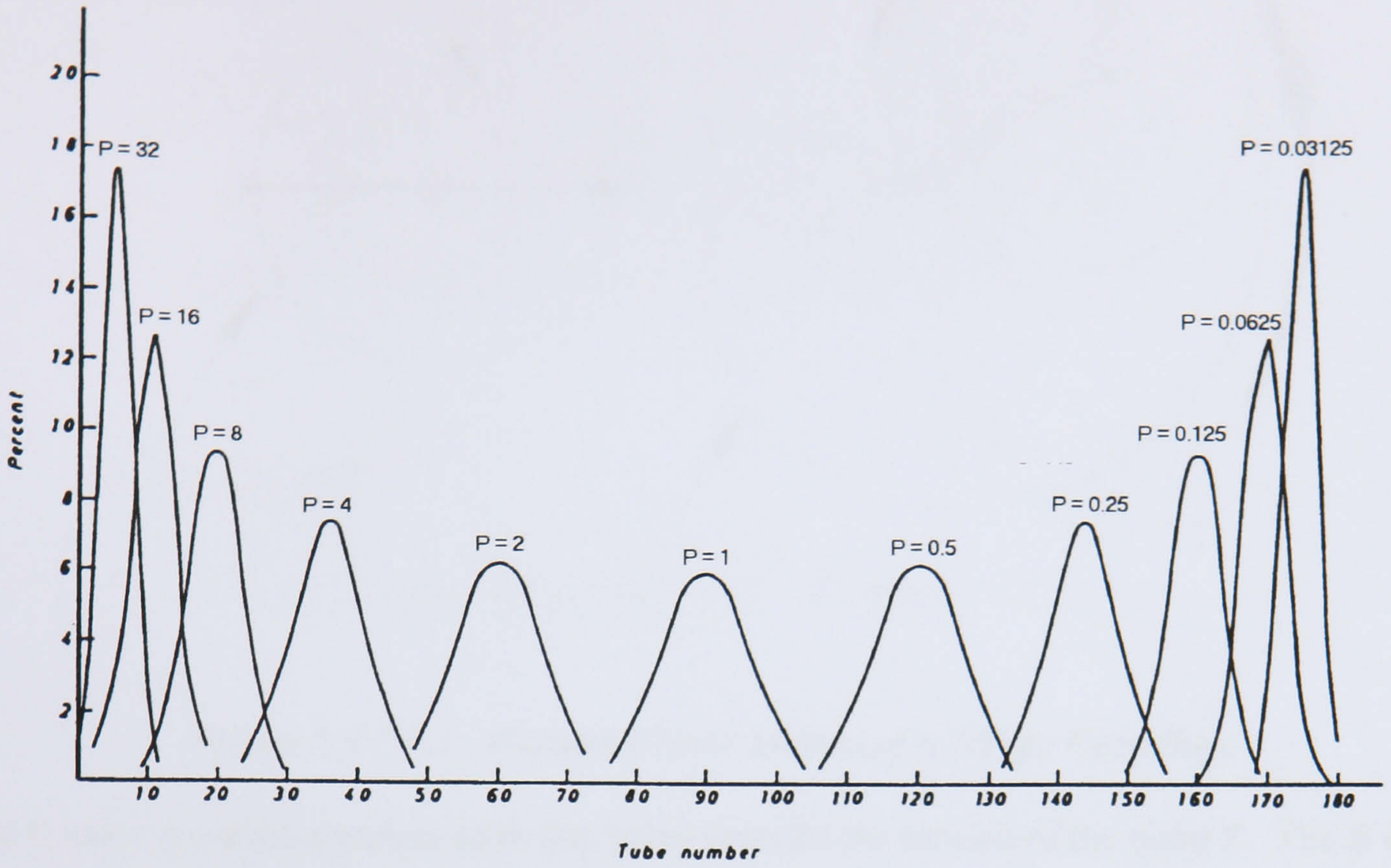

Figure 1.3.1.1.2 Theoretical countercurrent distribution of components with different distribution constants

1.3.2 Basic explanation of Countercurrent Chromatography

1.3.2.1 Planetary Gear Motion of the J-type Centrifuge and the motion's affects on Hydrodynamics of the two immiscible phases

The J-type centrifuge has a bobbin that rotates in planetary gear motion see figure 1.3.2.1.1. A coil of tubing is wound on this bobbin to form the column; hence the column rotates in planetary motion. The sun gear does not rotate, and the planet gear is attached to the bobbin. As the system rotates, the bobbin rotates around its own planetary axis and the planetary axis rotates about the sun gear or solar axis. As a result of the gear mechanism and the 1:1 gear ratio between the sun and planet gears, the rotational speed of the bobbin is equal to that of the rotor. Due to this motion, the coil is subjected to a varying centripetal acceleration. This centripetal acceleration is discussed in greater detail in the literature review in section 1.4.

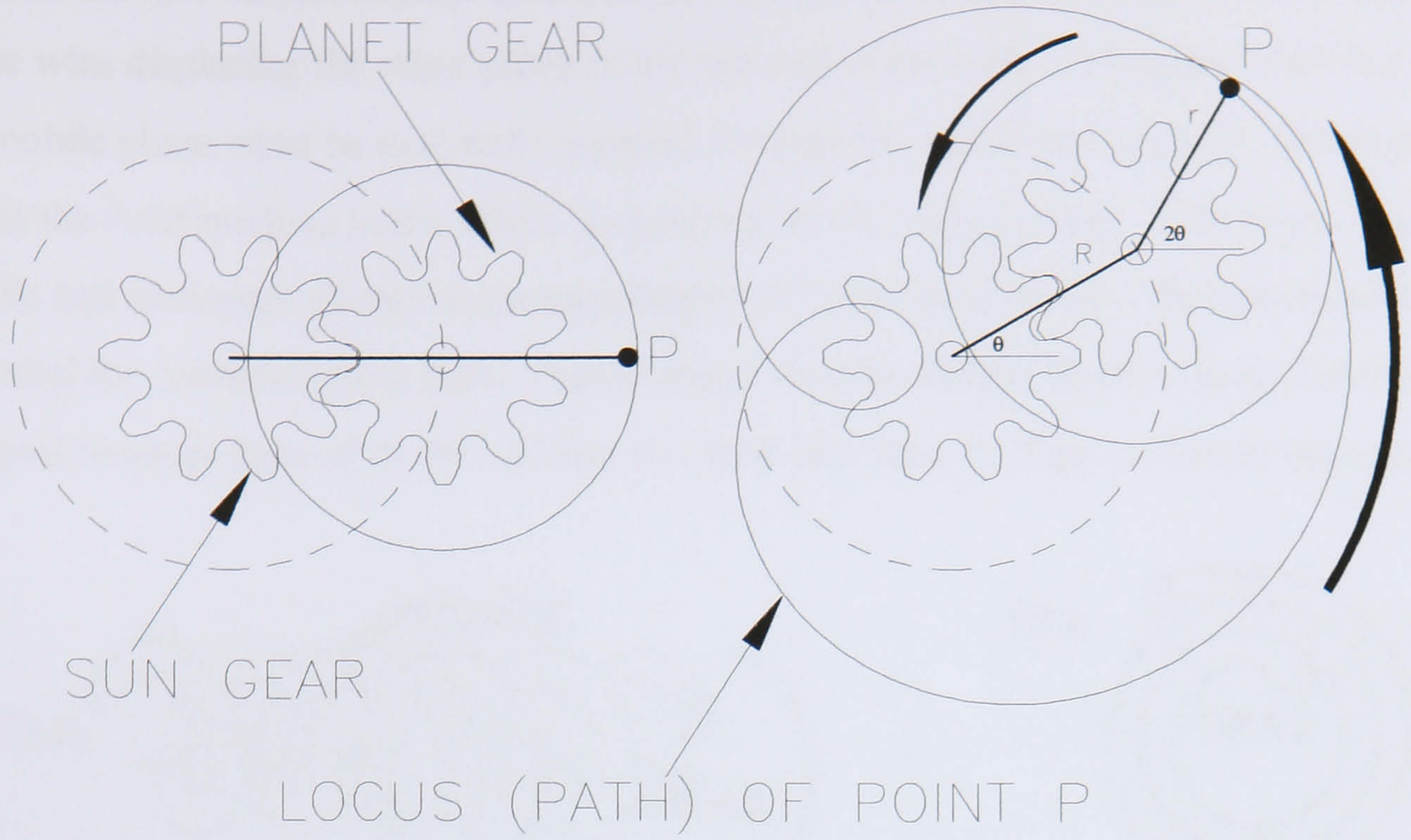

Figure 1.3.2.1.1. Planetary Gear Motion of a J-Type Centrifuge

The β value is a dimensionless term that helps describe the motion of the point P. The β value is the radial distance (r) between the centre of the coil and the point P divided by the radial distance (R) between the centre of the sun gear and the planet gear figure 1.3.2.1.1. In this figure the β value equals 1, which means r equals R and the locus of the point P is a cardioid. When the β value equals 0, r equals 0, and the locus of the point P is a circle.

A coil can be wound in a number of different ways: in an axial direction producing a helical coil, in a radial direction creating a spiral coil or in a combination of both, producing a multi-layer coil. In the separation process centripetal acceleration causes the lower phase to move to the radially outer part of the tubing and the upper phase to move to the radially inner part of the tubing, similar to a standard centrifuge.

For a separation to occur the externally pumped mobile phase must not completely displace the stationary phase ie some stationary phase must remain in the coil. This is achievable because of the Archimedean screw effect. This Archimedean screw effect is an internal pumping effect that redistributes the upper and lower phases to opposite ends of the coil when no externally pumped mobile phase is present. This effect occurs in all coils and can be visualised using a bead and a bubble placed somewhere in a coil, representing the lower phase and the upper phase respectively see figure 1.3.2.1.2 [Conway 1990]. When rotating the coil around its own axis, both the bead and the bubble try to maintain their original positions, the bead at the bottom of a loop and the bubble at the top of a loop. This causes the bubble and the bead to progress (screw) to one end of the coil; this end is called the head. The other end

is called the tail. In this manner both phases try to move towards the head end of the coil, one phase wins displacing the other phase to the tail end of the coil. To retain a stationary phase, the mobile phase must be externally pumped through the coil in the opposite direction to which the Archimedean screw effect is pumping the stationary phase. This means that the mobile and stationary phases are being pumped in opposite directions and hence have the potential for countercurrent flow. It also means that the mobile phase is being externally pumped towards the end of the coil that it would distribute to if the coil ends were sealed.

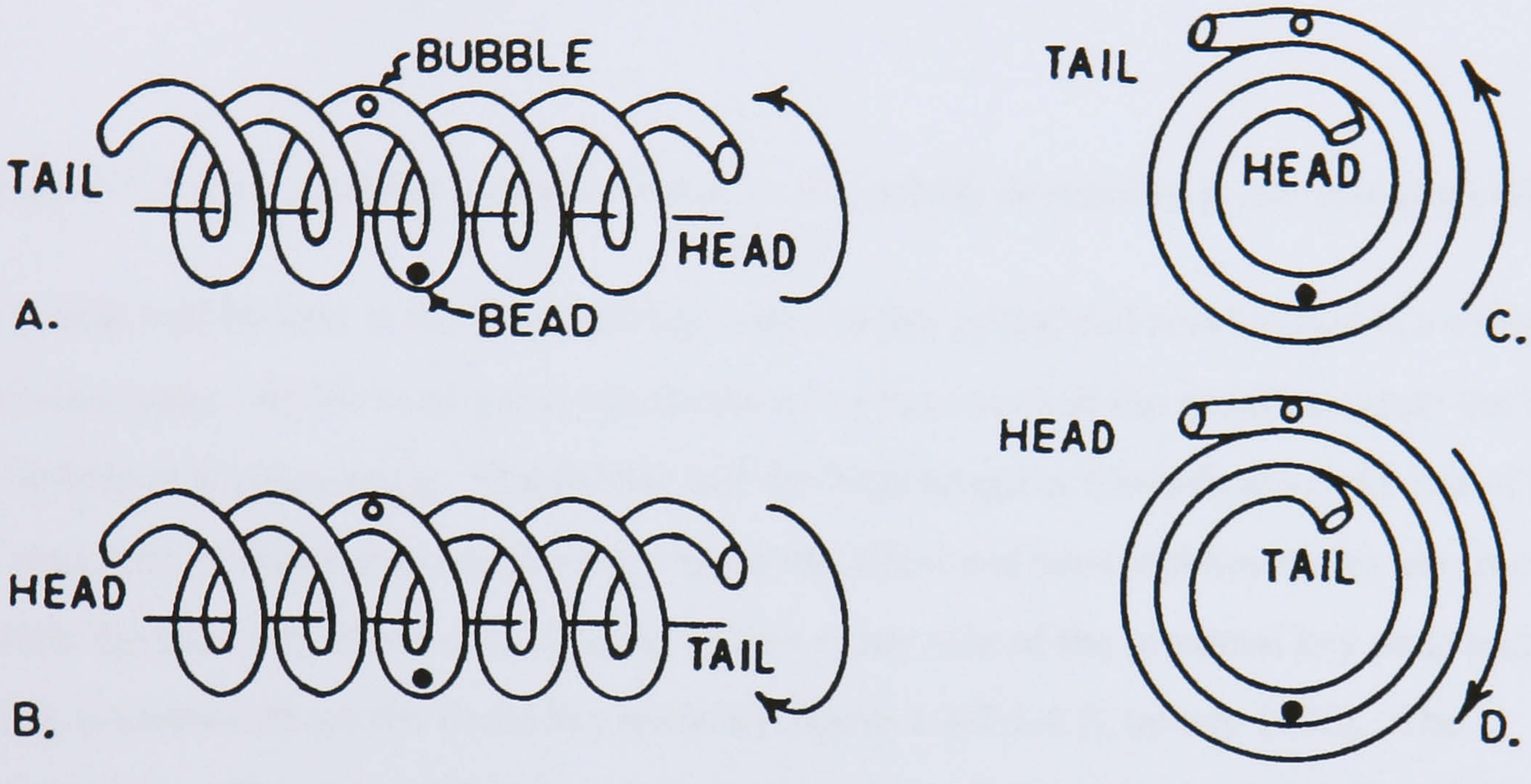

Figure 1.3.2.1.2 Visualisation of head and tail with a helical coil (A & B) and with a spiral coil (C & D) [Conway 1990].

In the figure 1.3.2.1.3 points A and B represent the distal and proximal key nodes respectively. As the coil rotates around the solar axis the path of the key nodes are concentric circles around the solar axis. The proximal key node has the path with the smaller radius and distal key node has the path with the greater radius. The schematic diagram on the left shows the point P placed at the distal key node. The right hand schematic shows the relative positions of the key nodes and the point P after the loop has rotated through an angle θ. The point P has moved away from the distal key node by the angle θ towards the proximal key node. When the loop has rotated through 180° the point P will be at the proximal key node. The point P will then move away from the proximal key and on towards the distal key node. When the loop has completed one rotation the point P will be at the distal key node again.

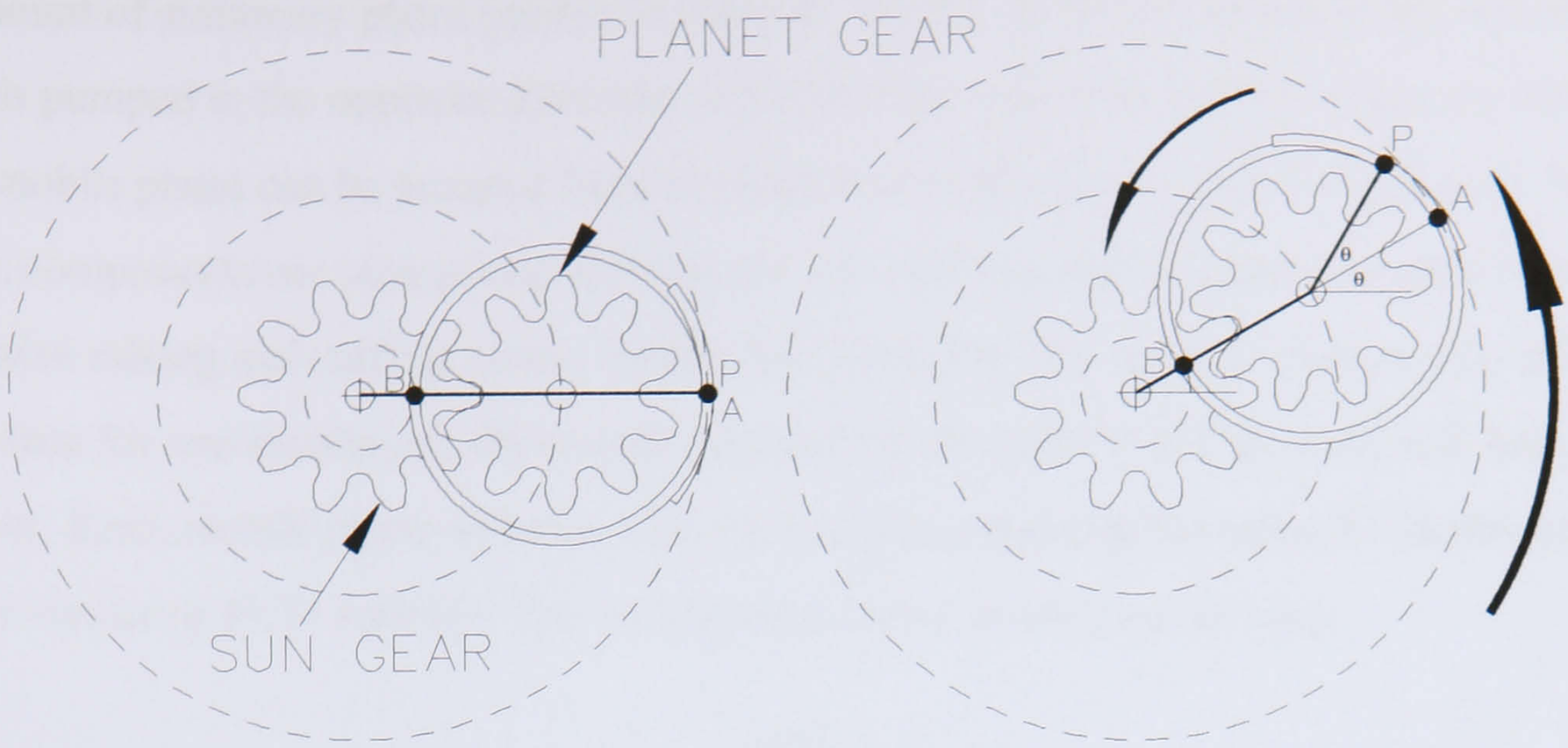

Figure 1.3.2.1.3 showing a single loop of coiled tubing in relation to the sun and planet gears.

The bubble will be held at the proximal key node, as the centripetal acceleration is a minimum at this key node. As the centripetal acceleration is a maximum at the distal key node the bead will be held at this key node. The bubble and the bead progress towards the head end of the coil under the Archimedean screw effect hence the distal and proximal key nodes also move towards the head end of the coil. Mixing occurs either side of the proximal key node and settling is centred about the distal key node see figure 1.3.2.1.4 [Conway 1990]. The transition from mixing to settling zones occurs between adjacent proximal and distal key nodes. Conversely the change from settling to mixing occurs between adjacent distal and proximal key nodes.

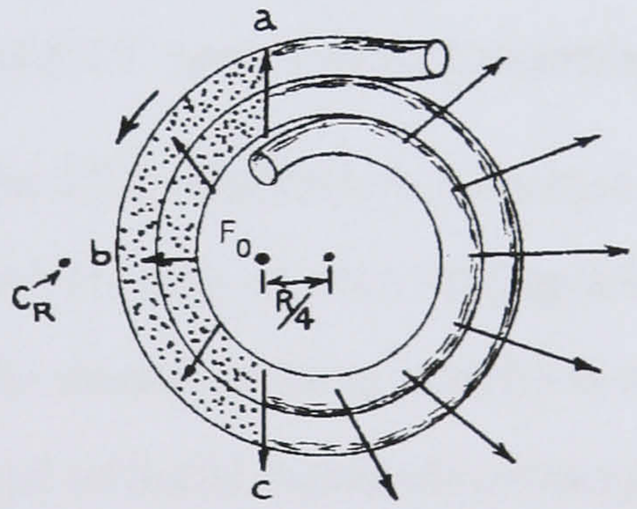

Figure 1.3.2.1.4 shows the relationship between the mixing, settling zones and the accelerations exerted on the immiscible phases, C_R is the solar axis [Conway 1990].

Each loop of a coil contains a mixing zone and a settling zone. As the coil rotates these zones travel towards the head end of the coil with the key nodes see figure 1.3.2.1.5. During a single rotation of a centrifuge a mixing zone and a settling zone will have travelled through a single loop. Therefore the rate of mixing and settling zones passing the point P in the coil is equal to the rotational speed of the centrifuge. This must not be confused with the rate at which the mobile phase is travelling through the coil, which is dependent on the flow rate and

the amount of stationary phase present in the coil. In fact, in reverse phase mode, the mobile phase is pumped in the opposite direction to which the mixing and settling zones are travelling ie the mobile phase can be pumped from the head end of the coil towards the tail end. The sample components are transported through the coil with the mobile phase and pass through successive mixing and settling zones. In the time taken for two mixing zones to pass the point P, the time for one revolution, the mobile originally at the point P will have moved, hence different, fresh, mobile phase will mix with the stationary phase at the point P. In this manner CCC is similar to CCD with the flow rate being equated to the transfer rate.

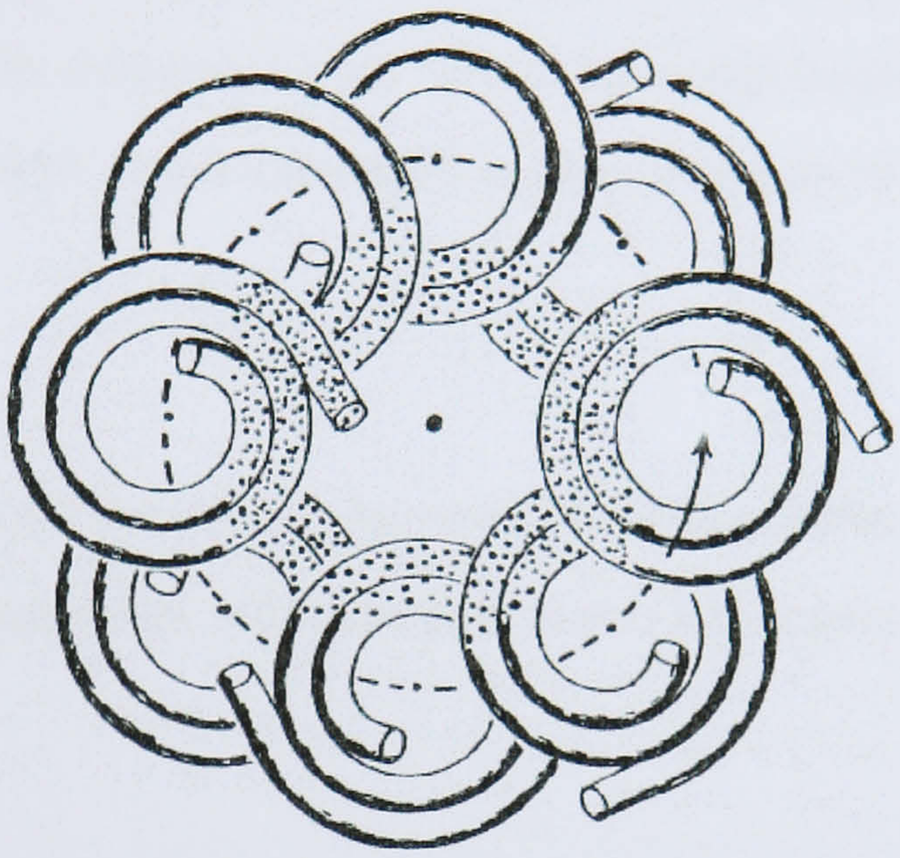

Figure 1.3.2.1.5 shows how the mixing and settling zones move through loops of a coil towards the head. The tail end of the coil is at the centre and the head end is at the periphery of the coil [Conway 1990].

1.3.2.2 Comparison of CCC in a J-type Centrifuge with CCD

CCC in principle is the same as the CCD separation technique as described above. However CCD can be described as a discrete process as each mixing-settling activity occurs in a self-contained (discrete) test tube. The mixing-settling activity is also discrete from the transfer activity. CCC is a continuous form of liquid-liquid chromatography as mixing, settling and transfer activities occur continuously in one container ie the coil. CCD is limited to the number of partition stages that it can use ie the number of test tubes that is practical. However, in the CCC process operating at 800rpm, injected samples undergo 48,000 (800 x 60) partitioning steps per hour. The slower the mobile phase flow rate the longer a sample component remains in a coil and the more partitioning steps it will have under gone. The larger the number of partitioning steps the higher the resolution. Therefore CCC has greater potential for producing high-resolution separations than CCD. However the chromatographic efficiency of the separation decreases the longer a sample remains in a coil.

The retention characteristics of these two separation techniques are different if the number of partitioning steps per unit time is kept constant for each technique. For CCC this means that the rotational speed is kept constant and for CCD the number of transfers per minute is kept constant. To increase the mobile phase flow rate in CCD while maintaining the same transfer rate means that the volume of mobile phase transferred per partitioning step must be increased. If the volume of the test tubes used is also kept constant the volume of stationary phase and hence the stationary retention must reduce accordingly. Therefore for CCD the mobile phase flow rate is inversely proportional to the stationary phase retention. For CCC the retention of stationary phase is less sensitive to mobile flow rate than CCD and therefore resolution is less sensitive to mobile phase flow rate than CCD. The relationship between stationary phase retention and mobile phase flow rate is discussed in more detail in section 1.4 of the literature review.

1.3.3 Resolution

Resolution is the true mark of a separation, however resolution varies with retention. Understanding how resolution varies with retention is one key aspect of being able to predict resolution.

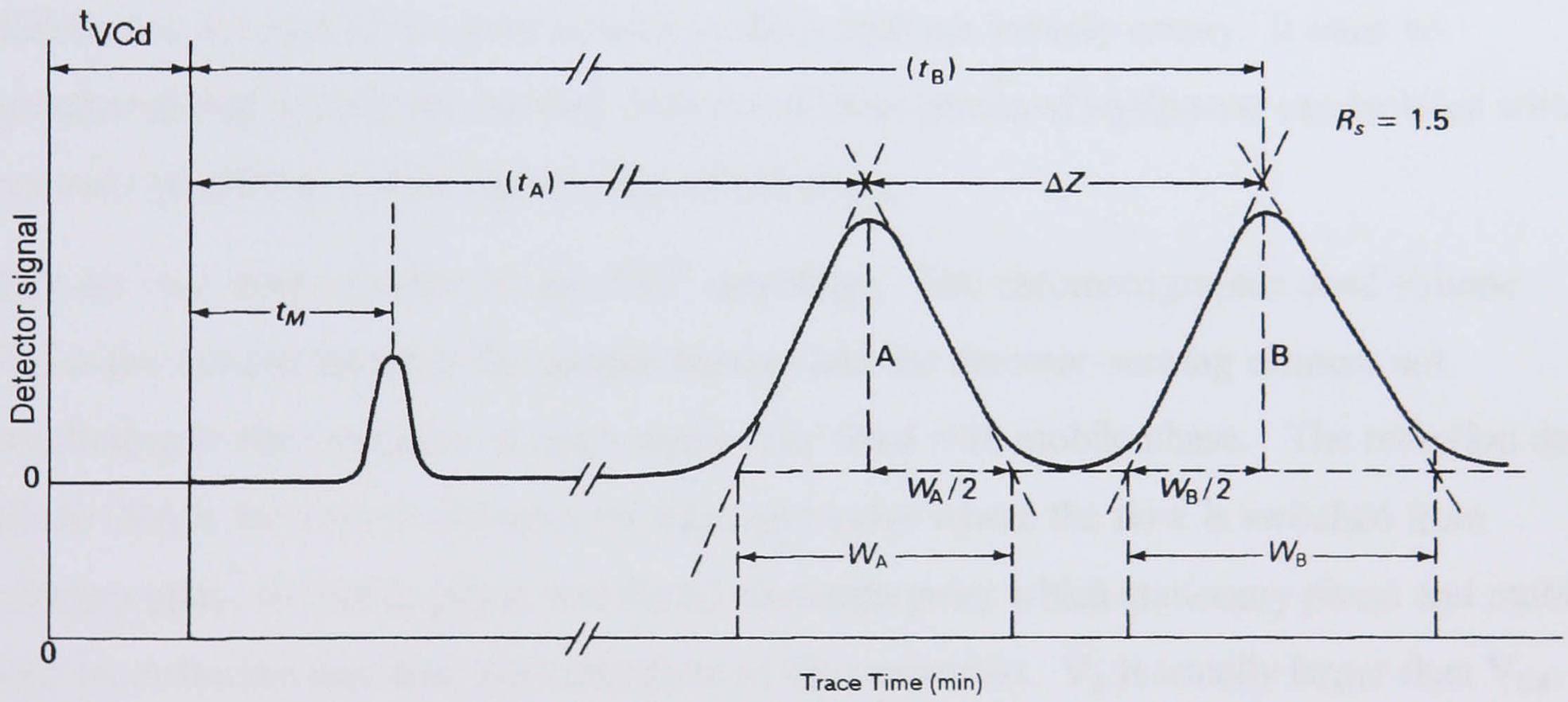

Figure 1.3.3.1 Example of chromatographic separation peaks of two sample components which is a modified version of a figure from [Conway 1990]

In figure 1.3.3.1 a typical chromatogram is shown for the separation of two sequential components from a sample, the resolution of this separation is 1.5. Here t_M is the mobile phase elution time or the P = 0 elution time, t_A and t_B are the elution times of the two sample components A and B, where W_A and W_B are the peak widths. The resolution can be calculated with the elution times of the peaks and the peak widths as shown below [Tswett 1906]:

$$R_S = \frac{2(t_B - t_A)}{W_A + W_B} \qquad (1.3.3.1)$$

where t is the elution time and W is the peak width of each peak. The width of a peak is measured by drawing tangents through the points of inflexion on each side of the peak. The peak width is the distance between the points of intersection between the tangents and the baseline of the trace see figure 1.3.3.1. If the resolution is greater than 1.5, components will be completely resolved and a baseline resolution has been achieved. A resolution of unity is described as a 4σ resolution [Karger 1973]. Before the resolution can be calculated the elution times and peak widths must be determined. A common error in measuring the elution time is to assume that the time period between switching the injector valve to inject and the appearance of a peak is the elution time of the peak. However this is not the case since the dead volume of the system has not been taken into account.

1.3.3.1 Dead Volumes

Dead volume in a CCC set up is mainly accounted for from the volume of the flying leads and associated plumbing such as switch valves, injectors, detectors and the delivery system inside of fraction collectors up to the dispensing nozzle. The volume of the vials used to collect the fractions are not part of the dead volume as these vials are initially empty. It must be remembered that initially the internal volumes of these pieces of equipment can be filled with stationary phase that will be replaced by mobile phase.

There are two dead volumes for any CCC centrifuge. The chromatographic dead volume (V_{Cd}) is the volume between the sample injector and the detector-sensing element not contributing to the separation ie any volume only filled with mobile phase. The retention dead volume (V_d) is the volume between the upstream valve where the flow is switched from stationary phase to mobile phase and the downstream point which stationary phase and mobile phase are collected that does not contribute to the separation. V_d is usually larger than V_{Cd} because the switching point between stationary and mobile phase is further upstream than the injector and the collection point (fraction collector) of stationary or mobile phase being further down stream than the detector-sensing element.

Usually when a separation is performed the trace from the detector is started when the sample is injected into the flow of the mobile phase see figure 1.3.3.1. However the sample will not start to separate until it reaches the coil after passing through some of the dead volume (V_{Cd}). There is also a period of time after a peak has left the coil before it is sensed at the detector. A peak elution time is the period between the sample entering the coil and the centre of a peak

appearing at the other end of the coil. The peak elution time ($t_{P=n}$) is determined by subtracting the time (t_{VCd}) spent in the chromatographic dead volume (V_{Cd}) from the trace time (t_{tn}):

$$t_{P=n} = t_{tn} - t_{VCd}$$

and $$t_{VCd} = \frac{V_{Cd}}{F}$$ where F is the mobile phase flow rate

hence $$t_{P=n} = t_{tn} - \frac{V_{Cd}}{F} \qquad (1.3.3.1.1)$$

Therefore it is necessary to know the dead volumes of a CCC experimental set up to accurately determine the elution time of a peak. The dead volumes are usually determined by calculation from the various volumes of the associated plumbing.

1.3.3.2 Predicting Elution times

The elution times of a separation can be measured or predicted. If measuring elution times, remember to subtract the time spent in the dead volume from the trace time see the above section. Walter Conway [1990] showed how the elution times for the P = 0 and the P = 1 peaks can be predicted. Conway also observed how the integer values of P eluted from a coil at regular intervals. The P = 0 peak elutes at a time determined by the mobile phase volume divided by the mobile phase flow rate because the P = 0 component does not transfer into the stationary phase and hence travels through the coil at the same speed as the mobile phase:

$$t_{P=0} = \frac{V_M}{F}$$

Now $$V_C = V_S + V_M \text{ and } S_f = \frac{V_S}{V_C}$$

Therefore $$V_C = V_C S_f + V_M$$

Therefore $$V_M = V_C(1 - S_f)$$

$$t_{P=0} = \frac{V_C(1 - S_f)}{F} \qquad (1.3.3.2.1)$$

The P = 1 peak elutes at a time calculated by dividing the coil volume by the mobile flow rate because the P = 1 component dissolves equally into both phases:

$$t_{P=1} = \frac{V_C}{F} \qquad (1.3.3.2.2)$$

For a given coil stationary phase retention and mobile phase flow rate, the elution times predicted by equations 1.3.3.2.1 and 1.3.3.2.2 are constant and can be plotted on the following figure. The elution time of a component is proportional to its distribution constant P so plotting a straight line through the P = 0 and P = 1 elution times allows the elution times for all other components to be predicted from the distribution constants [Conway 1990].

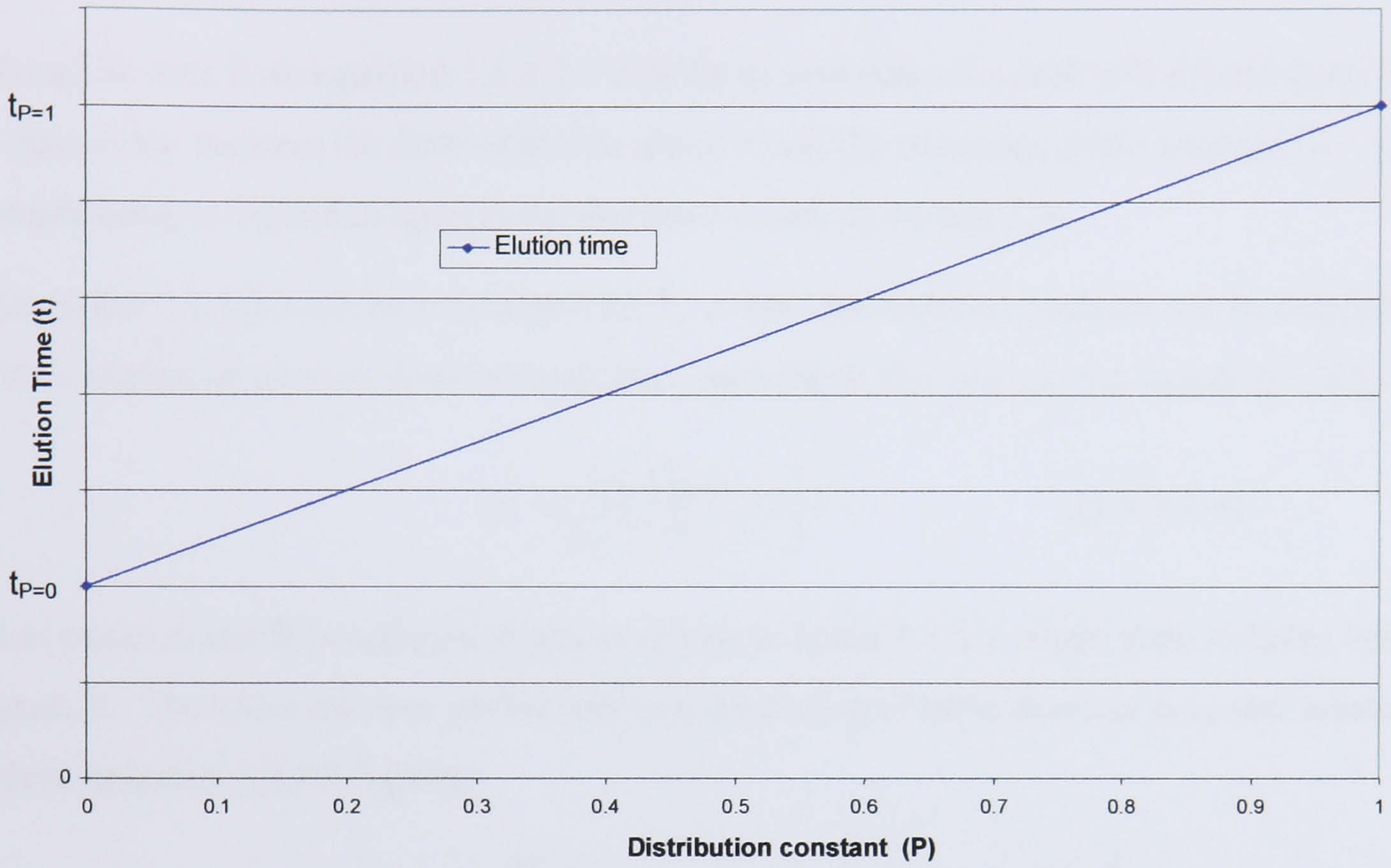

Figure 1.3.3.2.1 shows the Elution Time (t) plotted against Distribution constant (P).

The relationship shown on the above figure is governed by the basic equation y = mx + c where m is gradient of the relationship and c is the intercept on the vertical axis.

$$m = \frac{t_{P=1} - t_{P=0}}{1-0} \text{ and } c = t_{P=0}$$

Therefore m can be derived by subtracting equation 1.3.3.2.1 from equation 1.3.3.2.2 so that:

$$m = \frac{V_C}{F} - \frac{V_C\left(1-S_f\right)}{F}$$

$$m = \frac{V_C}{F}\left(1-\left(1-S_f\right)\right)$$

$$m = \frac{V_C S_f}{F}$$

Also from equation 1.3.3.2.1 $c = \frac{V_C\left(1-S_f\right)}{F}$

Therefore

$$t_{P=n} = \frac{V_C S_f}{F} P_n + \frac{V_C (1 - S_f)}{F}$$

$$t_{P=n} = \frac{V_C}{F} \left[S_f P_n + (1 - S_f) \right]$$

$$t_{P=n} = \frac{V_C}{F} \left[S_f (P_n - 1) + 1 \right] \qquad (1.3.3.2.3)$$

It can be seen from equation 1.3.3.2.3 that the elution time of a peak will depend upon the relationship between the flow of mobile phase F and the stationary phase retention S_f. This relationship is expanded upon in the literature review in section 1.4.

Equation 1.3.3.2.3 can be rearranged for P_n so that distribution constants can be determined from elution times once dead volumes have been taken into account see equation 1.3.3.1.1:

$$P_n = \frac{1}{S_f} \left(\frac{F t_{P=n}}{V_C} - 1 \right) + 1 \qquad (1.3.3.2.4)$$

Let peaks A and B be adjacent peaks as shown in figure 1.3.3.1 where peak A elutes before peak B. Therefore the time period between the elution of these peaks is t_B-t_A and substituting from equation 1.3.3.2.3 gives:

$$t_B - t_A = \frac{V_C}{F} \left[S_f (P_B - 1) + 1 \right] - \frac{V_C}{F} \left[S_f (P_A - 1) + 1 \right]$$

$$t_B - t_A = \frac{V_C}{F} \left[S_f (P_B - 1) + 1 - S_f (P_A - 1) - 1 \right]$$

$$t_B - t_A = \frac{V_C}{F} \left[S_f (P_B - 1) - S_f (P_A - 1) \right]$$

$$t_B - t_A = \frac{V_C S_f}{F} \left[P_B - 1 - P_A + 1 \right]$$

$$t_B - t_A = \frac{V_C S_f}{F} \left[P_B - P_A \right] \qquad (1.3.3.2.5)$$

Equation 1.3.3.2.5 forms the majority of the numerator of equation 1.3.3.1. Therefore equation 1.3.3.1 can be rewritten as:

$$R_S = \frac{2 V_C S_f (P_B - P_A)}{F (W_A + W_B)} \qquad (1.3.3.2.6)$$

1.3.3.3 Peak Width

It is known that the first component peak to elute from a coil is the narrowest and that the widest peak is the last peak to appear from the coil; therefore the peak width increases with elution time. The elution time is in turn related to the distribution constant see equation 1.3.3.2.3. It must therefore be possible to determine an equation for the peak width. The subject of an equation for peak width is expanded upon in the literature review in section 1.4.2.8.

1.4 Literature Review

This literature review is divided into three sections. The first is a review of the papers regarding the development of the CCC instrumentation. The second is related to papers and texts related to the retention of stationary phase. The third section reviews papers that are not directly related to CCC but are from the broader topic of the flow of two immiscible liquids and the onset of instability of the interfacial boundary between the liquids.

1.4.1 History of the Development of CCC

1.4.1.1 Background

The history of CCC begins in the early to middle 1960's and the first publication appeared in print in 1966 [Ito 1966, Foucault ISBN 0-8247-9257-2]. At this time Dr Yoshiro Ito was working in Japan. Dr Ito then moved to America where a large part of his job description was to invent new technologies that would help the American Health Services. However it appears that time has never been granted to the development of or a detailed understanding of his inventions.

1.4.1.2 I-Type and J-Type Centrifuges

The early papers describe the I-type coil plant centrifuges, the performance and the use of these centrifuges. Over the next decade Dr Ito and his team invented a number of variants on the I-type centrifuge and in the late seventies developed the J-type centrifuge. Dr Ito and others wrote a number of papers describing the design, use and performance of the J-type centrifuge between 1977 and 1980 [Ito 1977A, Ito 1978, Ito 1980]. The main advantage of the J-type over the I-type centrifuge is the higher stationary phase retentions that can be achieved. This means that the J-type centrifuge performs a given separation in a shorter time. This difference in performance must be related to the different motions of the two types of centrifuge.

1.4.1.2.1 Basic Description of I-type and J-type Centrifuges

The basic descriptions of the two types of centrifuge are similar in that a length of tubing is wound on a bobbin (circular drum) to form a coil. The coil is then rotated about its own axis and about a solar axis (the rotor axis). The motions of the coils are very similar to those of the planets orbiting the sun while rotating about their own axes. The coil on the I-type centrifuge rotates in the opposite direction about its own axis compared to the direction of rotation about the solar axis. If the coil is rotated clockwise about the solar axis, then the coil will rotate anti-clockwise about its own axis, the converse is also true; in this way the same portion of the

coil always faces the observer. The coil on the J-type centrifuge rotates in the same direction about its own axis compared to the direction of rotation about the solar axis see figure 1.3.2.1.1. If the coil is rotated clockwise about the solar axis, then the coil will rotate clockwise about its own axis, the converse is also true. The locus of a point P on the coil on an I-type centrifuge is a circle where as the locus on a J-type is a cardioid.

1.4.1.2.2 The Kinematics of a point P on a coil

Kinematics is the study of the motion of a point in space. If a point P is placed on a coil and the coil is rotated in planetary motion the locus (path) of the point P can be drawn. The mathematical equations of the locus can also be derived. Differentiating the equations for the locus will give the velocity equations of the point P. Differentiating the velocity equation will give the acceleration equations for the point P. Conway has done this in his book [Conway 1990] for the J-type centrifuges, see equations 1.4.1.2.2.1, 1.4.1.2.2.2 and 1.4.1.2.2.3. However in the Conway book the acceleration equations are described as the force equations. These equations do not contain mass terms and hence cannot be force equations, however these equations can be described as force/unit mass equations or equations of acceleration. The corrected equations are as follows:

$$\text{Accn } X = -R\omega^2(\cos\theta + 4\beta\cos 2\theta) \qquad (1.4.1.2.2.1)$$

$$\text{Accn } Y = -R\omega^2(\sin\theta + 4\beta\sin 2\theta) \qquad (1.4.1.2.2.2)$$

The magnitude of the resultant acceleration is given in equation 1.4.1.2.2.3.

$$\text{Accn (Resultant)} = (\text{Accn } X^2 + \text{Accn } Y^2)^{0.5} = R\omega^2(1 + 8\beta\cos\theta + 16\beta)^{0.5} \qquad (1.4.1.2.2.3)$$

The equations above describe the acceleration of the point P but need to be resolved tangentially and radially to the coiled tubing to be useful. Ito resolved these accelerations [Ito 1992], however the equations have again been described as force equations and again these equations are acceleration equations. The corrected equations are as follows:

$$\text{Accn Radial} = -R\omega^2(\cos\theta + 4\beta) \qquad (1.4.1.2.2.4)$$

$$\text{Accn Tangential} = R\omega^2\sin\theta \qquad (1.4.1.2.2.5)$$

For the derivation from first principles of the equations of motion for a J-type centrifuge see Appendix 1. Ito's equation for the Tangential acceleration has a negative sign. This is probably due to the Free Body diagram that he used having the acceleration vector pointing in the opposite direction to that in Free Body diagram 2 Appendix 1. If this is true then the equations represent exactly the same motion.

A similar treatment can be given to I-type centrifuges, see Appendix 2, and the corrected equation for radial and tangential accelerations are given below:

$$\text{Accn Radial} = -R\omega^2 \cos\theta \qquad (1.4.1.2.2.6)$$

$$\text{Accn Tangential} = -R\omega^2 \sin\theta \qquad (1.4.1.2.2.7)$$

Equations 1.4.1.2.2.3 to 1.4.1.2.2.5 can be used to generate diagrams that describe the kinematic accelerations for the point P see figures 1.4.1.2.2.1 to 1.4.1.2.2.6. Figures 1.4.1.2.2.1 to 1.4.1.2.2.3 can be redrawn to represent one loop of a coil, see figures 1.4.1.2.2.4 to 1.4.1.2.2.6.

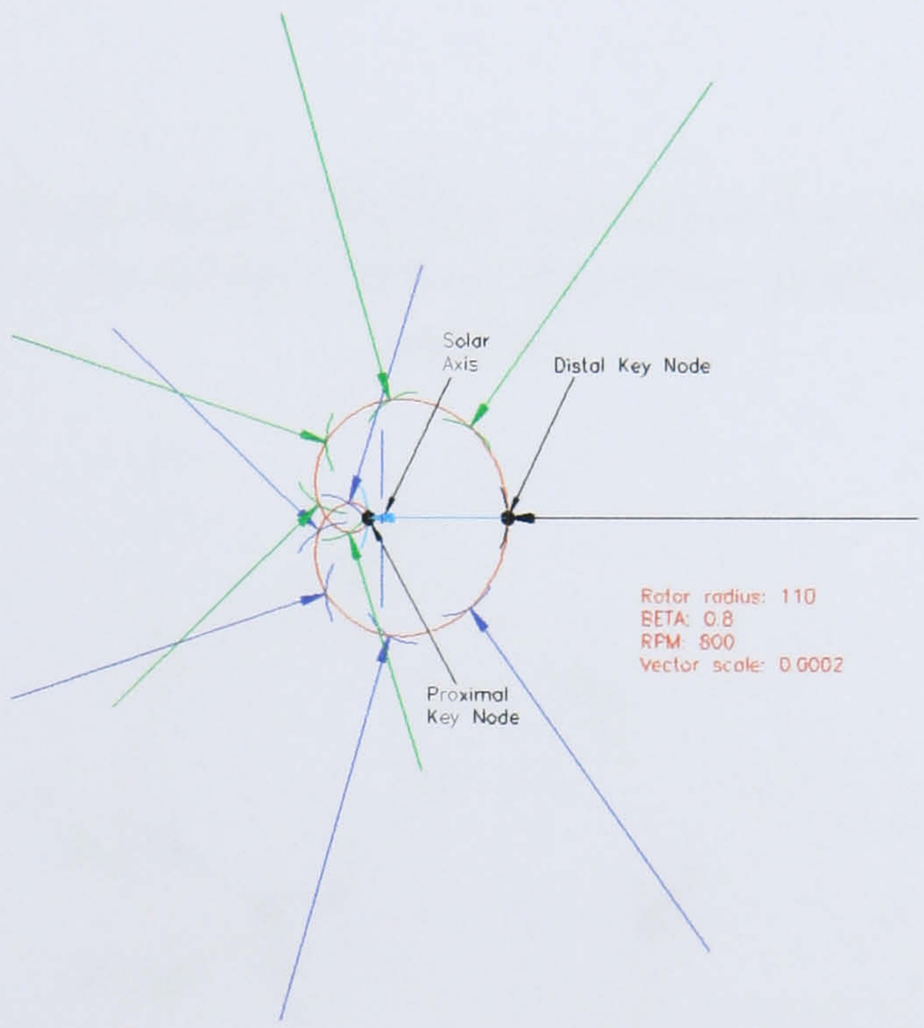

Figure 1.4.1.2.2.1 shows the kinematic Resultant Acceleration Vectors pointing inwards

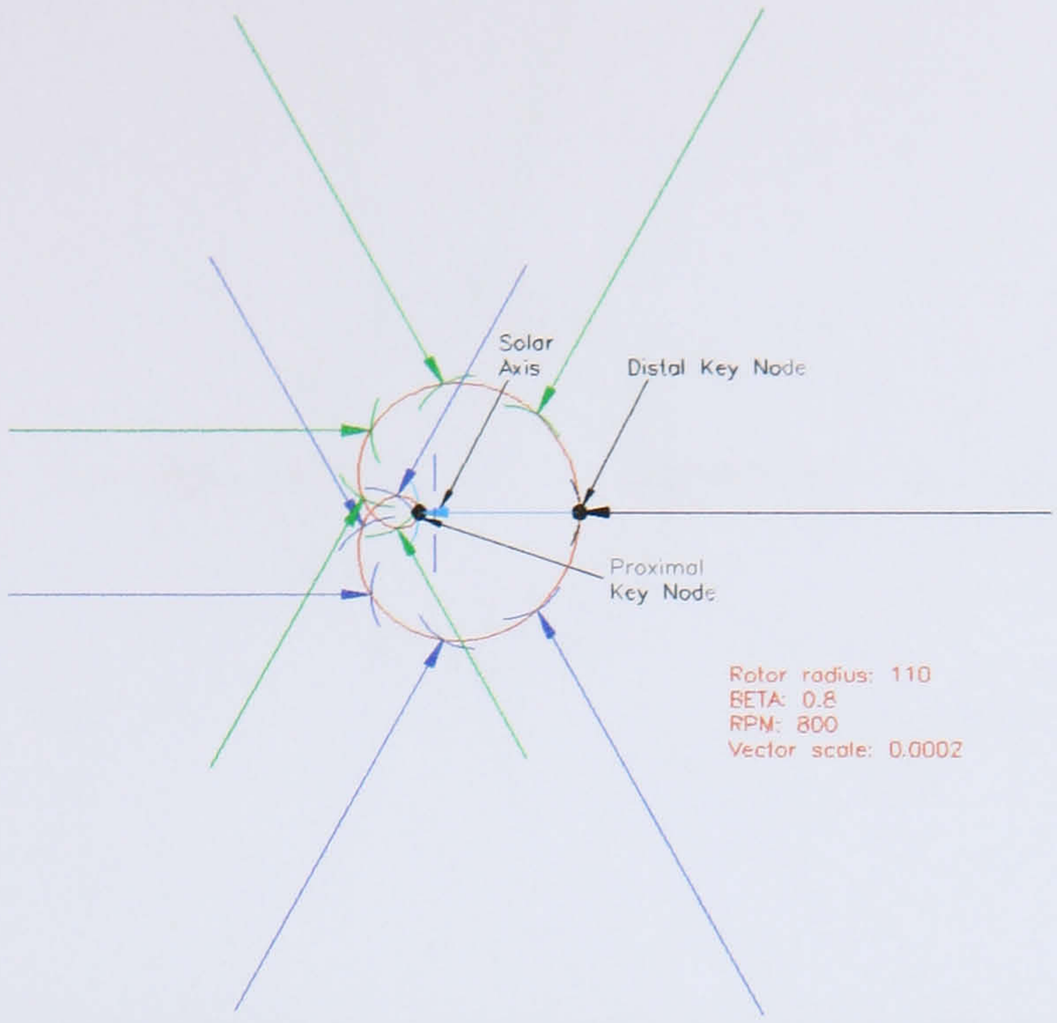

Figure 1.4.1.2.2.2 shows the kinematic Radial Acceleration Vectors, this presents the Radial Accelerations Vectors that the tubing exerts on the solvent system, and these vectors point inwards

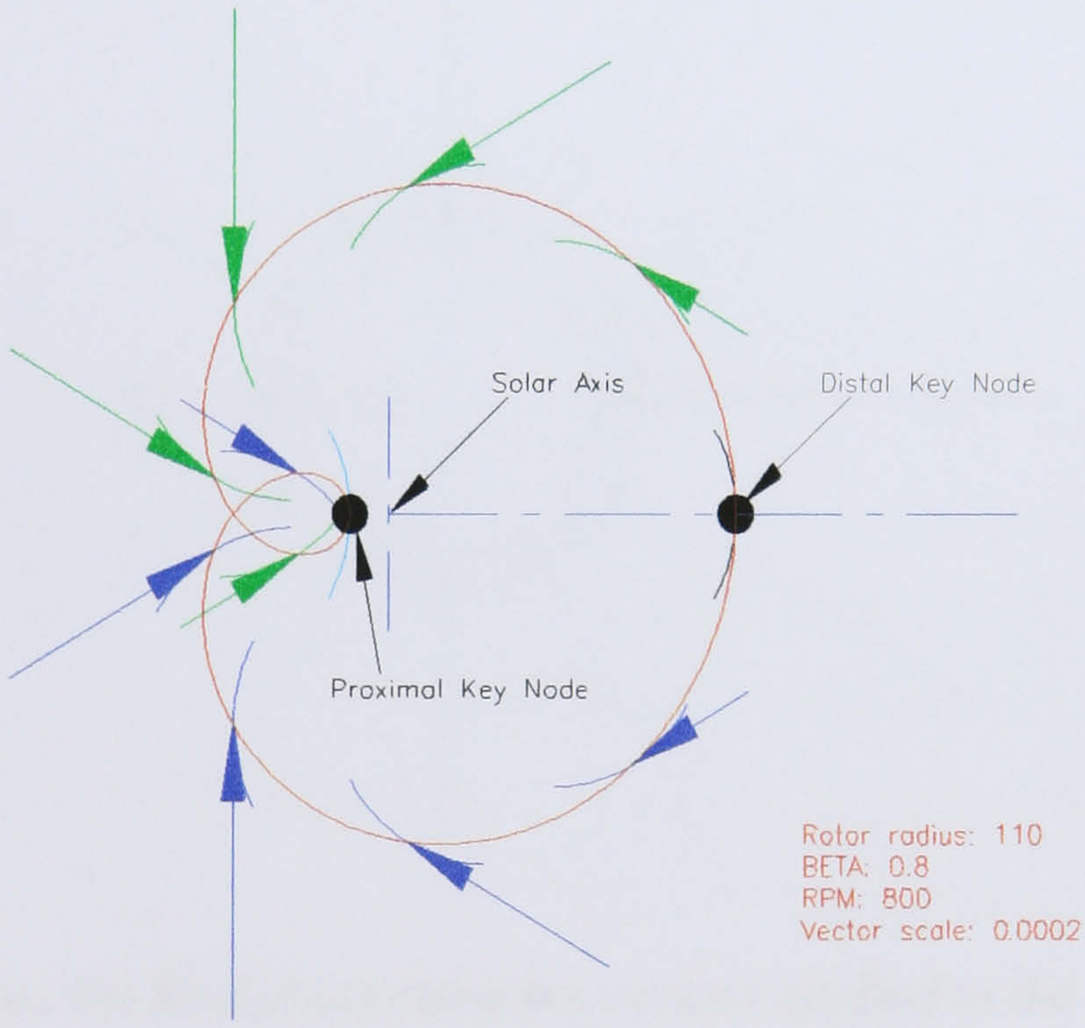

Figure 1.4.1.2.2.3 shows the kinematic Tangential Acceleration Vectors pointing towards the proximal key node; this presents the Tangential Accelerations Vectors that the tubing exerts on the solvent system

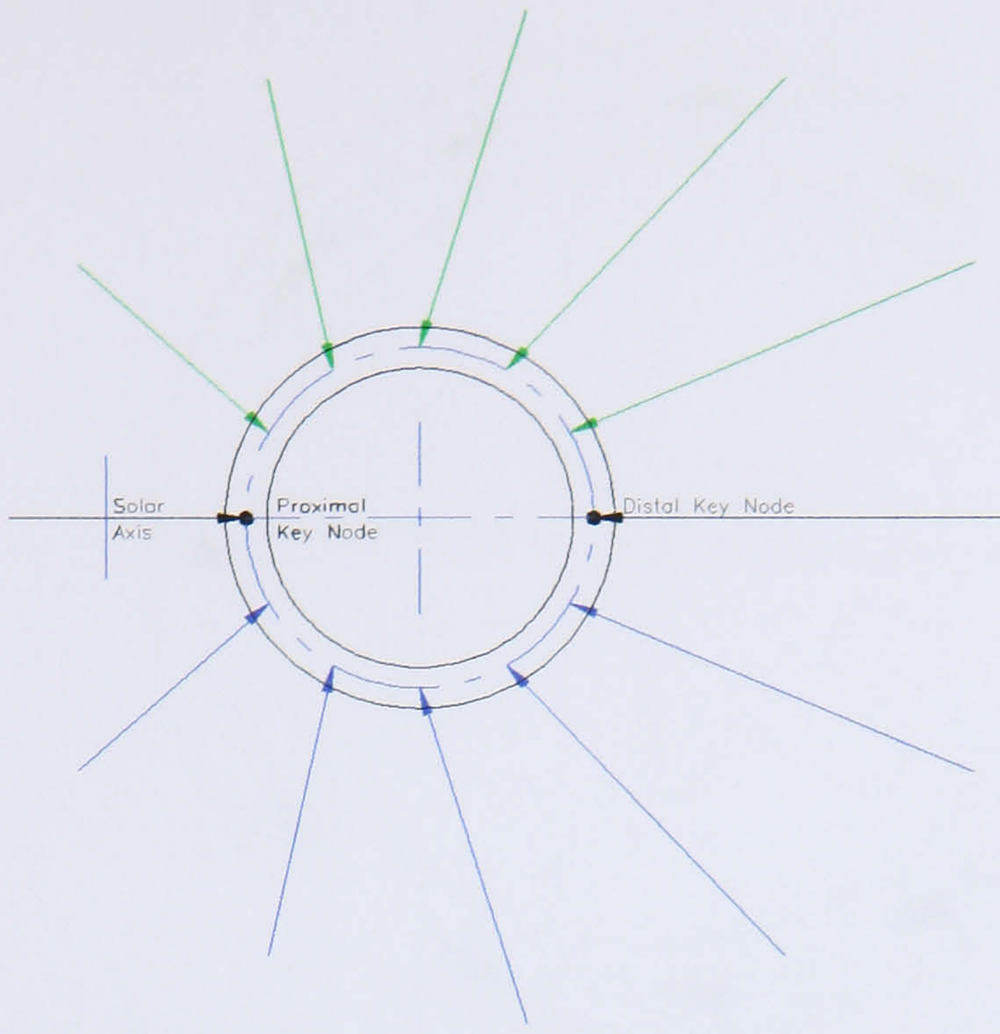

Figure 1.4.1.2.2.4 shows the Resultant acceleration vectors applied to the tubing for one loop of a coil

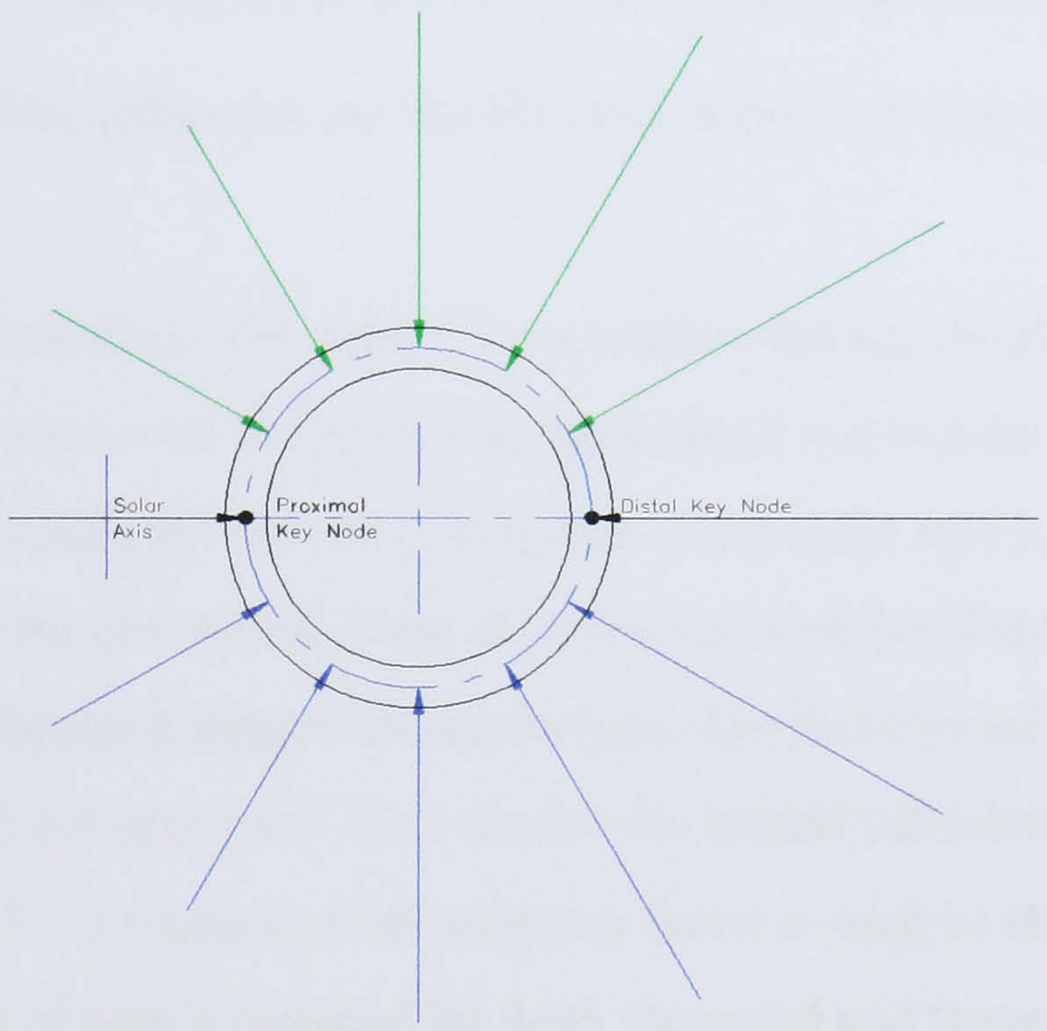

Figure 1.4.1.2.2.5 shows the Radial acceleration vectors applied to the tubing for one loop of a coil

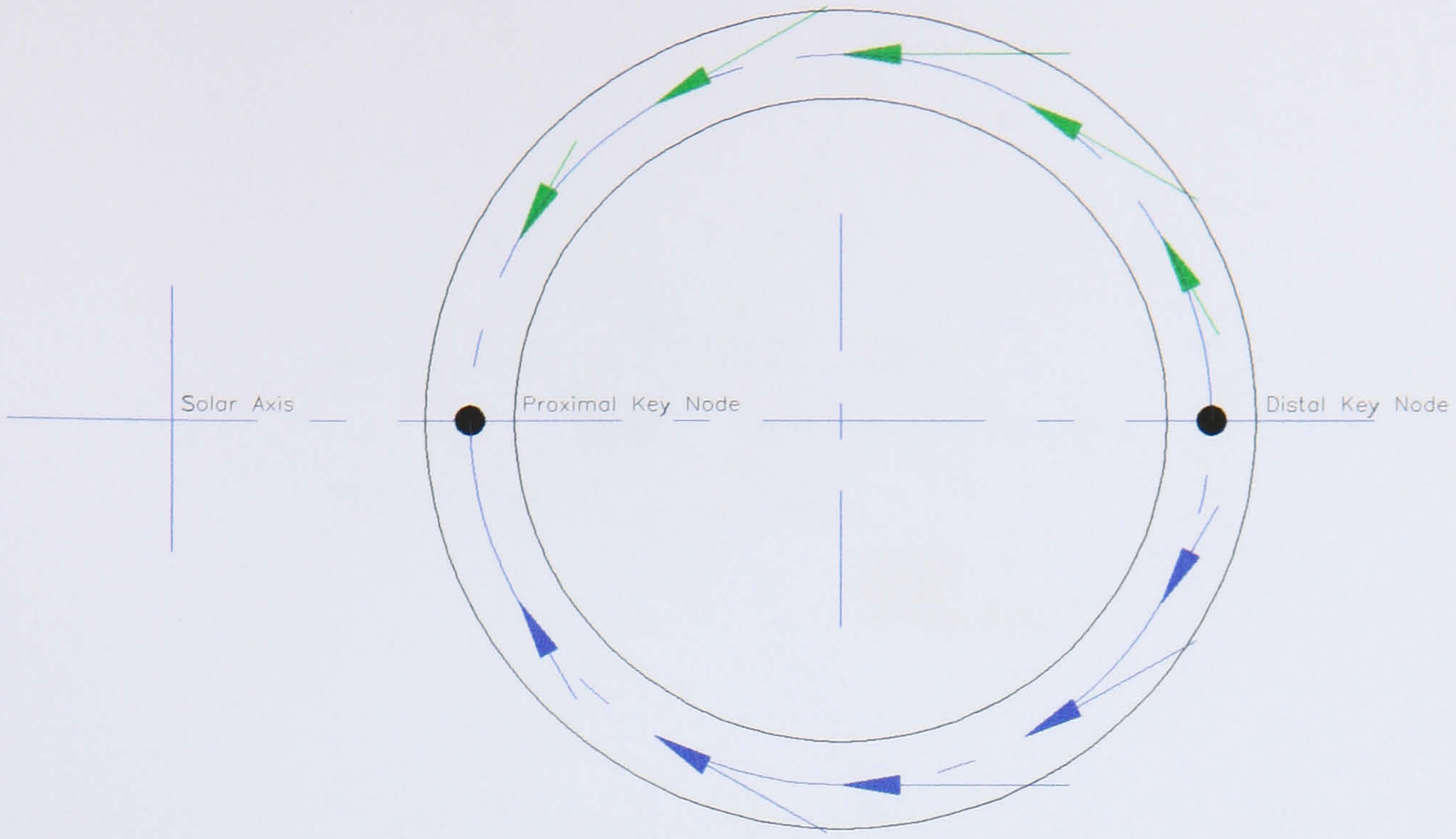

Figure 1.4.1.2.2.6 shows the Tangential acceleration vectors applied to the tubing for one loop of a coil. Note that these vectors point towards the proximal key node

1.4.1.2.3 The influence on the Hydrodynamics of the kinematics of a Point P

In the case of a J-type centrifuge, the point P on a coil has the accelerations shown in figures 1.4.1.2.2.1 to 1.4.1.2.2.6 because the point P is constrained to produce the cardioid shaped path. The resultant and radial accelerations in figures 1.4.1.2.2.1 and 1.4.1.2.2.2 point inwards towards the centre of rotation, these describe the centripetal acceleration. Figure 1.4.1.2.2.3 shows the kinematic tangential acceleration directed towards the proximal key node. Equations 1.4.1.2.2.4 and 1.4.1.2.2.5 are for the inertial (absolute) reference frame for the motion of the point P. If a non-inertial reference frame is used so that the coil is effectively held stationary a change of sign is required for both the radial and tangential components of acceleration of the point P. Therefore equations 1.4.1.2.2.4 and 1.4.1.2.2.5 can be rewritten as follows:

$$\text{Radial Acceleration of Liquid} = R\omega^2(\cos\theta + 4\beta) \qquad (1.4.1.2.3.1)$$

$$\text{Tangential Acceleration of Liquid} = -R\omega^2 \sin\theta \qquad (1.4.1.2.3.2)$$

Therefore the acceleration vectors are reversed in figures 1.4.1.2.3.1 to 1.4.1.2.3.3 to show the change of reference frame used. The radial acceleration component can be seen in figure 1.4.1.2.3.1. The tangential acceleration component is accelerating both of the phases towards the distal key node see figure 1.4.1.2.3.2. The equations above help determine the hydrodynamic motion of the fluids in a J-type centrifuge.

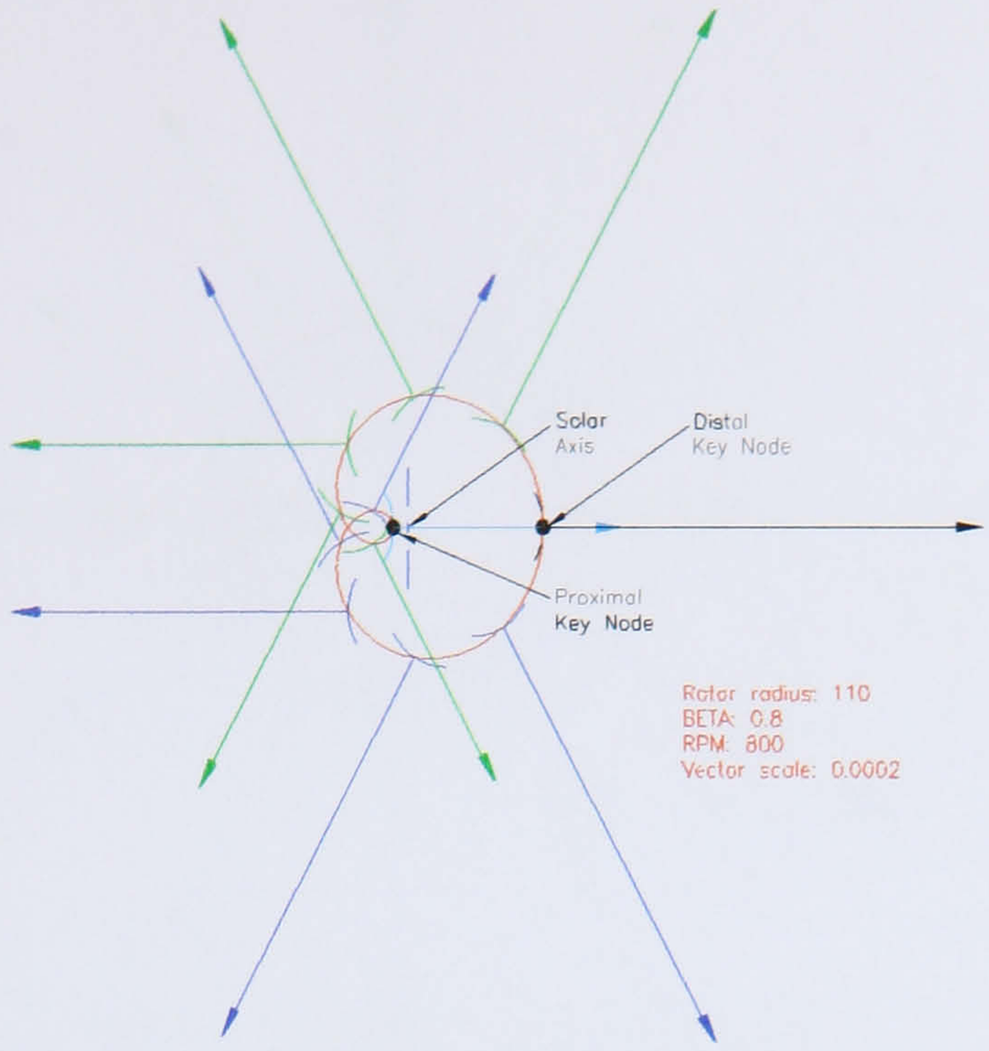

Figure 1.4.1.2.3.1 shows the Radial Acceleration Vectors that the solvent system exerts on the tubing, these Vectors point outwards from the coil's tubing

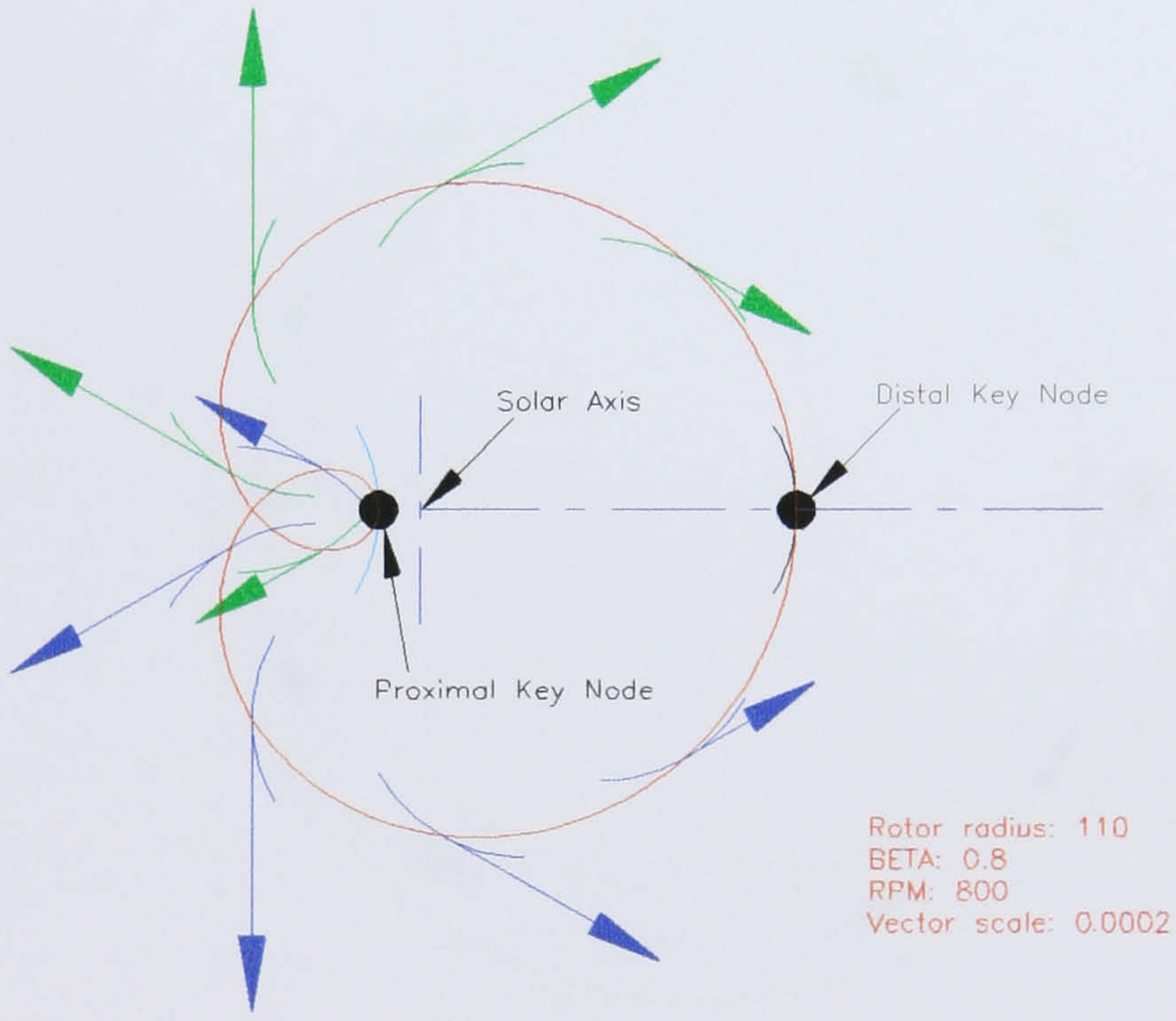

Figure 1.4.1.2.3.2 shows the Tangential Acceleration Vectors that the solvent system exerts on the tubing, these Vectors point towards the distal key node

Figures 1.4.1.2.3.1 and 1.4.1.2.3.2 can be represented for one loop of a coil, see figures 1.4.1.2.3.3 and 1.4.1.2.3.4.

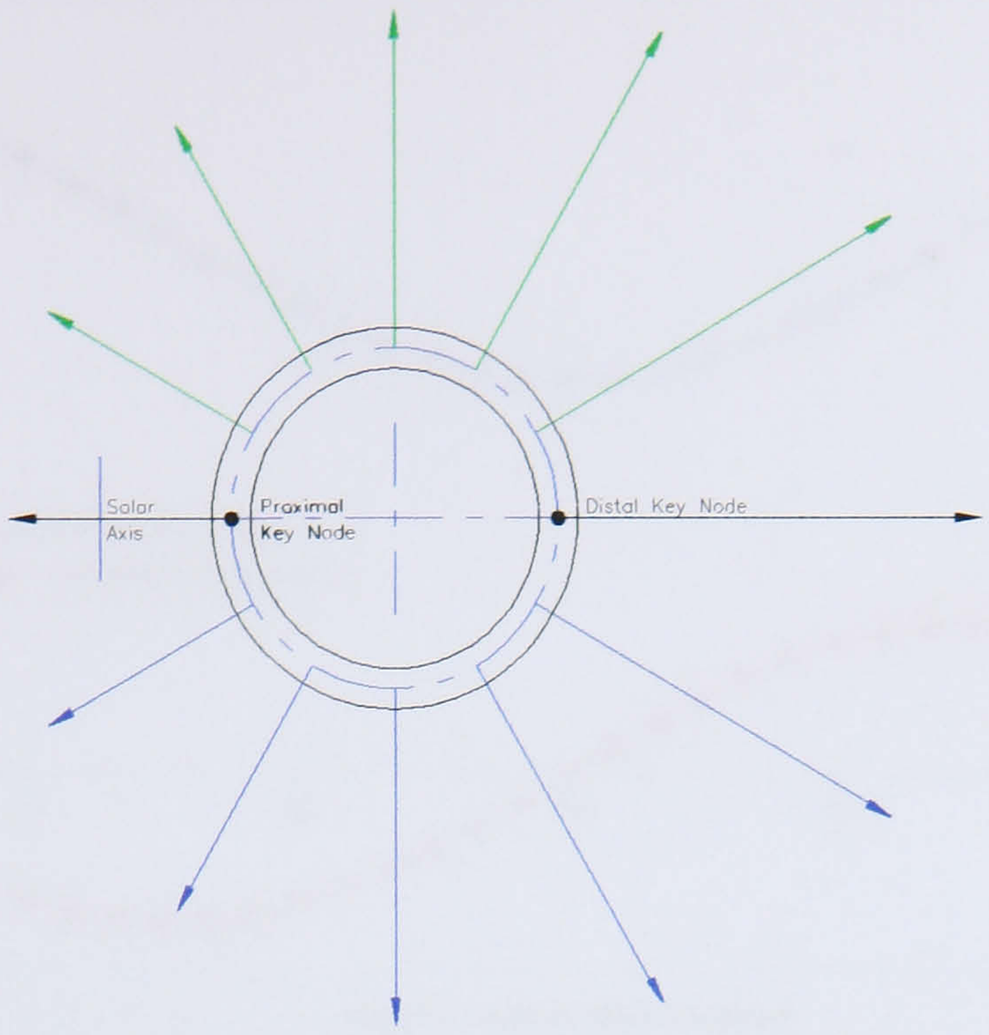

Figure 1.4.1.2.3.3 shows the Radial Acceleration Vectors that the solvent system exerts on the tubing for one loop of a coil, these vectors point outwards from the tubing

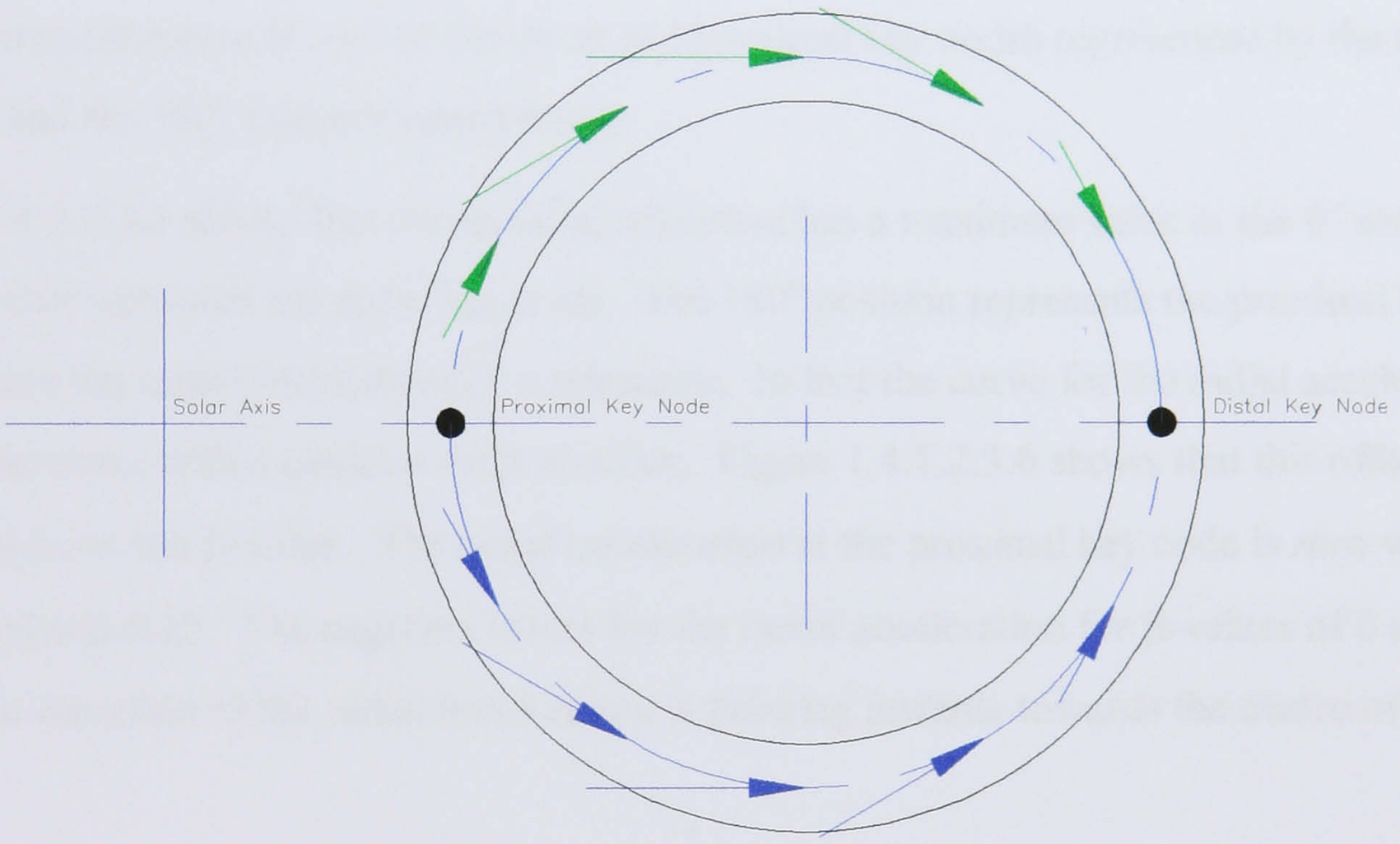

Figure 1.4.1.2.3.4 shows the Tangential Acceleration Vectors that the solvent system exerts on the tubing for one loop of a coil, these Vectors point towards the distal key node

Equations 1.4.1.2.3.1 and 1.4.1.2.3.2 can be used to determine the radial and tangential accelerations acting upon the phase system in a J-type centrifuge for one loop of a coil see figure 1.4.1.2.3.5[iv].

[iv] Figure 1.4.1.2.3.5 was generated using a rotor radius of 110mm, a β value of 0.9 and a rotational speed of 800 rpm.

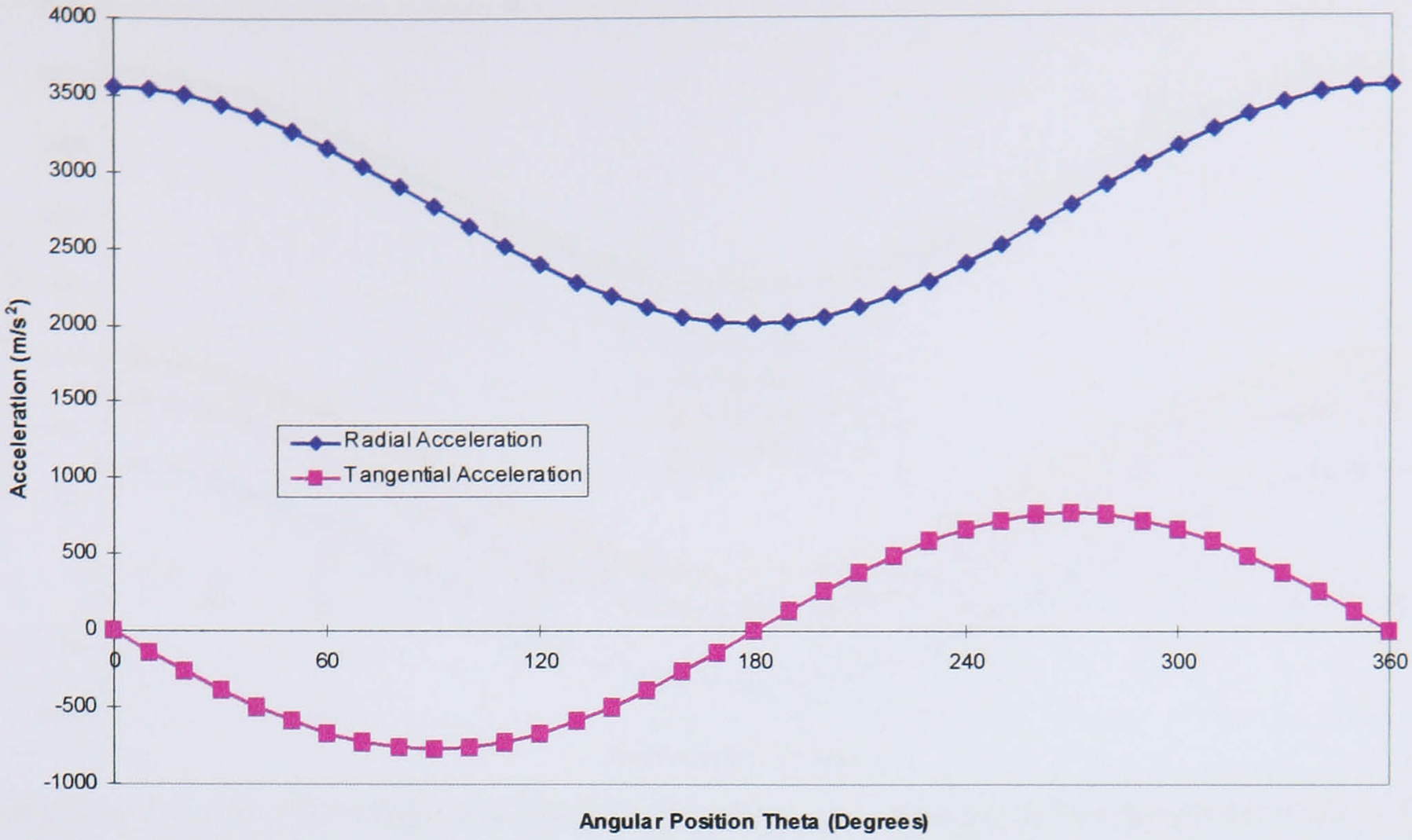

Figure 1.4.1.2.3.5 shows the variation of the radial and tangential accelerations against the angular position

Figure 1.4.1.2.3.5 shows that the tangential acceleration varies as a negative sine wave. The tangential acceleration is zero at the distal and proximal key nodes represented by the 0°/360° position and the 180° position respectively.

Figure 1.4.1.2.3.5 shows that the radial acceleration has a maximum value at the 0° and 360° position that represent the distal key node. The 180° position represents the proximal key node where the radial acceleration is a minimum. In fact the curve for the radial acceleration is a cosine curve with a positive vertical offset. Figure 1.4.1.2.3.6 shows that this offset is proportional to the β-value. The radial acceleration at the proximal key node is zero when the β-value equals 0.25. The negative values for the radial acceleration for β-values of 0 and 0.15 show that direction of the radial acceleration is pointing inwards towards the centre of the coil.

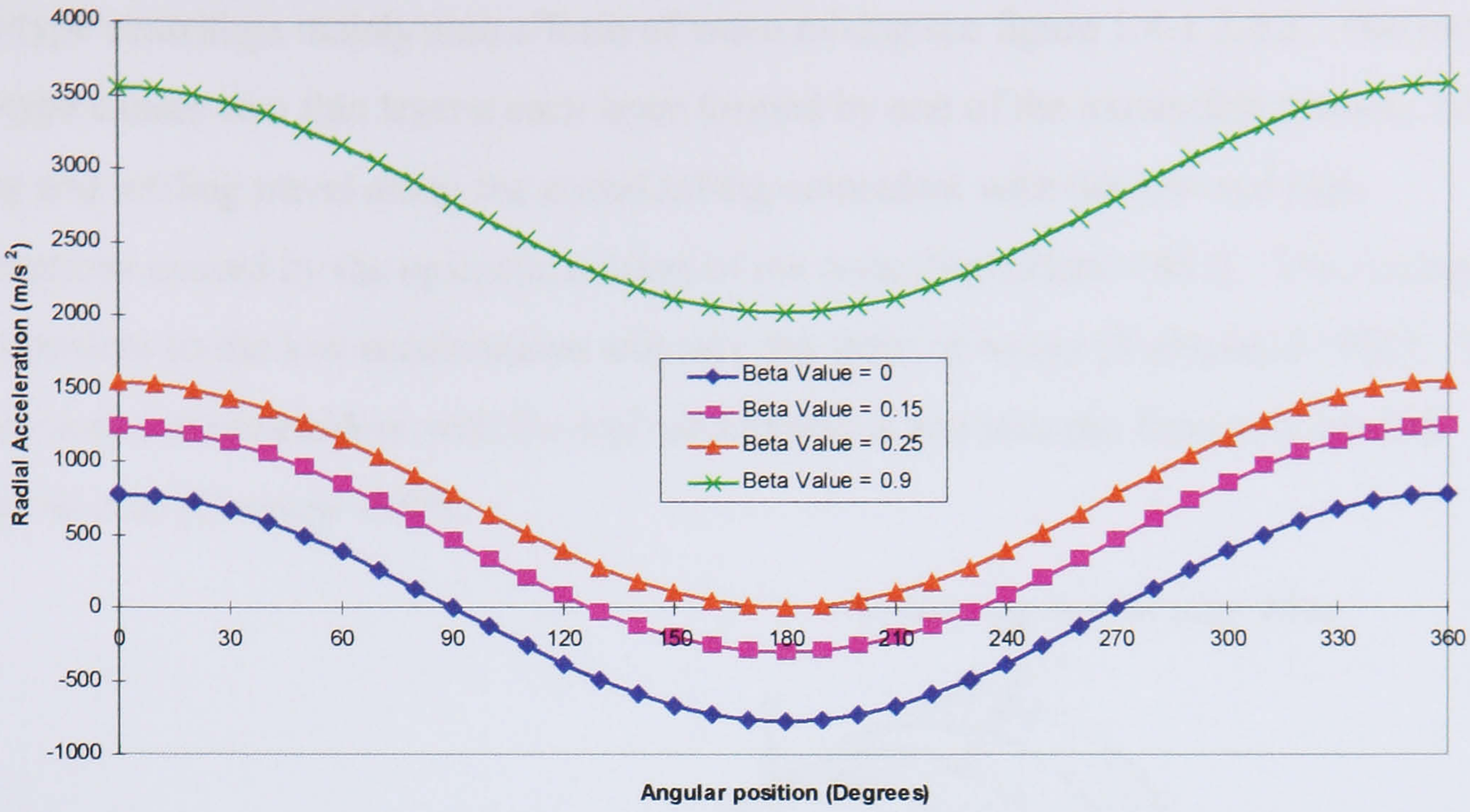

Figure 1.4.1.2.3.6 showing how Radial Acceleration changes with the β value for J-type Centrifuges, which is similar to a figure from [Conway 1990] but modified for the Brunel CCC machine

1.4.1.2.4 Comparison of the types of mixing in I-type and J-type centrifuges

The I-type centrifuge uses an increased acceleration field to retain one phase of an immiscible solvent system while the other phase is pumped through it, see figure 1.4.1.2.4.1. This cascade mixing is synchronous, however hydrodynamic constraints limit stationary phase retention to less than 50%, and high mixing rates cause carry over and loss of stationary phase. The process was limited to analytical scale, high-resolution separations using high interfacial tension solvent systems [Sutherland 1987]. Ito [1977B] has also produced similar results for a similar apparatus to the I-type centrifuge. This apparatus was a coil rotating slowly about its own axis in the earth's gravitational field that cascade mixing. Ito was able to produce "an efficient partition process" using the "low interfacial tension n-BuOH phase system".

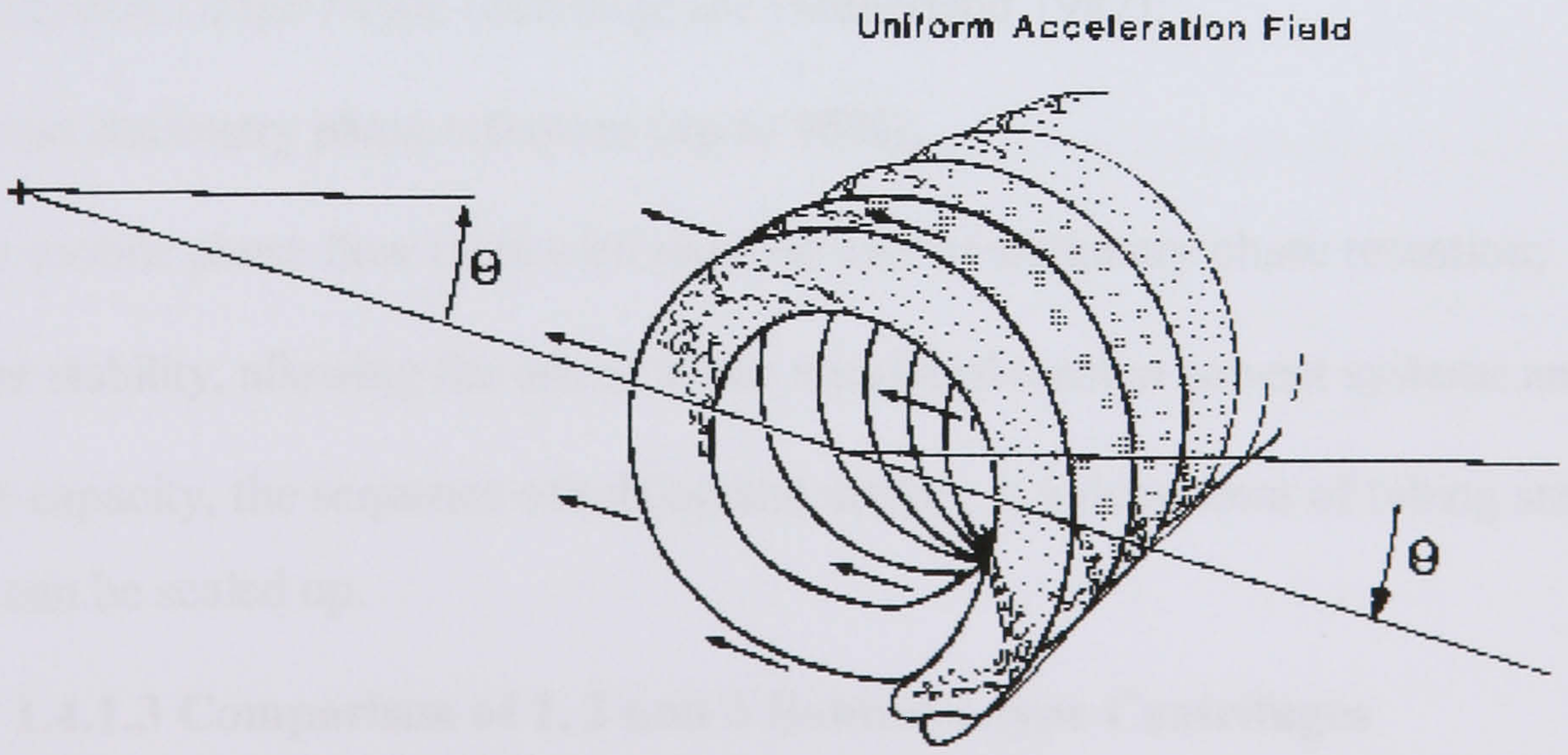

Figure 1.4.1.2.4.1 shows Cascade mixing of phases on an I-type Centrifuge [Sutherland 1987]

The J-type centrifuge mainly uses a form of wave mixing see figure 1.4.1.2.4.2. The motion of the J-type causes two thin layers; each layer formed by one of the immiscible phases. Zones of mixing and settling travel along the coiled tubing coincident with the low and high accelerations caused by the epicyclic motion of the coils [Sutherland 1987]. The mixing zones are coincident to the low accelerations and take the form of waves [Sutherland 1986]. The settling zones are coincident with the high accelerations and take the form of a smooth interfacial area [Conway 1990].

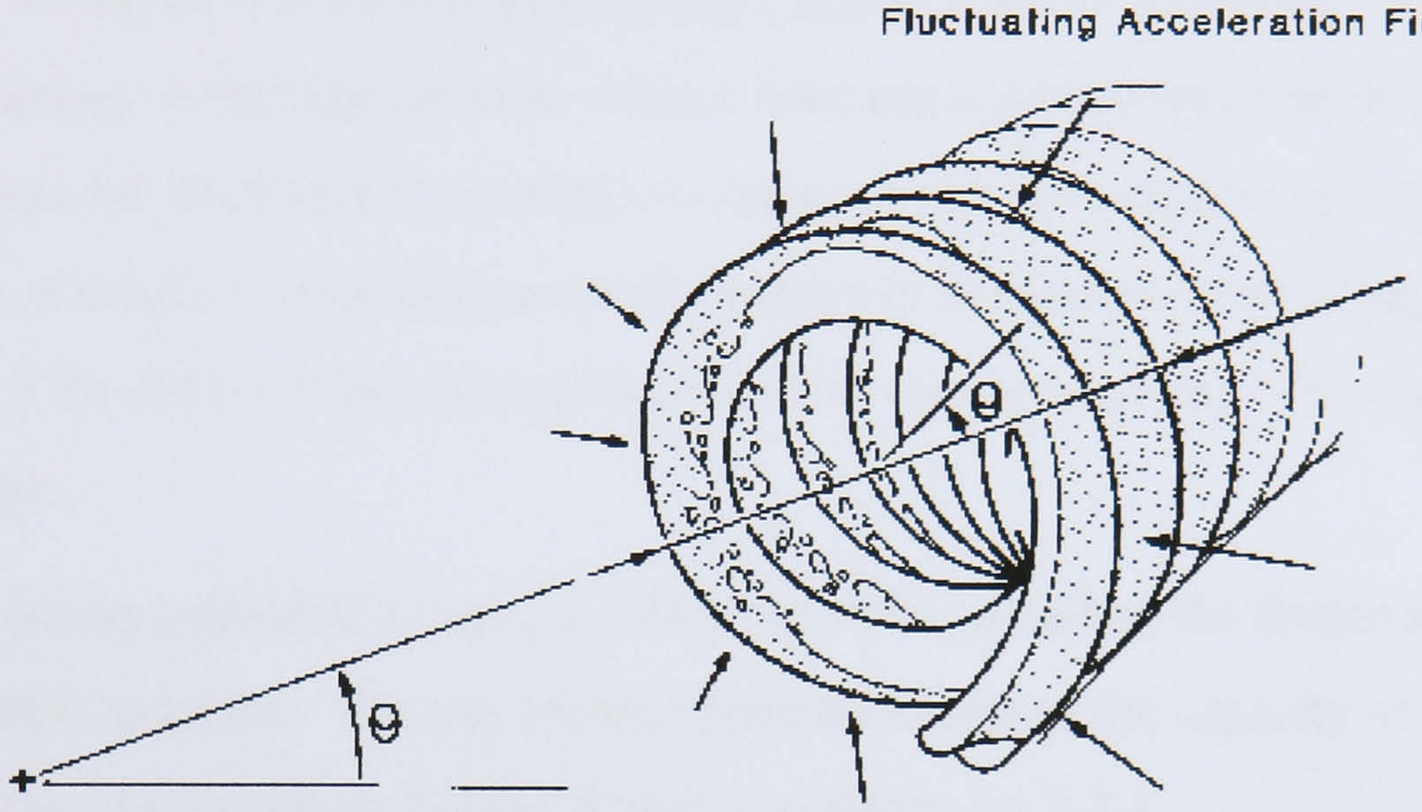

Figure 1.4.1.2.4.2 shows wave mixing as observed on J-type Centrifuges for β values above 0.25 [Sutherland 1987]

For a J-type centrifuge with a β-value below 0.25 a type of mixing resembling cascade mixing occurs due to the switching of the direction of the radial acceleration about the proximal key node. For a β-value of 0.25 the radial acceleration at the proximal key node is 0 and for β-values above 0.25 the radial acceleration increases proportionally but always points in the same direction relative to the tubing.

The main benefits of the J-type centrifuge are [Sutherland 1987]:

1. Increased stationary phase retention (up to 90%);
2. Higher mobile phase flow rates with reduced loss of stationary phase retention;
3. Greater stability, allowing the use of lower interfacial tension solvent systems and
4. Higher capacity, the sequence of mixing and settling is independent of tubing size and hence can be scaled up.

1.4.1.3 Comparison of 1, 2 and 3 Bobbin J-type Centrifuges

The simplest commercially available J-type centrifuge was produced and distributed by PC Inc [Marston 1994]. This machine had one bobbin upon which various types of coil could be wound. The bobbin was counter-balanced by a rotating mass placed symmetrically opposite

the bobbin. The main drive shaft passes through the space between the rotor plates reducing the maximum β value that a coil could achieve. This machine, when compared to modern instrumentation, has four main disadvantages. The first is, that it has a low capacity and the second is, a maximum β value of only 0.9. The third disadvantage is that it was difficult to keep balanced. The counter-balance mass would have to be adjusted to statically balance the bobbin when full of stationary and mobile phases in the correct proportions. The proportions of stationary and mobile phases change with operating conditions. Therefore the counter-balance mass would have to be changed for each different set of operating conditions. The fourth disadvantage is that the machine did not have any active form of temperature control but replied upon the ambient surroundings to minimise any temperature variations. Repeatability of results was poor because of changes in coil temperature using this machine; see section 1.5 for details of how temperature affects the repeatability of a separation in a J-type centrifuge.

Ito, Oka and Slemp published a paper in 1989 [Ito 1989] detailing the design and performance of a three-bobbin machine. The use of three bobbins increases the capacity of the machine compared to the original single bobbin device, see figure 1.4.1.3.1.

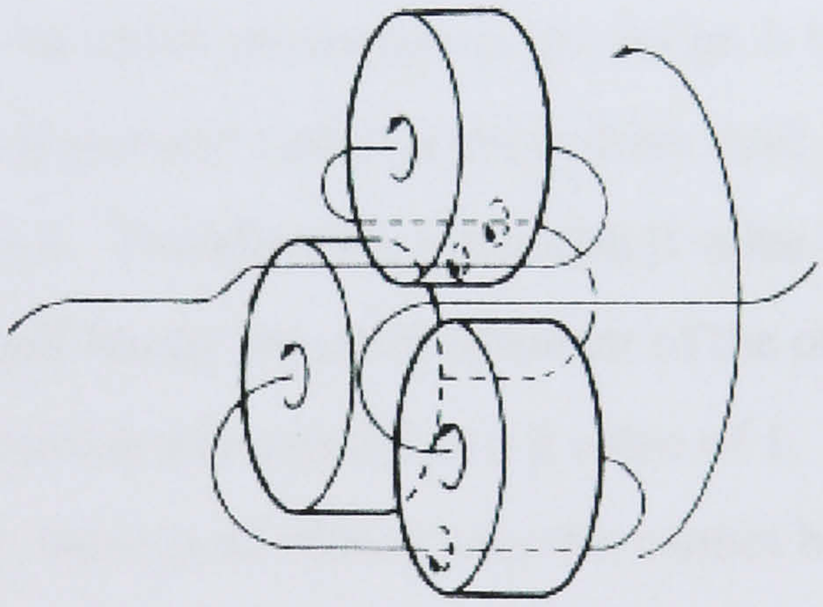

Figure 1.4.1.3.1 shows the schematic layout of the 3-bobbin J-type centrifuge with counter rotating flying leads [Ito 1989]

The three bobbins are connected in series and there are four flying leads. Three of these flying leads have to counter rotate to stop the leads from twisting. The counter rotation mechanism adds an extra level of complexity to the machine that will reduce its reliability, see figure 1.4.1.3.2. The number of flying leads also reduces the reliability. This machine does away with the need for a counter-balance mass or masses, each bobbin acts as a counter-balance for the other two bobbins. This machine also self-balances in that the bobbins are used in series, hence any change in operating conditions will eventually effect each bobbin in turn in the same manner, eventually the machine will become balanced. The β value range for this machine is

given as 0.5 to 0.75. The maximum β value is 0.866 for a 3-bobbin machine and will decrease as the number of bobbins increases, see figure 1.4.1.3.5.

However the repeatability of the results using the machine have been compromised due to having no form of active temperature control.

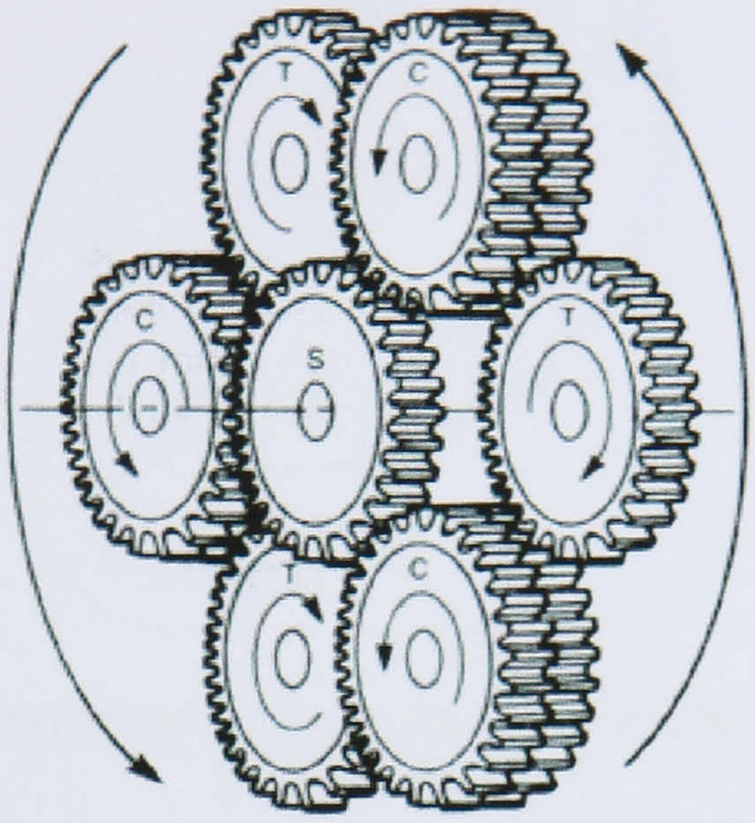

Figure 1.4.1.3.2 shows the complex counter rotating mechanism for the 3-bobbin J-type centrifuge [Ito 1989]

Sutherland et al [Sutherland 1998] described a two-bobbin machine that has the advantages of the three-bobbin machine without the added complexity. This machine has two flying leads one for each bobbin, see figure 1.4.1.3.3. These flying leads do not need to be counter rotated to stop them from twisting. An added advantage of the design is the ability to achieve a maximum β value of 1. This is possible since the main drive shaft does not pass between the rotor plates see figure 1.4.1.3.4. Therefore the maximum β value is not limited by the diameter of the main drive shaft but by the outer diameter of the other bobbin. The outer diameters of the bobbins will touch when each has a β value of 1. Currently the β value range of this machine is 0.7 to 0.91; there is no reason why this cannot be expanded to give a range of 0.5 to 0.95.

This machine also has active temperature control allowing the chromatography to experience an identical temperature from one separation to the next regardless of ambient temperature conditions. This ability increases the repeatability of separations when compared to the other machines.

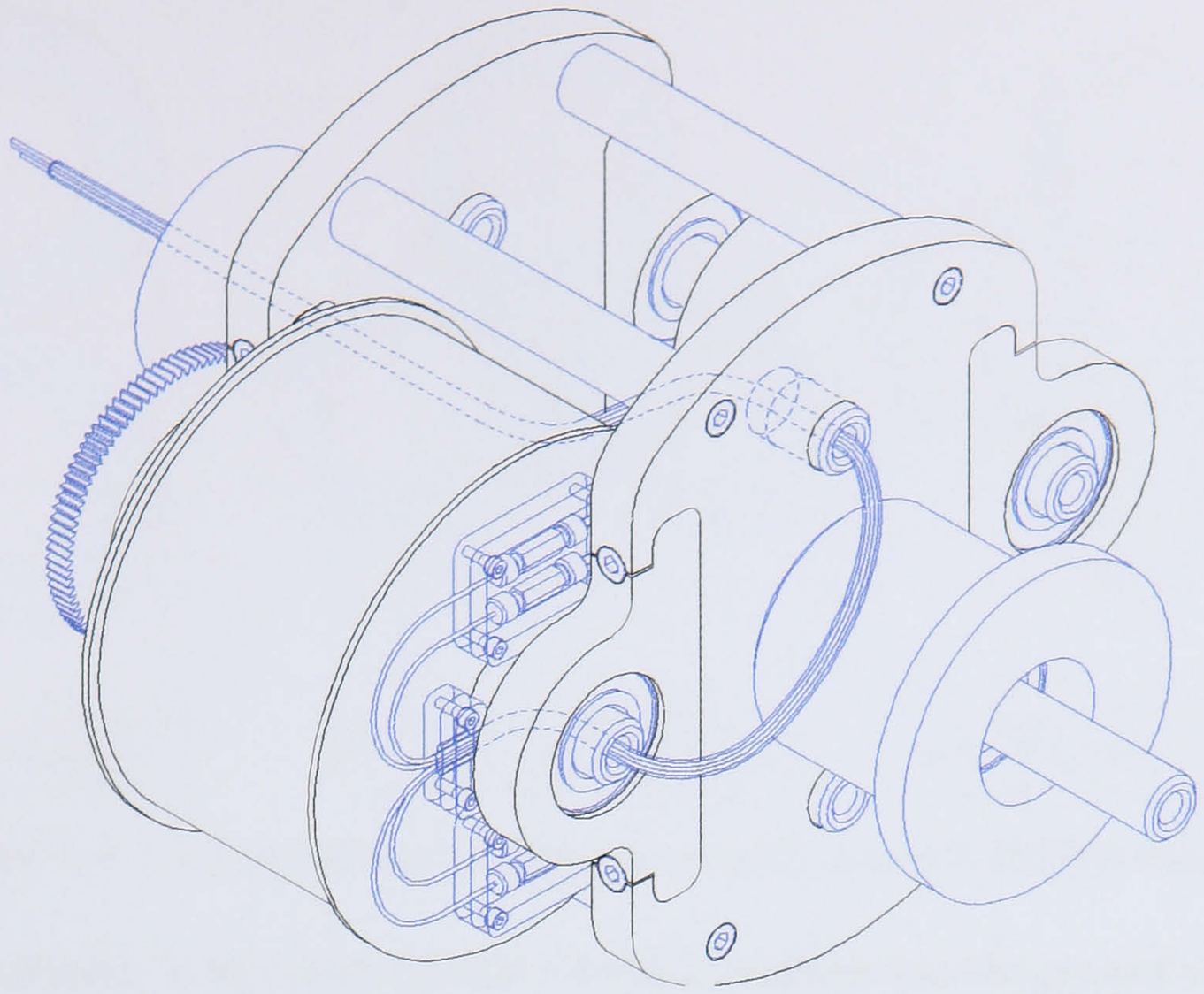

Figure 1.4.1.3.3 shows the routing of a Flying Lead out of the 2 Bobbin machine (only one Bobbin shown)

The main advantage the 2-bobbin machine has over all other configurations is that higher β values can be achieved. Section 1.4.1.2.3 showed that the radial acceleration increases with β value and higher radial accelerations increase stationary phase retention. Hence the 2-bobbin machine can achieve higher stationary phase retentions when compared to other configurations.

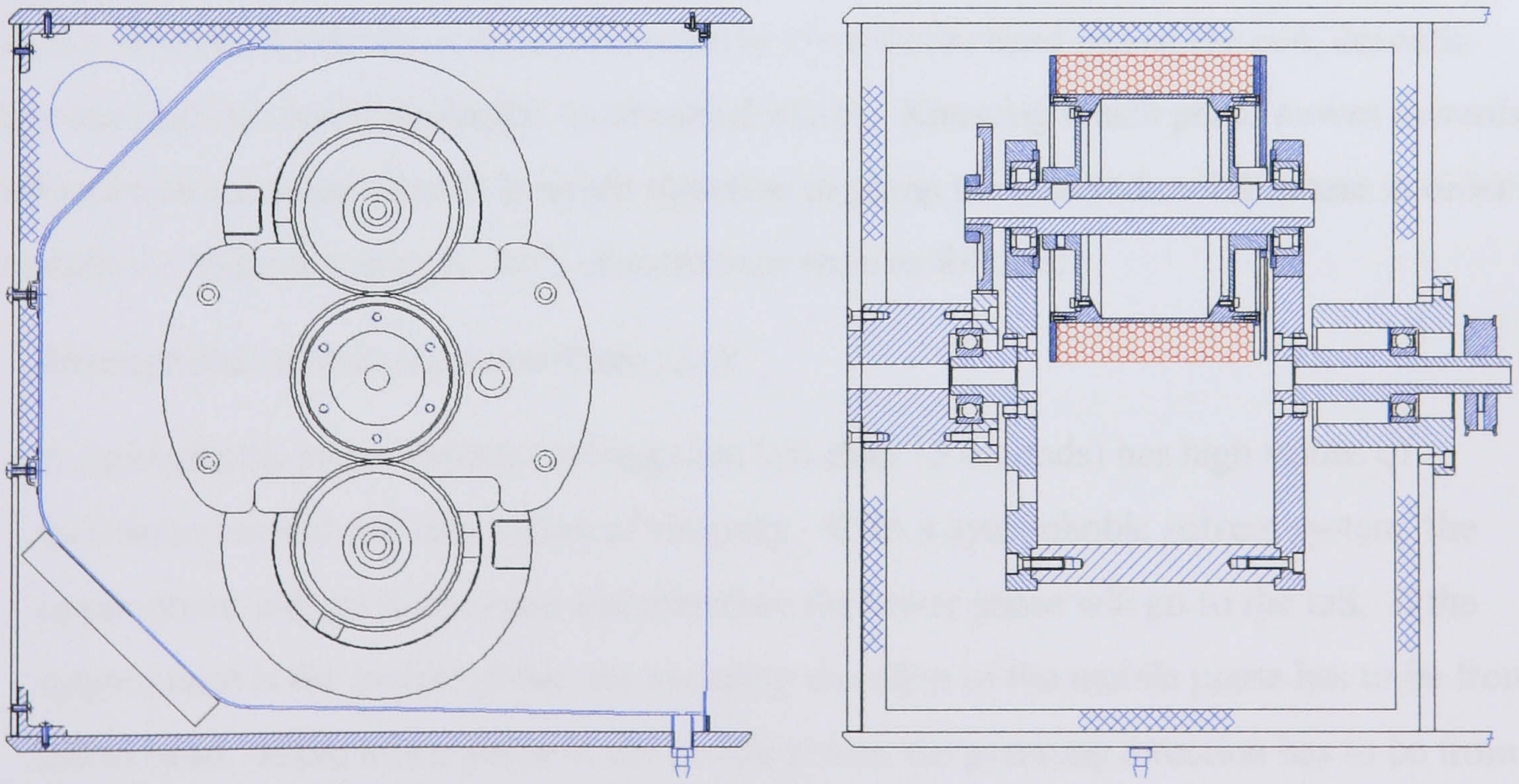

Figure 1.4.1.3.4 shows the 2 Bobbin machine with the drive shaft replaced by two half shafts

For a given rotor radius (R), bobbin axial length and tubing size, the 2 bobbin and 3 bobbin machines have the same capacity if the minimum β value is 0.5 assuming that the maximum β values are used on each machine, see figure 1.4.1.3.5.

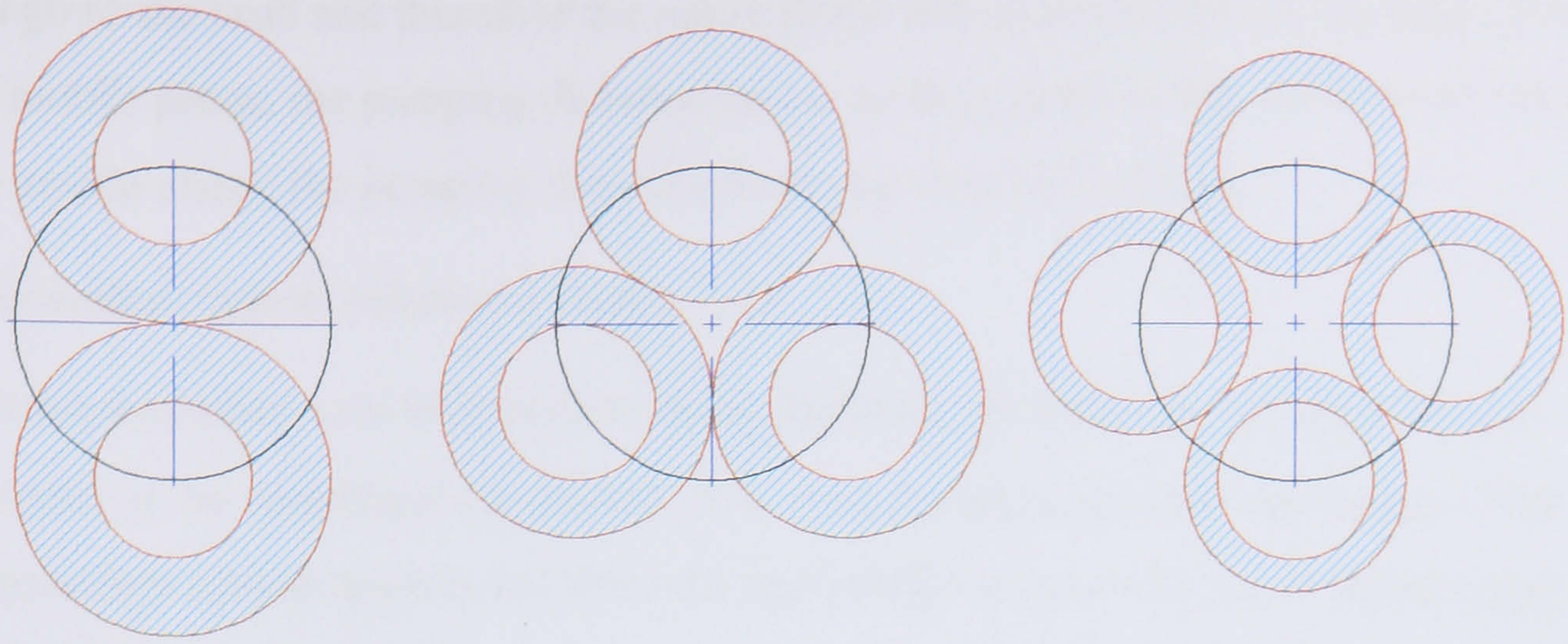

Figure 1.4.1.3.*5 shows the configuration of 2, 3 and 4 Bobbin machines*

If the minimum β value is less than 0.5 the 3-bobbin machine has the greater capacity and if the minimum β value is above 0.5 the 2-bobbin machine has the greater capacity. The capacity of multi-bobbin machines with more that 3 bobbins decreases with increasing number of bobbin regardless of the value of the minimum β value.

1.4.2 Head and Tail Theory and its affect on Retention

1.4.2.1 Ito's Observations

According to Ito [Ito 1984, Ito 1992, Mandava 1988 page 368], the behaviour of a phase system, whether the heavy or light phase moves towards the head end of the coil, depends upon the system's hydrophobicity; its chemical nature. Knowing which phase moves towards the head tells the experimenter in which direction to pump the selected mobile phase in order to retain the stationary phase. Ito's observations were as follows:

- *Hydrophobic system (Hexane-Water, 1:1)*

  A hydrophobic phase system (settling time less than 15 seconds) has high values of interfacial tension and low values of viscosity. With a hydrophobic solvent system, the upper phase will go to the head and therefore the lower phase will go to the tail. If the upper phase is the mobile phase, the pumping direction of the mobile phase has to be from tail to head. If the lower phase is the mobile phase, the pumping direction has to be from head to tail.

- *Hydrophilic system (sec.Butanol-Water, 1:1)*

  A hydrophilic system (settling time greater than 30 seconds) has low values of interfacial tension and high values of viscosity. With a hydrophilic solvent system, the lower phase

will go to the head and therefore the upper phase will go to the tail. If the upper phase is the mobile phase, the pumping direction has to be from head to tail. If the lower phase is the mobile phase, the pumping direction has to be from tail to head.

- *Intermediate system (nButanol-Water, 1:1)*

  In solvent systems with intermediate hydrophobicity, the head and tail preference is sensitive to the centrifugal conditions. For small β-values, the hydrodynamics of the intermediate system approaches that of a hydrophilic system with lower phase going to the head and the upper phase to the tail. For large β-values, the hydrodynamics approaches that of a hydrophobic system with the upper phase going to the head and the lower phase going to the tail.

- On the J-type centrifuge it is not worthwhile coiling below a β value of 0.25 because the centrifugal acceleration vectors point both inwards and outwards from the bobbin above a β value of 0.25 the acceleration vectors point only inwards towards the centre of a bobbin.

Maryutina et al [1998] used the above observations when researching the affect of physico-chemical properties of phase system on the retention of stationary phase; this is discussed in section 1.5.1.5 and expanded upon in chapters 3 and 4.

1.4.2.2 Review of Baalen's, Helden's and Ter Wee's Research

Baalen, Helden [Baalen 1997] and Ter Wee [Wee 1998] were Dutch undergraduate students that conducted research at the Brunel Institute for Bioengineering on the Countercurrent project. These three students were from Fontys University for the Department of Engineering Physics and were studying Applied Physics to honours degree level. Baalen and Helden were final year students and their work conducted at BIB was their final year project. Ter Wee was a second year student who had an industrial placement at BIB and extended the research conducted by Baalen and Helden. All three students studied the variation of stationary phase retention against β value for the following variables: rotational speed, direction of rotation, tube internal diameter, mobile phase flow rate and direction of mobile phase flow. These tests were conducted on three different phases systems. For all three phase systems the stationary phase retention increased with increasing rotational speed and coil tubing internal diameter. The stationary phase retention decreases with increasing mobile phase flow rate. The combination of the other variables determines the stationary phase retention, however the combination of these variables depends upon the solvent system being used and the relevant head and tail theory.

These students also conducted a basic investigation to verify the head and tail theory for the three phase systems. The head and tail testing was conducted at 800r.p.m with tubing of 1.6mm and 3.2mm internal diameter. This investigation tried to verify Ito's head and tail theory [Ito 1984 and Mandava 1988]. However the results of this investigation produced the first evidence that called Ito's head and tail theory into question.

1.4.2.3 Sutherland et al's Observations

After the investigation of Baalen, Helden and Ter Wee, Sutherland [2000A] felt that phase systems should not be characterised by hydrophobicity but by physical properties of the phase system such as: density difference between the upper and lower phases, viscosities and interfacial tension.

It is known that in a simple centrifuge the heaviest phase is driven to the furthest point away from the centre of rotation and the lightest phase is displaced towards the centre. In a spirally wound coil the heavier lower phase will try to move to the radially outer edge of the coil, called the periphery. This action displaces the lighter phase towards the centre of the coil. Hence the unilateral distribution of the phases is easily understood if the Archimedean screw effect is momentarily forgotten. For spiral or multi-layer coils it would be sensible to place the end of the coil to which the Archimedean screw effect was pushing the lower phase at the periphery. This means that the two pumping effects would push the lower phase to the periphery increasing the unilateral distribution. However knowledge of which end of a coil that the lower phase is pushed under the Archimedean screw effect is needed without the interference of the centrifuge effect. The unilateral distribution in helically wound coils is due purely to the Archimedean screw effect because no centrifuge effect is present. Ito [1984] has published results that inferred that the upper phase is unilaterally distributed to the head end and the lower is unilaterally distributed to the tail for β-values greater than 0.375. Sutherland [2000 A] hypothesised that the Archimedean screw effect pumps the upper phase to the head and the lower phase to the tail. Therefore to combine the centrifuge and the Archimedean screw effects in spirally wound coils the head should be at the centre and the tail at the periphery. Orientating the coil in this way will give the greatest unilateral distribution achievable and hence give the greatest retention of stationary phase. A number of phase systems from across the hydrophobicity range were tested and results showed that the best unilateral distribution was indeed achieved when a spiral coil is rotated so that the head is at the centre and the tail at the periphery. The paper concluded that the best retention would be achieved when pumping a mobile phase in the direction that the coil would naturally pump the

mobile phase. For example if the upper phase is the mobile phase, pump from tail periphery to head centre and if the lower phase is the mobile phase, pump from head centre to tail periphery. Ito's results [1984] confirmed this to be the true except for Butanol based systems, which are very viscous systems. Ito has comparable results for 1.6mm and 2.6mm bore tubing for Butanol based systems. The 2.6mm results are more consistent with the hypothesis put forward by Sutherland et al than the 1.6mm results. This suggests that if larger bore tubing is used then Butanol systems will show the same behaviour as other phase systems. Sutherland et al used 3.2mm bore tubing for their investigation with a spiral wound coil. A Butanol based system showed a very similar unilateral distribution to a Heptane water system, which had an upper phase dynamic viscosity 4 times less viscous than the Butanol system upper phase. The ratio of viscosities between the lower phases of the Heptane and Butanol system was 1:1.73. Therefore the same Butanol based system will exhibit the same behaviour as other phase systems if the tubing bore is large enough. This means that for larger bore tubing the viscosities of the phase system become less significant than the density difference. The affect of interfacial tension is difficult to determine since changes in interfacial tension are not independent of changes in density difference.

1.4.2.4 Comparison of Ito's and Sutherland et al's Observations

Ito observed the head and tail behaviour of a wide range of solvents systems on a number of J-type centrifuges in order to predict the direction that a given mobile phase should be pumped to obtain the maximum retention of stationary phase. The β-values of the centrifuges varied from 0.125 to 1.9 and rotation speeds from 200 to 1000rpm. Below a β-value of 0.25 the radial acceleration switches direction from inwards to outwards close to the proximal key node. The hydrodynamics is similar to that of an I-type centrifuge. Above a β-value of 0.25 the radial acceleration always points inwards to the centre of a coil. The hydrodynamic behaviour is as described by Conway [1990]. Ito categorised his observations in terms of the chemical properties of the solvent systems. Sutherland et al's hydrodynamic observations are based upon the physical properties of the phase systems and were made on a single J-type centrifuge. This centrifuge was operated at 800rpm, had an orbital radius (R) of 100mm and a β-value range of 0.38 to 0.85. Thus Sutherland et al's observations are more specific and are only applicable to the hydrodynamic behaviour as described by Conway for high-speed high β-value machines. As described in section 1.4.1.3 the most practical versions of the J-type centrifuge are the two and three bobbin varieties with minimum β-values greater than 0.25 to which the Sutherland observations can be applied.

1.4.2.5 Physical Properties of phase systems

Experience has shown that stationary phase retention changes from one phase system to the next. The retention also changes for a given phase system when switched from reverse phase to normal phase mode and visa versa. A number of papers have been published describing how the physical properties affect retention. The physical properties that effect retention for a given phase system are: the density of each phase, the density difference between the phases, the viscosity of each phase and the interfacial tension between the phases. The main contributors to research into the physical properties of the phase systems are a group of scientists from the Vernadsky Institute of Geochemistry and Analytical Chemistry in Moscow. Their published research work can be read in references [Maryutina 1998, Fedotov 1996, Fedotov 1998, Fedotov 2000]. Their research has focused on J-type centrifuges rotating at speeds between 350 and 700rpm with orbit radii between 63.5 and 85mm and β values between 0.37 and 0.53. The amplitude of tangential accelerations has been varied between 12 and 35 times the acceleration due to gravity (g). The radial acceleration has varied between 8g and 39g at the proximal key node and between 31g and 108g at the distal key node. These acceleration levels are at most half those used by other CCC users [Sutherland 1998, Conway 1990, Ito1998, Du 1999]. The interfacial tension is regarded as the most significant physical property of a phase system for retention, followed by density difference and viscosity difference between the phases. In [Maryutina 1998], mineral salts and surfactants were selectively added to a phase system to determine the affect of varying one physical property without changing the other properties; this is a very useful experimental technique. This allows the experimenter to change only one of the physical properties and hence determine the influence of the property on the retention of the stationary phase. The results from the Vernadsky Institute appear not to have been obtained under constant temperature conditions as none of the papers mentions temperature control. The Vernadsky research results were obtained at flow rates between 1.0 and 1.1ml/min. At such low flow rates the hydrodynamics of CCC are not being challenged.

1.4.2.6 Retention Characteristics

Understanding how the stationary phase retention changes with flow is fundamental to predicting the performance of a CCC separation given that elution times and resolution vary with retention and hence with mobile phase flow rate. In 1991 Olivier Bousquet published a paper titled "Efficiency and Resolution in Countercurrent Chromatography" [Bousquet 1991]. Bousquet et al studied how resolution and efficiency changed with the mobile phase flow rate.

Figure 1 of this paper shows the volume of mobile phase increasing with the mobile phase flow rate see below.

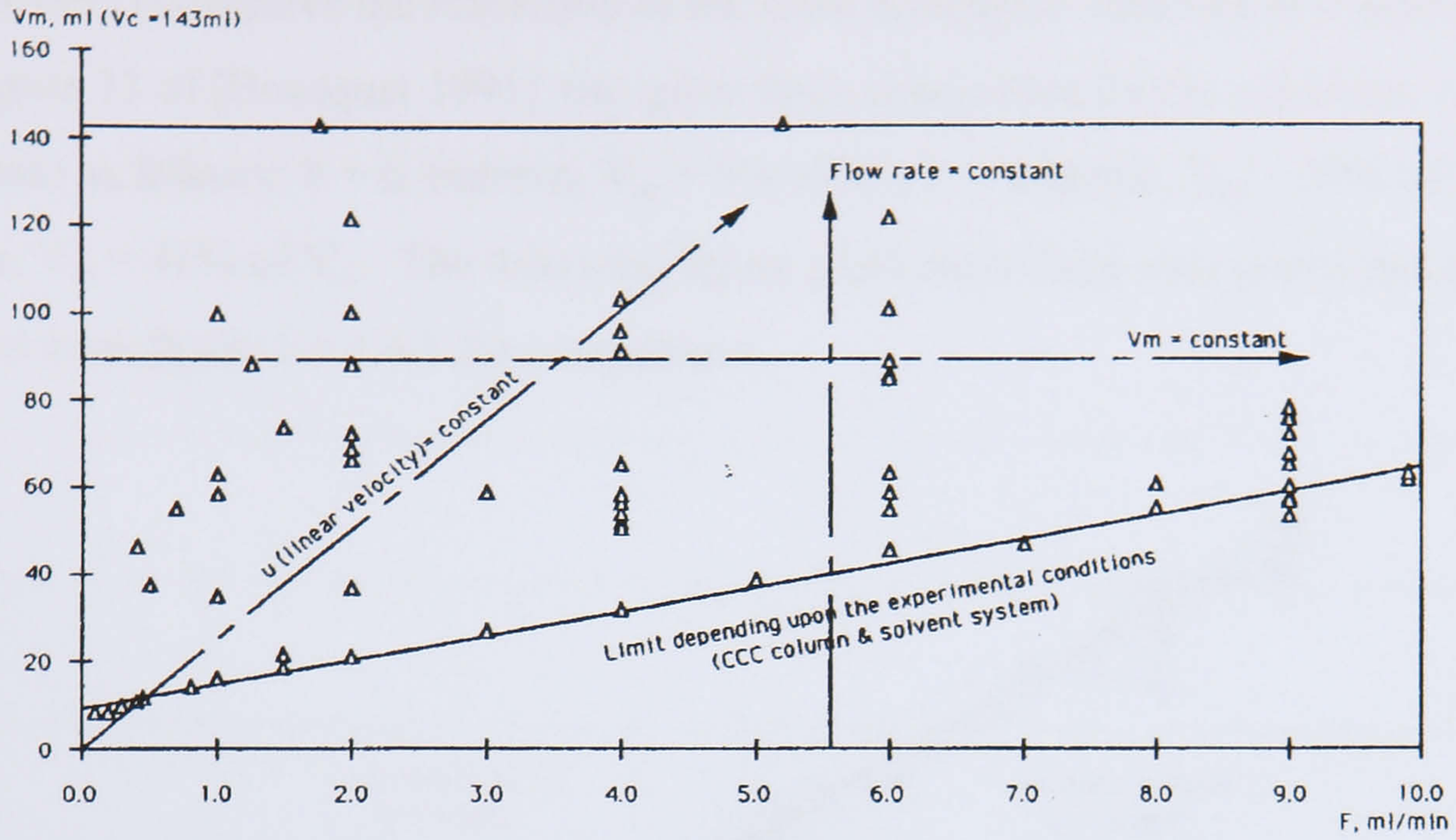

Figure 1 Map of the experimental points, with the various ways to vary the parameters, and the experimental limit $V_m^{min} = CF + D$

Figure 1.4.2.6.1 is figure 1 of [Bousquet 1991]

The above figure was produced using a PC Inc. J-type centrifuge with a 143ml coil made from 1.6mm bore Teflon tubing rotated at 710rpm. A Waters model 501 pump pumped the mobile phase. The phase system used was a hexane and 1% water in methanol as used by Armstrong et al [Armstrong 1988], the upper hexane rich phase was the stationary phase and the lower methanol rich phase was the mobile phase which was pumped from head to tail ie the coil was operated in reverse phase mode. The temperature of operation was approximately 25°C but no tolerance is given. The mobile phase was heated to 35°C before entering the ISCO model UA5 UV detector by a column temperature control unit supplied by Waters to achieve noiseless baselines. A 0.5ml injection loop was used to introduction the sample. The four-component sample was made up from diethyl phthalate, dipropyl phthalate, ethyl phenylacetate and butyl phenylacetate but the concentrations were not given. Armstrong et al reported that the dynamic viscosity of methanol is 0.54mNs/m^2 and hexane is 0.29mNs/m^2 at 25°C, the density of methanol is 791kg/m^3 and hexane is 661kg/m^3 at 20°C. However the actual physical properties of this phase system were not reported given that water was added changing the interfacial tension and the mutual solubilities. Bousquet et al fitted a first order linear equation to the minimum volume of mobile phase in the coil from figure 1.4.2.6.1 as follows:

$$V_m^{\min} = 5.51(\pm 0.11)F + 9.58(\pm 0.35) \qquad (1.4.2.6.1)$$

The correlation coefficient R^2 is given as 0.994 for equation 1.4.2.6.1 for 16 data points. However there appears to be 21 data points close to the fitted line in this figure. Figure 13 of [Bousquet 1991] compares the resolution of the same separation achieved at different flow rates. Figure 13 of [Bousquet 1991] also gives three data points for the minimum volume of mobile phase as follows: F = 0.4ml/min, V_m = 9% of V_C; F = 4ml/min, V_m = 23% of V_C and F = 9ml/min, V_m = 41% of V_C. The following figure plots these three data points and the 21 data points from figure 1.4.2.6.1 for comparison.

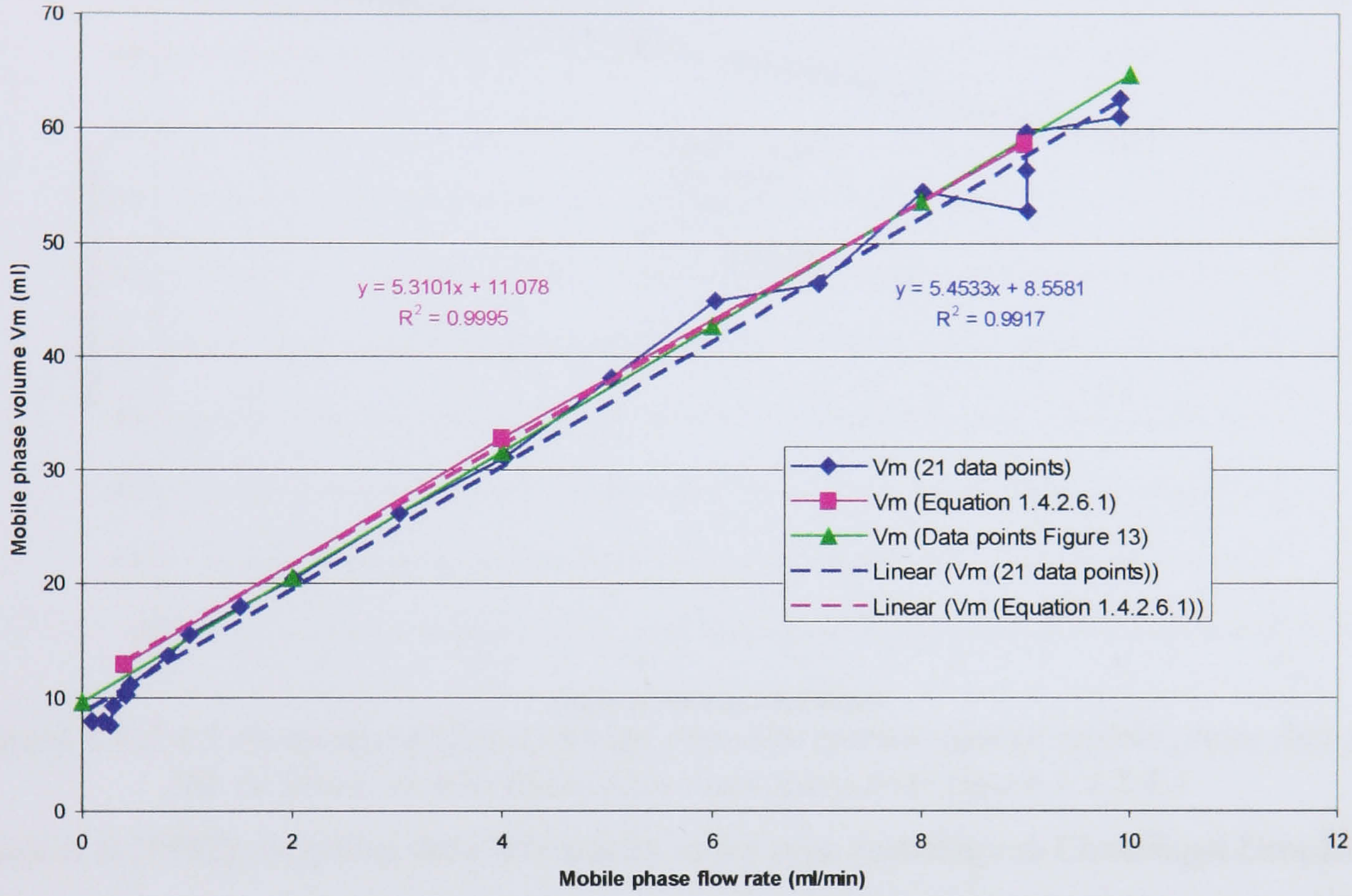

Figure 1.4.2.6.2 comparison of the 21 data points from figure 1.4.2.6.1, the 3 data points from Figure 13 of [Bousquet 1991] and equation 1.4.2.6.1

Figure 1.4.2.6.2 shows that there is very little difference between these two sets of results for the minimum volume of mobile phase. The difference can be attributed to experimental error. The fitted equation for the 21 data points is as follows:

$$V_m^{\min} = 5.4533F + 8.5581 \qquad (1.4.2.6.2)$$

The correlation coefficient R^2 is 0.9917 for equation 1.4.2.6.2 for 21 data points that is close to the correlation coefficient of 0.994 for equation 1.4.2.6.1. Equations 1.4.2.6.1 and 1.4.2.6.2 are very similar; the gradient term of 1.4.2.6.2 is within the tolerance of the gradient term of 1.4.2.6.1. The vertical axis intercept values differ by 1.02 ± 0.35 ml which is less than 1% of the coil volume V_C. Therefore the 21 data points taken from figure 1.4.2.6.1 must be accurate and can be used for plotting stationary phase retention characteristics. Figure 1.4.2.6.3 below shows the stationary phase retention plotted against the mobile phase flow rate for the 14 lowest flow rates of mobile phase taken from figure 1 of reference [Bousquet

1991]. The 7 highest flow rates of mobile phase have not been used as these are greater than 6ml/min which experience has shown to be high flow rates for 1.6mm bore tubing in a J-type centrifuge. The stationary phase retention was calculated by using equation 1.4.2.6.3:

$$S_f = \frac{V_S}{V_C} = \frac{V_C - V_M}{V_C} \qquad (1.4.2.6.3)$$

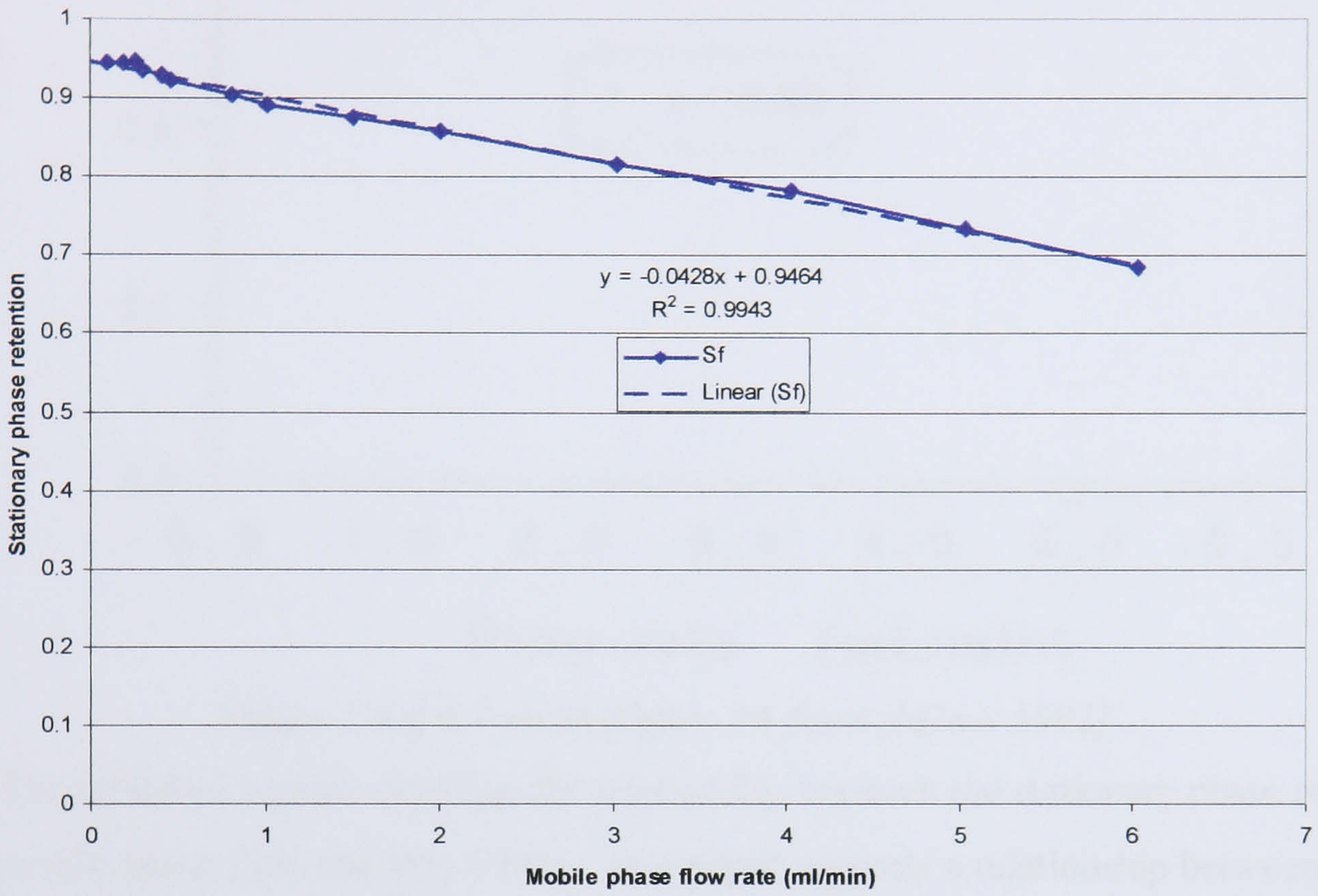

Figure 1.4.2.6.3 shows the stationary phase retention plotted against mobile phase flow for the 14 lowest mobile phase flow rtaes taken from figure 1.4.2.6.1

Menet et al [1992] compared the performance of a J-type centrifuge to Centrifugal Droplet CCC machine. The phase system used was n-heptane/acetic acid/methanol (1:1:1 v/v); the stationary phase was the lower phase, acetic acid/methanol phase saturated in n-heptane. Hence Menet et al were operating in normal phase mode. Again a PC Inc. J-type centrifuge was used with a 300ml coil wound from 1.6mm bore PTFE tubing giving a β-value range of 0.57 to 0.85. The centrifuge was rotated at 750rpm. A Gilson 303 HPLC pump was used to pump the mainly n-heptane mobile phase. A 0.5ml sample loop was also used to inject a sample of stearic acid, myristic acid and palmitic acid. The sample was made up in the mobile phase with each component having a concentration of 1g/litre. Figure 2A from this paper shows mobile phase flow rate plotted against stationary phase retention and a straight-line characteristic for the J-type centrifuge, the correlation coefficient is R = 0.99. Figure 2A is reproduced below:

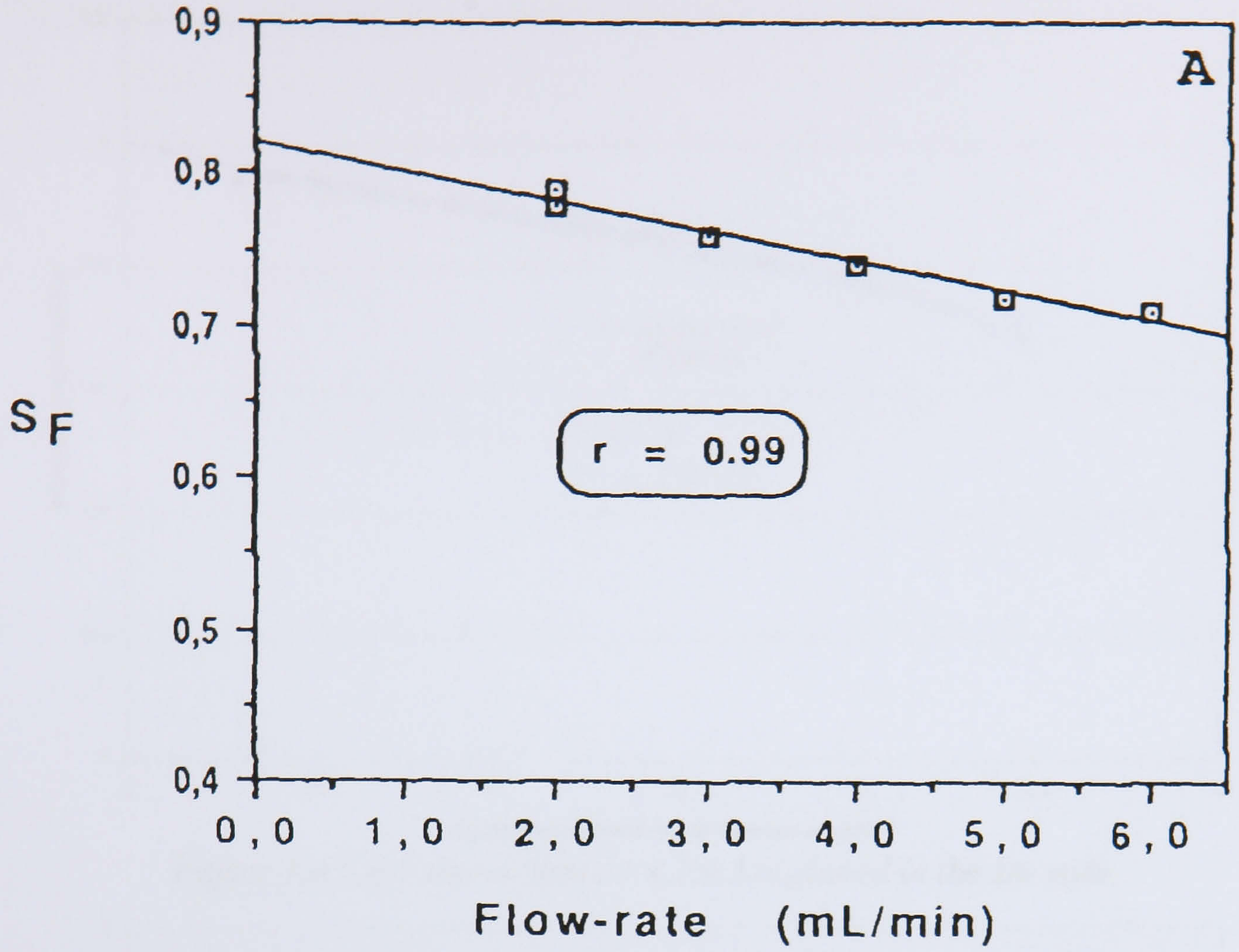

Figure 1.4.2.6.4 shows figure 2A from [Menet 1992]

In 1999 Du published a paper detailing the relationship between the stationary phase retention and the mobile phase flow rate [Du 1999]. This paper suggests a relationship between the percentage stationary phase retention (Sf) and the square root of the mobile phase flow rate (F). These retention plots have become known as Du plots see figure 1.5.1.6.5 for a typical example. Twelve phase systems had the Du style retention characteristics plotted for reverse phase mode only, the correlation coefficients varied between R = 0.99293 and 0.99976. Also the characteristics pass through the vertical axis close to the 100% stationary phase retention when the mobile phase flow rate will be zero. Theoretically the coil is full of stationary phase if no mobile phase is flowing through it. If Bousquet's and Menet's figures 1.4.2.6.3 and 1.4.2.6.4 are replotted in the Du style the figures below are produced:

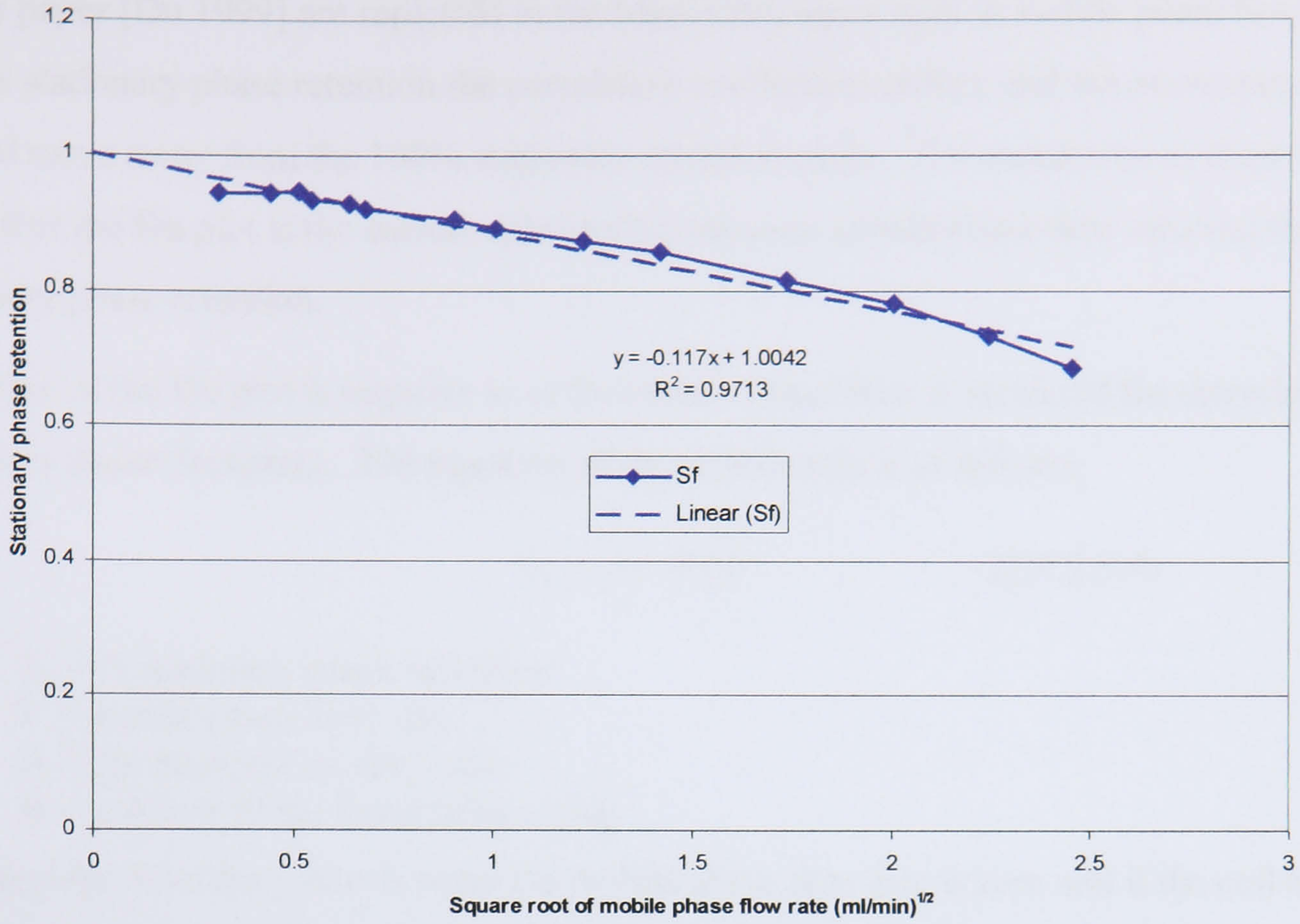

Figure 1.4.2.6.5 shows figure 1.4.2.6.3 replotted in the Du style

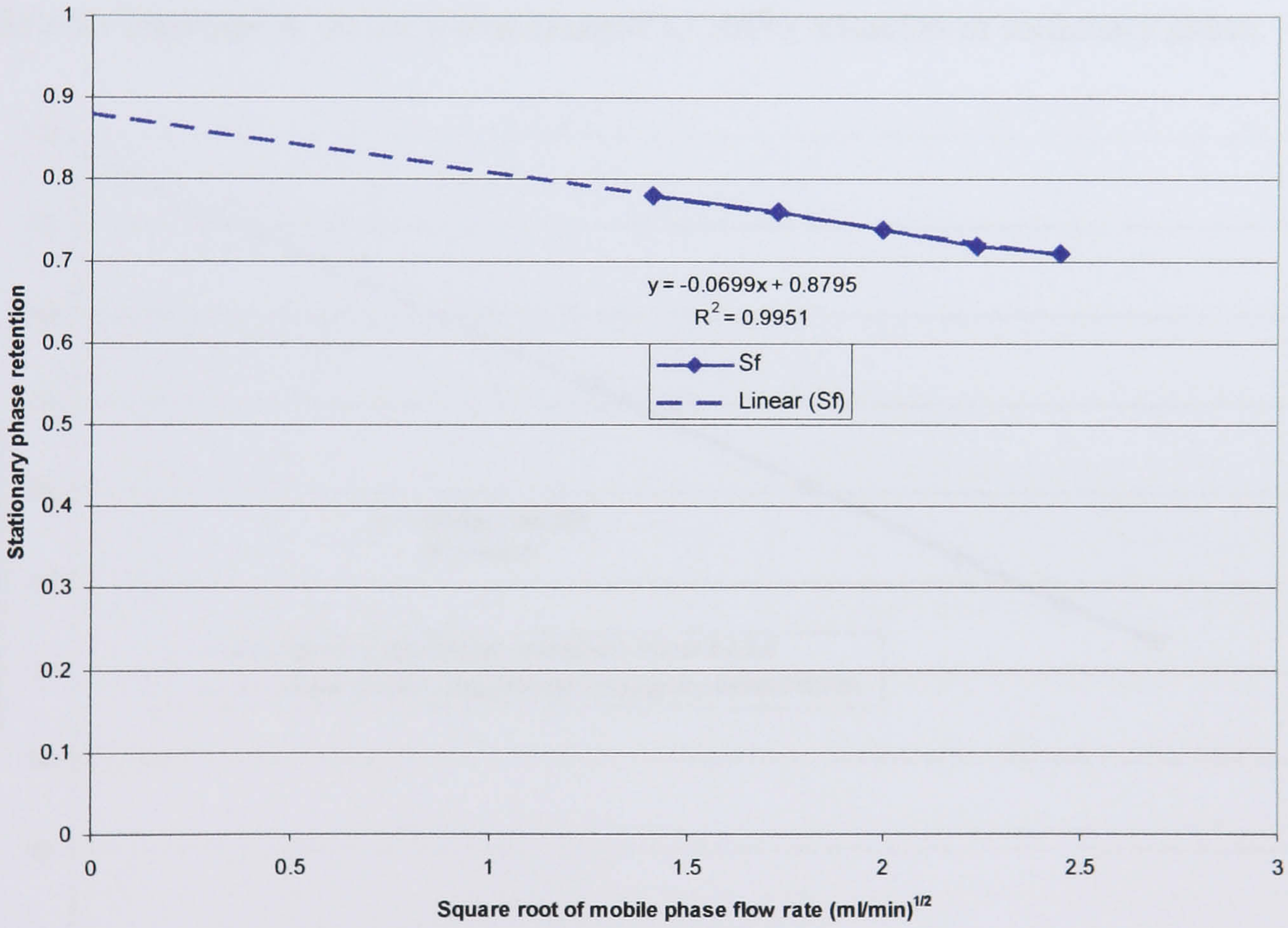

Figure 1.4.2.6.6 shows figure 2A from [Menet 1992] replotted in the Du style

Although the correlation coefficient from figure 1.4.2.6.5 is $R^2 = 0.9713$ has reduced from figure 1.4.2.6.3 of 0.9943 and the intercept on the vertical axis has moved closer to the point where the coil is full of stationary phase when the mobile phase flow rate is zero. The correlation coefficient from figure 1.4.2.6.6 is $R = 0.998$ an improvement from figure 1.4.2.6.4 of 0.990 and again the intercept on the vertical axis has moved closer to the $S_f = 1$ point where the coil is full of stationary phase when the mobile phase flow rate is zero. If the results from

the Du paper [Du 1999] are replotted in the Menet/Bousquet style ie mobile phase flow rate against stationary phase retention the correlation coefficients reduce and the intercepts on the vertical move away from the 100% stationary retention mark. The conclusion to draw from this is that the Du plot is the correct relationship between mobile phase flow rate and the stationary phase retention.

The slope of the Du plot is negative ie as the mobile phase flow is increased the retention of stationary phase decreases. The equation of the relationship is as follows:

$$S_f = A - B\sqrt{F} \qquad (1.4.2.6.4)$$

where S_f = % stationary phase retention
F = mobile phase flow rate
A = the intercept on the y axis
B = gradient of the linear relationship

The intercept A on the y-axis is when the mobile phase flow rate is zero and if the coil has just been primed with stationary phase then the stationary phase retention should be 100%.

Therefore the intercept A on the y-axis is equal to 100% retention of stationary phase.

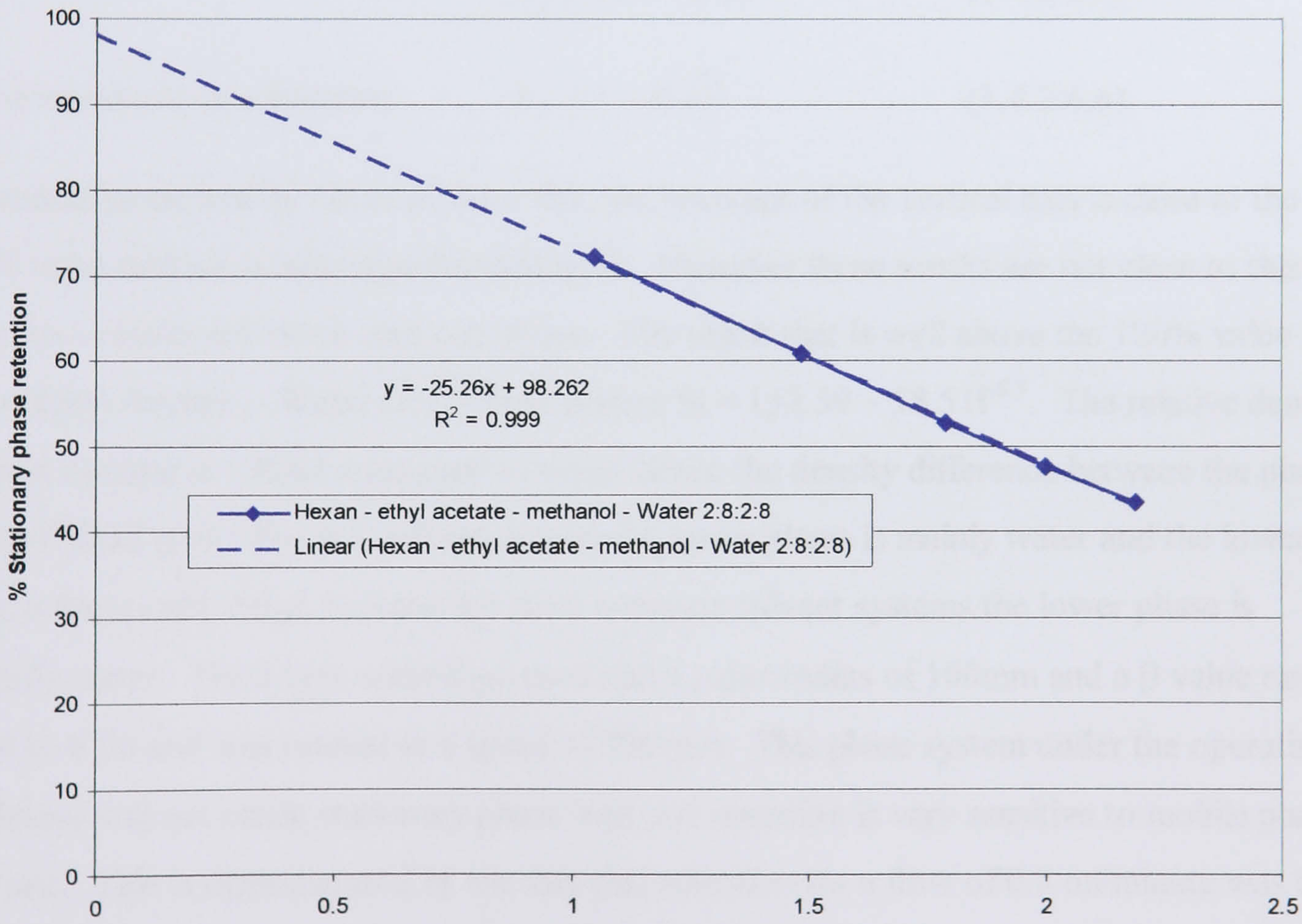

Figure 1.4.2.6.7 showing a typical retention characteristic or Du plot

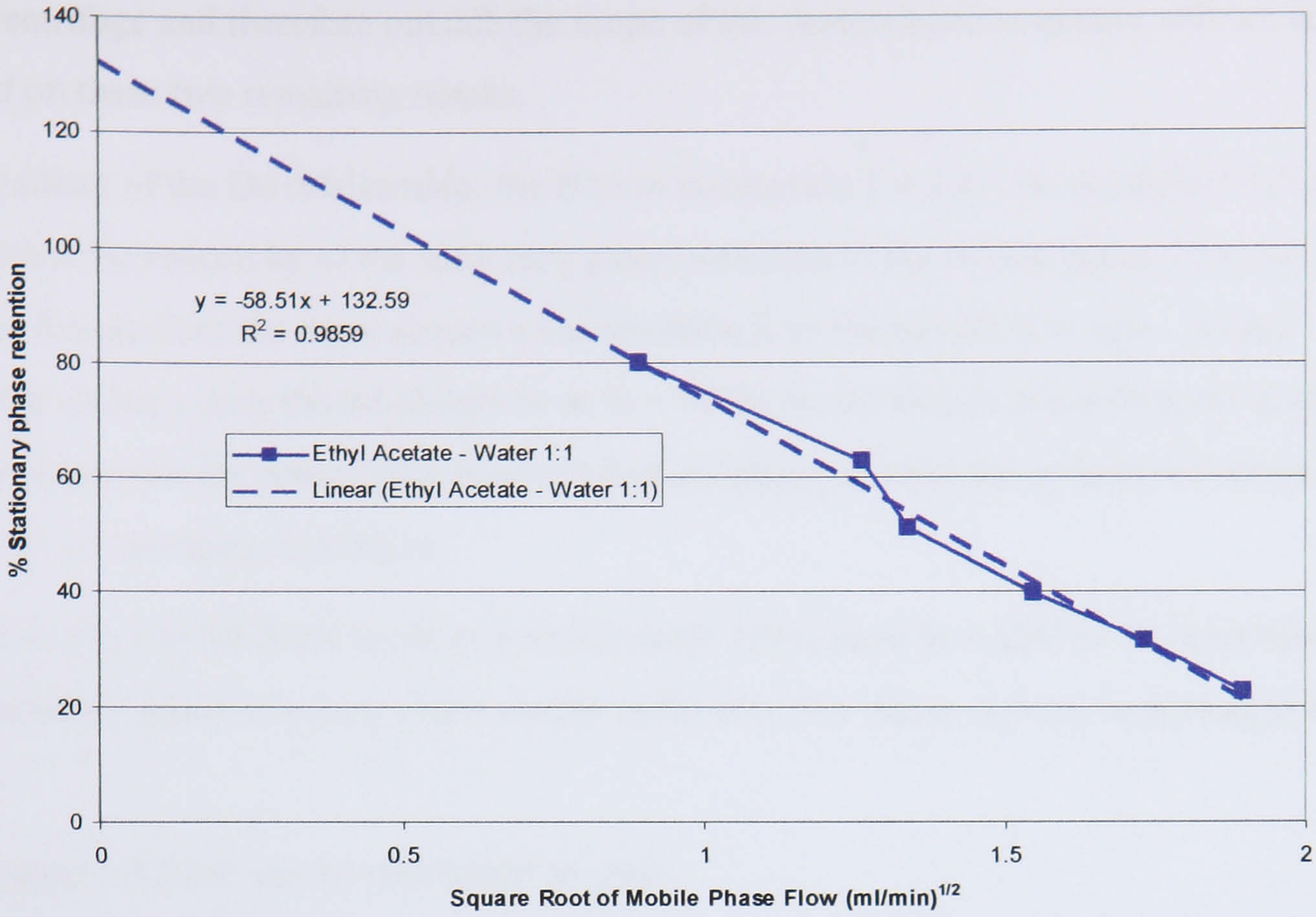

Figure 1.4.2.6.8 showing a the Du plot for the Ethyl acetate – water 1:1 phase system

Therefore equation 1.4.2.6.4 can be rewritten as if S_f is expressed as a percentage:

$$S_f = 100 - B\sqrt{F} \qquad (1.4.2.6.5)$$

If S_f is expressed as a fraction: $$S_f = 1 - B\sqrt{F} \qquad (1.4.2.6.6)$$

The results presented by Du et al show that the intercept of the vertical axis is close to the 100% value and are within experimental error. However three results are not close to this value, two results are below and one above. The result that is well above the 100% value is for an Ethyl Acetate – Water (1:1) phase system $S_f = 132.59 - 58.51F^{0.5}$. The relative density of Ethyl Acetate is 1.0282 compared to water hence the density difference between the phases is only 0.0282 g/ml. For this solvent system the upper phase is mainly water and the lower phase is the mostly Ethyl Acetate; for most common solvent systems the lower phase is normally water. The J-type centrifuge used had a rotor radius of 100mm and a β value range of 0.4 to 0.78 and was rotated at a speed of 750rpm. This phase system under the operating conditions will not retain stationary phase well and retention is very sensitive to mobile phase flow rate. This is demonstrated by the fact that retention for a flow of 0.8 ml/minute was 80% and only 22.6% at 3.6 ml/minute. There is also a discontinuity between the second and third readings see figure 1.4.2.6.8, which suggests gross experimental error for the low flow readings. The other two results with gross errors are for a different type of CCC instrument. The description of this apparatus in the paper is not clear and no diagram is given, it is not a J-

type centrifuge and therefore outside the scope of this research and comment will not be passed on these two remaining results.

The gradient of the Du relationship, the B term in equation 1.4.2.6.5 or equation 1.4.2.6.6, represents the sensitivity of the stationary phase retention to the mobile phase flow rate. The steeper the gradient the more sensitive the retention is to the mobile flow rate. As the intercept on the y-axis should always be at $S_f = 100\%$ for no mobile phase flow the gradient term is important for determining how a stationary phase of a solvent system will retain for a given set of operating conditions.

Menet et al's normal phase mode research [Menet 1992] must be added to, to determine if the Du stationary phase retention characteristic holds for other phase systems in normal phase mode.

If equation 1.4.2.6.6 can be rearranged to give:

$$F = \frac{\left(1 - S_f\right)^2}{B^2} \qquad (1.4.2.6.7)$$

Substituting equation 1.4.2.6.7 into equation 1.3.3.2.3 gives for the peak elution time:

$$t_{P=n} = \frac{V_C B^2}{\left(1 - S_f\right)^2}\left[S_f\left(P_n - 1\right) + 1\right] \qquad (1.4.2.6.8)$$

Substituting equation 1.4.2.6.7 into equation 1.3.3.2.6 gives for the resolution:

$$R_S = \frac{2V_C S_f B^2 \left(P_B - P_A\right)}{\left(1 - S_f\right)^2 \left(W_A + W_B\right)} \qquad (1.4.2.6.9)$$

Sutherland [2000 B] took the retention relationship, equation 1.4.2.6.6, from Du et al's paper [Du 1999] and derived a linear relationship between the mobile phase flow rate (F) and the square of the mean flow velocity (u) of the mobile phase:

$$u^2 = CF \qquad (1.4.2.6.10)$$

Sutherland hypothesised that the u^2 term is related to the Bernoulli's kinetic energy term ($\rho u^2/2$) for the mobile phase. This term represents the kinetic energy per unit volume. The higher the value of this term for a given flow rate the better the retention of the stationary phase. Hence this term could be used to compare the retention of different machines that used the same bore of tubing. Sutherland plotted this kinetic energy term against the flow of the mobile phase flow rate for all of Du et al's 12 phase systems. All of these relationships have correlation coefficients (R^2) greater than 0.97 and have intercepts on the vertical axis close to

the origin. Sutherland then hypothesised that this relation between the kinetic energy of the mobile phase and the mobile phase can be developed further to understand the hydrodynamics of a J-type centrifuge. He also stated that there were some phase systems that did not follow the relationship represented by equation 1.4.2.6.10, however he did not mention if these phase systems had been tested in normal or reverse phase. Sutherland recommended that standard phase systems could be used to determine the gradient of the Du retention characteristic for each design of J-type centrifuge. The gradient term would indicate the performance of each design.

Berthod and Billardello [2000] independently of Sutherland have suggested using a heptane-methanol-water phase system in normal phase mode with a standard sample to measure the performance of five CCC machines. Four of these machines were J-type centrifuges and the fifth was a droplet CCC centrifuge, the performance of the fifth machine will not be discussed as it outside of the scope of this document.

Table 1
Technical characteristics of the CCC machines evaluated

Apparatus	Volume (ml)	Spool				Tubing		
		Number	Average radius (cm)	Rotor radius (cm)	β Ratio	Diameter (mm)	Length (m)	Number of turns
SFCC 2000	156	3 (multilayer)	3.4	6.0	0.56	1.65	73	400
Kromaton 2	94	2 (multilayer)	10	15	0.67	2.6	15.5	28
Prototype 1	29	1 (spiral)	11.9	15.4	0.77	2.6	5.1	7.5
Prototype 2	25.5	1 (spiral)	10.3	15.4	0.67	1.65	12	18.5

Table 1.4.2.6.1 below reproduces the details of the four J-type centrifuges from table 1 of [Berthod 2000].

The phase system and sample components were selected because these items are commonly used to measure and compare the performance of HPLC columns. Mixing the methanol and water in a 90:10 volume ratio and then adding the heptane made up the phase system. The upper phase is 99.9% heptane (v/v) and the lower phase is heptane-methanol-water (5.1:85.4:9.5, v/v) at 20°C. The sample is made from Toluene and hexylbenzene, however concentrations were not given. The sample was injected into the mobile phase flow from a 20µl (0.02ml) sample loop. A Shimadzu LC10-AS pump was used to pump the mobile phase. These pumps are known for pulse free constant flow delivery unlike the pulsitile flow produced by some other HPLC pumps.

Berthod and Billardello [2000] took equation 1.4.2.6.6 and determined the "flush away" flow rate when no stationary phase is retained ie when S_f equals zero in equation 1.4.2.6.7:

$$F_{Sf=0} = \frac{1}{B^2} \qquad (1.4.2.6.11)$$

The larger the flow rate determined by the above equation the greater the ability of the centrifuge to retain stationary phase. This flow rate value acts as an easily understood measure of the retention ability of a CCC machine. The assumption underlining this method is that the nature of the mobile phase flow does not change at the higher flow rates determined by this equation. If the nature of the flow changes from say laminar to turbulent the stationary phase may be washed away before this flow rate is reached.

Berthod and Billardello [2000] also found that the mean linear velocity of the mobile phase varied with the square root of the rotational speed of a centrifuge for constant flow rates see equation 1.4.2.6.12:

$$u = C\sqrt{\omega} + D \qquad (1.4.2.6.12)$$

When the C and D parameters are known by performing a limited number of experiments it is possible to use this relationship to determine the minimum rotational speed above which the stationary phase will retain for a given mobile phase flow rate. The minimum flow velocity u_{mini} is determined by assuming that the mobile phase completely occupies the cross-sectional area of the tubing for the chosen flow rate. Once u_{mini} is known equation 1.4.2.6.12 can be used to determine the rotational speed (ω_{mini}) for the condition when the mobile phase completely occupies the cross-sectional area of the tubing. If the rotational speed is increased stationary phase will then be retained. Table 1.4.2.6.2 shows table 4 after Berthod [2000]. This table shows the C and D parameters for equation 1.4.2.6.12 plus the corresponding u_{mini} and ω_{mini} values. Comparison of ω_{mini} values from table 1.4.2.6.2 with those from table 1.4.2.6.4 shows good comparison of the SFCC 2000 and the Prototype 2 machines, both using 1.65mm bore tubing, however the comparison is not good for the other two machines that use 2.6mm bore tubing see table 1.4.2.6.1. Examination of the regression coefficients (r^2) in table 1.4.2.6.2 shows these coefficients are higher for the 1.65mm bore machines than the 2.6mm bore machines. In private communications between Dr Alain Berthod and the author, Berthod has stated that all the derived relationships were developed using the SFCC 2000 machine and then applied to the other machines. The relationships can be applied to the Prototype 2 machine that also uses 1.65mm bore tubing, however the relationships become less accurate when applied to the machines that use 2.6mm bore tubing, the conclusion to draw from this is that bore affects the retention of stationary phase.

Table 4
Regression parameters of the $u = C\omega^{1/2} + D$ lines

Apparatus	Flow-rate (ml/min)	C	D	r^2	Relationship of C and D with F [a]	u_{mini} for Sf=0 [b] (cm/s)	ω_{mini} for Sf=0 [c] (rpm)
SFCC 2000	1	0.571	−9.1	0.999	$C = 0.724F^{1/2} - 0.16$	0.78	300
	2	0.850	−14.4	0.999	$r^2 = 0.999$	1.56	340
	3	1.10	−19.4	0.999	$D = -14F^{1/2} + 5.1$	2.34	390
	4	1.29	−23.0	0.999	$r^2 = 0.998$	3.12	410
Kromaton 2	1	0.059	3.22	0.656	$C = 0.714F^{1/2} - 0.69$	0.78	–
	2	0.269	2.58	0.964	$r^2 = 0.979$	1.56	–
	3	0.516	0.841	0.999	$D = -4.6F^{1/2} + 8.35$	2.34	8
	4	0.778	−1.44	0.999	$r^2 = 0.894$	3.12	34
Prototype 1	1	0.089	0.019	0.996	$C = 0.238F^{1/2} - 0.15$	0.314	11
	2	0.175	−0.510	0.997	$r^2 = 0.996$	0.63	42
	3	0.254	−1.09	0.989	$D = -1.7F^{1/2} + 1.8$	0.94	64
	4	0.326	−1.68	0.982	$r^2 = 0.984$	1.26	81
Prototype 2	1	0.436	−4.57	0.999	$C = 0.733F^{1/2} - 0.30$	0.78	150
	2	0.731	−8.36	0.999	$r^2 = 0.999$	1.56	184
	3	0.966	−11.4	0.999	$D = -9.5F^{1/2} + 5.0$	2.34	202
	4	1.17	−14.1	0.998	$r^2 = 0.999$	3.12	217

[a] In the form: $C = EF^{1/2} + G$ and $D = HF^{1/2} + I$, the constants E, G, H and I are used in Eqs. (10) and (11).
[b] See text and Fig. 1.
[c] ω value for which Eq. (8) gives u_{mini}, compare with Table 3 corresponding value.

Table 1.4.2.6.2 shows table 4 of [Berthod 2000]

Berthod [2000] also uses the SFCC 2000 machine to determine an equation for the retention of stationary phase see below.

$$S_f = 1 - \frac{4\sqrt{F}}{\pi d^2 \left(E\sqrt{\omega} + H + G\sqrt{\frac{\omega}{F}} + \frac{I}{\sqrt{F}} \right)} \qquad (1.4.2.6.13)$$

F represents the mobile phase flow rate and d is the bore diameter of the tubing. The variable in this equation is the rotational speed (ω) of the centrifuge. The parameters E, H, G and I were obtained from a number of experiments for each machine see table 1.4.2.6.2. Equation 1.4.2.6.2 could then be used to predict the retention at different rotational speeds.

Apparatus	Rotor speed (ω, rpm)	A	B	r^2
SFCC 2000	400	1.40	0.72	0.9977
	500	1.11	0.34	0.9997
	600	1.04	0.20	1
	700	1.02	0.15	1
	800	1.01	0.12	1
Kromaton 2	300	0.96	0.030	0.9896
	400	0.94	0.016	0.9026
	500	0.94	0.007	0.4964
Prototype 1	300	0.92	0.117	0.9992
	400	0.92	0.087	0.9974
	500	0.92	0.069	0.9948
Prototype 2	300	0.98	0.24	1
	400	0.96	0.15	1
	500	0.96	0.11	0.9999

Table 1.4.2.6.3 shows the retention data for each machine predicted by equation 1.4.2.6.13

Table 3
Regression parameters of the $Sf = A - BF^{1/2}$ lines

Apparatus	Rotor speed (ω, rpm)	A	B	r^2	$F_{Sf=0}$[a] (ml)	ω_{mini} for $F_{Sf=0}$[c] (rpm)
SFCC 2000	400	1.22	0.56	0.990	4.8	430±20
	500	1.11	0.32	0.991	12	
	600	1.04	0.20	0.993	27	
	700	1.02	0.15	0.993	46	
	800	1.01	0.12	0.994	71	
Kromaton 2	300	0.90	0.080	0.983	126	150±50
	400	0.85	0.035	0.991	590	
	500	0.86	0.028	0.991	940	
Prototype 1	300	0.93	0.082	0.862	130	220±60
	400	0.94	0.070	0.956	180	
	500	0.93	0.048	0.941	370	
Prototype 2	300	0.99	0.25	0.998	16	220±60
	400	0.95	0.14	0.991	46	
	500	0.96	0.11	0.990	76	

Table 1.4.2.6.4 reproduces the retention equations of the four J-type centrifuges at different rotational speeds from table 3 of [Berthod 2000].

The predicted retentions compared well with measured retentions for the, compare results from tables 1.4.2.6.3 and 1.4.2.6.4, SFCC 2000 and Prototype 2 machines which both use 1.65mm bore tubing compare tables 1.4.2.6.3 and 1.4.2.6.4. However the comparisons between predicted and measured retentions for the Kromaton 2 and Prototype 1 machines are not very good, these machines both use 2.6mm bore tubing. Again in private communications between Dr Alain Berthod and the author [Berthod 2001], Berthod has stated that this is in fact the case and that more recent work with other phase systems is showing the weaknesses in the equation. In fact examination of the equation shows that the gradient term:

$$B = \frac{4}{\pi d^2 \left(E\sqrt{\omega} + H + G\sqrt{\frac{\omega}{F}} + \frac{I}{\sqrt{F}} \right)} \qquad (1.4.2.6.14)$$

varies with the square root of flow and hence will not be constant as shown by Du [1999]. This also undermines the assumption underpinning equation 1.4.2.6.11. The predicted retention characteristic for the Kromaton 2 machine confirms that the gradient is not constant using equation 1.4.2.6.14 see figure 1.4.2.6.9.

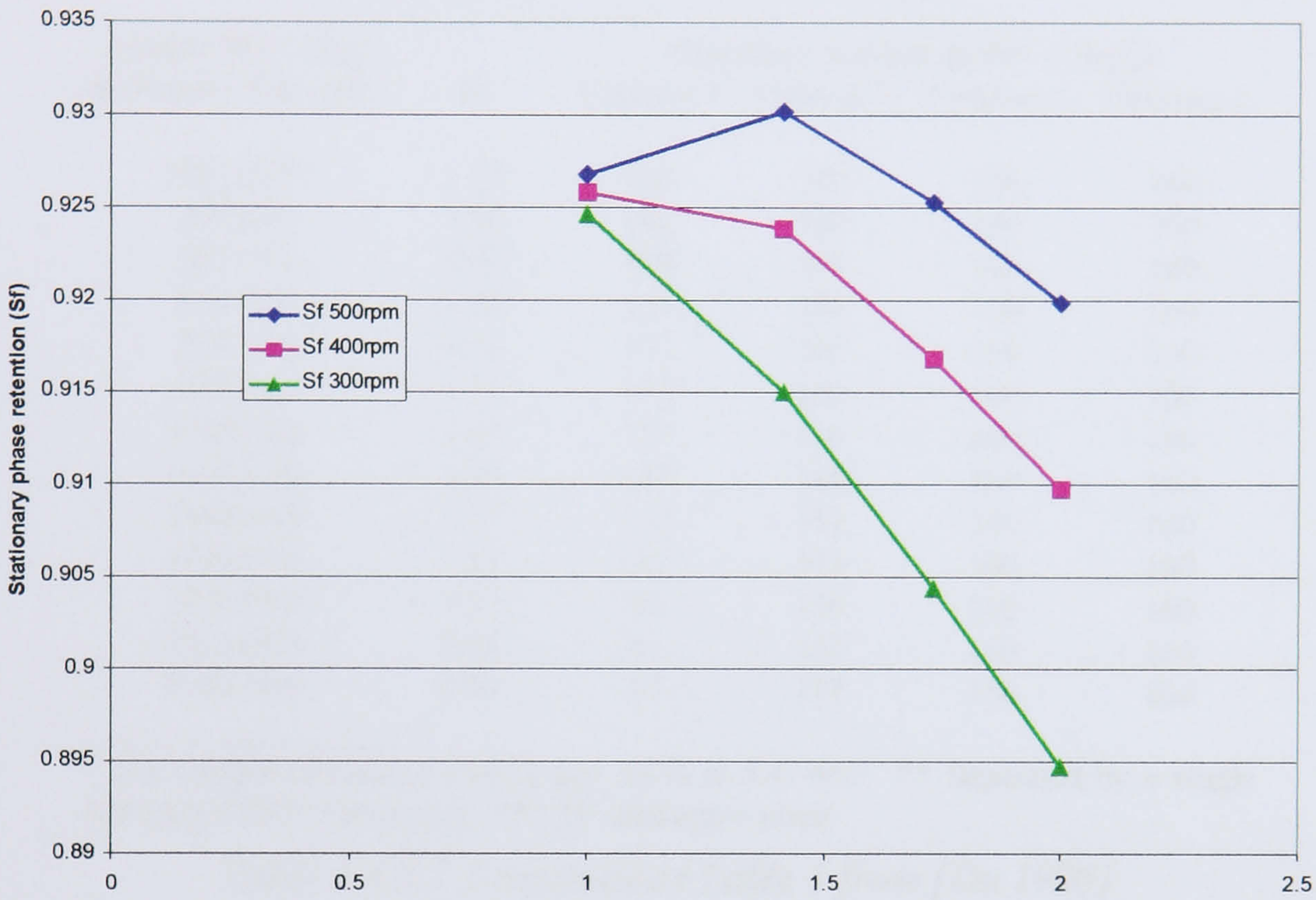

Figure 1.4.2.6.9 shows three Du characteristics for the Kromaton 2 machine as predicted by equation 1.4.2.6.13 that do not have constant gradients

A major problem with the work described in this paper is that there is no hydrodynamic theory underpinning the empirical equations presented.

1.4.2.7 Stationary Phase Retention, Resolution and Coil length

Du has also published a paper where four identical coils on four identical J-type centrifuges that were connected in series operating at the same rotational speed [Du 1998]. Epigallocatechin Gallate (EGCG) was separated from Gallocatechin Gallate (GCG) using hexane-ethyl acetate-water (1:2:3, v/v/v) phase system operating in reverse phase mode at 2.5ml/min. The two main points that this paper makes are: 1) that the resolution of a separation is proportional to the square root of the number of coils used and 2) that using four coils allows the sample loading capacity to be increased eleven times for the same resolution as one coil. The results also show that high sample loadings decrease the retention of stationary phase that in turn lowers resolution, see table 1.4.2.7.1. The reason put forward for this is that high concentrations of sample alter the physical properties of the phase system. Thus it is

important to measure how high sample concentrations and loadings affect the physical properties of the phase system. Examination of table 1.4.2.7.1 from [Du 1998] shows that the sample's concentration and volume did not affect the solvents systems physical properties enough to cause a loss of stationary phase retention for the resolution study shown in table 1.4.2.7.1.

Peak Resolution Between EGCG and GCG by High-Speed CCC Along With the Retention of the Stationary Phase for Each of Four Columns Connected in Series.

Sample Wt.* (mg) & Sample Vol. (mL)	R_s	Retention Volume of SP*** (mL) Column 1	Column 2	Column 3	Column 4
180 (30)**	1.00	160	160	160	160
180 (30)	1.98	160	160	160	160
360 (30)	1.95	160	160	160	160
540 (30)	1.88	152	160	160	160
720 (30)	1.73	135	160	160	160
900 (60)	1.55	143	160	160	160
1080 (60)	1.45	137	160	160	160
1260 (60)	1.36	133	160	160	160
1440 (60)	1.27	110	152	160	160
1620 (90)	1.14	115	143	160	160
1800 (90)	1.07	93	136	160	160
1980 (90)	0.98	81	133	160	160
2160 (90)	0.91	67	117	156	160

* The sample consists of EGCG and GCG at 5:4, w/w; ** Separated by a single high-speed CCC instrument; *** SP: stationary phase.

Table 1.4.2.7.1 reproduces Table 1 from [Du 1998]

As each coil on each centrifuge was identical ie made from the same bore and length of tubing to give the same volume the equation:

$$R_{s-n} = n^{\frac{1}{2}} R_{s-1} \qquad (1.4.2.7.1)$$

can be rewritten as:

$$R_{s-l} = \left(\frac{L}{L_{s-1}}\right)^{\frac{1}{2}} R_{s-1} \qquad (1.4.2.7.2)$$

or

$$R_{s-V_c} = \left(\frac{V_C}{V_{s-1}}\right)^{\frac{1}{2}} R_{s-1} \qquad (1.4.2.7.3)$$

where R_{s-1} equals the resolution from a single coil and l_{s-1} and V_{s-1} are the length and volume of a single coil respectively. Therefore it is possible to determine the length or volume of a coil necessary to achieve a desired resolution if sample loadings do not decrease stationary phase

retention. This can be applied to winding longer or shorter coils on a single centrifuge providing that: the same tubing is used, the tubing is wound over the same β-value range, the centrifuge is rotated at the same rotational speed, the coil is orientated with the head and tail in the same positions as the original coil and the same mobile phase is pumped in the same head-tail direction at the same flow rate. If the above conditions are met it can be seen that R_S is proportional to the square root of coil length or proportional to the square root of coil volume, hence:

$$R_S \propto L^{1/2} \qquad (1.4.2.7.4)$$

$$R_S \propto V_C^{1/2} \qquad (1.4.2.7.5)$$

Berthod and Billardello [Berthod 2000] also measured the resolution of the four J-type centrifuges compared in their study. Table 1.4.2.6.1 shows the details of the centrifuges tested. The SFCC 2000 and the Prototype 2 both use the same bore tubing, 1.65 mm, the mean β-value for both machines are similar however the rotor radii are different. The Kromaton 2 and Prototype 1 machines are very similar. Each centrifuge uses a different length of tubing and should give a different resolution for the Toluene and hexylbenzene separation.

Examination of Table 1.4.2.6.4 shows that similar Du retention characteristics for the:

1. SFCC 2000 at 800rpm and Prototype 2 at 500rpm.
2. Kromaton 2 at 300rpm and Prototype 1 at 300rpm.

Using $R\omega^2$ to calculate the acceleration at the centre of a rotating bobbin/spool the acceleration for the:

1. SFCC 2000 at 800rpm is 421.1m/s^2 and for Prototype 2 at 500rpm is 422.2m/s^2.
2. Kromaton 2 at 300rpm is 148.0m/s^2 and for Prototype 1 at 300rpm is 152.0m/s^2.

Figure 1.4.2.7.2 below shows how the resolution varies with mobile phase linear velocity for each machine tested.

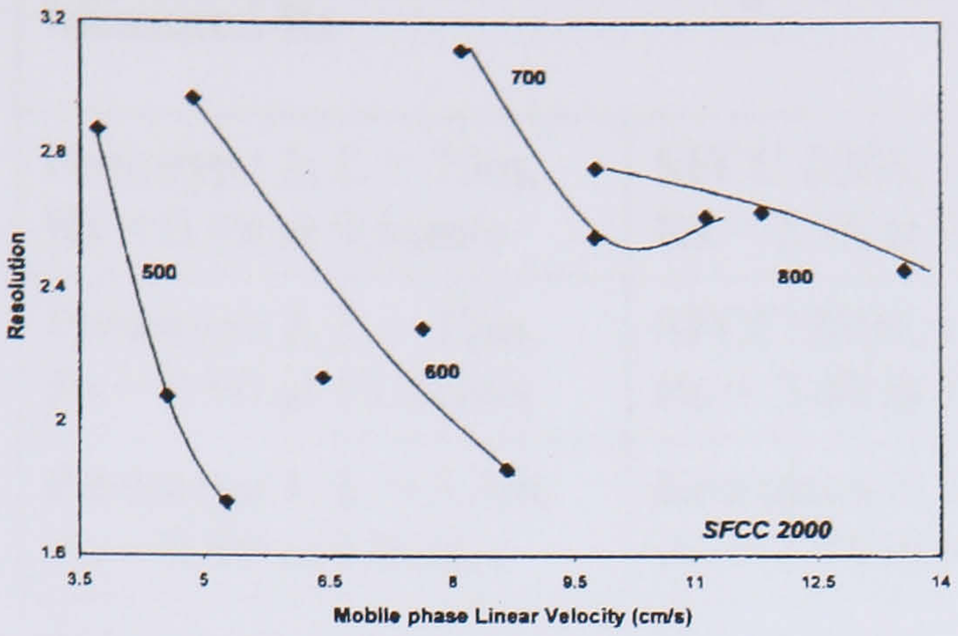

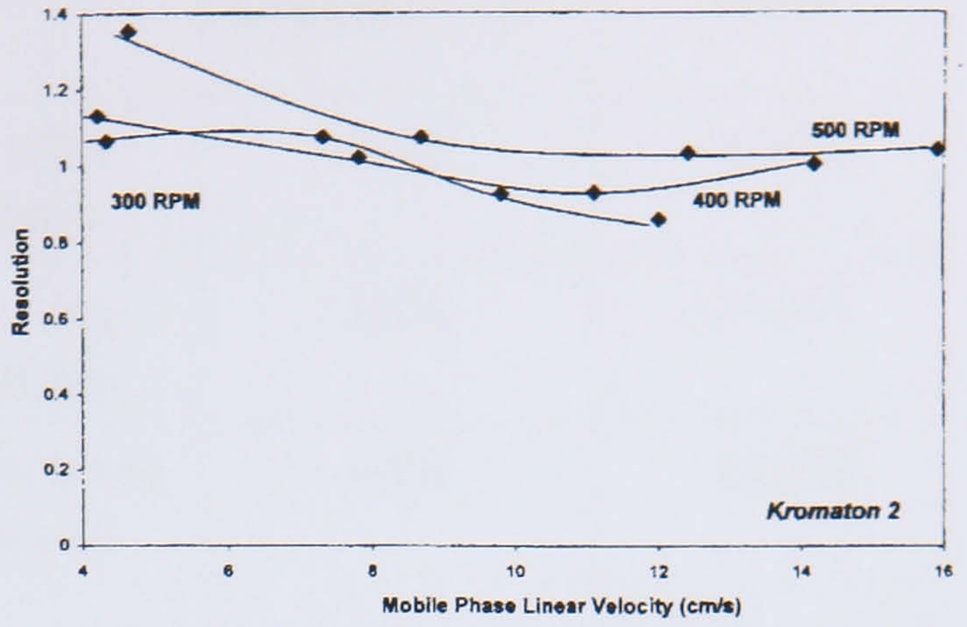

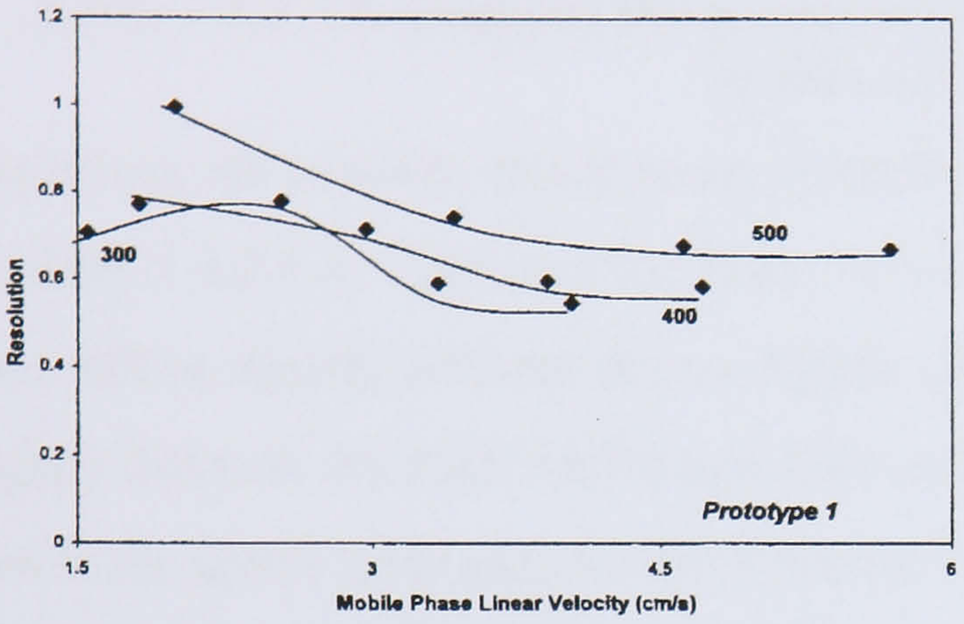

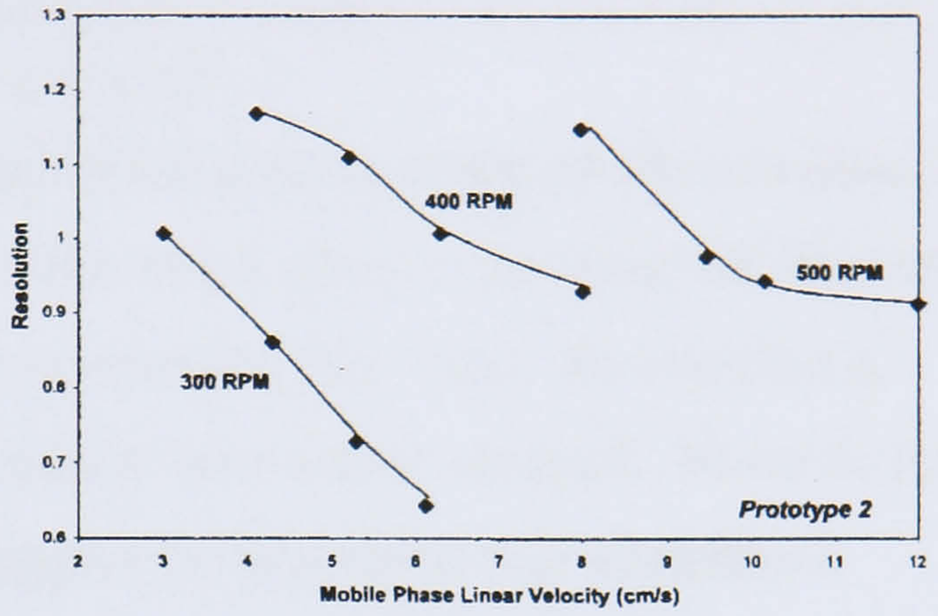

Fig. 4. The resolution factor, R_s, versus the mobile phase linear velocity for the four hydrodynamic machines.

Figure 1.4.2.7.2 is figure 4 from reference [Berthod 2000]

The resolution data given in figure 1.4.2.7.2 shows that:

1. SFCC 2000 at 800rpm and mobile phase linear velocity of 9.5cm/s gives a resolution of 2.75 and for Prototype 2 at 500rpm and mobile phase linear velocity of 9.5cm/s gives a resolution of 0.98.
2. SFCC 2000 at 800rpm and mobile phase linear velocity of 12cm/s gives a resolution of 2.6 and for Prototype 2 at 500rpm and mobile phase linear velocity of 12cm/s gives a resolution of 0.9.
3. Kromaton 2 at 300rpm and mobile phase linear velocity of 4cm/s gives a resolution of 1.07 and for Prototype 1 at 300rpm and mobile phase linear velocity of 4cm/s gives a resolution of 0.55.

If equation 1.4.2.7.2 is applied to the shorter coil a calculated resolution close to the measured resolution is obtained, the coil lengths are taken from table 1.4.2.6.1, see table 1.4.2.7.3 below for the comparison of results.

Measured Rs		Calculated Rs	Error
Prototype 2, L = 73m, Rs = 0.98 at 9.5cm/s	SFCC 2000, L= 12m, Rs = 2.75 at 9.5cm/s	2.42	-12.0%
Prototype 2, L = 73m, Rs = 0.90 at 12.0cm/s	SFCC 2000, L= 12m, Rs = 2.60 at 12.0cm/s	2.22	-14.6%
Prototype 1, L = 5.1m, Rs = 0.98 at 4.0cm/s	Kromaton 2, L= 15.5m, Rs = 2.75 at 4.0cm/s	0.96	-10.4%

Table 1.4.2.7.3 compares the measured and calculated resolution for the Toluene and hexylbenzene separation.

The errors can be taken into account given the slightly different Du retention characteristics, see table 1.4.2.6.4. Although the linear velocity of the mobile phase is the same, the flow rate used will be slightly different due to slightly different retention (S_f). Since the retention is slightly different the peak widths and differential elution times will be obtained. However the data in the above table adds further evidence to support the hypothesis that resolution is proportional to the square root of coil length. This hypothesis can even be used to approximately predict the resolution obtain from different machines operating with similar levels of acceleration.

1.4.2.8 Modelling of the CCD process

In 1998 another Dutch student from Eindhoven came to work at the Brunel Institute for Bioengineering (BIB), his name was Joost de Folter. While at BIB de Folter worked on how resolution changes with mobile phase flow and hence stationary phase retention. His work is detailed in his work placement report [Folter 1998]. A large part of this work was compiling a piece of software that runs in the Microsoft Windows environment that models the separation of two sample components in the CCD process. The software has been used to study how the resolution is affected by changes to the following parameters: the component sample partition constants, stationary phase retention, sample volume and number of mixing settling and transfer cycles and the transfer efficiency between the test tubes. The software has shown that:

1. The resolution is directly proportional to the square root of the number of mixing, settling and transfer cycles.
2. The peak elution time is directly proportional to the number of mixing, settling and transfer cycles.
3. The elution time between peaks is directly proportional to the number of mixing, settling and transfer cycles.

4. The peak width is directly proportional to the square root of the number of mixing, settling and transfer cycles.
5. The peak height is inversely proportional to the square root of the number of mixing, settling and transfer cycles.

It has been shown in section 1.4.2.1 that the rate of mixing and setting in a J-type centrifuge is the rotational speed. The number of mixing, settling and transfer cycles that a peak will undergo in a J-type centrifuge is the product of the peak elution time and the rotational speed. Therefore if the length of a coil is doubled the elution time will double and the number of mixing, settling and transfer cycles will double. In turn the differential elution time between peaks will double, the peak widths will increase by root two, the resolution will increase by root two and the peak height/concentration will decrease by root two. From observation 4 the following equation for peak width can be formed for CCD [Sutherland 2002A, 2002B]:

$$W = 4\sqrt{H_{P=n}k'} \qquad (1.4.2.8.1)$$

where W and $H_{P=n}$ are measured in the number of CCD transfer steps therefore the constant 4 has the units of the square root of the number of transfer steps and

$$k' = \frac{PS_f}{1-S_f} \qquad (1.4.2.8.2)$$

Now the model shown that:

$$H_{P=n} = \frac{PS_f h}{\left(1-S_f\right)} + h$$

where h is the number of transfer stages in a CCD column.

$$H_{P=n} = h\left[\frac{PS_f}{\left(1-S_f\right)} + 1\right] \qquad (1.4.2.8.3)$$

Comparing to a CCC coil on J-type centrifuge:

$$h = \frac{NV_C\left(1-S_f\right)}{F} \qquad (1.4.2.8.4)$$

Where N is the rotational speed in rpm. Substituting equation 1.4.2.8.4 in equation 1.4.2.8.3 gives:

$$H_{P=n} = \left[\frac{NV_C\left(1-S_f\right)}{F}\right]\left[\frac{PS_f}{\left(1-S_f\right)}+1\right]$$

$$H_{P=n} = \frac{NV_C PS_f}{F} + \frac{NV_C\left(1-S_f\right)}{F}$$

$$H_{P=n} = \frac{NV_C}{F}\left[PS_f + 1 - S_f\right]$$

$$H_{P=n} = \frac{NV_C}{F}\left[S_f\left(P-1\right)+1\right] \qquad (1.4.2.8.5)$$

Now $H_{P=n} = t_{P=n}N$ and substituting in equation 1.4.2.8.5 gives equation 1.3.3.2.3:

$$t_{P=n} = \frac{V_C}{F}\left[S_f\left(P-1\right)+1\right] \qquad (1.3.3.2.3)$$

Now $W = W_{P=n}N$ where W is measured in the number of CCD transfer steps to elution and N is the rotational speed in rpm of the centrifuge and $W_{P=n}$ is the elution time measured in minutes. Hence equation 1.4.2.8.1 can be rewritten for the CCC process as:

$$W_{P=n} = \frac{C}{N}\sqrt{H_{P=n}k'} \qquad (1.4.2.8.6)$$

Where C is a constant related to the separation efficiency and has the units of the square root of the number of transfer steps. Using the equation $H_{P=n} = t_{P=n}N$ and substituting in 1.4.2.8.6 for $H_{P=n}$ gives:

$$W_{P=n} = C\sqrt{\frac{t_{P=n}k'}{N}} \qquad (1.4.2.8.7)$$

The minimum value that C can have is 4 since in the CCD model it was assumed that there was complete mixing, settling and transfer between each test tube, see equation 1.4.2.8.1. Hence a CCC efficiency equation can be defined:

$$\%\ \text{CCC Efficiency} = \frac{100\times 4}{C} = \frac{400}{C} \qquad (1.4.2.8.8)$$

Now substituting equation 1.4.2.8.2 into equation 1.4.2.8.7 gives:

$$W_{P=n} = C\sqrt{\frac{t_{P=n}PS_f}{N\left(1-S_f\right)}} \qquad (1.4.2.8.9)$$

Substitute equation 1.4.2.6.8 into equation 1.4.2.8.9 for W_A to give:

$$W_A = C\sqrt{\frac{t_A P_A S_f}{N(1-S_f)}}$$

$$W_A = C\sqrt{\frac{P_A S_f V_C B^2 \left[S_f(P_A-1)+1\right]}{N(1-S_f)^3}}$$

$$W_A = \frac{CB\sqrt{S_f V_C}}{N^{1/2}(1-S_f)^{3/2}}\sqrt{P_A\left[S_f(P_A-1)+1\right]} \qquad (1.4.2.8.10)$$

By a similar process $$W_B = \frac{CB\sqrt{S_f V_C}}{N^{1/2}(1-S_f)^{3/2}}\sqrt{P_B\left[S_f(P_B-1)+1\right]} \qquad (1.4.2.8.11)$$

Therefore $$W_B + W_A = \frac{CB\sqrt{S_f V_C}}{N^{1/2}(1-S_f)^{3/2}}\left[\sqrt{P_B\left[S_f(P_B-1)+1\right]}+\sqrt{P_A\left[S_f(P_A-1)+1\right]}\right] \qquad (1.4.2.8.12)$$

Substituting equation 1.4.2.8.12 and into equation 1.4.2.6.9 gives:

$$R_S = \frac{2V_C B^2 S_f(P_B-P_A)}{(1-S_f)^2}\,\frac{N^{1/2}(1-S_f)^{3/2}}{CB\sqrt{V_C S_f}\left[\sqrt{P_B\left[S_f(P_B-1)+1\right]}+\sqrt{P_A\left[S_f(P_A-1)+1\right]}\right]}$$

$$R_S = \frac{2B\sqrt{NV_C S_f}(P_B-P_A)}{C(1-S_f)^{1/2}\left[\sqrt{P_B\left[S_f(P_B-1)+1\right]}+\sqrt{P_A\left[S_f(P_A-1)+1\right]}\right]} \qquad (1.4.2.8.13)$$

Figure 1.4.2.8.1 was produced for three different machines and two different phase systems. For each machine and phase system used the Du retention gradient B was determined from a retention study with the same operating conditions as the appropriate resolution study. For each machine the constant C was determined from one resolution result for that machine. These values were then used in equation 1.4.2.8.13 to produce figure 1.4.2.8.1. It can be seen from figure 1.4.2.8.1 that the predicted and measured resolution compare well for the range of retentions and mobile phase flow rates tested. Table 1.4.2.8.1 contains the ranges of the values for the constant C and the CCC efficiency determined by equation 1.4.2.8.8 for the results displayed in figure 1.4.2.8.1.

Machine	Range of constant C	Range of CCC % Efficiency
Analytical	12.8	31.2
Process	15.2 to 16.5	24.2 to 26.3
Quattro	26.5 to 41.4	9.7 to 15.1

Table 1.4.2.8.1 shows the values of C determined from the experimental data used to plot figure 1.4.2.8.1 and the corresponding efficiencies achieved

It remains to be seen if the chromatographic efficiency changes significantly when the retention is varied from say 50 to 98% ie the usable potion of stationary phase retention.

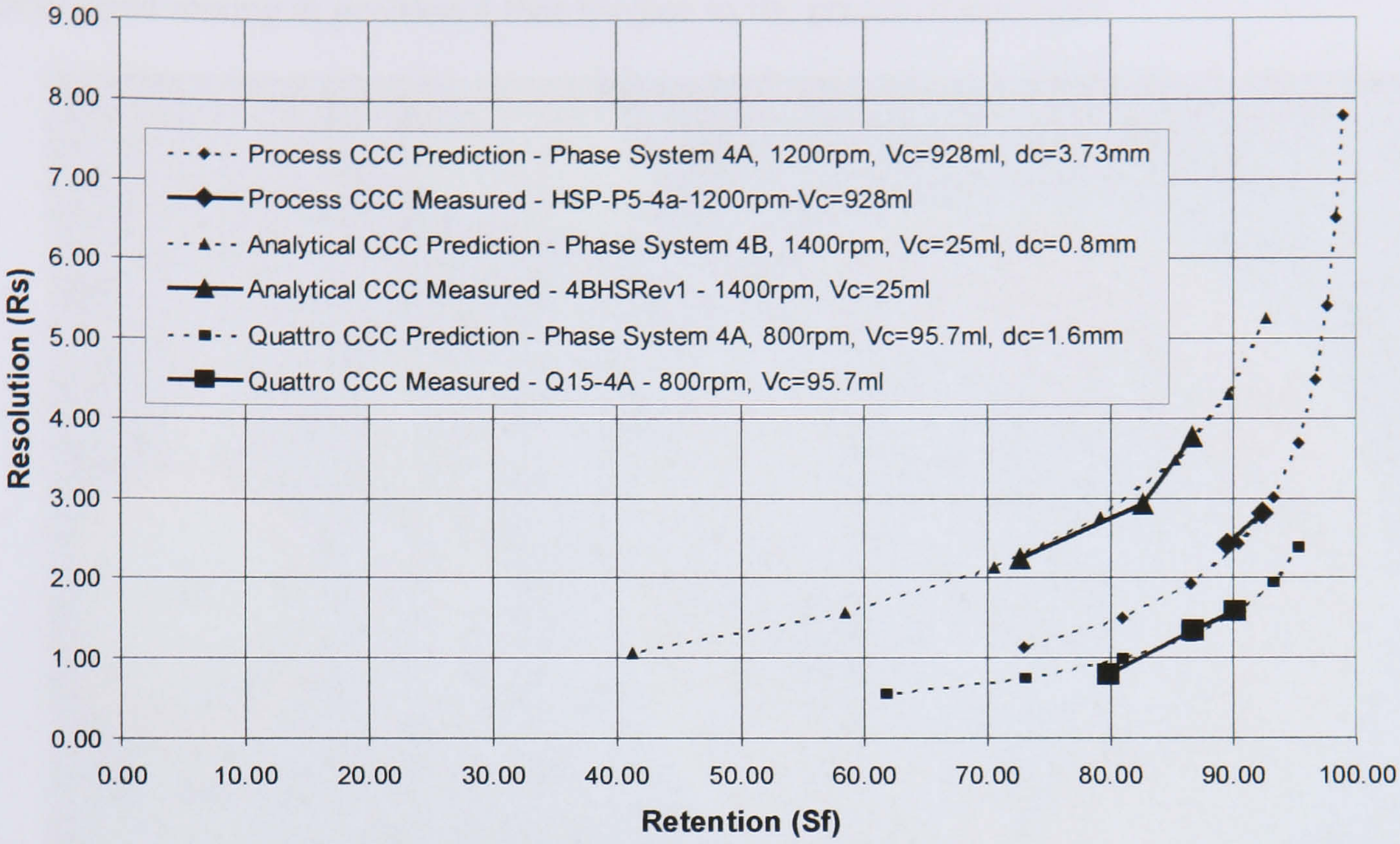

Figure 1.4.2.8.1 compares theoretical and measured resolutions for three different instruments and two different phase systems. This figure is taken from [Sutherland 2002A]

1.4.3 Hydrodynamics

The hydrodynamics of CCC perform two tasks for the chromatographic process: the first task is the retention of the stationary phase and the second task is the creation of zones of mixing and settling that move towards the head end of a coil. The retention of the stationary phase is caused by the pumping action of the coil motion and is discussed in section 1.4.2 "Head and Tail Theory and its affect on Retention". The role of the mixing and settling zones are discussed in sections 1.3.1.1 "Countercurrent Distribution" and 1.3.2 "Basic Explanation of Countercurrent Chromatography". This following section discusses the mixing phenomenon that occurs around the proximal key node and settling about the distal key node. Section 1.4.3.2 introduces secondary flow phenomena that may affect the fluid dynamics of CCC.

1.4.3.1 Mixing

The following figures show wave mixing and settling occurring in zones as shown originally by Conway [Conway 1990] and discussed in section 1.3.2.1. Figure 1.4.3.1.1 shows that the lower phase is the mobile phase and is being pumped at 4ml/min from head centre to tail periphery following the recommendations of Sutherland et al [2000 A]. The phase system used was Chloroform/Acetic Acid/ Water (2:2:1). These photographs are taken from [Sutherland 1999]. The coil is wound in the clockwise direction hence the mobile phase is also being pumped in the clockwise direction. Starting at position 1 which is close to the

distal key node figure 1.4.3.1.2 shows the 2 liquid phases stratified into layers. Figure 1.4.3.1.3 taken at position 3 shows wave mixing developing and figure 1.4.3.1.4 shows fully developed mixing at position 4 that is close to the proximal key node.

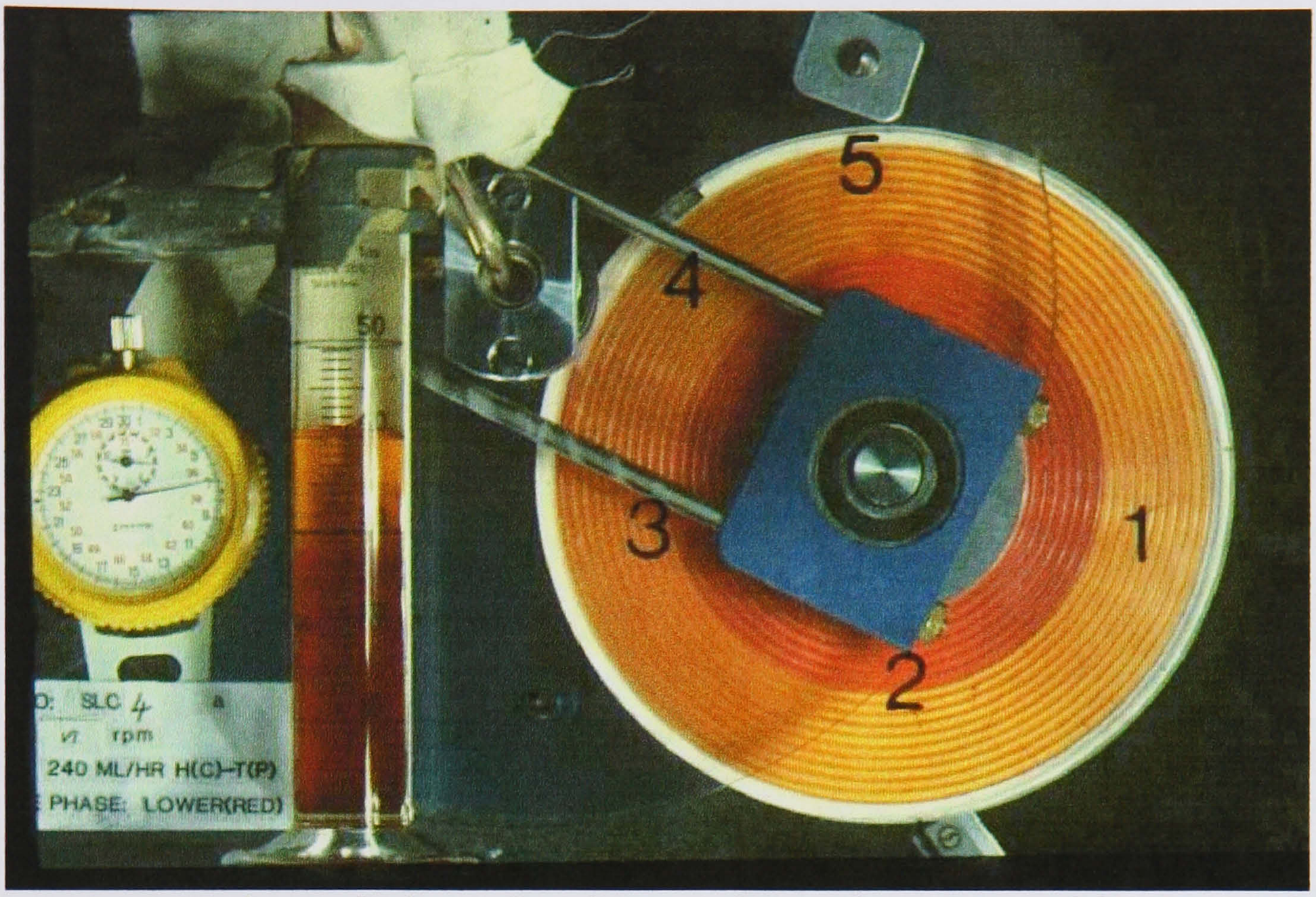

Figure 1.4.3.1.1 shows a high-speed stroboscopic figure of a rotating coil filled with a dyed phase system, the following figures show close up views of positions 1, 3, and 4 [Sutherland 1999]

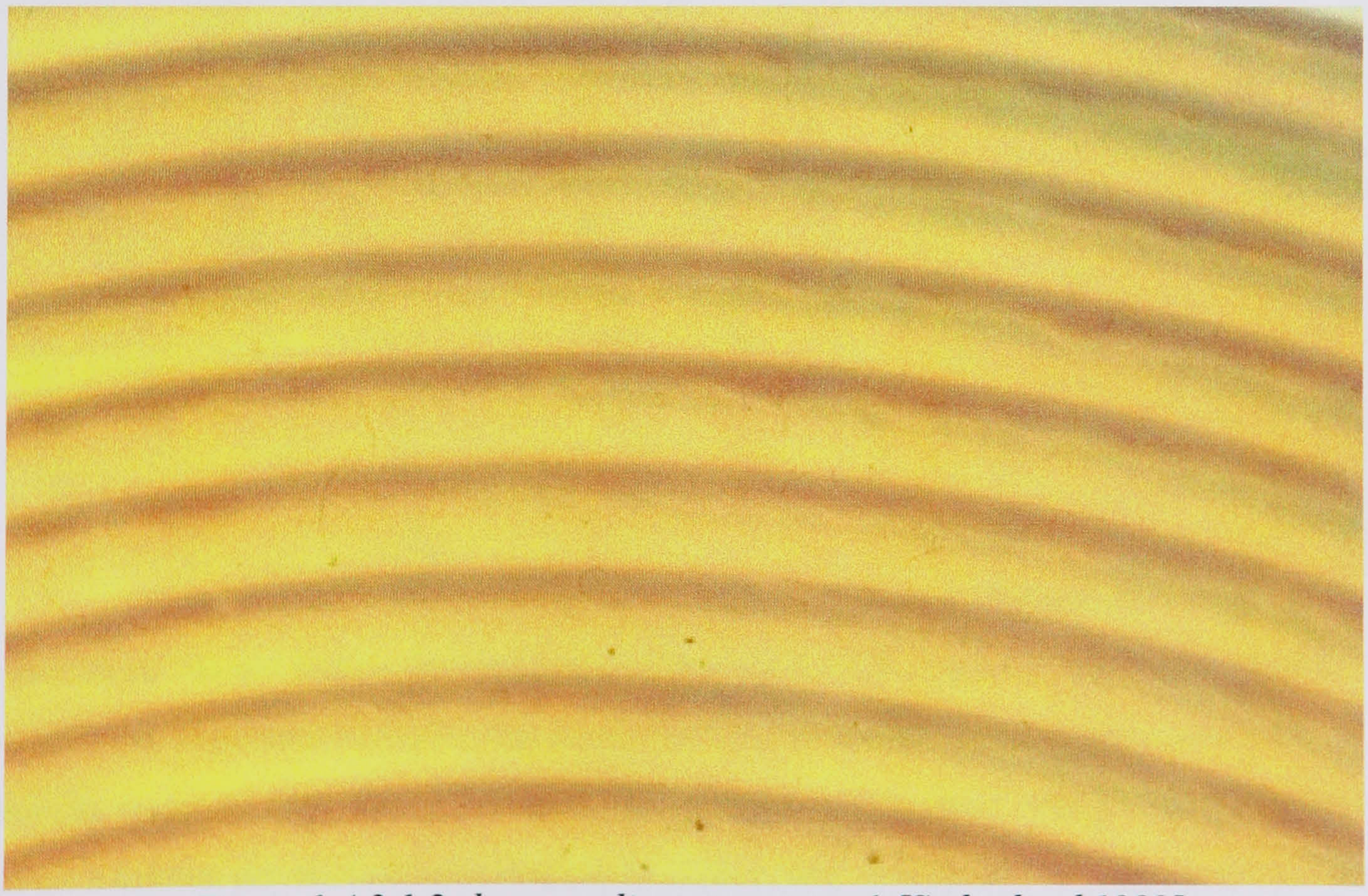

Figure 1.4.3.1.2 shows settling at position 1 [Sutherland 1999]

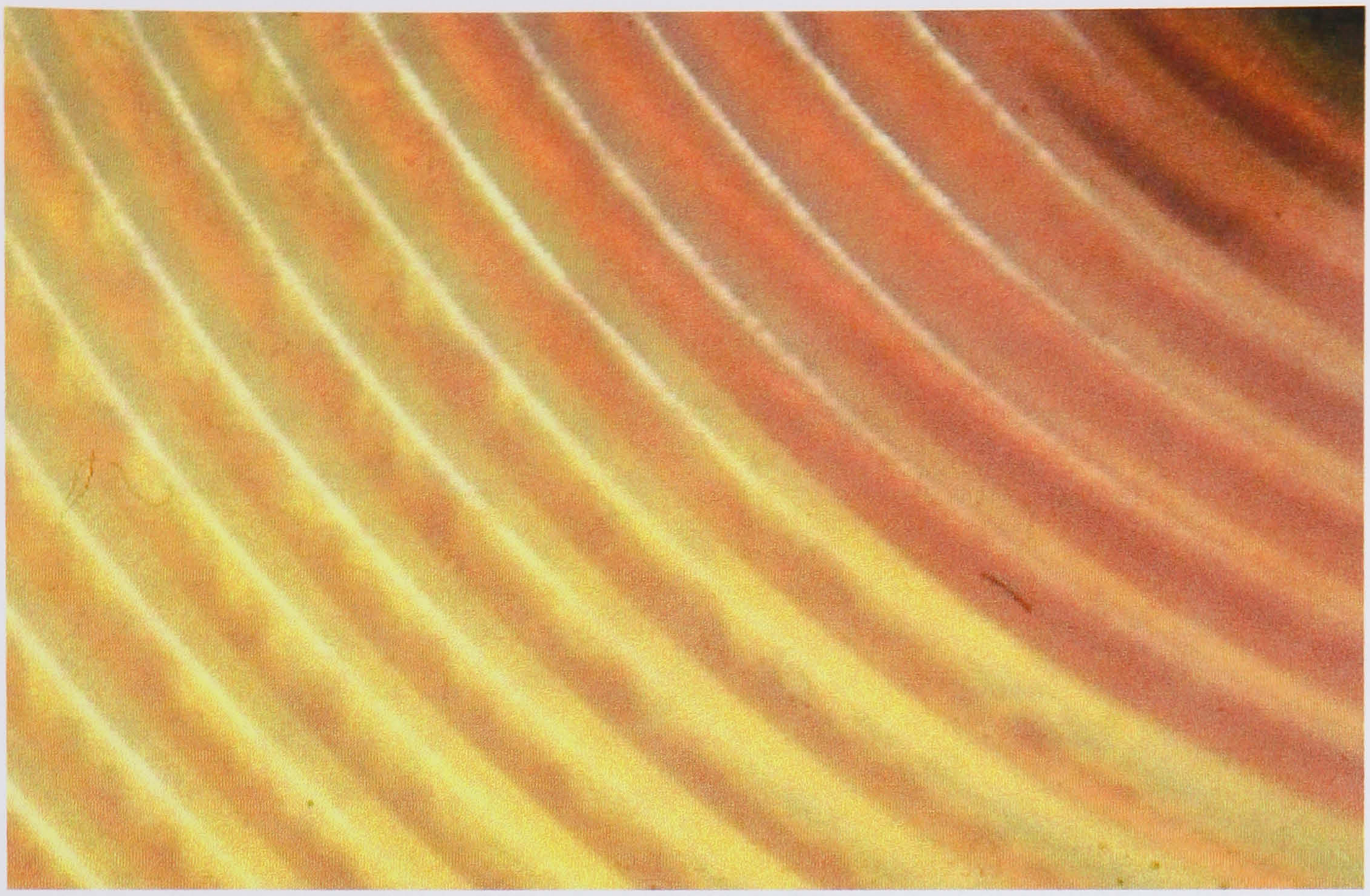

Figure 1.4.3.1.3 shows wave mixing building at position 3 [Sutherland 1999]

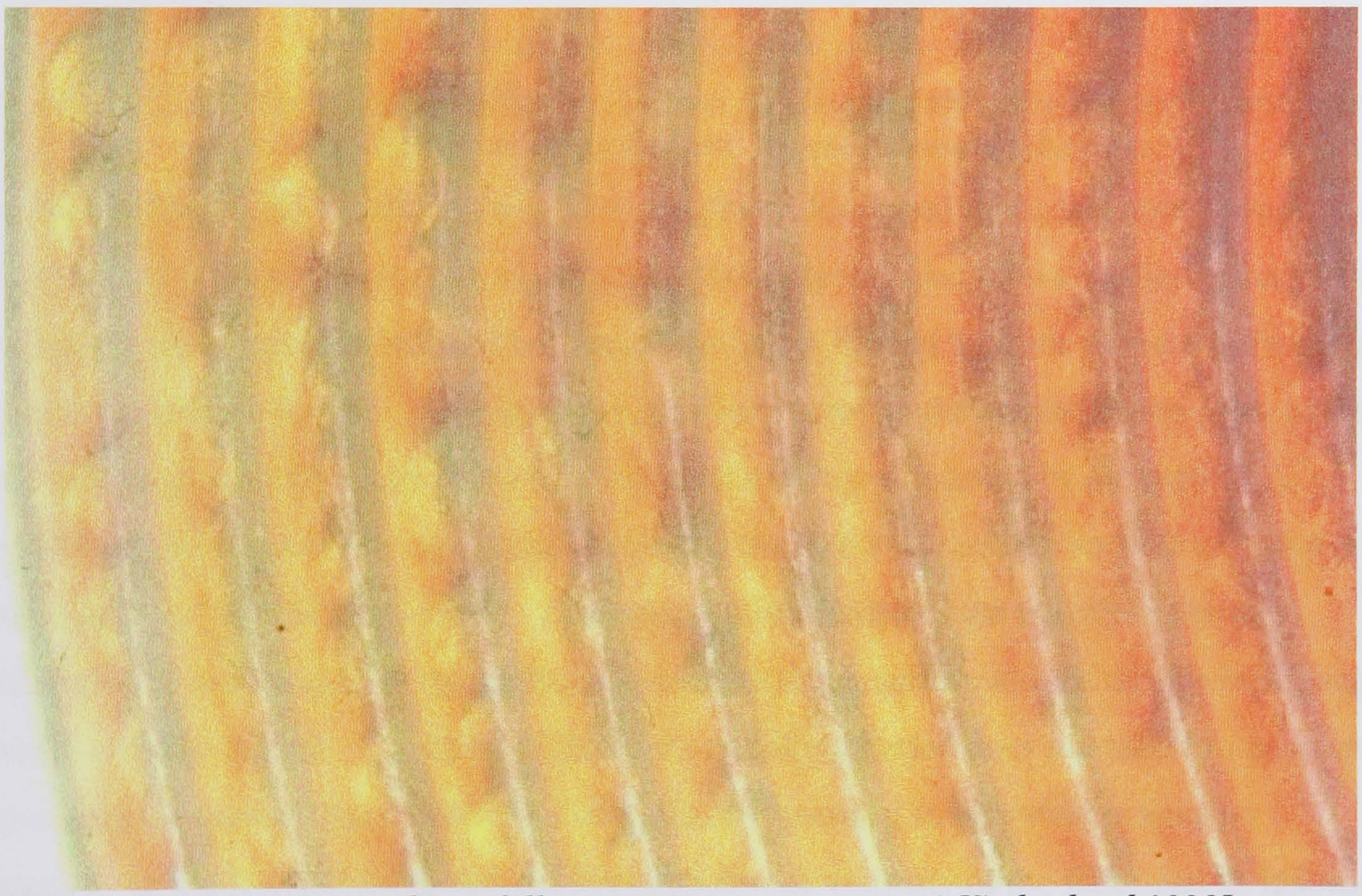

Figure 1.4.3.1.4 shows full wave mixing at position 4 [Sutherland 1999]

To date there has not been a detailed study of mixing in CCC, such a study would need to determine the important variables that cause the flow instability that creates waves that eventually cause mixing. The paper by Sutherland et al [Sutherland 1986] is the first paper to describe a known physical process that could explain why mixing and settling occurs in CCC. The ideas postulated in this paper are based upon the Kelvin-Helmholtz stability criterion; developed in the late 19th and early 20th century [Kelvin 1871, Helmholtz 1868]. The

conditions for the flow to become unstable can be calculated from the Kelvin-Helmholtz stability criterion:

$$\frac{(u_1 - u_2)^4}{g} < \frac{4T_i(\rho_2 - \rho_1)(\rho_1 + \rho_2)^2}{(\rho_1\rho_2)^2} \qquad (1.4.3.1.1)$$

Where u_1 and u_2 are the velocities of the two liquids, T_i is the interfacial tension between the two liquids and ρ_1 and ρ_2 are the densities of the two liquids and g is the acceleration due to gravity, see figure 1.4.3.1.5.

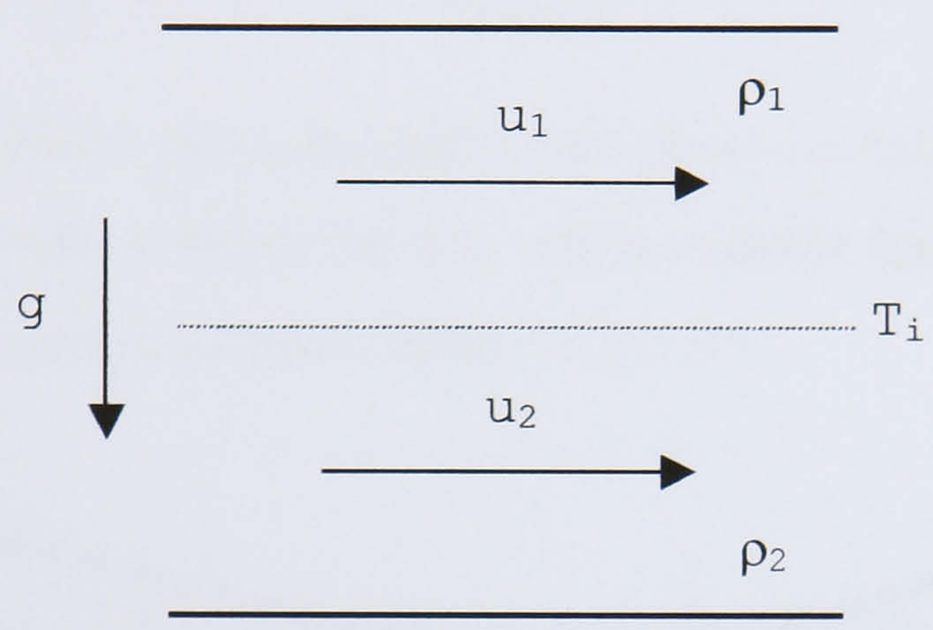

Figure 1.4.3.1.5 shows a longitudinal-section of coil tubing containing the upper and lower phases the dotted line represents the interface between the phases

The Kelvin-Helmholtz stability criterion was originally developed to explain how waves are generated on the sea by the action of the wind. Basically the wind blows on the surface of the sea causing small waves to form. These small waves are formed by some of the wind's energy being transferred to the sea. If enough energy is transferred to the sea the waves grow in size until the energy transferred from the wind equals the energy dissipated by the waves. A complete explanation of the under lying theory for the Kelvin-Helmholtz stability criterion is give in chapter 11 of [Levich 1962]. The wave motion dissipates the transferred energy because work is done against the surface tension due to the surface area of the sea increasing when waves are formed. The Kelvin-Helmholtz stability criterion does not take into account any energy dissipation due to viscosity, the fluids are assumed to be invisid ie have no viscosity. In the Kelvin-Helmholtz stability criterion the viscosity of the fluids can be ignored because the boundaries, the seabed and the stratosphere, are assumed to be at infinity or a very great distance from the interface. The Kelvin-Helmholtz stability criterion predicts instability when the waves are growing in size and stable when the waves are decreasing in size.

Sutherland [1986] uses the radial acceleration as shown in figure 1.4.1.2.3.5 to explain why mixing occurs at the proximal key node and why settling occurs at the distal key node. The g

term in equation 1.4.3.1.1 can be replaced by equation 1.4.1.2.3.1 for the radial acceleration experienced by the phase system to give:

$$\frac{(u_1-u_2)^4}{R\omega^2(\cos\theta+4\beta)} < \frac{4T_i(\rho_2-\rho_1)(\rho_1+\rho_2)^2}{(\rho_1\rho_2)^2} \qquad (1.4.3.1.2)$$

Equation 1.4.3.1.2 rearranged to calculate the Kelvin-Helmholtz threshold velocity (u_1-u_2) between the phases. Equation 1.4.3.1.3 shows the rearranged formula:

$$(u_1-u_2) = \left(\frac{4T_i R\omega^2(\cos\theta+4\beta)(\rho_2-\rho_1)(\rho_1+\rho_2)^2}{(\rho_1\rho_2)^2}\right)^{1/4} \qquad (1.4.3.1.3)$$

A relative flow velocity below that calculated by the above equation means that mixing will not occur and a velocity above means the flow will be unstable and mixing will occur. Equation 1.4.3.1.3 was used to generate figure 1.4.3.1.6[v].

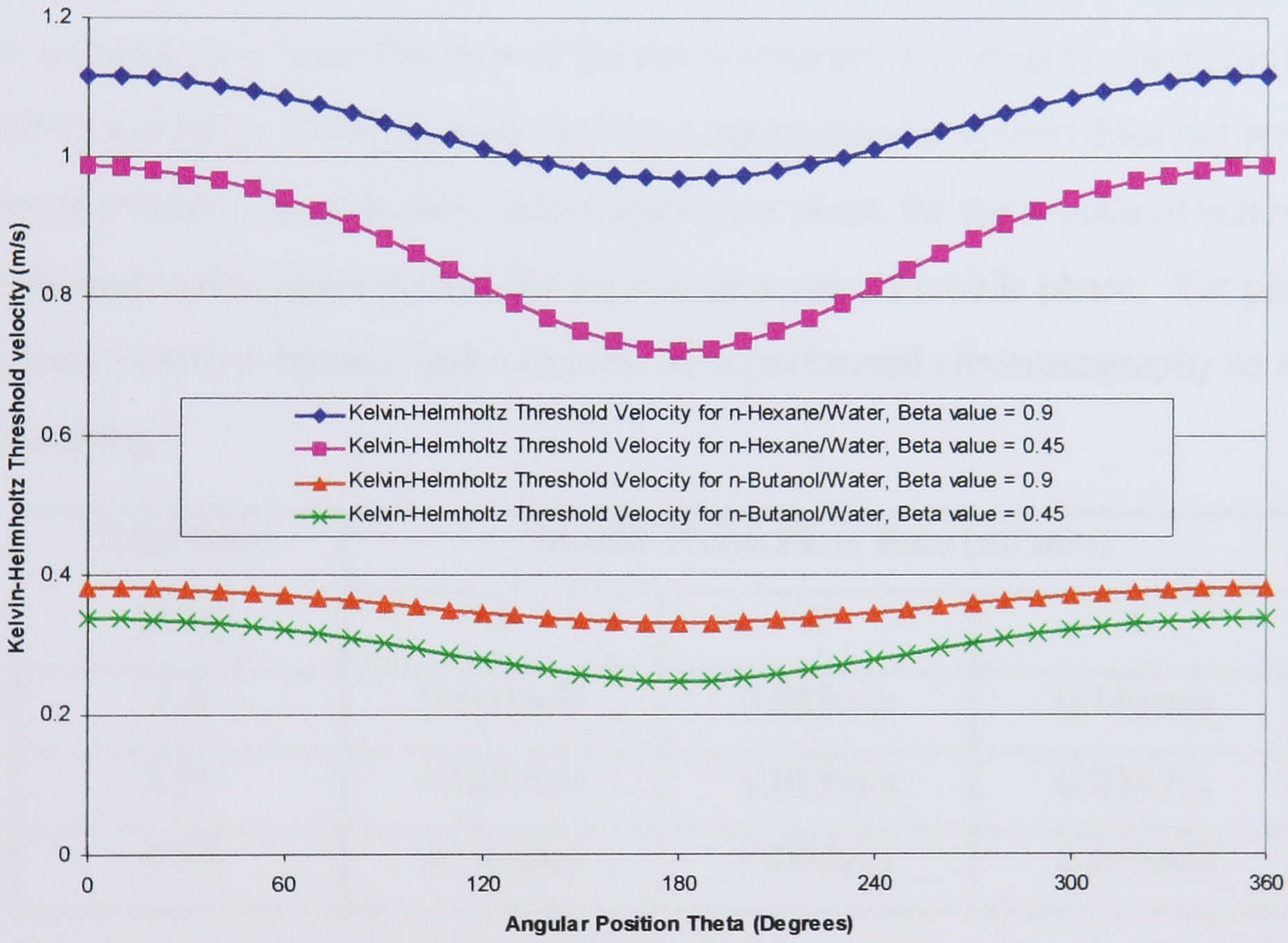

Figure 1.4.3.1.6 shows how the threshold velocity for mixing varies with angular position around a single loop of a helical coil for two different phase systems at two different β-values

The figure clearly shows that the linear flow velocity required for mixing is lowest at the proximal key node and highest at the distal key node as suggested by Sutherland et al [1986]. The figure also shows that the n-hexane/water phase system requires higher flow velocities

---

[v] Figure 1.4.3.1.6 was generated using a rotor radius (orbital radius) of 110mm and rotational speed of 800rpm. The density difference for the n-Hexane/Water system was 340kg/m^3 and interfacial tension was 51.1mN/m. The density difference for the n-Butanol/Water system was 190kg/m^3 and interfacial tension was 1.58mN/m.

than the n-butanol/water phase system, this is because the interfacial tension of the n-hexane/water is approximately 32 times that of the n-butanol/water phase system. However n-butanol is approximately 9 times more viscous than n-hexane and should therefore require more kinetic energy from the flow in order for mixing to occur. If the mobile phase was the lower aqueous phase in both cases then the mobile phase mean velocity would need to be approximately 3 times greater when the stationary phase was n-butanol than when n-hexane in order to supply enough kinetic energy for mixing. If using this simple explanation for the affect of viscosity on mixing the n-butanol/water curves would be in the same region as the n-hexane/water curves on figure 1.4.3.1.1. If the same retention were achieved for both phase systems the n-butanol/water system would need to have 3 times the flow rate of the n-hexane/water system. The work of Baalen-Helden [Baalen 1997], Ter Wee [Wee 1998] and Du et al [Du 1999] has shown that the retention for each phase system under the same operating conditions is different. Therefore the same retention for the n-butanol/water system will not be obtained at 3 times the flow as for the n-hexane/water system. In fact references [Baalen 1997] and [Wee 1998] showed that the n-butanol/water system does not retain as well as the n-hexane/water system ie there is less stationary phase for the n-butanol/water system than the n-hexane/water phase system for a given flow rate of mobile phase. Yet phase systems based on both n-butanol and n-hexane have performed chromatography so mixing must be occurring.

Tube Bore (mm)	Mobile Phase Flow Rate (ml/min)		
	1	2	4
1.6	0.041m/s	0.083m/s	0.166m/s
3.35	0.009m/s	0.019m/s	0.038m/s
4.75	0.005m/s	0.009m/s	0.019m/s

Table 1.4.3.1.1 shows the mean flow speed (m/s) of the mobile Phase for various tube bores and stationary Phase Retention of 80%

If the stationary phase is truly stationary relative to the tubing, the velocity of the mobile phase is the determining velocity as to whether mixing or settling occurs. Also if the stationary phase retention is constant at all points in the coil the mean linear velocity of the mobile phase can be calculated easily. The values in table 1.4.3.1.1 were calculated assuming a constant 80% retention through out the coil. The cross-sectional area occupied by the mobile phase can be calculated, 20% of the cross-sectional area of the tubing, and the velocity is determined by dividing the flow rate by the cross-sectional area of the mobile phase. However, the external pumped velocity of the mobile phase does not exceed the Kelvin-Helmholtz threshold

velocity, as shown in table 1.4.3.1.1 and figures 1.4.3.1.6 and 1.4.3.1.7 [vi]. Linear velocities are at least an order of magnitude lower than that required to produce wave mixing like that shown in Figures 1.4.3.1.1-1.4.3.1.3. If the pumped flow rate of mobile phase were increased to a value where the threshold velocity was achieved the more stationary phase would displaced from the coil. With no stationary phase present in the coil no mixing can occur. It is concluded that for mixing to occur there must be other factors influencing the relative velocity between the mobile and stationary phases. There may also be other factors that lower the mean flow velocity for which mixing can occur such as viscosity and boundary effects.

Equation 1.4.3.1.3 does not take into account the viscosities of the liquid phases or the presence of the boundary formed by the tubing inner wall.

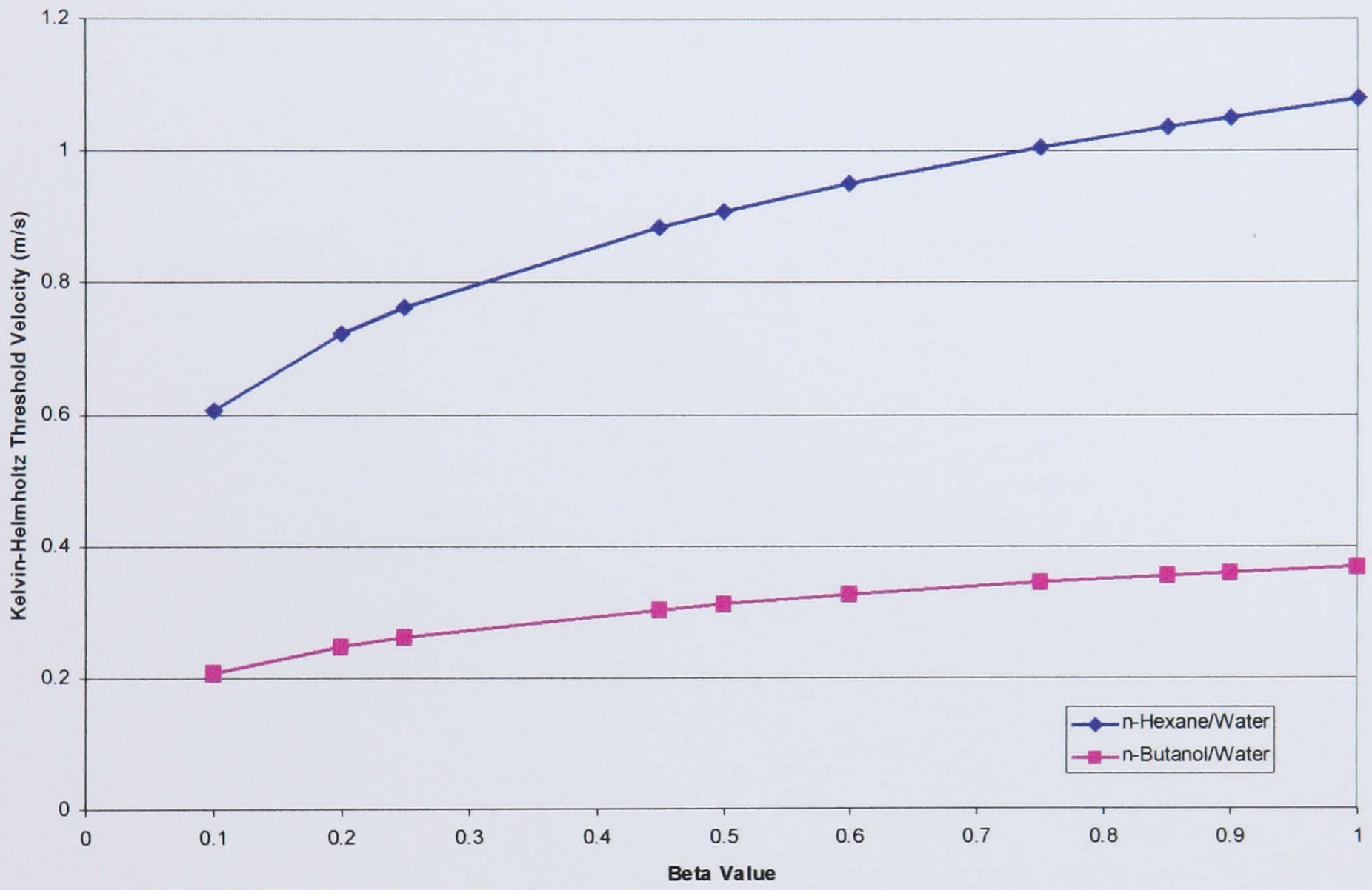

Figure 1.4.3.1.7 shows the relation between Kelvin-Helmholtz threshold velocity and β-value for n-hexane/water and n-butanol/water phase systems

Four papers published by Thorpe [Thorpe 1968, Thorpe 1969 A, Thorpe 1969 B, Thorpe 1971] expand upon the work conducted by Kelvin and Helmholtz. These papers develop the theoretical analysis of a flow similar to that observed by Conway [1990] in a J-type CCC instrument. The viscosities of the liquids and the presence of boundaries are included in the analysis. The analysis is also backed up by experimental results and observations. The

---

[vi] Figure 1.4.3.1.7 was generated using a rotor radius of 110mm, a rotational speed of 800rpm, the Kelvin-Helmholtz Threshold Velocity formula for two inviscid liquids and the values shown are for an angular position of 90° for all β-values.

channel section used in the analysis and experiments is a rectangle. The experimental method used to create relative flow between the two immiscible liquids is to fill a channel with both liquids, seal the ends of the channel and then tilt the channel relative to the horizontal. The acceleration due to gravity (g) causes the liquids to flow past each other. The heavier phase collects at the lower end of the channel and the lighter phase collects at the higher end of the channel. As the flows accelerate towards each end of the channel the relative velocity between the two liquids quickly increases forming waves that grow rapidly see figure 1.4.3.1.8.

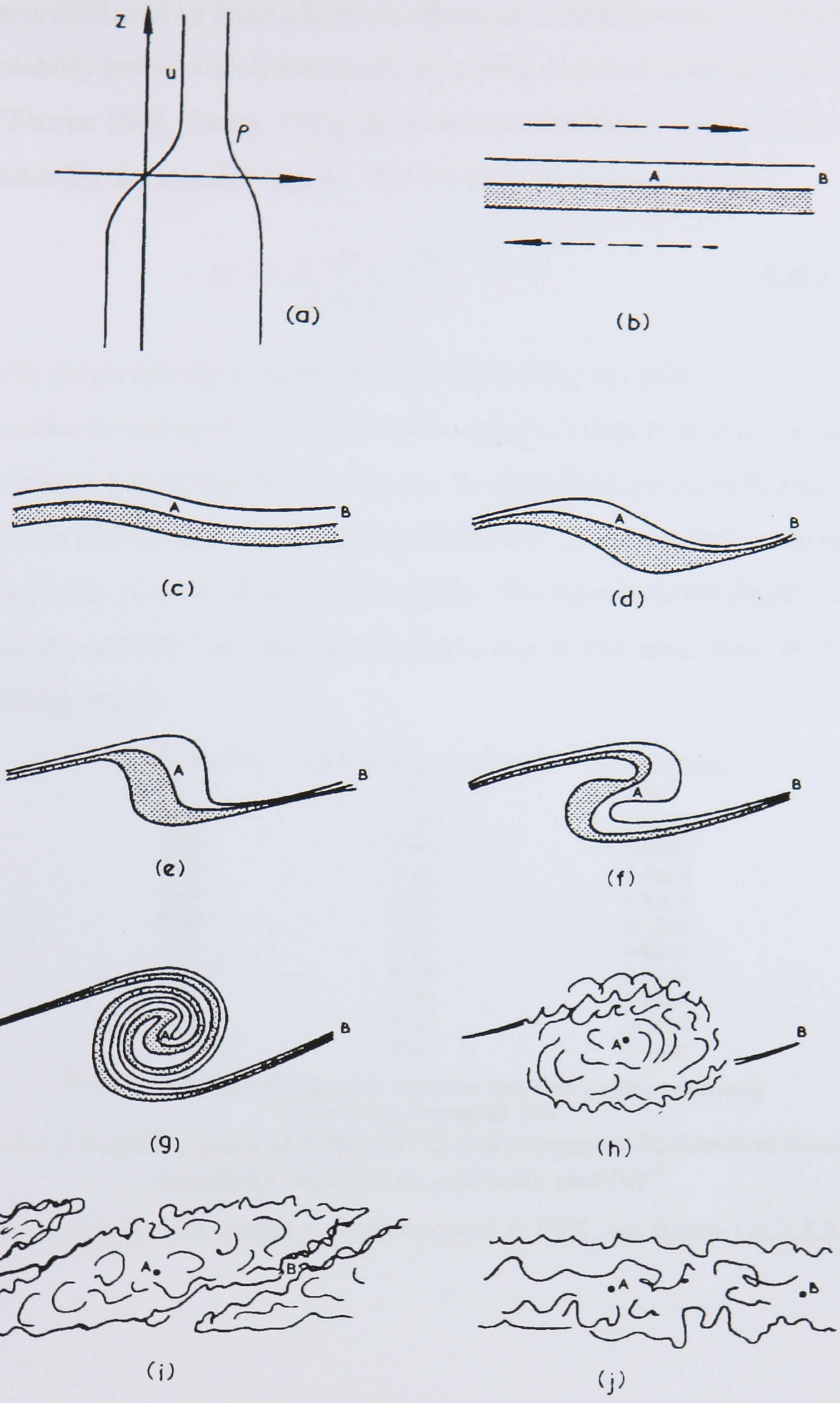

Fig. 3. The growth of disturbances. (*a*) The density ρ and velocity u distributions. (*b*) The lines mark a fluid of constant density; the points *A* and *B* are fixed; the arrows indicate the direction of flow. Drawings (*c*) to (*j*) show the development of instability. The points *A* and *B* remain fixed, and the lines continue to mark a fluid of constant density.

Figure 1.4.3.1.8 is figure 3 from [Thorpe 1969 B] and shows the type of wave motion and instabilities investigated by Thorpe that are similar to those see in figures 1.4.3.1.3 and 1.4.3.1.4

The Kelvin-Helmholtz theory was used to predict the time at which instability would be observed, the experiments used cine film to record the onset of instability. The predicted and observed times were stated to be very similar although no raw data was supplied. However the wavelength of the observed waves was significantly greater than that predicted, in [Thorpe

1969 A] this was attributed to finite amplitude effects or to development of Tollmien-Schlichting instability before Kelvin-Helmholtz instability, however again no raw data was supplied. In [Thorpe 1968, Thorpe 1971] the Richardson number is used to help determine the onset of instability for miscible liquids. The Richardson number (R_i) is:

$$R_i = -\frac{g}{\rho}\frac{d\rho}{dz}\Big/\left(\frac{du}{dz}\right)^2 \qquad (1.4.3.1.4)$$

The lower the R_i the greater the growth rate of the instability see table 1.4.3.1.2. The problem using the R_i number for immiscible liquids is that it requires a density gradient close to the interface. It could be argued that for CCC there is be a small region on both sides for the interface where the phases have not completely settled out due to successive mixing waves giving rise to a density gradient close to the interface. For the immiscible liquids used in CCC the density gradient could be very small giving rise to low R_i and hence rapid growth of the instability or mixing waves.

Wave-number α	Richardson number (J)	Growth rate (αc_i)
0·40	0·20	0·0446
0·40	0·15	0·0885
0·40	0·10	0·1264
0·40	0·05	0·1602
0·40	0·01	0·1848
0·44	0·20	0·0474
0·44	0·15	0·0896
0·44	0·10	0·1270
0·44	0·05	0·1606
0·44	0·01	0·1855

TABLE 1. The growth rates for the error function profiles of density and velocity, equation (11)

Table 1.4.3.1.2 is table 1 from [Thorpe 1971] and compares Richardson number with instability growth rate and wave number[vii]

This mechanism is clearly very similar to that observed in CCC see figure 1.4.3.1.9.

[vii] A wave number is the reciprocal of the wave length

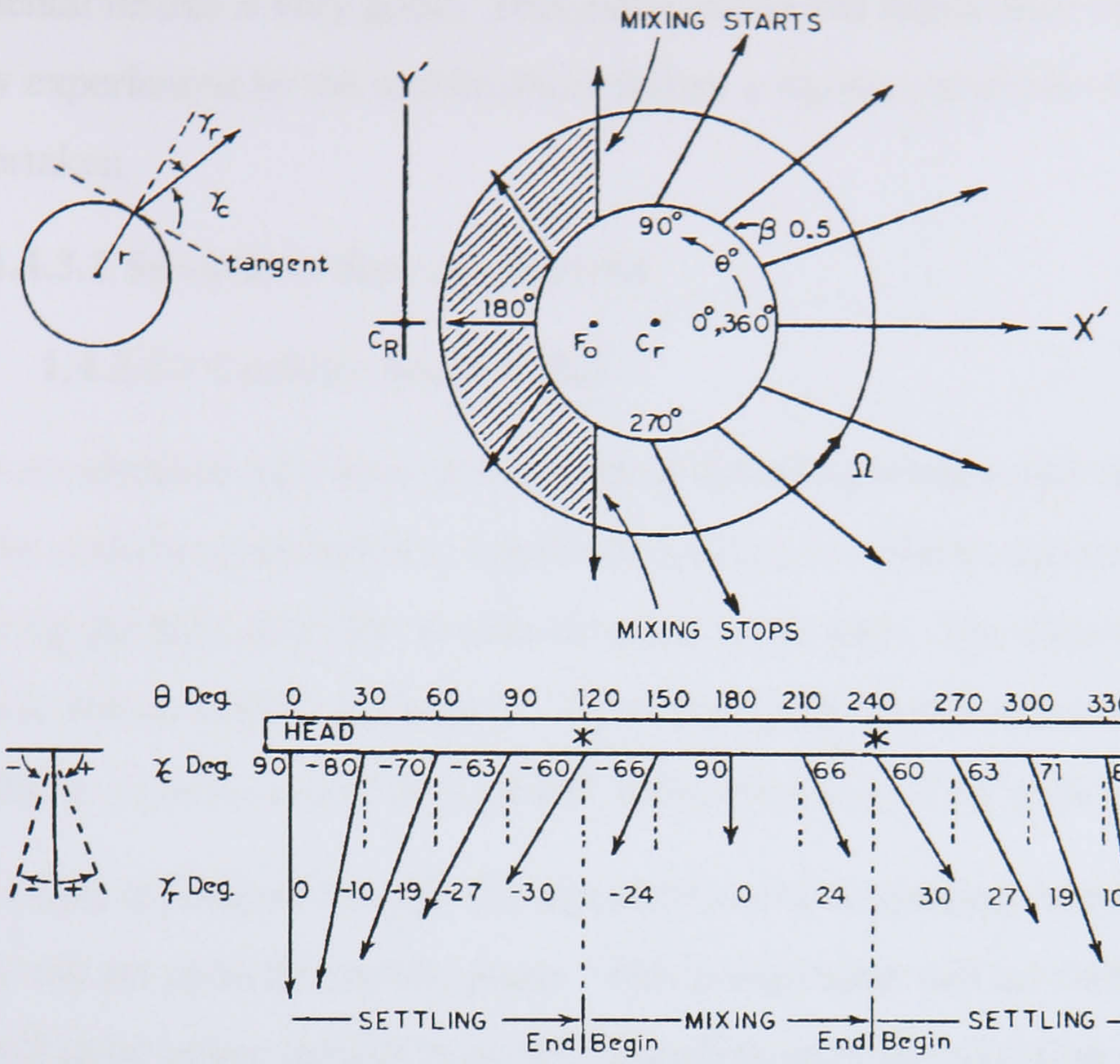

Relationship of γ_r and γ_c to a planet-gear column coil at $\beta = 0.5$ for acceleration-field vectors at 30° intervals of θ. Lower diagram shows the uncoiled column moving in a tailward direction relative to the field vectors.

Figure 1.4.3.1.9 shows how the resultant acceleration vector changes its angle relative to the coil tubing that is similar to a straight channel rocking to and fro [Conway 1990]

If the acceleration vectors in the above figure are repositioned vertically but the angle between the vector and the tubing is kept the same the tubing will no longer be horizontal and this is similar to a short length of tubing rocking to and fro. The short length of tubing will be horizontal at the 0° (distal key node), 180° (proximal key node) and the 360° (distal key node) positions. However, in CCC the channel cross-sectional area is much smaller, the time period for the mixing and settling to occur is very much shorter and the accelerations normal and tangential to the tube are much greater. Finally a paper written by Gardner and Kubie [Gardner 1975] details experiments similar to those conducted by Thorpe. These experiments conducted by Gardner and Kubie differ for those of Thorpe in two ways. The first difference is that a circular shaped section for the channel is used. The second difference is that the channel is inclined at a set angle i.e. the channel is not tilted from the horizontal. Pumping each phase separately up the inclined channel generates the flow of each phase. The theoretical analysis contained in this paper discusses various different conditions of flow between the two phases and equations are given for the flow velocities that separate these different flow conditions. These flow conditions are: stable interface at low relative velocity, droplet formation of the upper phase in the lower phase and turbulent flow of the upper phase while the lower phase remains laminar. The agreement between the theoretical analysis and

the experimental results is very good. This paper shows the importance of determining the type of flow experienced by the mobile phase before a rigorous analysis of the flow dynamics can be undertaken.

1.4.3.2 Secondary flow phenomena

1.4.3.2.1 Coriolis Acceleration

The coriolis acceleration acts upon an item that is travelling along a path when the path itself is rotating. The coriolis acceleration's magnitude is twice the relative speed of the item travelling along the path times the rotational speed of the path. The direction of the acceleration is always normal to the path. The sense of the direction is obtained by rotating the items relative velocity vector through 90° in the direction of the path's rotation.

The mobile phase is pumped through the coil and the coil is rotating, hence coriolis acceleration will act upon the mobile phase. This acceleration will act radially to the coil tubing. It will point either radially in or out depending upon the direction in which the mobile phase is pumped, head to tail or tail to head. The magnitude of this acceleration will depend upon the linear velocity of the mobile and will increase proportional with the velocity. As linear flow rates increase as the process is scaled up the affect of the coriolis acceleration will increase.

If the stationary phase is truly stationary, there is no relative motion between the stationary phase and the coil tubing, then the stationary phase will not experience a coriolis acceleration. However if the stationary phase does move relative to the tubing (ie back and forth) it will experience coriolis acceleration.

1.4.3.2.2 Secondary Flow due to flow through coiled tubing

For a liquid to flow through a curved length of tubing there must be a force acting radially inwards to provide an inward acceleration. In CCC this force is provided by the radial component of force see equation 1.4.1.2.3.1 plus a coriolis force due to the relative motion between the fluid and the tubing see section 1.4.3.2.1. Under the action of these radial forces the pressure near the outer wall is greater than the pressure close to the inner wall. Figure 1.4.3.2.2.1 simplifies the following explanation using only one liquid and rectangular section tubing.

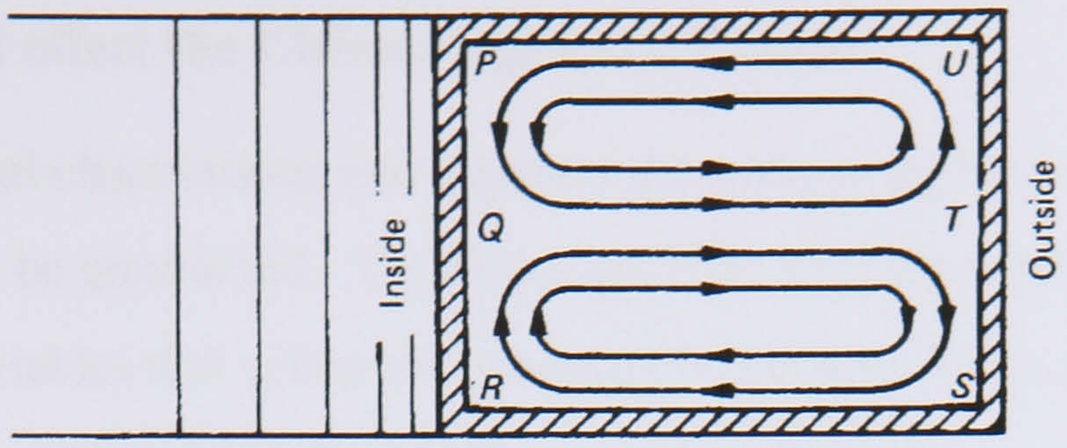

Figure 1.4.3.2.2.1 shows the secondary flow pattern for a single liquid flowing through curved rectangular section tubing. This diagram is taken from figure 7.10 of ref [Massey 1989]

Under the action of the radial acceleration the liquid wants to flow from the inner wall PQR to the outer wall UTS. Viscous drag from the boundaries is much greater close to the surfaces PU and RS than in the central region Q to T. Therefore the liquid flows much more easily from Q to T than from P to Q or R to S hence the flow pattern seen above. This flow pattern can be described as twin eddies. The liquid is also travelling axially along the tubing that produces a double spiral motion in three dimensions. Generally in CCC circular bore tubing is used which combined with a second immiscible liquid and a boundary gives the following flow pattern.

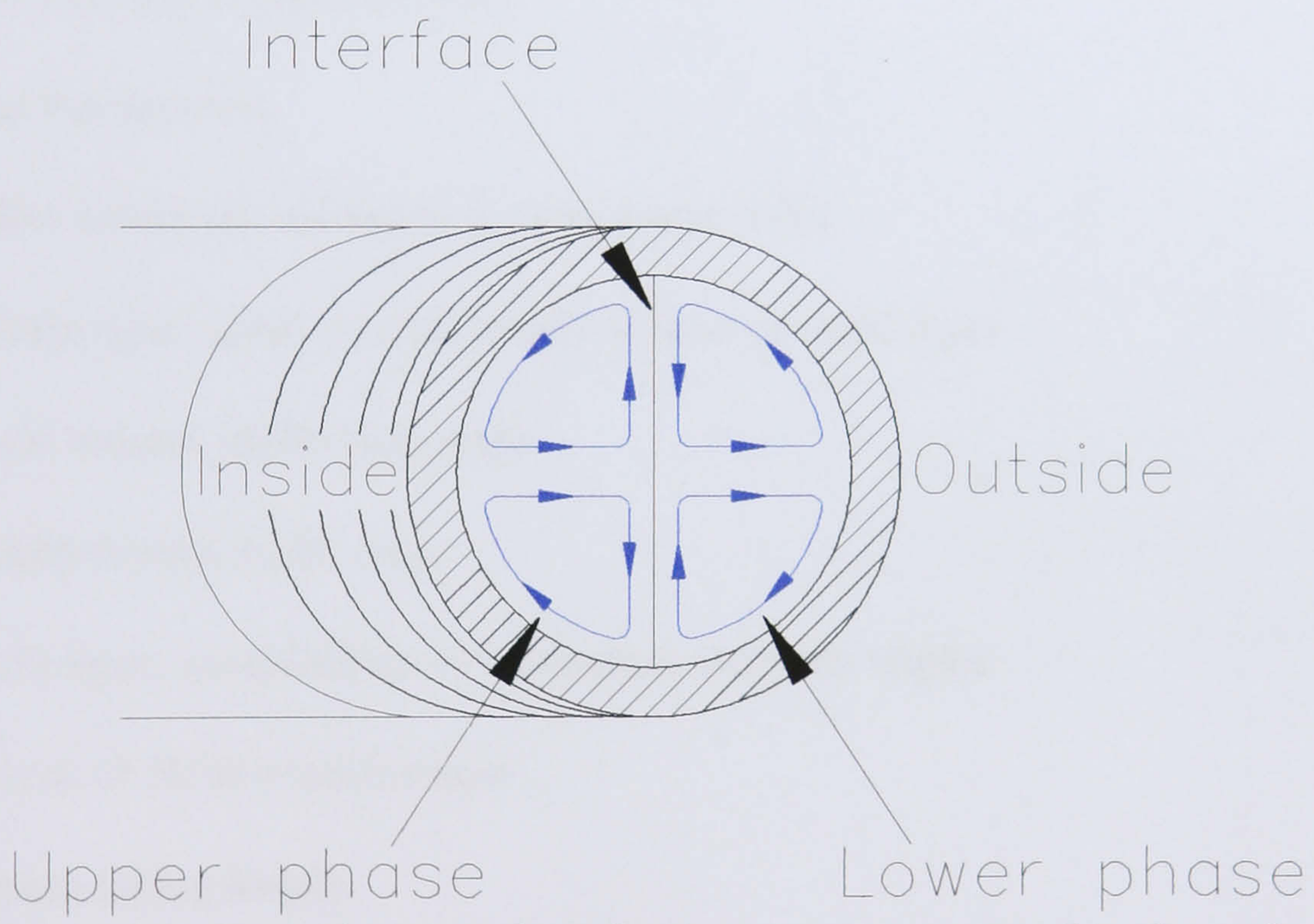

Figure 1.4.3.2.2.2 shows the secondary flow pattern encountered in the coil of a J-type centrifuge

The secondary flow of the upper phase may cause the initial disturbance of the interface that initiates wave growth on the approach to the proximal key node. The transverse flow of the upper and lower phases in opposite directions may also cause the interface to become unstable near the proximal key node. These secondary flow patterns may cause a sample component to evenly mix within a single liquid phase. This secondary mixing is important as tubing bores become bigger as the process is scaled-up since distances from the interface increase. However these effects are likely to small when compared to the primary flow.

1.5 The variables that effect the Chromatographic Process

To explain the anecdotal observations and improve the understanding of CCC an investigation of the process needs to be conducted. The major problem regarding such an investigation is the large number of variables that affect the process [Sutherland 2001A]. These variables or parameters can be broken down into four main groups, as follows:

Phase System

- Densities of upper and lower phases
- Viscosity of upper and lower phases
- Interfacial Tension

Rotor Parameters

- Planetary Radius (R)
- Maximum axial length of Bobbin
- Maximum rotational speed of Rotor

Coil/Column Parameters

- Coil Radius values (r) and hence β value range (r/R)
- Coil/Column type: spiral wound; axially wound or multi-layer
    - If spiral wound, inclination angle
    - If axially wound, helix angle
    - If multi-layer, combination of inclination and helix angles
- Coil/Column or Bobbin axial length
- Coil/Column tubing length
- Coil/Column tubing material
- Coil/Column tubing internal diameter (bore)
- Shape of Coil/Column cross section

Operational Variables

- Rotational Speed (rpm)
- Direction of Rotation (clockwise or anticlockwise)
- Choice of mobile phase (upper phase or lower phase)
- Mobile phase pumped flow rate (ml/min)
- Mobile phase direction of pumped flow (head to tail or tail to head)
- Process Temperature (°C)

The most important group of variables is the choice of phase system to use. This choice has the greatest influence on the separation to be conducted. The choice of phase system will depend upon the sample and the components of the sample to be separated. The combination of the phase system and the sample determines the number of mixing, settling and transfer stages that the sample must undergo for a given resolution. The correct selection of phase system will minimise the number of mixing, settling and transfer stages that the sample will need to undergo for a given resolution of separation. The next set of variables is the choice of Rotor Parameters (type of CCC machine to use). The choice of which Rotor to use will be determined by the type of separation required. For fast, high-resolution separations with small sample volumes (volumes in milligrams) use a high-speed (greater than 800rpm) analytical machine. For larger sample volumes (10-100 grams) use a preparative scale machine (800rpm maximum). The third sets of variables to use are the Coil/Column parameters. These parameters are controlled by the choice of coil. The final parameters to vary are the operational parameters. Table 5.1 lists all of the above variables and discusses each variable's probable effect upon the fluid mechanics and the separation.

1.5.1 Variables Effecting the Fluid Mechanics

Table 1.5.1.1 below lists the variables and describes the probable effect or effects upon the fluid mechanics and the differential partitioning process of the separation.

Variable	Effect upon Fluid Mechanics	Effect upon the Differential Partitioning Process
Speed of Rotation (ω radians/sec)	The induced accelerations acting upon the liquids increase with the square of the speed of rotation. Hence the fluid mechanics will be affected by some square function of the rotational speed. Another effect of the rotational speed is that it defines the period in which a single mixing and settling cycle must be completed. This time is inversely proportional to the rotational speed.	The total number of mixing and settling stages affects the resolution (R_s). R_s increases with the increasing number of mixing and settling stages. The total number of mixing and settling stages in a given time increases with the rotational speed, hence R_s is affected by rotational speed. Also increase "g" can inhibit wave mixing – so there is a trade off.
Rotor Radius (mm)	The induced accelerations acting upon the liquids are proportional to the rotor radius. Hence the fluid mechanics will be affected by some proportional function of the rotor radius.	A change in rotor radius will have to compensated by changing rotational speed to maintain the same "g" level. – hence the rate and wavelength of mixing and settling zones will change.

Variable	Effect upon Fluid Mechanics	Effect upon the Differential Partitioning Process
Rotor Orientation relative to the Earth's Gravitational Field	The Earth's Gravitational Field will influence the acceleration field produced by a spinning J-type planet centrifuge. The possible orientations of the Rotor assembly main axis are: vertical, horizontal and inclined at various angles in space. The influence is likely to be small due to the relative size of accelerations produced by a spinning centrifuge and that of the gravity.	
β value (ratio of rotor radius to bobbin radius)	The induced accelerations are proportional to the β value. Hence the fluid mechanics will be affected by some proportional function of the β value range. Also on a spiral the β value from point to point changes, hence the magnitude of the induced accelerations will change from point to point. For a layer on a multi-layer coil the β value is constant and hence the accelerations will be constant for that layer. For the next layer the accelerations will be different but still constant for that next layer.	Ito[1984] has shown that β value can affect the head tail relationship

Variable	Effect upon Fluid Mechanics	Effect upon the Differential Partitioning Process
Tube internal diameter (mm)	The internal diameter of the coil tubing has a number of effects. It determines the pressure drop across a coil for a given pumped flow rate and phase system. It also defines the settling distance. More importantly it defines the boundaries to the fluid mechanics. In the Kelvin-Helmholtz analysis boundaries encourage the onset of instability and the closer the boundaries the more unstable a wave becomes [Craik 1982]. However the smaller the internal diameter the slower the liquids can move and hence the less likely an unstable relative flow velocity will be achieved.	Surface effects at small bore and bulk fluid effects at large bore
Tube internal roughness factor (μm)	The internal roughness factor for the internal surface of the tube helps to define the pressure drop across a coil.	

Variable	Effect upon Fluid Mechanics	Effect upon the Differential Partitioning Process
Tube stiffness	If the tube is not stiff enough it will deform under the action of the acceleration field and the induced fluid motions. All polymers that are not re-enforced deform with time when exposed to uni-directional forces for extended periods. The Radial acceleration's magnitude varies with the angular position and above a β value of 0.25 the direction does not reverse. Hence for β values above 0.25 the radial acceleration generates a uni-directional force of varying magnitude that will differentially stretch the tubing. The Tangential acceleration's magnitude varies with the angular position and the direction reverses at the proximal and distal key nodes. The tangential acceleration compresses the tubing longitudinally about the proximal key node and stretches the tubing about the distal key node. Hence the tangential acceleration induces a cyclic fatigue loading in the tubing. The combined effect of these accelerations is to weaken and stretch the tubing. The stretching and weakening of the tubing in turn affects the fluid motions and the CCC process. The stiffness of the tubing also partly determines the induced pressure that the tubing can withstand. The higher the mobile phase flow rate the higher the induced back pressure therefore tube stiffness partly determines the maximum mobile phase pumped flow rate.	

Variable	Effect upon Fluid Mechanics	Effect upon the Differential Partitioning Process
Tube Material	The material from which the tubing is made will affect the tube stiffness, internal roughness factor and contact properties with the phase system. The stronger the material used the stronger the tubing will be hence the greater pressure the tubing will be able to withstand. This will allow higher mobile flow rates to be used that may lead to better mixing. The internal roughness factor and the contact properties will effect the adhesion of the phases to the tubing walls this in turn will effect the fluid mechanics.	
Tube length (m)	The pressure drop across a coil, for a given internal diameter, is proportional to its length. The combination of tube length, tube internal diameter, internal roughness and the tube safe working pressure define which liquids can be pumped through at given flow rates. The tube length also affects the resolution of the CCC process since the length determines the number of mixing and settling zones in a coil.	The length of tubing in a coil also partly determines the resolution of a separation. The longer the coiled length the greater the resolution. It must also be remembered that the longer the tube the greater the process time will be for a given separation.

Variable	Effect upon Fluid Mechanics	Effect upon the Differential Partitioning Process
Tube inclination angle, degrees (Spiral wound coils). Spiral wound coils are wound radially on a bobbin.	The inclination angle is the angle between the tube axis and an imaginary cylindrical surface for a given radius. As the coil radius increases the inclination angle will decrease. Hence a spiral coil will have a range of inclination angles. The inclination angle determines the gradient that the liquid will be pumped up or down (up hill or down hill). The direction of up or down is controlled by the pumping direction of the mobile phase.	
Tube helix angle, degrees (Axially wound coils). Layer would coils are wound axially on a bobbin.	The helix angle is the angle between the tube axis and a transverse plane normal to the bobbin's rotational axis. This helix angle determines the effect that Archimedean screw action has upon the fluid mechanics. On traditionally wound coils the helix angle has been determined by the outside diameter (O.D.) of the tubing. The helix angle decreases as the mean radius of a layer increases. The angle also reverses from one layer to the next (but not with respect to the head/tail relationship).	
Coil volume (ml)	The coil volume combined with stationary phase retention defines the amount of stationary phase in a coil under hydrodynamic equilibrium.	

Variable	Effect upon Fluid Mechanics	Effect upon the Differential Partitioning Process
Direction of Coil Winding combined with the direction of rotation	The direction of rotation plus the direction of the coils winding defines which end of the coil is the head and which end is the tail. In the case of a spiral coil if the J-type centrifuge is rotated in the same direction as the coil is wound (winding from centre to periphery) the head is at the centre and the tail is at the periphery. This in turn effects the stationary phase retention see section 1.4.2.3.	
Pumped Flow rate (ml/min)	Increasing the pumped flow rate of the mobile phase decreases the stationary phase retention, increases the pressure drop across the coil and increases the effect of the Coriolis acceleration. However it also increases the mean velocity of the mobile phase over the stationary phase and will increase the amount of mixing per loop but also reduces the number of mixing and settling stages for a peak before the peak is eluted from a coil.	

Variable	Effect upon Fluid Mechanics	Effect upon the Differential Partitioning Process
Direction of pumped flow Head to tail or tail to head	The direction of pumped flow can radically affect the stationary phase retention. Changing the flow direction can cause the stationary phase retention to drop from as much as 80% to as low as 0%. The direction in which the coil was wound relative to the direction of rotation and direction of pumping will determine the final acceleration that will be produced upon the liquids. In one combination of the above factors the linear velocity of the mobile phase adds to the total induced acceleration. In another combination this velocity subtracts from the total induced acceleration. The acceleration causing the addition or subtraction is called the Coriolis acceleration. The Coriolis acceleration is adding to or subtracting from the radial acceleration, see section 1.4.3.2.1.	
Densities of upper and lower phases (g/ml)	The relative densities of the upper and lower phases will have an effect upon the fluid dynamics. If these two densities were equal the forces acting upon the upper and lower phases would also be equal and the only relative motion between the phases would be from the pumped flow of the mobile phase. However with vastly different densities the forces acting upon each phase would be vastly different. Hence there would be relative motion between the two phases as they are pushed towards the preferred positions at the head and tail ends of a coil. The pumped flow of the mobile phase would be superimposed over this relative motion.	

Variable	Effect upon Fluid Mechanics	Effect upon the Differential Partitioning Process
Viscosity's of upper and lower phases (centipoises)	The viscosity of a liquid is a resistance to its flow. The higher the viscosity the higher the force required to achieve a given flow. Hence high viscosity liquids will require higher induced accelerations to achieve flows that are unstable and for the on set of mixing to occur. The viscosity of the second phase also affects the motion of the first phase since the second phase has to be displaced by the first phase. The converse could also true. Viscosity also can act to increase the likelihood of instability as it causes eddies in waves formed in shallows, where the wave height is close to the depth of liquid in which the wave is formed and turbulence [Craik 1982].	
Upper and lower phase compressibility.	The compressibility of the phases may affect the CCC process itself if the tube's mechanical stiffness is not great enough. This all depends upon the pressures developed in the system. If a phase does compress its density will change and possibly its viscosity. Fortunately most liquids can be regarded as incompressible under the pressures developed during CCC.	

Variable	Effect upon Fluid Mechanics	Effect upon the Differential Partitioning Process
Interfacial tension between upper and lower phases	Interfacial tension tries to minimise the interfacial area between the two phases. Put simply, the interfacial tension tries to damp the motion of interfacial waves. A phase system with a low interfacial tension will more readily mix than a system with a high interfacial tension. The Kelvin-Helmholtz threshold velocity is proportional to the fourth root of the interfacial tension. The settling time of the high interfacial tension phase system will be quicker than that of the low interfacial tension phase system. It must be remember that the interfacial tension of a phase system increases with the immiscibility of the two phase of the phase system.	
Additions of tertiary and quaternary solvents such as Acetic Acid	Acetic Acid is added to a number of two-phase systems to help partition the product being processed. The proportions of the two solvents and additives are known for the system overall. Adding an additive to a solvent system will change the solvents' densities, viscosities and the interfacial tension between the solvents, which in turn will affect the solvents system's behaviour in the CCC process. One known effect of adding acetic acid is that it shortens the settling time.	Additives (tertiary and quaternary solvents) also effect the partitioning of sample components between the phases; this is the main reason why tertiary and quaternary phases are added. These additives can increase the separation between distribution constants of adjacent components of a sample. Effectively these additives can increase the resolution of a separation.

Variable	Effect upon Fluid Mechanics	Effect upon the Differential Partitioning Process
Stationary phase Retention in coil %	It is not known if retention is constant through out a loop of a helical coil or if it is different at each position within such a loop. The retention affects the fluid mechanics by determining the volumes of the two solvents in a coil or a single winding. The mean velocity of flow of the mobile phase through the coil is also determined by the stationary phase retention for a given tube internal diameter. This will also affect any relative motion between the two phases.	For a given coil the higher the retention the greater the resolution of a separation.
pH	Changes in pH of the phase system can cause the distribution constants of the various components in a sample to change causing the separation of the components to change accordingly. The stationary phases uses a retainer acid (or base) while the mobile phase uses an eluent acid (or base) [Ito 1995]. As the mobile phase moves through a coil the two acids chemically react changing the pH along the length of the coil allowing different sample components to be extracted at different times according to the acidity and hydrophobicity of each component. The pH of a phase system can also be affected by the sample components and may require the use of chemical buffers.	Changes the distribute constants of the sample components.

Variable	Effect upon Fluid Mechanics	Effect upon the Differential Partitioning Process
Dynamic balance of the rotating parts of the Counter Current Chromatography	If a CCC machine is perfectly dynamically balanced the machine will not vibrate and will be silent while running. If the same machine was not dynamically balanced it will vibrate and generate a lot of noise. The amount of vibration and noise is proportional to the degree of imbalance. No machine can ever be perfectly dynamically balanced; hence there will always be some vibration. Vibration will affect the fluid dynamics and hence the CCC process. Such effects can be minimised by dynamically balancing the machine as much as possible. This will mean the induced acceleration will be due to the motion of the planet centrifuge only, which is predictable. Since this vibration is a source of error it therefore needs to be controlled for the results to be scientifically rigorous and for the process to have improved repeatability.	Vibration could induce more mixing and hence affect the mass transfer between the phases.
Induced Pressure	The induced pressure inside a section of coil tubing will affect the fluid mechanics of the phase system in that section. The induced pressure has two sources: the first is the accumulative effect of pumping a liquid through a long narrow piece of tubing and the second is from the induced accelerations, which vary with the β value.	

Variable	Effect upon Fluid Mechanics	Effect upon the Differential Partitioning Process
Temperature (°C)	As the temperature increases a two-phase solvent system can form one phase and the whole CCC process stops. As the ambient temperature increases the viscosity of the solvents will decrease. The temperature of the mobile phase is likely to increase as it is pumped through the coil since it accumulates the amount of work that it has had done to it. Some of this heat energy will be transferred to the adjacent stationary phase. Therefore the viscosities of both phases are likely to decrease the further their position through a coil. The lower the viscosity of both phases the greater the amount of mixing and the shorter the settling time. For repeatable results the temperature should be controlled as this affects both the fluid mechanics and the differential partitioning. When the process is scaled-up for manufacturing repeatability is a prime goal therefore temperature control is a must.	Solubility of the sample changes with temperature in one or both solvent phases. This will affect the resolution of a separation. Increased temperature will also increase the diffusion rate (mass transfer rate) of sample components between the solvent phases and hence increase the speed of a separation for a given resolution.

Variable	Effect upon Fluid Mechanics	Effect upon the Differential Partitioning Process
Atmospheric Pressure (mmHg)	The atmospheric pressure may affect the fluid dynamics but this is likely to be a small effect. At low atmospheric pressure cavitation may occur as it does in other pieces of rotodynamic equipment (pumps and turbines). The induced pressures in the coil are likely to be much greater than fluctuations in atmospheric pressure. The atmospheric pressure at each end of the coil will also be the same.	Cavitation (the formation of bubbles) could cause a loss of stationary phase retention and reduce the amount of mobile phase in the coil effectively lowering the coil volume and the resolution of a separation.
Relative Humidity %	The relative humidity will affect the stiffness of the PTFE tubing that may in turn affect the fluid motion. Again, this is liable to be a small effect.	

1.6 Concluding Remarks

The Introduction and literature review has shown that the retention of the stationary phase is an important variable of the CCC process, that it is not fully understood and cannot be predicted from the range of variables listed in Section 1.5.1. Summarising conclusions from section 1.4.2.6 it appears that Du has found the correct stationary phase retention characteristic for both normal and reverse phase modes. This characteristic plots stationary phase retention against the square root of mobile phase flow rate. In section 1.5.1 of the Literature Review a number of the variables listed affect the retention. Understanding stationary phase retention and thus being able to predict the retention will enable large scale manufacturing centrifuges to be designed that when built will perform as planned. The basic aim of the following chapters is to investigate retention and to develop an understanding of how it is affected by various parameters and eventually allow the retention, and hence sample elution characteristics in CCC, to be predicted based upon the Du retention characteristic.

Chapter 2 Methods and Materials

2.1 Summary

This chapter describes the materials and test methods used in the research work reported in this thesis. It describes the phase systems used and the method by which these systems are made up. The measurement of the phase system physical properties is also described; these properties are densities, viscosity and interfacial tension. Test methods for the measurement of stationary phase retention are described for both normal and reverse phase mode. The method for conducting the head and tail study on three helical FEP, Fluorinated Ethylene Propylene, coils is also discussed.

The majority of the densities, viscosities and interfacial tensions of the phase systems used in this study were already known and measured by Prins and Timmers [Prins 1998, Timmers 2001]. The measurement tests for these properties are included in this document to verify that the physical properties of the phase systems used did not change significantly during the retention tests and the Head/Tail studies in this thesis.

The J-type centrifuge used in the research was a modified Brunel CCC. The main modification was fitting a more powerful drive motor to allow the centrifuge to rotate at speeds up to 1200rpm; the standard version has a maximum rotational speed of 800rpm. The rotor or solar radius was unmodified and remains 110mm. The rotor design was also unchanged see figures 1.4.1.3.3 and 1.4.1.3.4. The descriptions of the various coils under test are described in the appropriate chapters.

2.2 Phases systems and Degassing of the Phase systems

Table 2.2.1 shows all the used phase systems, the components and the component ratios. Table 2.2.2 shows the densities, viscosities and interfacial tension for each of the phase systems listed in table 2.2.1.

All the solvents used are either "Analar" or " Chromatography" grade. The water used was laboratory standard "purite" water that has been filtered by reverse osmosis.

Phase System	Solvents	Ratios
4A	Heptane-Ethyl Acetate-Methanol-Water	1.4:0.1:0.5:1
4B	Heptane-Ethyl Acetate-Methanol-Water	1.4:0.6:1:1
4C	Heptane-Ethyl Acetate-Methanol-Water	1.4:4.5:1:1

Table 2.2.1 showing the chemical composition of the Phase Systems and the ratios of the various components [Wood 2001A]

Phase System	Density kg/m^3	Density Diff. kg/m^3	Dynamic Viscosity cp (mNs/m^2)	Interfacial Tension mN/m
4A Upper	679	268	0.36	17.8
4A Lower	947		1.36	
4B Upper	708	230	0.35	6.2
4B Lower	938		1.35	
4C Upper	833	98	0.42	1.1
4C Lower	931		1.35	

Table 2.2.2 showing the Physical Properties of the Phase Systems, at 30°C, this table was taken from [Wood 2001A]

2.2.1 Making up a phase system

2.2.1.1 Apparatus

- Desired measuring cylinders (100 ml/500 ml/etc) for each component,
- Pipette for each component,
- 10 litre aspiration flask to store phases system in (500 ml/1000 ml/2000 ml/ etc) and a rubber stopper,
- Large Stainless steel funnel.

2.2.1.2 Procedure

1. Fill out a COSHH (Risk Assessment) Form stating all the components and hazards.
2. From the component ratio, calculate the amount of liquid needed for each component. For example, the component ratio is 4/1/4 parts. For example, if 9 litres of solvent system is to be made up, 4 litres of the first component would be used followed by 1 litre of the second component and finally 4 litres of the third component.
3. Always wear a laboratory coat, gloves and goggles when making up a phase system. Always perform this task in a fume cupboard in case of solvent spillages.
4. Measure out the required volume of each component in a separate clean measuring cylinder. Adjust the desired volume of each component with a pipette. If too much of a component has been used, do not pour it back into the solvent bottle but dispose of it in a waste container, see below.
5. Use a large stainless steel or glass funnel to pour each component into a 10litre aspiration flask. Remove funnel and place the bung in the opening of the flask. Carefully shake the flask to ensure that both phases mix thoroughly.
6. Before a phase system can be used it must be degassed, using a vacuum degasser see section 2.2.2, and then left for a minimum of 12 hours to equilibrate at the temperature at which it will be used. If the upper and lower phases are decanted into different containers and each container only holds a single phase then these containers can be stored at room temperature. However if the phase system is stored in one container, this container must be stored at the temperature at which the solvents system is to be used. If it is not stored in this manner, the solvent system will be constantly re-equilibrating, changing the various amounts of its constituent solvent components, as the temperature changes. This means that the physical and chemical properties of the

upper and lower phases will change with temperature and this is a source of experimental error.

2.2.1.3 Waste Containers (Waste-Winchesters)

If waste has been generated while testing or making up a phase system, dispose of waste in a waste-Winchester using a stainless steel or glass funnel. Always label waste-Winchesters with the appropriate hazard stickers, listing the ingredients.

2.2.1.4 Solvent Recycling

A chemical becomes waste when it has been contaminated with other chemicals, i.e. impurities or sample material. Therefore, when a phase, or phase system, has remained pure during a retention test, it can be reused for further tests once it has been degassed and re-equilibrated at the operational temperature for a minimum of 12 hours.

2.2.2 Solvent Degassing

Both the upper and lower phases of a solvent system need to be degassed before they can be used in a J-type centrifuge. The solvents need to be degassed before use because air bubbles have been observed in the downstream flying lead when un-degassed solvents have been used. The air bubbles have caused errors in the measurement of stationary phase retention.

2.2.2.1 Apparatus

- Two 10-litre aspirator flasks to store phases system in and a rubber stopper,
- Large Stainless steel funnel,
- Vacuum degasser, Jones Chromatography 7600 series D-Gasser,
- Gilson 302 HPLC pump with a 100ml pump head,
- Mobile and stationary phase containers.

2.2.2.2 Degassing Procedure

1. Using a large stainless steel funnel pour the solvents that are to be degassed in the lower 10-litre aspirator flask that is connected to the inlet of a Gilson 302 HPLC pump, see figure 2.2.2.2.1.
2. Check that the all the lines between the two 10-litre aspirator flasks are primed with solvent. It may be necessary to activate the priming function on the Gilson pump. Any solvent pumped through the system should be collected in

a glass container and poured back into the lower 10-litre aspirator flask when priming is complete.

3. Ensure the ends of the three outlet tubes from the degasser are touching the bottom of the upper 10-litre aspirator flask, this minimises the formation of air bubbles that would cause the solvents to absorb gas.

4. Switch the degasser and HPLC pump on. The maximum flow rate through a vacuum degassing unit is 4ml/min/channel. It will take a minimum of 12.5 hours for nine litres of phase system to be degassed using a three-channel degasser.

5. Once degassing of the solvents is complete the degassing unit and the Gilson pump should be switched off. Care should then be taken when decanting the upper and lower phases into mobile and stationary phase containers. Air bubbles should not be allowed to form. Also, once decanted, there should not be more than one phase in a mobile or stationary phase container. If both phases are present the composition of the mobile or stationary phase will change with temperature, this will change the phase's physical and chemical properties that will cause errors in results.

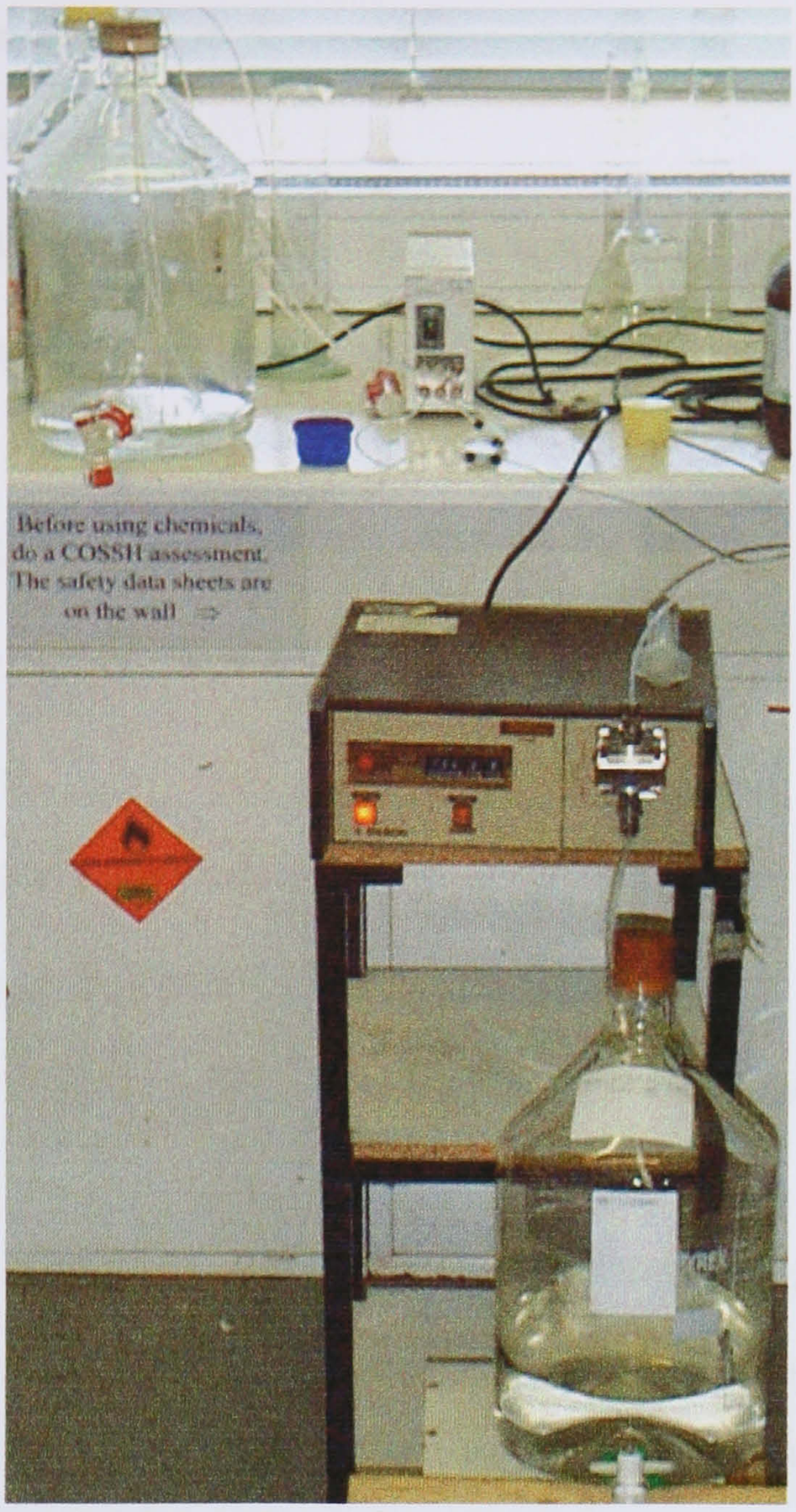

Figure 2.2.2.2.1 shows the solvent degassing set up

2.3 Density

Density is defined according to the following equation:

$$\rho = \frac{mass}{volume} \tag{2.3.1}$$

To measure the density of a liquid at a certain temperature, take an accurate known volume and measures its mass. Equation 2.3.1 yields the density of the fluid; the measurement error can be calculated using equation 2.3.2:

$$\Delta\rho = \pm\rho \cdot \left(\frac{\Delta m}{m} + \frac{\Delta V}{V} \right) \tag{2.3.2}$$

2.3.1 Density of a fluid at 30 °C

2.3.1.1 Apparatus

- Temperature controlled water bath (Grant Instruments);
- Volumetric flask (e.g. 100 ml) and stopper;
- Accurate balance (Precisa 80 A – 200 M, see [Prins 1998]);
- Thermocouple and thermocouple meter;
- Pipette and pipetter;
- Drying cloth/paper.

2.3.1.2 Measurement procedure

1. Measure the mass of the clean dry flask and stopper.
2. Fill the flask with fluid; do not fill completely as fluid will expand slightly when heated to 30 °C.
3. Heat up the flask in the water bath to 30° C, using thermocouple to check temperature.
4. When at 30° C, remove flask from water bath, dry the flasks external surfaces and add or remove solvent until the correct volume to 100 ml is obtained.
5. Weigh the flask, stopper and liquid. Subtract weight of flask and stopper to obtain the mass of the liquid and use equation 2.3.1 to obtain the density.

After density tests, the phase systems can be recycled.

2.4 Viscosity

There are two definitions of viscosity: *dynamic* (or absolute) viscosity (μ) and *kinematic* viscosity (ν). These two are related by the density of the fluid:

$$\mu = \rho \cdot \upsilon \qquad (2.4.1)$$

The most commonly used unit for dynamic viscosity is the *poise* (p), which is 1g/cm.s. The common unit for kinematic viscosity is the *stoke* (St) which is 1 cm^2/s.

Dynamic viscosity is defined as follows: the ratio of the shearing stress to the rate of change of shearing strain. The following equation illustrates this:

$$\mu = \frac{F \; A}{dv \; dy} \qquad (2.4.2)$$

Dynamic viscosity quantifies the force (F) that must be exerted to cause one layer of fluid to slide past another, or to cause one (solid) surface to slide past another, if there is a layer of fluid between the solid surfaces. To measure kinematic viscosity, one uses a device similar to that shown in figure 2.4.1.1.1.

The measurement of kinematic viscosity for Newtonian liquids is done using a capillary viscometer, where a certain amount of fluid flows through a bulb and a capillary tube. The time needed for the liquid to pass through this capillary tube is called the Efflux time (t). The kinematic viscosity is obtained by using the following equation:

$$\upsilon = C \cdot t \tag{2.4.3}$$

The viscometer constant (C) is obtained by calibration with a fluid of known viscosity (i.e. deionised water). To obtain reproducible results, the same volume of liquid should be used for all measurements (including calibration). The error can be calculated with equation 2.4.4:

$$\Delta\upsilon = \pm\upsilon \cdot \left(\frac{\Delta C}{C} + \frac{\Delta t}{t} \right) \tag{2.4.4}$$

When calculating dynamic viscosity, the following error is introduced:

$$\Delta\mu = \pm\mu \cdot \left(\frac{\Delta\rho}{\rho} + \frac{\Delta\upsilon}{\upsilon} \right) \tag{2.4.5}$$

2.4.1 Viscosity of a fluid at 30 °C

2.4.1.1 Apparatus

- Capillary viscometer (Cannon-Fenske) as depicted in figure 2.4.1.1.1; preferably calibrated;
- Temperature controlled water bath (Grant Instruments);
- 0°C to 100 °C thermometer;
- Stopwatch;
- 25/50 ml flask;
- Tubing and pipetter;
- Retort stand;
- Ethanol;

- Distilled/deionised water;
- Oven to dry viscometers.

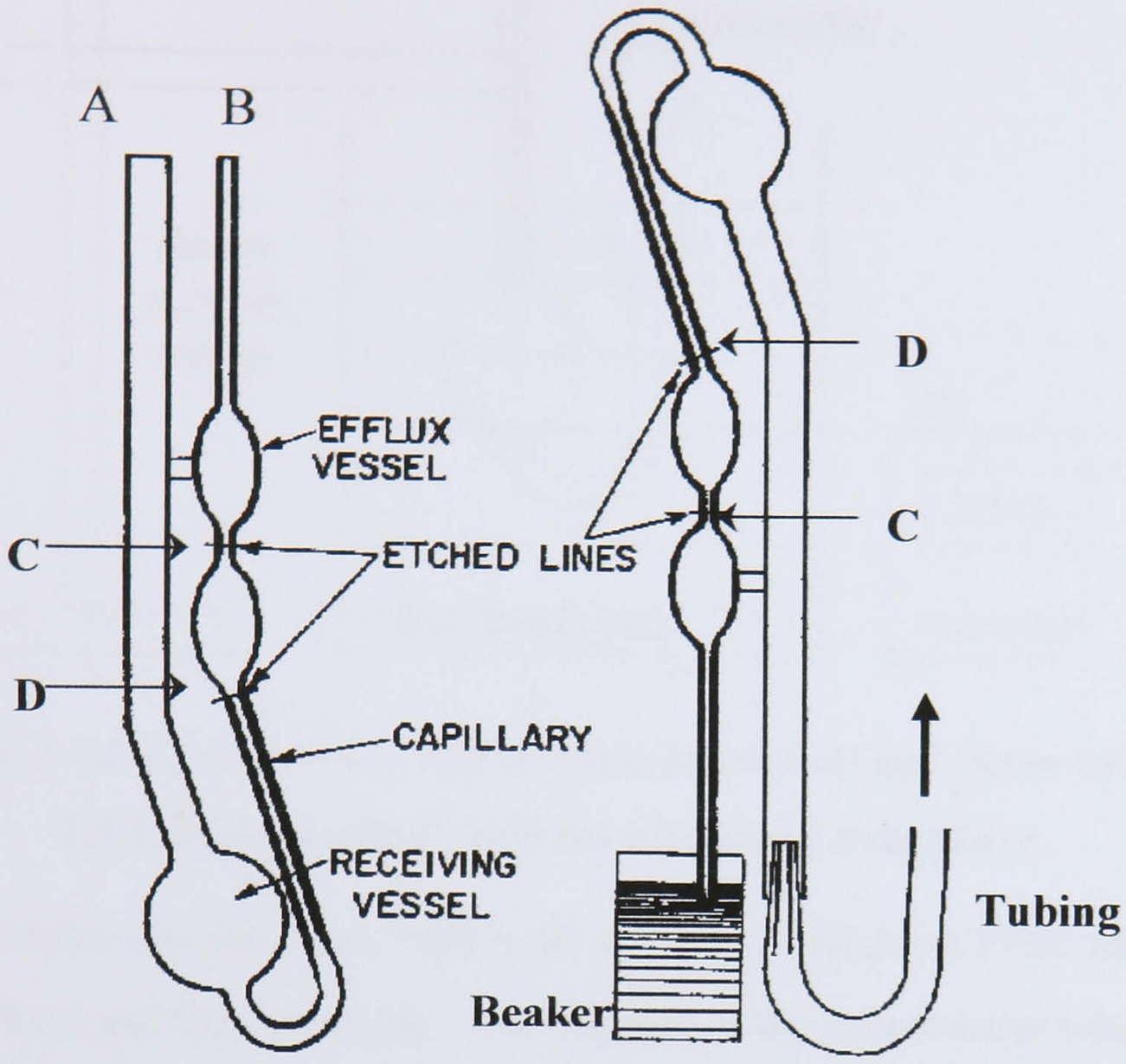

Figure 2.4.1.1.1 Cannon-Fenske viscometer for transparent liquids. Filling technique is shown on the right. 'A' and 'B' are openings. 'C' and 'D' are the etched marks; figure taken from [Timmers 2001]

The Cannon-Fenske viscometers listed in table 2.4.1.1.1 were used. The pre-calibrated viscometers are delivered with instruction sheets and calibration certificates. The calibration certificate shows the viscometer constants and the instruction sheet shows the correct measurement procedure to use.

Size	Viscosity range [cSt]	Pre-calibrated	Viscometer No.	Viscometer constant C (cSt/s)
25	0.4 – 1.6	No	156	0.0001T+0.0134[viii]
50	0.8 – 3.2	No	113	0.011[i]
25	0.5 – 2	Yes	F439	0.00187
50	0.8 – 4	Yes	Y664	0.003765

Table 2.4.1.1.1 Specifications of the Cannon-Fenske viscometers

The experimental set up for calibration and measurement is shown in figure 2.4.1.1.2.

[viii] The T in the formula for the viscometer constant is the absolute temperature (°K) of the liquid at which the measurement is taken. The viscometer constants for the uncertified viscometers were determined by Timmers [2001].

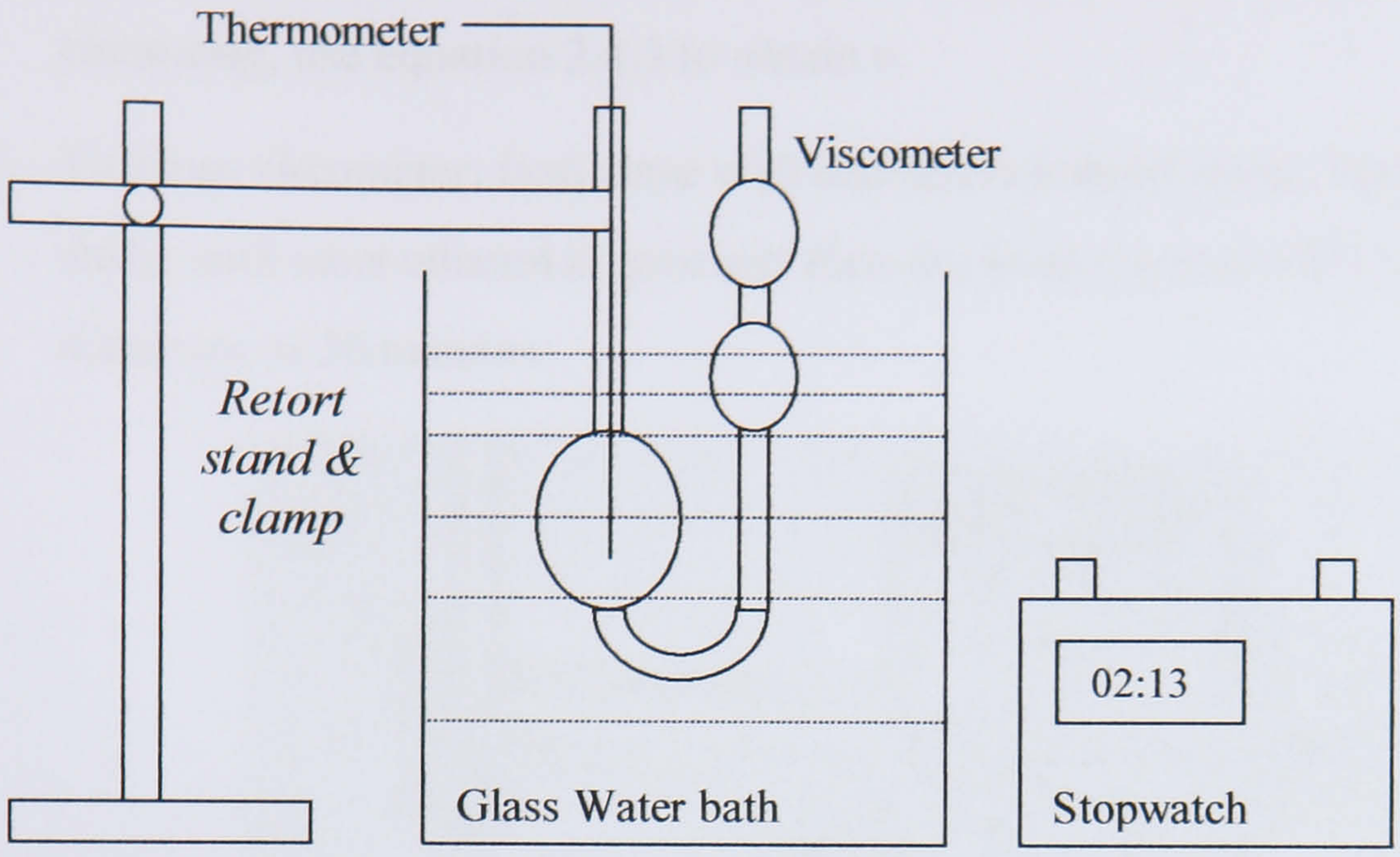

Figure 2.4.1.1.2 Schematic view of experimental set up; figure taken from [Timmers 2001]

2.4.1.2 Calibration[ix] and measurement procedure

1. Make sure the water bath is set at 30.0°C. Heat up 25/50 ml flask to 30°C using water bath and thermocouple. Use distilled or deionised water when calibrating size 25 and size 50, use more viscous fluids (oils) for size 50 and 100.

2. Fill viscometer as in figure 2.4.1.1.1 using a pipette, not shown, connected to the tubing shown and fill until the liquid has reached the mark D. Filling to the Mark D ensures that the viscometer is filled with the same volume of solvent for each test and that consistent readings are obtained.

3. Turn viscometer upright, as per the left hand side of figure 2.4.1.1.1and place in water bath as in figure 2.4.1.1.2 ensure that the mark C is below the water surface see figure 2.4.1.1.2. Remove tubing and pipette.

4. Leave the viscometer in the water bath for a minimum of 20 minutes to allow the viscometer and liquid to equilibrate at 30°C before starting the calibration or measurement.

5. Reconnect the tubing and pipetter to the viscometer as before, pull the meniscus of the liquid above mark C and disconnect the tubing and pipetter.

6. Start the stopwatch when meniscus passes mark C.

[ix] Only applies to the un-calibrated viscometers.

7. Stop the stopwatch when meniscus passes mark D. The time obtained is the efflux time. When calibrating, use equation 2.4.3 to obtain the viscometer constant. When measuring, use equation 2.4.3 to obtain υ.

8. To clean viscometer: first, rinse with distilled/deionised water, then rinse with ethanol, shake until most ethanol is gone and then dry in an oven, at 60°C to 80°C, for a minimum of 30 minutes.

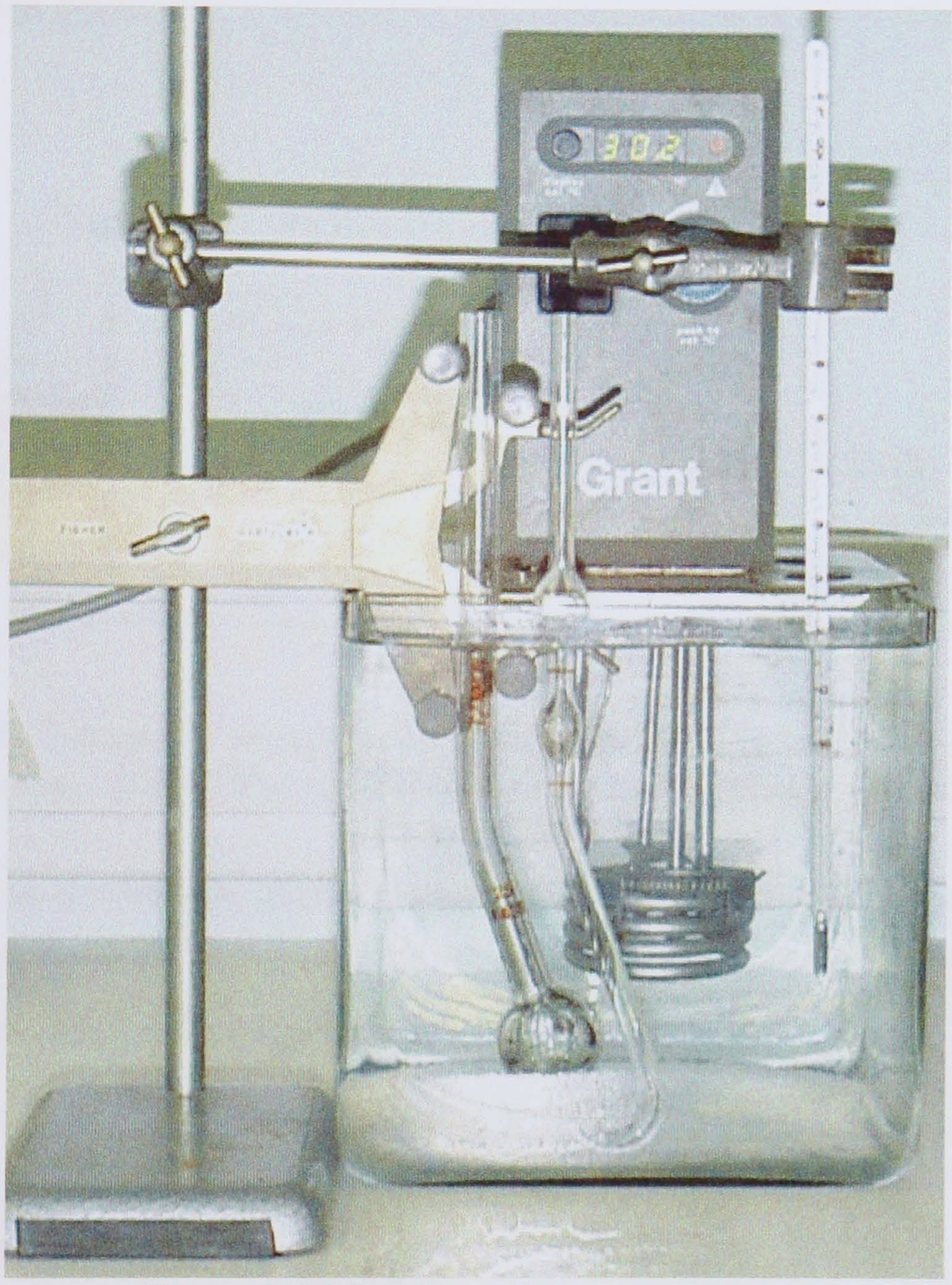

Figure 2.4.1.2.1 shows the viscosity test rig

Always use the appropriate viscometer size, see table 2.4.1.1.1 for viscosity ranges. Each size requires its own calibration. Calibrate the viscometer at different temperatures, for example 25 °C, 28 °C, 30 °C and 32 °C. Construct a calibration graph from such results. With some sizes the calibration constant remains the same at different temperatures, meaning that it is not necessary to calibrate at different temperatures.

2.5 Interfacial tension

If two immiscible fluids are present in a container an interface will be created between these fluids. The force that keeps the fluids separated from each other determines the strength of this interface. This force, per unit length, is known as the interfacial tension (τ). If a metal ring is pulled up through the interface the ring will be subjected a force equal to the interfacial tension multiplied by the total length along which the interfacial tension is applied, see figure 2.5.1 and equation 2.5.1.

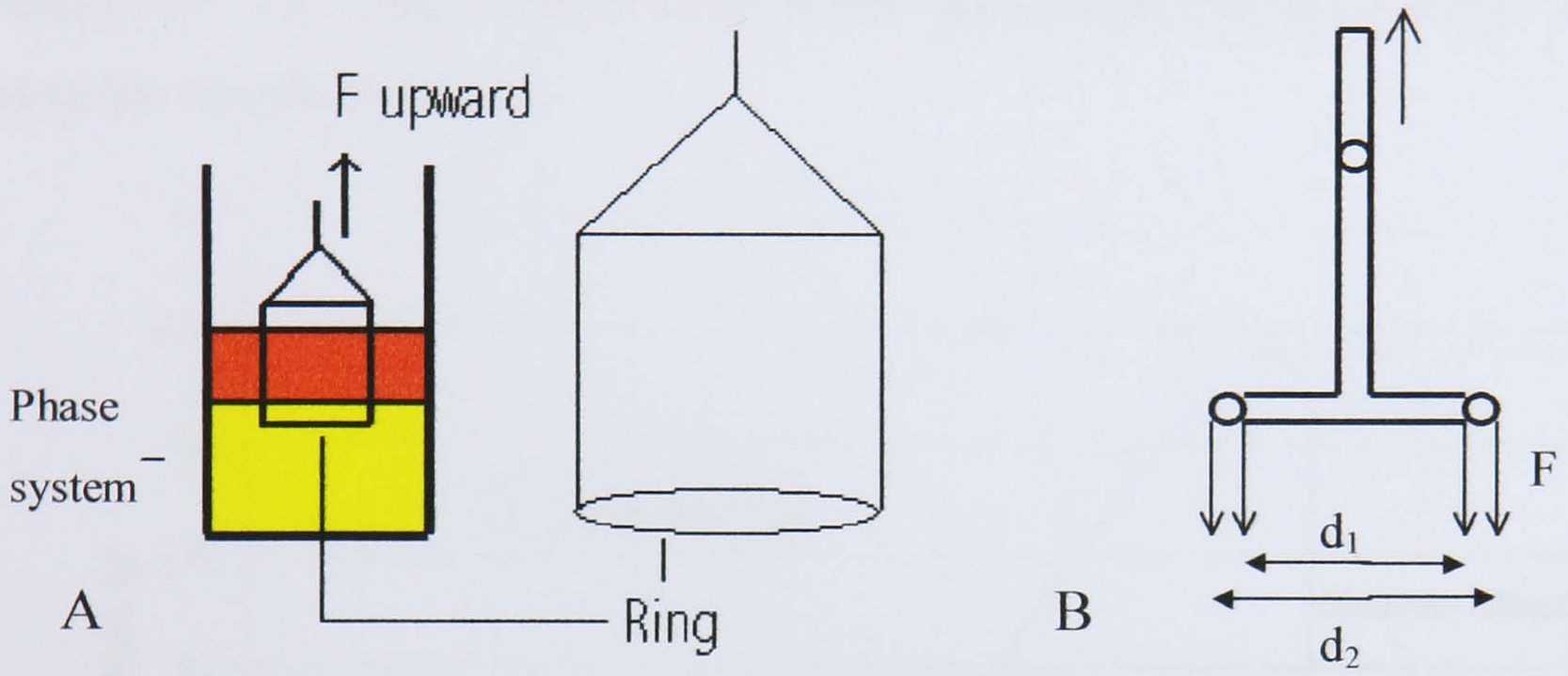

Figure 2.5.1. A. Principle of measuring interfacial tension. The metal ring is submerged in the phase system. B. The forces acting on the ring (sideways view); figure taken from [Timmers 2001]

The total length along which the interfacial tension acts is the addition of the inner and outer circumferences of the ring. Therefore the relationship between the force applied to the ring and the interfacial tension is governed by equation 2.5.1:

$$Force = \pi(d_1 + d_2)\tau \qquad (2.5.1)$$

rearrange to give:

$$\tau = \frac{Force}{\pi(d_1 + d_2)} \qquad (2.5.2)$$

If the container holding the two immiscible liquids is placed on a set of weighing scales the force applied to the ring by the interfacial tension can be measured. The rapid increase in the measured mass as the ring breaks through the interface represents the force applied to the ring by the interfacial tension. The force is change in mass (ΔM) multiplied by the acceleration due to gravity ($g = 9.81 m/s^2$). Hence equation 2.5.2 can be modified to give:

$$\tau = \frac{g\Delta M}{\pi(d_1 + d_2)} \qquad (2.5.3)$$

Plot a graph of mass versus time, as shown in figure 2.5.2. The graph obtained will depict mass lifted by the ring versus time, which will be positive since the balance was zeroed at the start of each test and the software used for data logging converts the negative measured mass from the balance into an increasing mass supported by the ring by multiplying by minus one. The term ΔM is represented by the rapid decrease in the lifted mass as shown in figure 2.5.2.

There are two other forces that are applied to the ring as it is pulled upwards. These are viscous drag and buoyancy forces. These forces account for the shallow slopes indicated on figure 2.5.2. To minimize these forces, the ring is pulled upwards slowly at approximately 1mm/minute. The affect of these forces is then insignificant and the measured ΔM is mainly due to the interfacial tension.

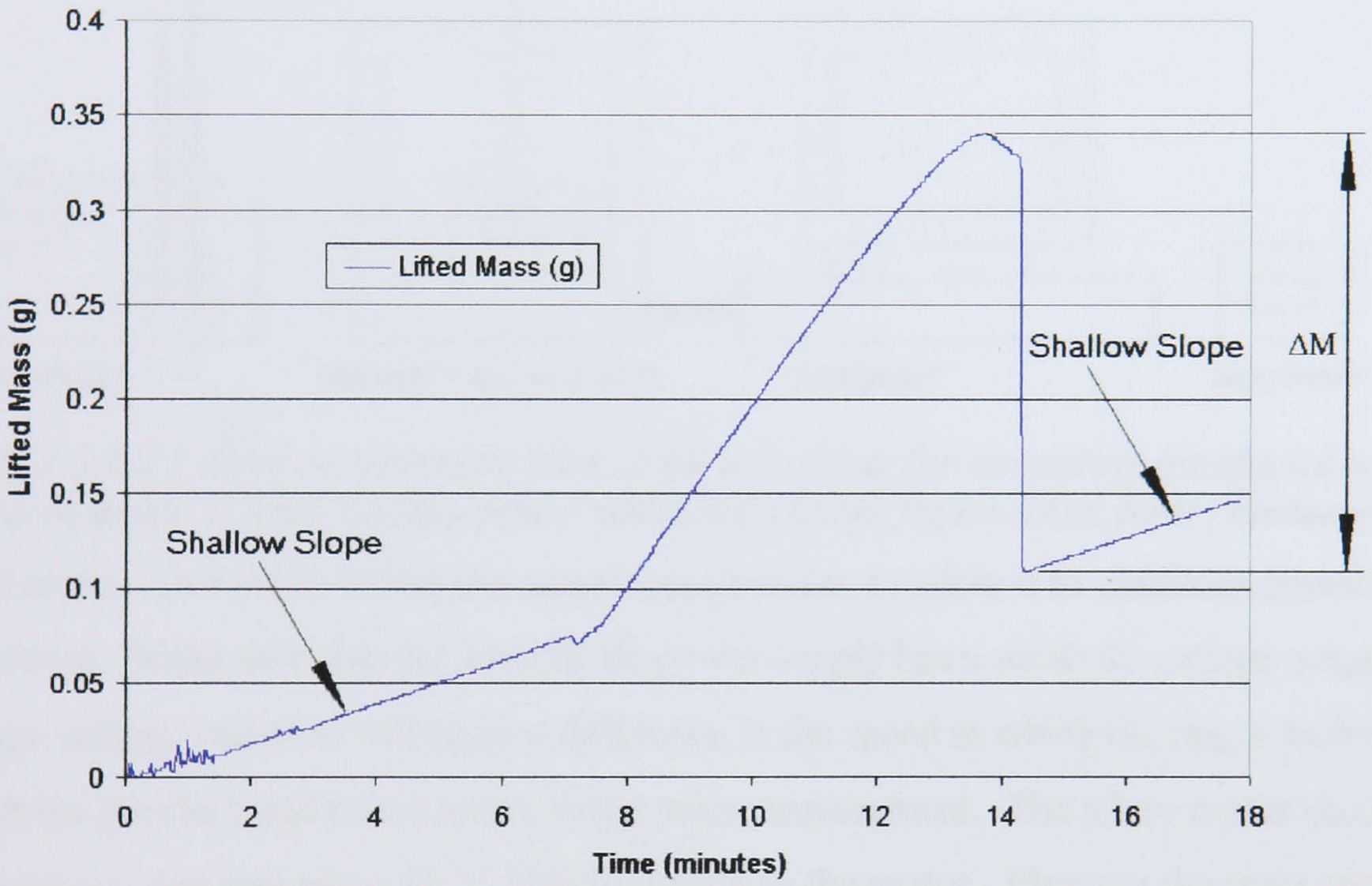

Figure 2.5.2 obtained from an interfacial tension test on the 4A phase system

2.5.1 Interfacial tension between the phases of a 2-phase system

2.5.1.1 Apparatus

- Accurate balance (Precisa 80A – 200 M);
- Stopwatch;
- Faulhaber DC-Micromotor & high gear ratio gear head;
- Thurlby PL310 DC power supply;
- Banana leads;

- Interfacial measurement ring, $d_1 = 18.78 \pm 0.01$mm, $d_2 = 19.37 \pm 0.01$mm [Timmers 2001];
- RS232 cable;
- Data logging computer and data logging software: Windows® Terminal;
- Beaker, 50 to 100 ml.

2.5.1.2 Test Set up

The experimental set up is shown in figure 2.5.1.2.1.

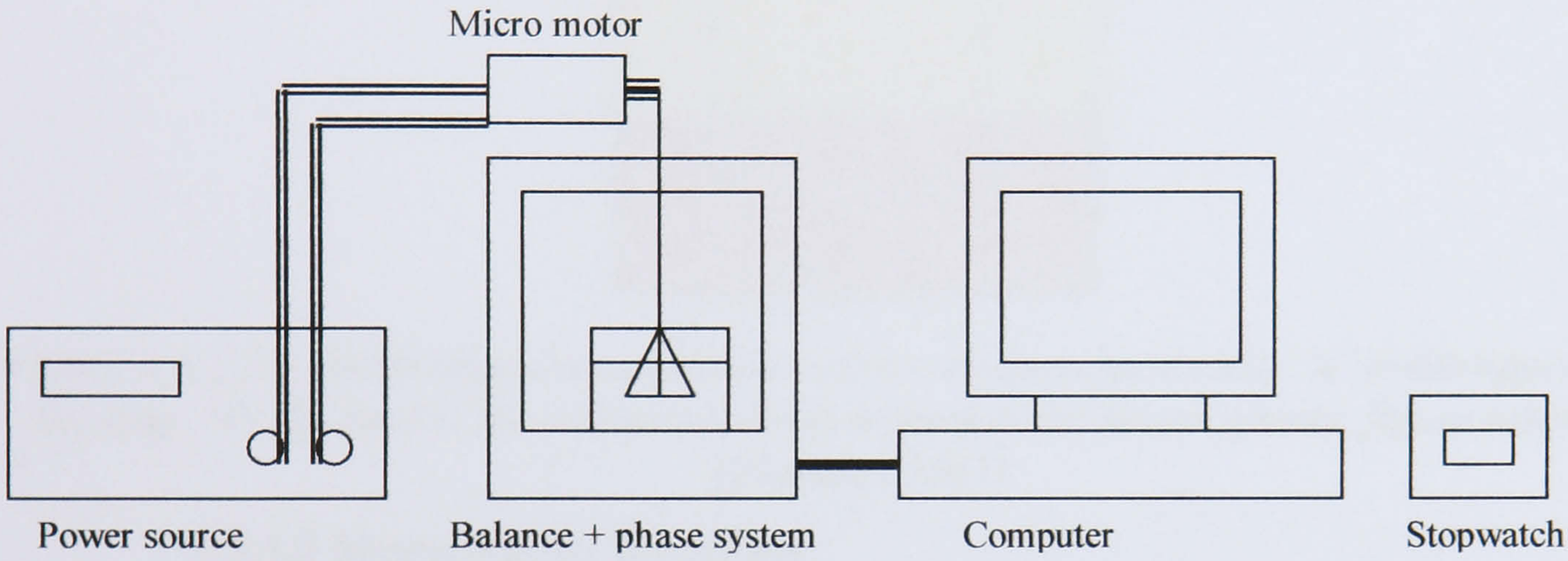

Figure 2.5.1.2.1 shows a schematic view of the test set up for measuring interfacial tension. The micro motor is held in place with a stand and clamp; figure taken from [Timmers 2001]

Let the motor run a while before the actual measurement to allow it to obtain an operating temperature. Make sure that the Thurlby dc power supply has a stable dc voltage output, as any large voltage variation will cause a difference in the speed at which the ring is pulled through the interface and hence errors in the mass measurement. The micro motor should lift the thread at 1 mm/min when 11.55 Vdc is applied to the motor. Measure the inner and outer radii of the metal ring. Tie the thread to part A of the metal ring as shown in figure 2.5.1.2.2. Pass the thread through the small hole in the top Perspex cover of the Precisa balance. Tie the other end of the thread to the output shaft of the micro motor in such a way that it does not slip, if necessary wind a number of loops of thread around the motor shaft. Make sure that the ring hangs vertically directly below the motor and that the thread is not touching the inside surfaces of the hole through the Perspex cover. The ring needs to hang vertically directly below the motor to ensure that the ring is orientated in the horizontal plane. An accurate reading of the interfacial tension is only obtained when the interface releases the whole of the ring instantaneously. If the ring is not orientated in the horizontal plane, the ring will not be released instantaneously and the reading obtained will underestimate the interfacial tension.

When submerging the ring in the phase system, make sure that part A is still in air see figure 2.5.1.2.2. If it is not, this part will stick to the liquid-air interface, causing an increase in the mass peak leading to a false test result. To establish this situation, the 'thickness' of the layer of upper phase should be less than the length of the suspension wires of the ring. It is also advised to place the ring, part B, just below the interface. A measurement will then take up less time to perform and the results are easier to obtain.

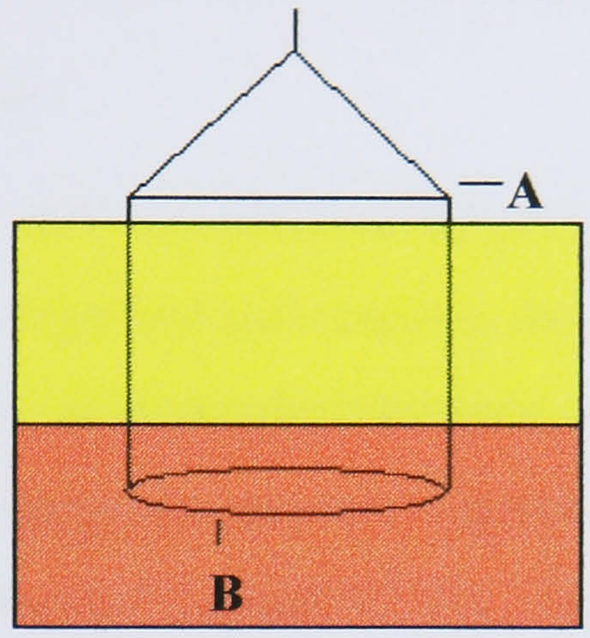

Figure 2.5.1.2.2 positioning the interfacial tension measurement ring, 'A' is the upper part of the ring, 'B' the lower. The coloured blocks represent the phase system; figure taken from [Timmers 2001]

2.5.1.3 Measurement procedure

1 Ensure that the test set up is as described above and that the Perspex side covers on the Precisa balance are closed.

2 Double click on Terminal.exe, the path is c:\windows\Terminal.exe

3 Click on 'File', then 'Open' and select 'TIES.TRM', the path is c:\windows\Ties\Ties.trm. If this file is not present, re-configure the terminal under 'Settings'. Set up the balance with the same configuration, as described in the Precisa weighing scale operational manual.

4 Select 'Transfers', then 'Receive text file' and name the target file, remember to add the suffix '.txt' to the filename.

5 Press 'OK', this will immediately start the transfer of data to the named file.

6 Tare the balance and start the stopwatch.

7 Start the motor.

8 When the ring reaches the interface, record the time.

9 When the ring has passed the interface, stop the motor.

10 Tare the balance and stop the stopwatch at the same time

11 Stop the terminal by selecting 'Stop' under 'Transfers'.

12 Copy the terminal files on a floppy disk and store them on a personal computer.

The reason to record the time when the ring hits the interface is that this will provide a way of locating the right mass peak on the resulting graph see figure 2.5.2.

Between measurements, make sure that the metal ring is dry, when using a different phase system, and still vertically aligned. If the metal ring is not vertically aligned adjust it so that it is vertically aligned and repeat the previous test to ensure the accuracy of the results obtained.

2.6 Calibration of Pressure sensor

One of the aims for the retention tests is to measure the pressure drop across the coil upon which the retention test is being performed and compare the measured results with theoretical prediction. The pressure drop is to be determined for both normal and reverse phase modes. A pressure transducer that measures gauge pressure was connected just downstream of the upstream switching valve see figures 2.7.2.1 and 2.7.4.1. The pressure transducer measures the pressure drop across: 1) the in and out flying leads; 2) the coil; 3) the downstream switching valve and 4) the 25psi backpressure valve plus associated 1/16" bore PTFE tubing. The pressure drop across all of the above items, except the coil, needs to be removed in order to just measure the pressure drop across the coil. In this calibration test all of the above items, except the coil, are connected together and a mobile phase is pumped through at the same flow rates as used in the retention tests. The pressure reading is noted for each flow rate and a pressure verses flow characteristic is created. The pressure readings at each flow rate can then be subtracted from those obtained during the retention tests to determine the pressure drop across the coil. The pressure sensor will need to be calibrated for both the upper and lower phases for each phase system tested.

If the test set up is changed in any manner between the upstream switching valve and the exit through the 25psi backpressure valve this calibration will need to be conducted for the new set up.

2.7 Retention Tests

2.7.1 Apparatus

- J-type Centrifuge (Brunel CCC),
- Grant chiller (RC1400G),
- Grant Water Bath,
- Mobile and stationary phase reservoirs,
- Non-pulsitile flow HPLC pump, Dynamax SD-1 with a set of 800ml heads for pumping the mobile phase,
- Gilson 302 HPLC pump with 100ml pump head for pumping stationary phase,
- Switching valve and back pressure valves,
- Pressure transducer,
- Stationary phase collector (normal and reverse phase mode types),
- Stopwatch,
- Nitrogen gas bottle with regulator,
- Glass measuring cylinders: 100ml, 250ml and 500ml,
- Glass beakers: 100ml and 150ml.

2.7.2 Test Set up

The test set for reverse phase mode can be seen in figure 2.7.2.1, with a schematic layout given in figure 2.7.2.2.

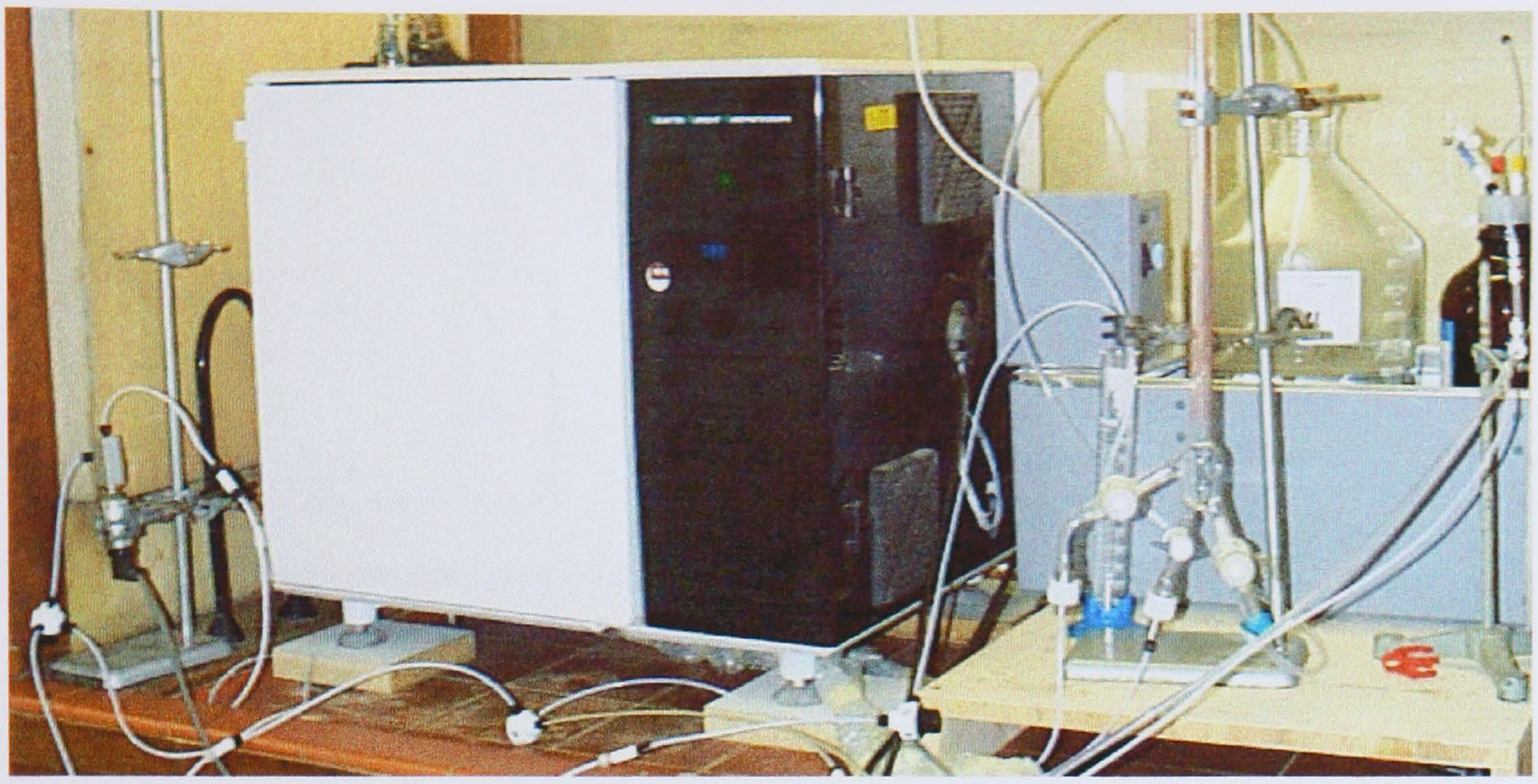

Figure 2.7.2.1 shows the test set up for reverse phase mode in a fume-cupboard

Brunel CCC centrifuge rotational speed (rpm)	Grant Chiller set operating temperature (°C)
600	16
700	11
800	9
900	3
1000	-1
1200	-4

Table 2.7.2.1 shows the chiller operating temperatures for various rotational speeds of the Brunel CCC centrifuge

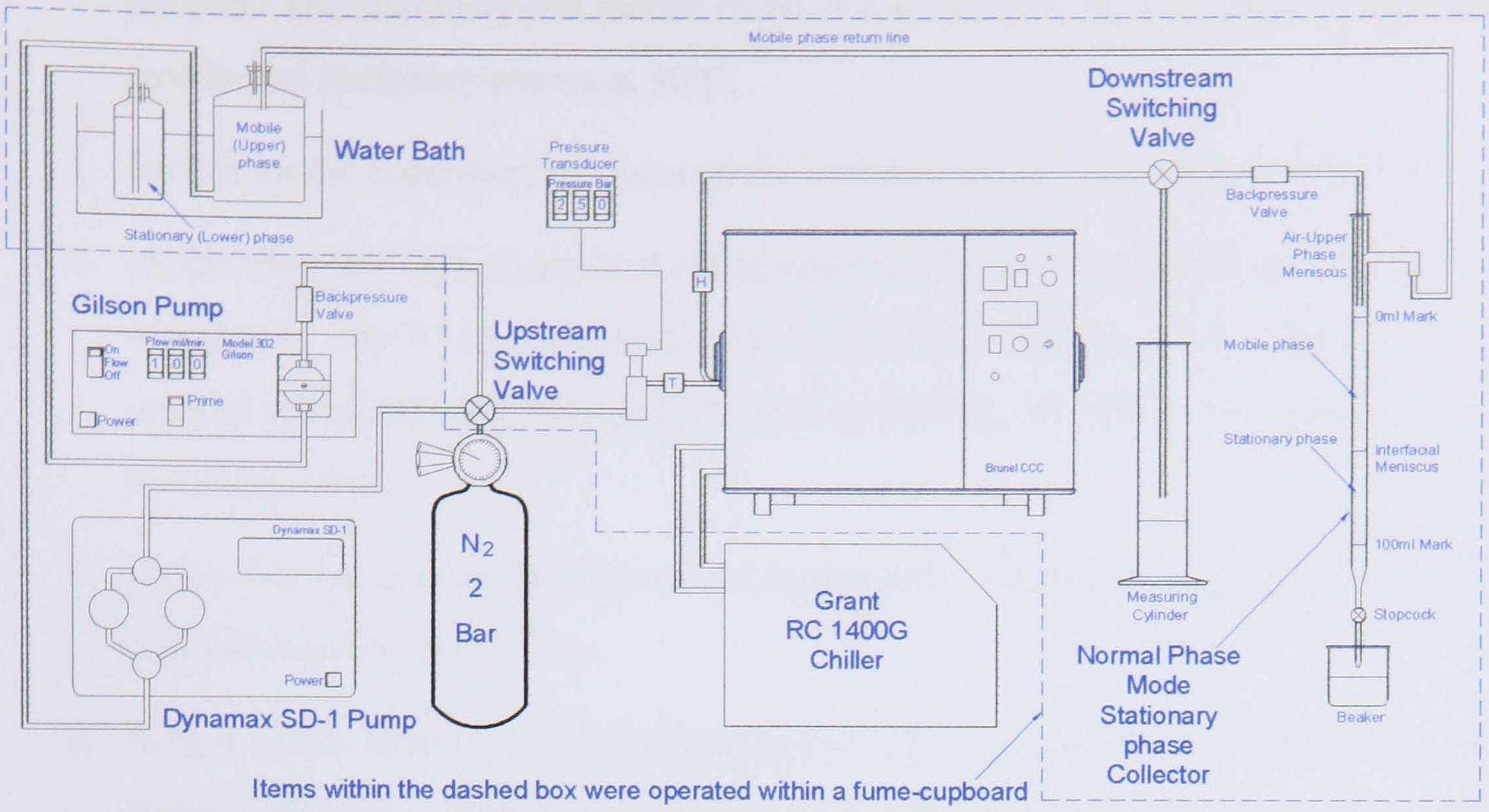

Figure 2.7.2.2 shows a schematic of the retention test set for normal phase mode

2.7.3 Normal phase mode Procedure

For the normal phase mode of operation the upper organic phase is the mobile phase and the lower aqueous phase is the stationary phase for the phase systems listed in tables 2.2.1 and 2.2.2.

At the start of this procedure it is assumed:

- That the delivery lines to the HPLC pumps are primed with their respective solvents.
- That the coil upon which the retention test is to be performed is empty.
- That the centrifuge and solvents are not at the 30°C operating temperature.
- That the stationary phase collector is empty.

In this procedure the mobile phase is pumped in tail to head direction through the coil as recommended by Sutherland [2000A]. Refer to figure 2.7.2.2 for the named items in the following procedure.

1. Determine the dead volume of the system between the upstream switching valve and the stationary phase collector by measuring the length of the flying leads and associated tubing and then calculating the volume from the cross-sectional area of the tubing. Ensure that this dead volume is recorded with the other test data.
2. Check that the mobile phase reservoir is filled with enough upper phase to perform the retention test. Ensure that the stationary phase reservoir has enough lower phase to fill

the coil. The stationary and mobile reservoirs are kept in the water bath to keep the mobile and stationary phases at 30°C.

3. Switch on the water bath to warm up the mobile and stationary phases to 30°C.
4. Ensure that the TAIL flying lead of the selected coil is connected to the pressure transducer. The TAIL flying lead is marked with a T and the HEAD flying lead is marked with an H. The HEAD flying lead should be connected to the downstream switching valve.
5. Check that the normal phase mode stationary phase collector is connected to the downstream switching valve.
6. Switch on the Brunel CCC centrifuge; ensure that the heater is set to 30°C. For the detailed operation of the Brunel Centrifuge see Wood [2000].
7. Position the upstream switching valve to allow stationary phase to be pumped into the centrifuge. Position the downstream switching valve to allow excess stationary phase to drain into a 100ml glass measuring cylinder through the backpressure valve.
8. Set the Gilson 302 pump to 20ml/min and switch on.
9. Set the Brunel centrifuge to rotate at 200rpm in the reverse direction of rotation. This will cause the stationary phase to collect at the end of the coil into which the coil is being filled ie the tail end in the reverse direction of rotation. Any trapped air will be pumped towards the head end of the coil. This process continues until the coil is full of stationary phase and no air is present.
10. Switch off the Gilson 302 pump once a continuous stream of lower (stationary) phase is draining into the 100ml glass measuring cylinder.
11. Place a 100ml glass beaker directly under the stopcock of the stationary phase collector and check that the stopcock is closed.
12. Turn the downstream switching valve to allow the stationary phase to be pumped through the backpressure valve. Place the outlet PTFE from the backpressure valve into the top of the stationary phase collector.
13. Switch on the Gilson 302 pump and fill the stationary phase collector to just above the 100ml mark (the normal phase mode stationary phase collector is made from a 100ml burette and the 100ml mark is at the bottom and the 0ml mark is at the top).

14. Stop the Gilson 302 pump and adjust the level of the stationary phase so that the meniscus is level with the 100ml mark by opening the stopcock at the stationary phase collector.

15. Increase the speed of the centrifuge, reverse direction of rotation, to the desired speed for the test.

16. Switch on the Grant chiller and ensure that it is set to the correct operating temperature to allow the centrifuge to maintain 30°C. The operation instructions for the Grant chiller are printed on its top surface. See table 2.7.2.1 for the correct temperature setting of the chiller, given the desired rotational speed for the test.

17. Allow the centrifuge time to reach 30°C.

18. Once the centrifuge has reached 30°C check the level of the meniscus in the stationary phase collector and adjust if necessary, see steps 13 and 14.

19. Turn the upstream switching valve to allow mobile phase to flow into the centrifuge and ensure that the mobile phase return tube is connected between the stationary phase collector and the mobile phase reservoir.

20. Set the Dynamax pump to the desired mobile phase flow rate. Set the ramp time to the 0.1 minutes per 10ml/min increase in flow rate. Start the Dynamax pump; once the set flow rate is achieved after the ramp time has elapsed start the stopwatch[x].

21. Allow three minutes for equilibrium to be achieved between the mobile and stationary phases and then take a set of readings. Record the following readings: rotational speed; cabinet (centrifuge) temperature; backpressure and displaced volume of stationary phase. The displaced volume of stationary phase is the volume of lower phase between the interfacial meniscus and the 100ml mark.

22. Take a set of readings every two minutes until the same volume of displaced stationary phase is recorded twice.

23. Increase the mobile phase flow rate remembering to alter the ramp time as required. Repeat from step 20 until a minimum of five flow rates have been tested.

---

[x] The set flow rate is assumed to be the actual flow rate because during the commissioning of the retention test rig the actual flow rate was measured and compared to the set flow rate and found to be within ± 0.7%. The test rig is also fitted with backpressure valves to ensure that the non-return valves in the pump heads work accurately and that siphoning through the pump heads does not occur.

24. Stop the Dynamax pump.

25. Stop the rotation of the centrifuge.

26. Position the downstream switching valve to allow the contents of the coil to drain into a dry empty measuring cylinder. The volume of the measuring cylinder should be great enough to accommodate the volume of the coil and the dead volume from the upstream switching valve to the measuring cylinder.

27. Turn the upstream switching valve to allow nitrogen gas to force the contents of the coil into the measuring cylinder. Check that the regulator is set to a maximum pressure of 2bar, adjust if necessary and then open the valve on top of the nitrogen gas bottle.

28. Start the centrifuge rotating at 200rpm in the reverse direction of rotation. This will pump the liquids within the coil towards the downstream end of the coil ie the head end in the reverse direction of rotation. Any trapped air will be pumped towards the tail, upstream, end of the coil. This process continues until the coil is empty of both mobile and stationary phase.

29. Close the valve on top of the nitrogen gas bottle when only gas is draining into the measuring cylinder connected to the downstream switching valve.

30. Stop the rotation of the centrifuge.

31. Record the total volume of the upper and lower phases in the measuring cylinder and the individual volumes of the upper and lower phases. The volume of the upper phase in the measuring cylinder should be similar to the displaced volume of stationary phase in the stationary phase collector ie the volume of lower phase between the interface meniscus and the 100ml mark. In theory these volumes should be the same however due to the different accuracies of volume measurement between the stationary phase collector and the measuring cylinder these measured volumes will differ slightly. If the difference between these two volumes is greater than 3ml the retention test may need to be repeated.

32. Drain the contents of the stationary phase collector into a 150ml beaker via the collector's stopcock.

33. Empty the contents of the measuring cylinder and 150ml beaker into the lower 10-litre aspirator flask of the degassing rig (see section 2.2.2).

The test is now finished and the results can be processed.

2.7.4 Reverse phase mode Procedure

The test set up for reverse phase mode can be see in figures 2.7.4.1 and 2.7.2.1.

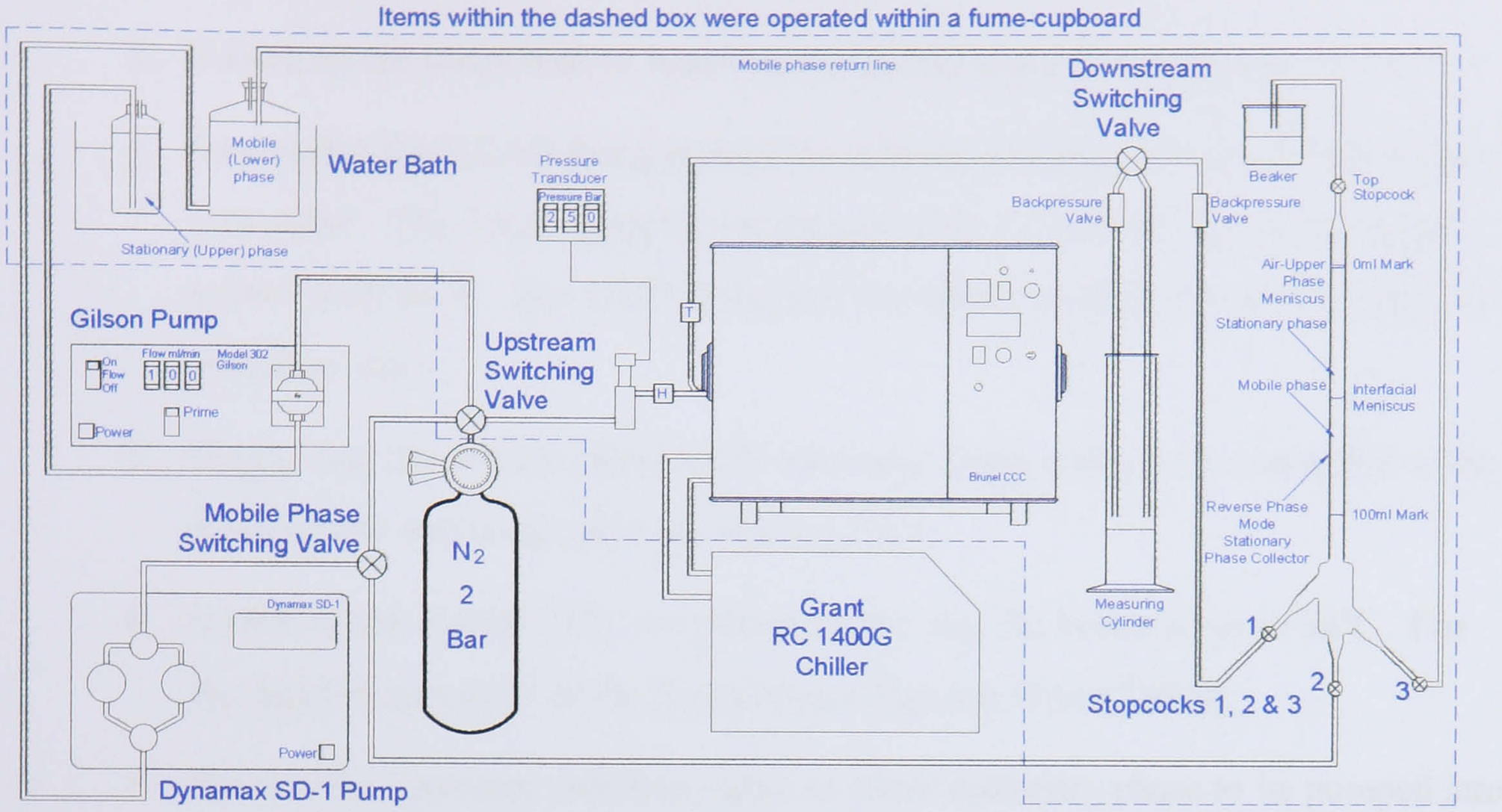

Figure 2.7.4.1 shows a schematic of the retention test set for reverse phase mode

For the reverse phase mode of operation the lower aqueous phase is the mobile phase and the upper organic phase is the stationary phase for the phase systems listed in tables 2.2.1 and 2.2.2.

At the start of this procedure it is assumed:

- That the delivery lines to the HPLC pumps are primed with their respective solvents.
- That the coil upon which the retention test is to be performed is empty.
- That the centrifuge and solvents are not at the 30°C operating temperature.
- That the stationary phase collector is empty.

In this procedure the mobile phase is pumped in head to tail direction through the coil as recommended by Sutherland [2000A].

1. Determine the dead volume of the system between the upstream switching valve and the Stationary phase collector by measuring the length of the flying leads and associated tubing and then calculating the volume from the cross-sectional area of the tubing. Ensure that this dead volume is recorded with the other test data.

2. Check that the mobile phase reservoir is filled with enough lower phase to perform the retention test. Ensure that the stationary phase reservoir has enough upper phase to fill the coil. The stationary and mobile reservoirs are kept in the water bath to keep the mobile and stationary phases at 30°C.
3. Switch on the water bath to warm up the mobile and stationary phases to 30°C.
4. Ensure that the HEAD flying lead of the selected coil is connected to the pressure transducer. The TAIL flying lead is marked with a T and the HEAD flying lead is marked with an H. The TAIL flying lead should be connected to the downstream switching valve.
5. Checks that the reverse phase mode stationary phase collector is connected to the downstream switching valve see figure 2.7.4.1.
6. Switch on the Brunel CCC centrifuge; ensure that the heater is set to 30°C. For the detailed operation of the Brunel Centrifuge see Wood [2000].
7. Position the upstream switching valve to allow stationary phase to be pumped into the centrifuge. Position the downstream switching valve to allow excess stationary phase to drain into a 100ml glass measuring cylinder through the backpressure valve.
8. Set the Gilson 302 pump to 20ml/min and switch on.
9. Set the Brunel centrifuge to rotate at 200rpm in the forward direction of rotation. This will cause the stationary phase to collect at the end of the coil into which the coil is being filled ie the tail end in the forward direction of rotation. Any trapped air will be pumped towards the head end of the coil. This process continues until the coil is full of stationary phase and no air is present.
10. Switch off the Gilson 302 pump once a continuous stream of upper (stationary) phase is draining into the 100ml glass measuring cylinder.
11. Stop the centrifuge rotation.
12. Place the end of the PTFE tubing that is connected to the top stopcock of the stationary phase collector in a 100ml glass beaker open the top stopcock. Close the stopcocks 1 and 3. Open the stopcock 2. Turn the mobile phase switching valve to pump mobile phase into the stationary phase collector.

13. Set the Dynamax pump to pump at 40ml/min and set the ramp time to 0.4 minutes and then switch the Dynamax pump on.

14. Stop the Dynamax pump once a continuous stream of lower phase is draining into the 100ml glass beaker.

15. Close the top stopcock on the stationary phase collector and close the stopcock 2.

16. Open the top stopcock and then slightly open the stopcock 3. Allow the lower phase in the stationary phase collector to drain into the mobile phase reservoir. Close the top stopcock when the lower phase-air meniscus is level with or just below the zero ml mark. Care should be taken as the lower phase can drain very quickly and the meniscus may settle far below the zero ml mark, if this occurs follow steps 17 to 19, if the meniscus is in the correct position go to step 20.

17. Close the stopcock 3 and then open the top stopcock.

18. Open the stopcock 2. Set the Dynamax pump to pump at 5ml/min and set the ramp time to 0.1 minutes and then switch the Dynamax pump on.

19. Stop the Dynamax pump when the lower phase-air meniscus is level with or just below the zero ml mark. Close the top stopcock and close the stopcock 2. Open the stopcocks 1 and 3.

20. Switch on the centrifuge in the reverse direction of rotation and increase the speed of the centrifuge to the desired speed for the test.

21. Switch on the Grant chiller and ensure that it is set to the correct operating temperature to allow the centrifuge to maintain 30°C. The operation instructions for the Grant chiller are printed on its top surface. See table 2.7.2.1 for the correct temperature setting of the chiller, given the operating rotational speed of the Brunel CCC.

22. Once the centrifuge has reached 30°C check the level of the meniscus in the stationary phase collector and adjust if necessary, see steps 17 to 19.

23. Turn the mobile phase and upstream switching valves to allow mobile phase to flow into the centrifuge and ensure that the mobile phase return tube is connected between the stationary phase collector and the mobile phase reservoir.

24. Set the Dynamax pump to the desired mobile phase flow rate. Set the ramp time to the 0.1 minutes per 10ml/min increase in flow rate. Start the Dynamax pump.

Once the set flow rate is achieved after the ramp time has elapsed start the stopwatch[xi].

25. Allow three minutes for the equilibrium to be achieved between the mobile and stationary phases and then take a set of readings. Record the following readings: rotational speed; cabinet (centrifuge) temperature; backpressure and displaced volume of stationary phase. The displaced volume of stationary phase is the volume of upper phase between the interfacial meniscus and the air-upper meniscus.

26. Take a set of readings every two minutes until the same volume of displaced stationary phase is recorded twice.

27. Increase the mobile phase flow rate remembering to alter the ramp time as required. Repeat from step 20 until a minimum of five flow rates have been tested.

28. Stop the Dynamax pump.

29. Stop the rotation of the centrifuge.

30. Position the downstream switching valve to allow the contents of the coil to drain into a dry empty measuring cylinder through the line without the backpressure valve. The volume of the measuring cylinder should be great enough to accommodate the volume of the coil and dead volume from the upstream switching valve to the measuring cylinder.

31. Turn the upstream switching valve to allow nitrogen gas to force the contents of the coil into the measuring cylinder. Check that the regulator is set to a maximum pressure of 2bar, adjust if necessary and then open the valve on top of the nitrogen gas bottle.

32. Start the centrifuge rotating at 200rpm in the forward direction of rotation. This will pump the liquids within the coil towards the downstream end of the coil ie the head end in the forward direction of rotation. Any trapped air will be pumped

---

[xi] The set flow rate is assumed to be the actual flow rate because during the commissioning of the retention test rig the actual flow rate was measured and compared to the set flow rate and found to be within ± 0.7%. The test rig is also fitted with backpressure valves to ensure that the non-return valves in the pump heads work accurately and that siphoning through the pump heads does not occur.

towards the tail, upstream, end of the coil. This process continues until the coil is empty of both mobile and stationary phase.

33. Close the valve on top of the nitrogen gas bottle when only gas is draining into the measuring cylinder connected to the downstream switching valve.

34. Stop the rotation of the centrifuge.

35. Record the total volume of the upper and lower phases in the measuring cylinder and the individual volumes of the upper and lower phases. The volume of the lower phase in the measuring cylinder should be similar to the displaced volume of stationary phase in the stationary phase collector ie the volume of upper phase between the interface meniscus and the air-upper phase meniscus. In theory these volumes should be the same however due to the different accuracies of volume measurement between the stationary phase collector and the measuring cylinder these measured volumes will differ. If the difference between these two volumes is greater than 3ml the retention test may need to be repeated.

36. Empty the contents of the measuring cylinder and 150ml beaker into the lower 10-litre aspirator flask of the degassing rig see section 2.2.2.

The test is now finished and the results can be processed.

2.8 Head/Tail Studies

2.8.1 Dyed phase systems

Head/Tail experiments were conducted on a 3.18mm bore diameter FEP coil using dyed phase systems. The dyes used are:

- Procion Brilliant Yellow
- Sudan III (red)
- Sudan Blue

The Sudan III and Sudan Blue can both be used to dye the organic (often the upper phase) phase. Procion Brilliant Yellow is used to dye the aqueous (often the lower phase) phase.

2.8.2 Apparatus

- J-type Centrifuge (Brunel CCC),
- Two FEP, Fluorinated Ethylene Propylene, coils,
- Grant chiller (RC1400G),
- Grant Water Bath,
- Two Gilson 302 HPLC pumps each with a 100ml pump head,
- Mobile and stationary phase reservoirs,
- Four switching valves,
- Glass measuring cylinders: 100ml and 250ml,
- Stopwatch,
- 500ml of distilled water.

2.8.3 Test Set up

For the test set up see figure 2.8.3.1.

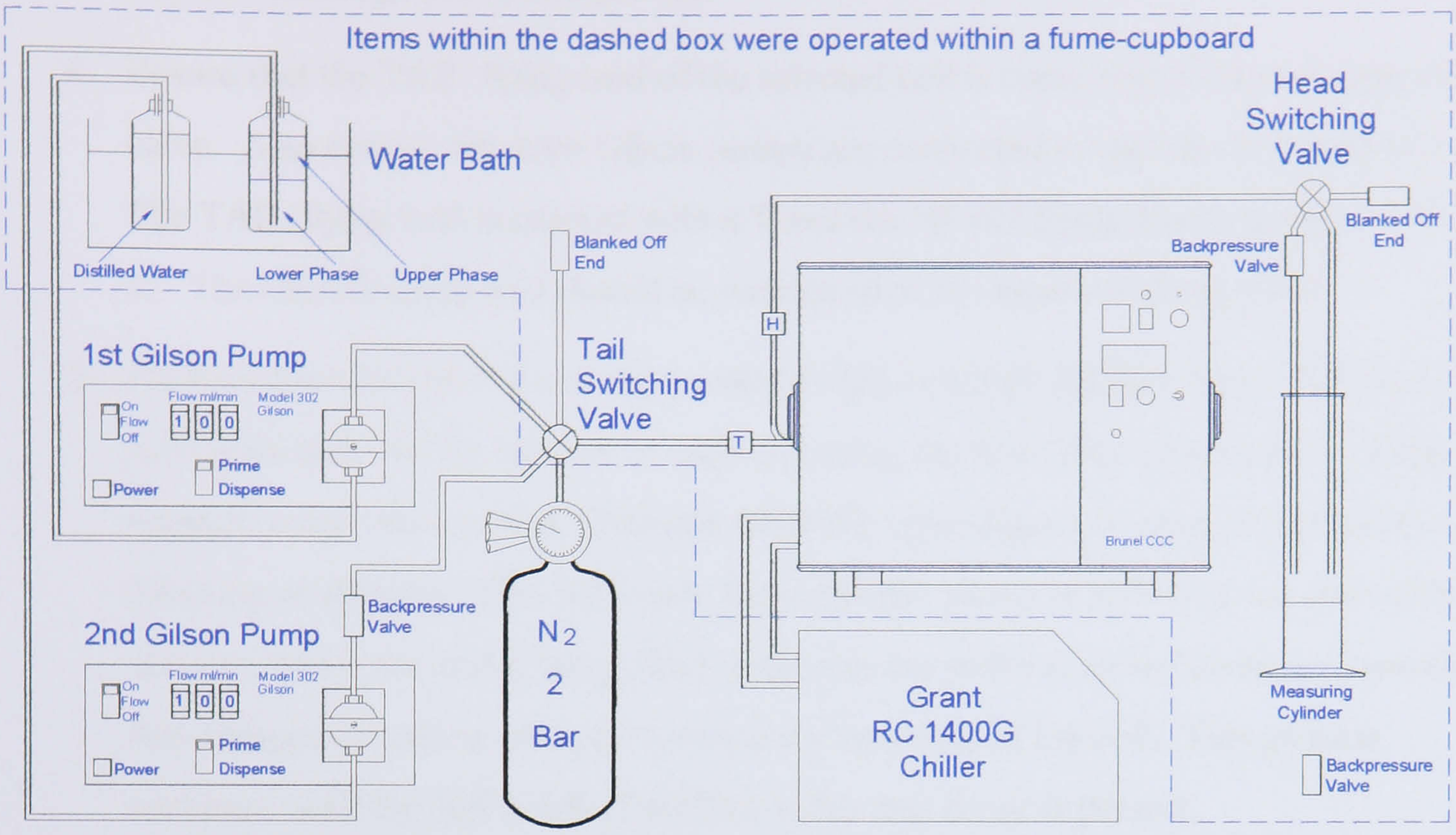

Figure 2.8.3.1 shows a schematic of the head and tail study test set up

2.8.4 Head and Tail Study Experimental Procedure

For the three helical FEP, Fluorinated Ethylene Propylene, coils used in this study - the left hand end, while facing the rotor, is the head end when rotating in the reverse direction, thus the right hand end is the tail. For the forward direction of rotation the head and tail swap over.

At the start of this procedure it is assumed:

- That the delivery line to the first Gilson pump is primed with distilled water.
- That the coil, upon which the Head/Tail experiment is to be performed, is empty.
- That the centrifuge and solvents are not at the 30°C test temperature.

1. Dye a minimum of 125ml of each phase of the selected solvent system in a suitable glass container; details of the dyes are given in the previous section. Filter the 250ml of solvent to remove any particles of dye and then degass as per section 2.2.2. Place the degassed solvent, contained in a 250ml glass container, in a water-bath set to 30°C for a minimum of 20 minutes.
2. Photograph the dyed phase system in the 250ml glass container to show which phase is dyed with which colour.

3. Mount the selected coils on the rotor of the Brunel CCC centrifuge and check that the rotor is balanced with the counterweight bobbin. For the detailed operation of the Brunel Centrifuge see Wood [2000].

4. Ensure that the TAIL flying lead of the selected coil is connected to the tail-switching valve. Also ensure that both Gilson pumps are connected to the tail-switching valve. The TAIL flying lead is marked with a T and the HEAD flying lead is marked with an H. The HEAD flying lead should be connected to the head switching valve.

5. Fill both the selected coil and the counterweight coil with distilled water. Fill these coils separately via the tail end of each coil using the first Gilson pump set to pump distilled water into a coil at 10ml/min while the centrifuge is rotating in the reverse direction at 200rpm. This will cause the stationary phase to collect at the end of the coil into which the coil is being filled ie the tail end in the reverse direction of rotation. Any trapped air will be pumped towards the head end of the coil. This process continues until the coil is full of distilled water and no air is present.

6. Once a coil is full, stop the Gilson pump and seal the open end of head flying lead and then repeat the previous step for the other coil. Connecting the head and tail flying leads together seals the counterweight coil. The selected coil is sealed by turning the tail switching valves to the blanked off position. The head end of the coil is sealed because the backpressure valve connected to the second Gilson pump does not allow liquid to flow in the direction of the Brunel CCC towards the second Gilson pump.

7. Once both coils are full increase the speed of the centrifuge to the operating speed of the Head/Tail experiment.

8. Switch on the Grant chiller and ensure that it is set to the correct operating temperature to allow the centrifuge to maintain 30°C. The operation instructions for the Grant chiller are printed on its top surface. See table 2.7.2.1 for the correct temperature setting of the chiller, given the operating rotational speed of the Brunel CCC.

9. Check that the centrifuge heater is switched on and set to 30°C and then allow the centrifuge time to reach 30°C.

10. Once the centrifuge temperature has reached 30°C stop its rotation.

11. Turn the head switching valve to allow the contents of the coil to drain into a dry empty 100ml measuring cylinder through the line fitted without the backpressure valve.

Empty the selected coil of its contents by turning the tail-switching valve to allow nitrogen gas to force the contents of the coil into the measuring cylinder. Check that the regulator is set to a maximum pressure of 2bar, adjust if necessary and then open the valve on top of the nitrogen gas bottle.

12. Start the centrifuge rotating at 200rpm in the forward direction of rotation. This will pump the liquids within the coil towards the downstream end of the coil ie the tail end in the forward direction of rotation. Any trapped air will be pumped towards the head, upstream, end of the coil. This process continues until the coil is empty of both mobile and stationary phase.
13. Close the valve on top of the nitrogen gas bottle when only gas is draining into the measuring cylinder connected to the head switching valve.
14. Stop the rotation of the centrifuge and open the door.
15. Rotate the centrifuge rotor by hand so that the empty coil is facing you and an imaginary line through the centre of both coils is lying in the horizontal plane.
16. Turn the tail-switching valve to select the second Gilson pump and connect an empty 100ml glass measuring cylinder to the head switching valve. Turn the head switching valve to allow excess solvent to drain into the measuring cylinder via the line with the backpressure valve.
17. Place the inlet tube to the second Gilson pump in the 250ml of dyed phase system that is resting in the water bath and prime the pump.
18. Fill the coil with lower phase and then continue filling with upper phase until the coil is half full of each phase. This is done by firstly raising the inlet tube of the second Gilson pump through the interface of the dyed phase system when the coil is full of lower phase. Secondly the Gilson pump is switched off when the interface between the two dyed phases is approximately positioned half way through a coil.
19. Check whether phase distribution is 50:50, if not empty coil and repeat last step.
20. Seal off both the head and tail flying leads by turning both the head and tail switching valves to the closed position.
21. Repeat from step 11 to first empty the second coil of distilled water and fill with dyed phase system.
22. Start the rotation of the centrifuge in the reverse direction.

23. Once the cabinet temperature of the centrifuge has reached 30°C stop the rotation of the centrifuge.

24. Open the main door of the centrifuge and by hand position the coils one above the other so that both coils can be clearly seen, see figures A.3.2 to 3.11 Appendix 3. Leave the coils in this position for 2 minutes to allow the upper and lower phases to settle and then photograph the distribution of the upper and lower phase.

25. Photograph the phase distribution in both coils.

26. Close the Brunel CCC main door.

27. Start the rotation of the centrifuge in the forward direction.

28. After 5 minutes has elapsed record the cabinet temperature and stop the rotation of the centrifuge.

29. Open the main door of the centrifuge and by hand position the coils one above the other so that both coils can be clearly seen, see figures A.3.2 to 3.11 Appendix 3. Leave the coils in this position for 2 minutes to allow the upper and lower phases to settle and then photograph the distribution of the upper and lower phase.

30. Start the rotation of the centrifuge in the reverse direction and the stopwatch simultaneously. This is done to determine if the upper and lower phases redistributed to the opposite ends of the coil to those for the forward direction of rotation.

31. After 5 minutes has elapsed record the cabinet temperature and stop the rotation of the centrifuge.

32. Open the main door of the centrifuge and by hand position the coils in the vertical plane so that both coils can be clearly seen. Leave the coils in this position for 2 minutes to allow the upper and lower phases to settle and then photograph the distribution of the upper and lower phase.

33. Empty the selected coil of dyed phase system by repeating steps 10 to 13.

The next phase system can now be tested for its head and tail preferences.

Chapter 3 Head and Tail Studies

3.1 Summary

Experimental results on two helical coils on the 4A (Hydrophobic), 4B (Intermediate) and 4C (Hydrophilic) phase systems show that the upper phase will distribute to the head end of a helical coil and the lower phase will distribute to the tail end. This confirms that the distribution of the upper and lower phases during a head and tail study in a helical coil is the same as that in a spiral coil operated head-centre to tail-periphery. It shows that the directions of pumping the mobile phase through a helical coil are the same as those for a spiral coil operated head-centre to tail-periphery [Sutherland 2000A]. If the upper phase is the mobile phase, the mobile phase should be pumped from tail to head and if the lower phase is the mobile phase, the mobile phase should be pumped from head to tail.

3.2 Introduction

Sutherland et al [2000A] have shown that the lower phase will collect at the tail end of a coil and the upper, lighter, phase will collect at the head end when there is no externally pumped mobile phase. An unambiguous distribution of the upper and lower phases was observed for spiral coils when Archimedean and Hydrostatic forces acted together. This condition is achieved when the coil is orientated so the head is at its centre and the tail is at the periphery. In helical coils the pumping effect is purely Archimedean, whereas spiral coils have an additional Hydrostatic pumping effect due to changes in radius. The combination of the J-type planetary motion, the geometry of the helical coil produces the Archimedean pumping effect. To date it has been assumed that the head and tail preferences of the upper and lower phases are identical for both spiral and helical coils. The main aim of the experiments described in this chapter is to test this assumption. Two coils made from transparent FEP, Fluorinated Ethylene Propylene, tubing with approximately equal volumes and the same bore but different β-values were tested with three dyed phase systems, 4A, 4B and 4C, to determine if the lower phase would collect at the tail end of a coil and if the upper phase would collect at the head.

Previous experimental research has shown that for hydrophobic phase systems the lower phase moves towards the tail even when the tail has been placed at the centre of a spiral coil [Sutherland 2000A]. Hydrophobic phase systems often have a high-density difference between the upper and lower phases, which may explain this behaviour. Also for high β-values in a J-type centrifuge the lower phase will preferentially move towards the tail [Sutherland 2000A]. One of the aims of this study is to examine the effect of β-value by using the two FEP helical coils that have β-values of 0.615 and 0.863. Another aim of this study is to determine if helical coils show the same head and tail behaviour at both β-values.

3.4 Methods and Materials

The experimental method used to produce the following results is described in Chapter 2 section 2.8 and is similar to that used in Sutherland [2000A] but adapted for helical coils used in a Brunel CCC J-type centrifuge.

A rotational speed of 763rpm is used for the experimental studies conducted in this chapter as this speed gives the same tangential acceleration at a rotor radius of 110mm as 800rpm gives at a rotor radius of 100mm. This allows the results of these studies to be compared directly to those of Sutherland [2000A].

The 4A, 4B and 4C phase systems were studied in the FEP coils described below and are described in tables 2.2.1 and 2.2.2 of Chapter 2. The 4A phase system is hydrophobic, the 4B phase system is intermediate and the 4C phase system is classed as hydrophilic.

The coils used were wound from the similar lengths of tubing and hence have similar volumes. The greater the β-value the lower the number of loops since a similar length of tubing was used for each coil. The helical pitch was increased proportionally to the increase in β-value to keep the helical pitch angle the same for each coil. The helical pitch angle determines the orientation of the tubing, through which the immiscible liquids are flowing, to the tangential accelerations affecting the motion of the immiscible liquids.

The two FEP, Fluorinated Ethylene Propylene, coils were designed to have:

1. Two different β-values of 0.615 and 0.863 for a rotor radius of 110mm.
2. Approximately the same length of tubing (bore = 3.175mm or 1/8 inch) and approximately the same volume, 34.3ml (β-value = 0.615 coil) and 34.2ml (β-value = 0.863 coil).
3. As β-value increases the number of loops decreases, integer number of loops 10 (β-value = 0.615) and 7 (β-value = 0.863).
4. The same helix angle, 1.09°, to maintain the same orientation of the tubing to the tangential acceleration.
5. The same helix angle at different β-values gives different helical pitches that increase with β-value. The helical pitches are 8.1mm (β=0.615) and 11.3mm (β=0.863).

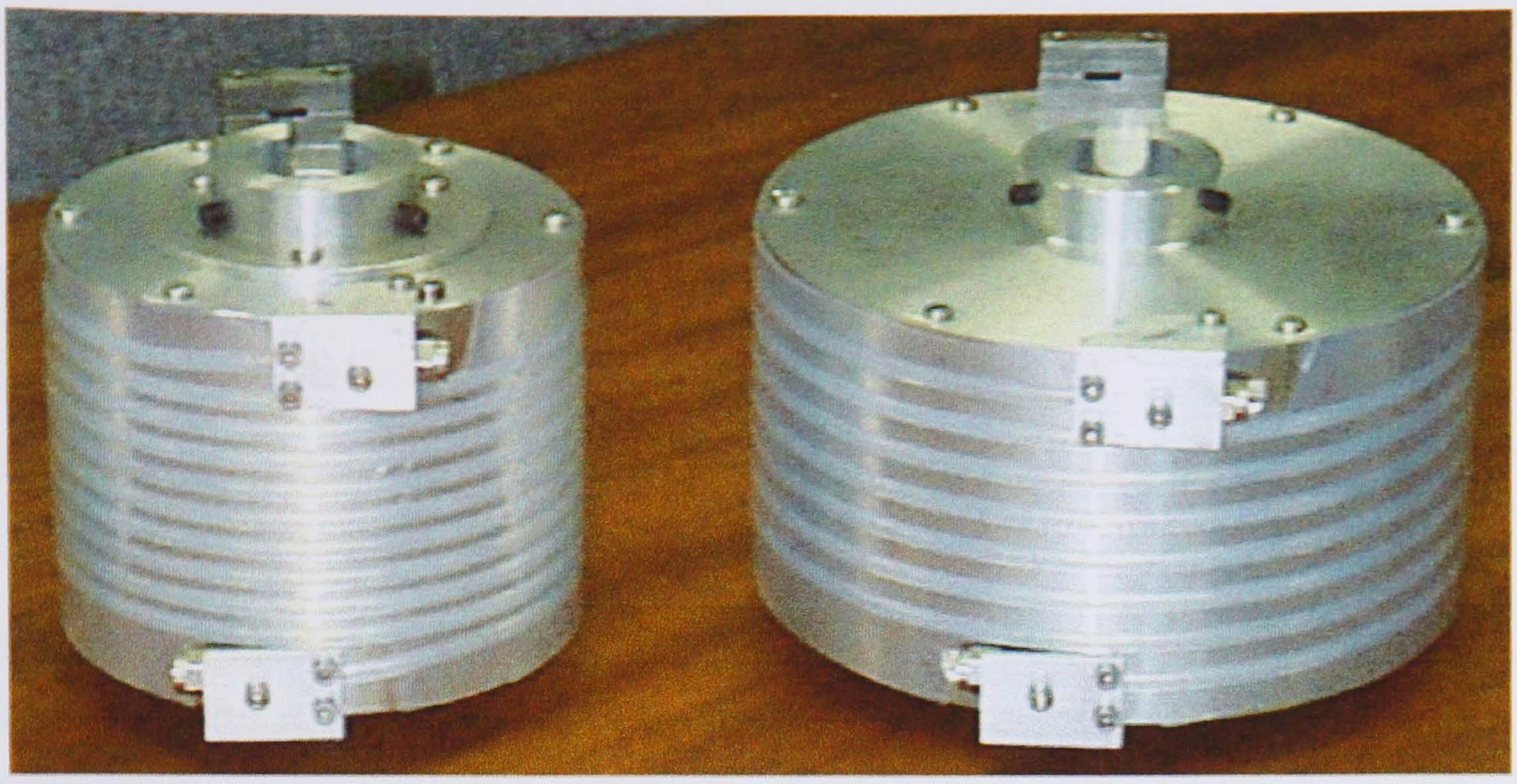

Figure 3.4.1 shows the two FEP helical coils used in this head and tail study

3.5 Results

3.5.1 Experimental Results

Figure A.3.1 from Appendix 3 shows that the upper organic phase for the 4A, 4B and 4C phase systems are all dyed blue. This figure also shows that the lower aqueous phase of each phase system is dyed yellow.

In figures A.3.2 to A.3.11 from Appendix 3 the 0.863 β-value coil is at the bottom and the 0.615 β-value coil is at the top of each photograph.

In figures A.3.2 to A.3.11 the forward direction of rotation is clockwise from the right hand side and the reverse direction of rotation is anti-clockwise from the right hand side. This means that for the forward direction of rotation the tail of both coils is on the left hand side and the head is on the right hand side of the figures A.3.2, A.3.4, A.3.6 and A.3.7. This means that for the reverse direction of rotation the head of both coils is on the left hand side and the tail is on the right hand side of the figures A.3.3, A.3.5, A.3.8, A.3.9, A.3.10 and A.3.11.

Figures A.3.2 and A.3.3 shows that the blue upper phase of the 4A phase distributes to the head end of both helical coils for both the forward and reverse directions of rotation. These figures also show that the yellow lower phase of the 4A phase system distributes to the head end of both coils in both directions of rotation.

Figures A.3.4 and A.3.5 shows that the blue upper phase of the 4B phase distributes to the head end of both helical coils for both the forward and reverse directions of rotation. These figures also show that the yellow lower phase of the 4B phase system is distributes to the head end of both coils in both directions of rotation.

Figure A.3.6 shows that the blue upper phase of the 4C phase system at the tail end of the coil before rotation in the reverse direction and the yellow lower phase at the head. The left hand photograph of figure A.3.7 shows the distribution of upper phase at the head and the lower at the tail end of both coils after 5 minutes of rotation in the forward direction. However the right hand photograph shows that there is still some lower phase at the head end of the coil after the rotor has been rotated through 45° by hand in the forward direction.

Figure A.3.8 shows that the blue upper phase is at the tail end of both coils and the yellow lower phase is at the head end of both coils before rotation in the reverse direction. Figure A.3.9 shows that the blue upper phase does not completely occupy the head end of the coil after 5 minutes of rotation in the reverse direction. Figure A.3.10 appears to show that the blue upper phase completely occupies the head end of both coils after rotation in the reverse

direction for 10 and 30[xii] minutes. However it was found that the blue upper phase did not completely occupy the head after 10 and 30 minutes of rotation once the rotor was rotated through 45° by hand in the reverse direction, the result was similar to the right hand photograph in figure A.3.7. Figure A.3.11 taken after 60 minutes of rotation in the reverse direction shows the blue upper phase still does not completely occupy the head end of both coils however the yellow lower phase does completely occupy the tail end of both coils.

[xii] The times shown on the photographs are the total time rotating in the appropriate direction. Therefore the photograph taken after 10 minutes was taken after 5 more minutes of rotation after the photograph in figure A.3.9.

3.6 Discussion

3.6.1 Experimental Results

The results presented in section 3.5.2 show that the upper phase will be distributed or be pumped to completely occupy the head end of a coil for the 4A (Hydrophobic) and 4B (Intermediate) phase systems. The upper phase for the 4C (Hydrophilic) phase system does not completely occupy the head end of a helical coil, however the upper phase does occupy the vast majority of the head end. However the lower phase completely occupies the tail end of both coils for all three phase systems, even the hydrophilic 4C phase system after just 5 minutes. These findings are the same as Sutherland et al's [2000A] findings for spiral wound coils orientated head-centre to tail-periphery. This means that the recommendations in [Sutherland 2000A] for the direction of pumping the mobile phase depending on whether the mobile phase is the upper or lower phase are the same for helical and spiral coils. The only difference being that a helical coil does not have a centre or periphery in the same sense that a spiral does. This means that if the lower phase is the mobile phase it should be pumped tail to head and that if the mobile phase is the lower phase it should be pumped head to tail.

3.6.2 Phase distribution of the two phase in a coil – a simple explanation

The experimental results show that there is pumping action that distributes the phases to opposite ends of a coil. The following description is a possible qualitative explanation of the pumping effect.

Take a sealed cylindrical vessel that is completely filled with two immiscible liquids of different densities and accelerate it along the axis of the cylinder. The denser liquid will collect at the rear end of the cylinder and the lighter liquid will collect at the front end. If the cylinder is decelerated ie accelerated in the opposite direction when travelling with a given velocity the immiscible liquids will change ends.

Take another sealed cylindrical vessel that is again completely filled with two immiscible liquids and one end is placed on a flat surface. Under the acceleration due to gravity the denser liquid will occupy the bottom end of this vessel while the lighter phase will occupy the top end. If this vessel is quickly placed on its other end the two immiscible liquids will switch ends so that the denser phase will still occupy the lower end and the lighter liquid the upper end. this is simply hydrostatics.

In the accelerating or decelerating cylindrical vessel example the acceleration or deceleration of the vessel is in the direction of the acceleration or deceleration when using the inertial

(absolute) reference frame. However if the vessel is held still using a non-inertial (relative) reference frame, see section 1.4.1.2.2 from Chapter 1, an additional acceleration or deceleration must be applied that is equal to the acceleration or deceleration of the inertial reference frame but in the opposite direction. The pressure gradient is in the direction of the accelerations applied in the non-inertial reference frame. Therefore the pressure gradient is in the opposite direction to the acceleration or deceleration of the vessel in the inertial or absolute reference frame. In the case of the cylindrical vessel on the flat surface the vessel is not applying acceleration to the liquids as both the vessel and liquids are stationary. However the liquids and the vessel are being accelerated towards the earth by the acceleration due to gravity and the pressure gradient is in the same direction as the acceleration due to gravity.

In the case of a helical coil on a J-type centrifuge the acceleration when using the inertial (absolute) reference frame is directed towards the head end of the coil. If a non-inertial (relative) reference frame is again used, see section 1.4.1.2.3 Chapter 1, so that the coil is effectively held still an addition acceleration that has the same magnitude but is directed towards the tail end of the coil is required. This means that the pressure gradient is directed towards the tail end of the coil and hence the denser or lower phase will collect at the tail while the lighter or upper phase will collect at the head. The acceleration applied in the non-inertial reference frame is applied via the helix of the coil in a similar manner to that of the helix in a traditional Archimedean screw pump but made more complex by the J-type motion. This hypothesis can be applied to a J-type centrifuge because the radial component of the acceleration applied to the tubing by the immiscible phases, above a β-value of 0.25, always points outwards from the centre of a coil, see section 1.4.1.2.2 from Chapter 1, and stratifies the phases into layers as observed by Conway [1990]. This stratification allows the phases to flow past one another to reach opposite ends of a coil. The hypothesis is not applicable to an I-type centrifuge because the radial component of acceleration cycles between pointing inwards or outwards during each complete rotation of the coil or loop. This means that stratification of the upper and lower phase cannot occur along the axis of the tubing and hence a zone of a loop is completely occupied by one phase followed by a zone completely occupied by the other phase, see figure 1.4.1.2.4.1 of Chapter 1. These zones are related to the regions where the radial acceleration points inwards or outwards of the loop. The result is that the phases cannot flow past one another to reach opposite ends of the coil but re-circulate within the same loop of a coil.

As described above the combination of the J-type motion and the geometry of the helical winding is the cause of the head and tail pumping or Archimedean pumping effect. Therefore

if CFD (Computational Fluid Dynamics) was used to model the two-phase flow in a three-dimensional loop of a helical coil the cause of the head and tail pumping may become apparent.

3.7 Concluding Remarks

The head and tail preferences of the upper and lower phases in helical coils is the same as for a spiral coil orientated head-centre to tail-periphery. This means that in a head and tail study the upper phase will distribute to the head while the lower phase will distribute to the tail. Therefore recommendations made by Sutherland et al [2000A] for the direction for pumping the mobile phase in spiral coils are also valid for helical coils.

Chapter 4 Retention Studies

4.1 Summary

In this chapter the first hypothesis that a J-type centrifuge acts as a constant pressure pump regardless of the mobile phase flow rate is developed and then experimental results are given that show the pressure drop is constant and independent of mobile phase flow rate. The second hypothesis that the constant pressure drop is the same in normal and reverse phase modes is also tested and results supporting this hypothesis are given. These hypotheses have allowed the development of an alternative theory of retention to that proposed by Fedotov et al [1996]. The results and conclusions of this chapter are used in Chapter 5 to determine an expression for the constant pressure drop across a coil and further the work presented in this chapter.

A new technique for determining the dead volume of an experimental set up, which is a development from Du's retention characteristic [1999], is also presented in this chapter. This gives a more accurate way of determining the dead volume without needing to calculate the volume in the flying leads and other associated plumbing. This new technique enables the Du retention characteristic to pass through the 100% retention mark for a zero flow rate of mobile phase. Results supporting this new technique are presented in this chapter.

4.2 Introduction

Large-scale production versions of J-type centrifuges will be expensive to design and construct. In order to obtain the required level of capital expenditure it will be necessary to show that such a machine will retain stationary phase for a number of phase systems in both normal and reverse phase modes. It will also be necessary to predict the stationary phase retention for a given flow rate and other sets of operating parameters before such expenditure can begin. To make such predictions requires a quantitive understanding of how the stationary phase is retained in the coil. A qualitative understanding of retention has been given by Sutherland et al [2000A] this paper used a head and tail study to show that a J-type centrifuge will pump the upper phase towards the head end of a coil and the lower phase towards the tail for spiral wound coils. If the upper phase is the mobile phase then the mobile phase is pumped from the tail end of the coil towards the head end. If the lower phase is the mobile phase then the mobile phase is pumped from the head end of the coil towards the tail end. Chapter 3 of this thesis showed that this is also true for helically wound coils. Du [1999] has shown that the stationary phase retention decreases proportionally to the square root of the mobile phase flow rate. This chapter builds on these observations and develops a hypothesis that the pressure drop across a coil is constant regardless of the mobile phase flow rate and regardless of whether the coil is operated in normal or reverse phase mode.

To predict the retention of stationary phase for a particular centrifuge-coil configuration and set of operating conditions requires an understanding of how retention is affected by each variable. These variables are: rotor radius, coil β-value, helical pitch, spiral pitch, tubing bore, length of coil, coil volume, rotational speed, mobile phase viscosity and density difference between the phases. Three stainless steel helical coils with the same β-value, helical pitch and coil length but different tubing bores were used to study the effect of tubing bore on retention. A PTFE coil is used to determine if the pressure drop is the same in normal and reverse phase mode. This is done by predicting the normal phase retention characteristic from the measured reverse phase characteristic and then comparing to the measured normal phase retention characteristic.

4.3 Theory

The assumption that *the intercept on the vertical axis of a Du plot is 100% retention of the stationary phase when the mobile phase flow rate is zero* is used to derive an equation that allows the dead volume to be determined from the displaced volumes of stationary phase from a coil and its flying leads see section 4.3.1.

Two hypotheses and two assumptions are used to develop an understanding of the controlling parameters for retention of the stationary phase see section 4.3.2. The two hypotheses are:

1. That the total pressure drop across a coil is independent of flow rate for a given set of operational parameters.
2. That the pressure drop across a coil is independent of whether the coil is being used in normal or reverse phase mode for the same operational parameters provided the mobile phase is pumped through the coil as specified by Sutherland [2000 A].

The assumptions are: 1) that the mobile phase flow is laminar and 2) that the interface between the mobile and stationary phases forms one surface of the conduit through which the mobile phase flows.

4.3.1 Dead Volume

The dead volume (V_d) of a CCC centrifuge is the system volume (V_{SYS}) minus the coil volume (V_C), hence:

$$V_d = V_{SYS} - V_C \qquad (4.3.1.1)$$

Traditionally the dead volume has been determined by measuring the length of the inlet and outlet flying leads and then calculating the dead volume by multiplying the total length by the cross-sectional area of the flying lead, hence:

$$V_d = V_{in} + V_{out} \qquad (4.3.1.2)$$

This traditional method does not take into account the volume of the tubing from the ends of the flying leads to the centre or periphery of the coil. These short lengths of tubing are called delivery tubes and are usually made from the same tubing as the coil. During CCC operation when both stationary and mobile phase can be present in the coil the delivery tubes will be filled with mobile phase, thus increasing the dead volume above that determined by measuring the length of the flying leads, hence:

$$V_d = V_{in} + V_{out} + V_{DT} \qquad (4.3.1.3)$$

where V_{in} = input volume upstream of the coil

V_{out} = output volume downstream of the coil

V_{DT} = dead volume in the delivery tubes, both in and out

It is not always easy to measure the length of the delivery tubes and hence determine the dead volume contained within these tubes particularly as it is possible for some retention of stationary phase in these tubes. The following method can be used to determine the total dead volume of the CCC system without measuring the lengths of the delivery tubes or the flying leads.

Du et al [1999] have shown that there is a linear relationship between the square root of the mobile phase flow rate and the stationary phase retention. Equation 1.4.2.6.4 from Chapter 1 describes the mathematical relationship of a Du plot.

$$S_f = A - B\sqrt{F} \qquad (1.4.2.6.4)$$

where S_f = % stationary phase retention

F = mobile phase flow rate

A = the intercept on the y axis

B = gradient of the linear relationship

It can be assumed that the intercept A on the y-axis is 100% when the coil has just been filled with stationary phase and before any mobile phase has been pumped in to the coil ie the mobile phase flow rate is zero. This assumption allows equation 1.4.2.6.4 to be modified as follows:

$$S_f = 100 - B\sqrt{F} \qquad (4.3.1.4)$$

Now by definition

$$S_f = \frac{100V_S}{V_C} \qquad (4.3.1.5)$$

Substituting equation 4.3.1.5 into equation 4.3.1.4 gives:

$$\frac{100V_S}{V_C} = 100 - B\sqrt{F}$$

$$\frac{V_S}{V_C} = 1 - \frac{B}{100}\sqrt{F}$$

$$V_S = V_C - \frac{BV_C}{100}\sqrt{F} \qquad (4.3.1.6)$$

The displaced volume of stationary phase (V_E) from a CCC system equals the amount of mobile phase in the dead volume (V_d) plus the volume of mobile phase in the coil (V_m) ie:

$$V_E = V_m + V_d$$

Therefore $$V_m = V_E - V_d \qquad (4.3.1.7)$$

Also the coil volume (V_C) equals the volume of stationary phase (V_S) in the coil plus the mobile phase (V_m) in the coil ie:

$$V_C = V_S + V_m$$

Therefore $$V_S = V_C - V_m \qquad (4.3.1.8)$$

Substituting for V_m in equation 4.3.1.8 from equation 4.3.1.7 gives:

$$V_S = V_C - V_E + V_d \qquad (4.3.1.9)$$

Substituting in equation 4.3.1.6 for V_S from equation 4.3.1.9 gives:

$$V_S = V_C - V_E + V_d = V_C - \frac{BV_C}{100}\sqrt{F}$$

$$-V_E + V_d = -\frac{BV_C}{100}\sqrt{F}$$

$$V_E - V_d = \frac{BV_C}{100}\sqrt{F}$$

$$V_E = \frac{BV_C}{100}\sqrt{F} + V_d \qquad (4.3.1.10)$$

Equation 4.3.1.10 governs the relationship between the displaced volume of stationary phase from the coil and flying leads and the square root of the mobile phase flow rate and V_d is the intercept on the y-axis. Plotting the displaced volume of stationary phase against the square root of the mobile phase flow rate and then fitting a linear relationship to the data points will allow the dead volume to be determined as it will be the intercept on the y-axis, see figure 4.5.1.1. A linear trend line is fitted to the plotted points and the equation of the trend line is in the form of equation 4.3.1.10.

Equation 4.3.1.10 shows that the $\frac{BV_C}{100}\sqrt{F}$ term should be a volume and have the dimensional term [L^3]; this is confirmed in Appendix 7.

If the magnitude of the gradient term in equation 4.3.1.10 is G then the magnitudes of the gradient terms from equations 4.3.1.10 and 4.3.1.4 are governed by the following relationship:

$$G = \frac{BV_C}{100} \qquad (4.3.1.11)$$

The magnitudes of the gradient terms of equations 4.3.1.6 and 4.3.1.10 are identical. Hence if the Du retention characteristic was modified to plot the actual volume of stationary phase (V_S) in the coil against the square root of mobile phase flow rate as per equation 4.3.1.6 then the magnitude of the gradients of the modified Du characteristic and the dead volume plot would be equal.

4.3.2 Stationary phase Retention

Mathematically it is possible to develop Du's empirical equation for retention [Du 1999], see equation 1.4.2.6.4 in the previous section, using the Hagen-Poiseuille equation for laminar flow applied with the first hypothesis. The first hypothesis may seem to break physical laws governing the flow of fluids however it must be remembered that as the mobile phase flow rate increases, the amount of stationary phase in a coil reduces, allowing the mobile phase to flow through a greater cross-sectional area of the coil. One use of the Hagen-Poiseuille formula is to determine the viscosity of a liquid by applying a known pressure to one end of a glass capillary tube of known length and bore and then measuring the flow rate obtained. Imagine a number of capillary tubes of the same length but different bore diameters, if the same pressure were applied to each capillary tube in turn the measured flow rate would increase for each increase of capillary bore diameter.

In the following derivation it is assumed that the upper and lower phases stratify as observed by Conway [1990] and shown in figures 1.4.3.1.1 to 1.4.3.1.4 Chapter 1. The interfacial surface formed between the phases by stratified flow forms a boundary of the conduits through which each phase flows. The internal wall of the tubing and the interfacial surface forms the boundary of each conduit. The Hagen-Poiseuille equation for laminar flow was developed for a single phase flowing through straight lengths of circular bore tubing. To use the Hagen-Poiseuille equation in this derivation it is assumed that:

1. The mobile phase flows in a laminar fashion and that Reynolds numbers are kept below 4000 as shown in Appendix 5. Sutherland et al [2001B] have also suggested that mobile phase flows in a laminar fashion.
2. The interface between the mobile and stationary phases can be treated as a solid but moveable boundary.
3. The cross-sectional area occupied by the mobile phase can be treated as circular, although in practice it is more like a segment of a circle.

4. The mean cross-sectional area occupied by the mobile phase is constant through out the coil.

5. That the mixing waves observed by Conway [1990] do not interfere significantly with the retention of stationary phase.

6. Helically or spirally wound tubing can be treated as straight tubing given that the bend radius is much greater than the radius of the tubing bore ie secondary flows as described in section 1.4.3.2.2 of Chapter 1 do not affect stationary phase retention.

The Hagen-Poiseuille equation for laminar flow is as follows:

$$F = \frac{\pi r_m^4 \Delta P}{8 \mu_m L} \qquad \text{(Hagen-Poiseuille)}$$

where F is the volumetric flow rate of mobile phase, r_m is the mean radius of the cross-sectional area occupied by the mobile phase, ΔP the total pressure drop across the coil (measured pressure drop plus pressure drop due to Archimedean action), μ_m the viscosity of the mobile phase and L the length of the column/coil.

The Hagen-Poiseuille equation can be reorganised as follows:

$$\Delta P = \frac{8 \mu_m L}{\pi} \frac{F}{r_m^4} \qquad (4.3.2.1)$$

Applying the first hypothesis to the above equation shows that:

$$\Delta P = \frac{8 \mu_m L}{\pi} \frac{F}{r_m^4} = \text{constant} \qquad (4.3.2.2)$$

The mean cross-section area occupied by the mobile phase is $A_m = \pi r_m^2$ and $V_m = A_m L$ therefore $V_m = \pi r_m^2 L$. Rearranging the equation for r_m^2 gives:

$$r_m^2 = \frac{V_m}{\pi L} \Rightarrow r_m^4 = \frac{V_m^2}{\pi^2 L^2}$$

Substituting into equation 4.3.2.2 for r_m^4 gives:

$$\Delta P = 8 \pi \mu_m L^3 \frac{F}{V_m^2} = \text{constant} \qquad (4.3.2.3)$$

For the first hypothesis to be true the $\frac{F}{V_m^2}$ must also be a constant since the μ_m and L terms of equation 4.3.2.3 are constants. Rearranging equation 4.3.2.3 as follows:

$$V_m^2 = \frac{8\pi\mu_m L^3}{\Delta P} F \qquad (4.3.2.4)$$

Equation 4.3.2.4 shows that plotting V_m^2 against F should produce a straight-line characteristic that passes through the origin if the first hypothesis is correct and the gradient would be $\frac{8\pi\mu_m L^3}{\Delta P}$ see figures 4.5.2.1 to 4.5.2.3.

Rearranging equation 4.3.2.4 for V_m gives:

$$V_m = \sqrt{\frac{8\pi\mu_m L^3}{\Delta P}}\sqrt{F} \qquad (4.3.2.5)$$

Taking equation 4.3.1.8 from the previous section:

$$V_S = V_C - V_m \qquad (4.3.1.8)$$

And multiply both sides by $\frac{100}{V_C}$ gives:

$$\frac{100V_S}{V_C} = 100 - \frac{100V_m}{V_C} \qquad (4.3.2.6)$$

Equation 4.3.1.5 from the previous section shows that:

$$S_f = \frac{100V_S}{V_C} \qquad (4.3.1.5)$$

Substituting equation 4.3.1.5 into equation 4.3.2.6 gives:

$$S_f = 100 - \frac{100V_m}{V_C} \qquad (4.3.2.7)$$

Substituting for V_m from equation 4.3.2.5 into equation 4.3.2.7 gives:

$$S_f = 100 - \frac{100}{V_C}\sqrt{\frac{8\pi\mu_m L^3}{\Delta P}}\sqrt{F} \qquad (4.3.2.8)$$ Equation 4.3.2.8 can be compared to the Du retention characteristic, $S_f = A - B\sqrt{F}$ equation 1.4.2.6.4 from Chapter 1, where the constant A = 100 and the gradient B is as shown below:

$$B = \frac{100}{V_C}\sqrt{\frac{8\pi\mu_m L^3}{\Delta P}} \qquad (4.3.2.9)$$

Now $V_C = A_C L$ and $A_C = \frac{\pi d_C^2}{4}$ hence $V_C = \frac{\pi d_C^2 L}{4}$ therefore equation 4.3.2.8 can be written as:

$$S_f = 100 - \frac{400}{\pi d_C^2 L}\sqrt{\frac{8\pi\mu_m L^3}{\Delta P}}\sqrt{F}$$

$$S_f = 100 - \frac{400}{d_C^2}\sqrt{\frac{8\pi\mu_m L^3}{\pi^2 L^2 \Delta P}}\sqrt{F}$$

$$S_f = 100 - \frac{800}{d_C^2}\sqrt{\frac{2\mu_m L}{\pi\Delta P}}\sqrt{F}$$

(4.3.2.10)

Comparing equations 1.4.2.6.4 and 4.3.2.10 shows that the formula for the gradient B is also as shown below:

$$B = \frac{800}{d_C^2}\sqrt{\frac{2\mu_m L}{\pi\Delta P}}$$

(4.3.2.11)

Equation 4.3.2.10 shows that equation 4.3.2.11 should have the fundamental dimensions $[TL^{-3}]^{0.5}$ this is confirmed in Appendix 7.

The gradient of a given Du plot is constant therefore equation 4.3.2.11 must produce a constant result. In this equation the only likely variable is the ΔP term, all of the other symbols represent constants for the given Du plot, therefore the ΔP term must also be a constant for the given Du plot. This means that the pressure drop across the coil must be independent of the flow rate of the mobile phase, which is consistent with the first hypothesis.

Equation 4.3.2.11 can be used to determine the ratio of the Du gradients for lower phase mobile and upper phase mobile, hence:

$$\frac{B_L}{B_U} = \frac{800}{d_C^2}\sqrt{\frac{2\mu_L L}{\pi\Delta P_L}} \Big/ \frac{800}{d_C^2}\sqrt{\frac{2\mu_U L}{\pi\Delta P_U}}$$

$$\frac{B_L}{B_U} = \sqrt{\frac{\mu_L}{\Delta P_L}} \Big/ \sqrt{\frac{\mu_U}{\Delta P_U}} \qquad (4.3.2.12)$$

The second hypothesis is that the pressure drop across a coil is the same for both normal and reverse phase modes ie $\Delta P_L = \Delta P_U$. If correct, the ratio of the Du plot gradients for normal

and reverse phase mode will depend upon the viscosities of the upper and lower phases see equation 4.3.2.13 below.

$$\frac{B_L}{B_U} = \sqrt{\frac{\mu_L}{\mu_U}} \qquad (4.3.2.13)$$

The second hypothesis is based upon the assumption that the same coil, the same phase system, the same rotational speed and the same rotational direction are used for both normal and reverse phase. It is also assumed that the mobile phase is pumped through the coil in the direction that coil will pump the mobile phase as recommended by Sutherland et al [2000A]. This means that if the upper phase is the mobile phase then it is pumped from the tail end of the coil to the head end. If the lower phase is the mobile phase then it is pumped from the head end of the coil to the tail end. When using spiral or multi-layer coils the best retention results are obtained when the coil is rotated so that it is oriented head-centre, tail-periphery. The viscosities of the upper and lower phases are almost always different hence the Du gradients for lower phase mobile and upper phase mobile will also be different. The viscosity data is taken from table 2.2.2 Chapter 2 and the ratios of the reverse to normal Du gradients were calculated using equation 4.3.2.13.

4.4 Methods and Materials

Detailed experimental procedures are given in Chapter 2. This chapter only contains experimental methodologies that are additional to those in Chapter 2. Chapter 2 also gives details of the phases used and the physical properties of these phase systems. The J-type centrifuges used in these experiments are based upon the Brunel CCC described in section 1.4.1.3 and Sutherland et al [1998], each had a rotor radius of 110mm and could rotate at any speed between 200 and 1400rpm. Each machine used has two bobbins with each bobbin having a maximum possible β-value of 0.95.

The volume of displaced stationary phase (ie the V_E for the highest flow rate of mobile phase) was subtracted from the pump out volume of the mobile phase[xiii]. If the result of the subtraction is more than 3ml[xiv] the results were rejected and the experiment was repeated. If the difference between these volumes was less than 3ml the dead volume determined as described in section 4.3.1 and the retention characteristic was plotted.

4.4.1 Dead Volume

A retention study was performed using a Brunel CCC centrifuge with the 4A phase system in reverse phase mode using a syringe driver instead of a HPLC pump for pumping the mobile phase through the coil. For details of the composition phase systems see table 2.2.1 Chapter 2. The volume of the PTFE coil used was 95.9ml[xv] and was rotated at 800rpm so that the coil was orientated head-centre, tail-periphery. The mobile phase flow rate was determined by measuring the time taken to fill measuring cylinders.

The experiments using a syringe (60ml glass Summit syringe) and syringe driver (Harvard Apparatus Millis. Mass. USA Infusion/Withdrawal Pump Model No. 944A) to pump the mobile phase used a 50ml glass-measuring cylinder to measure the displaced stationary phase. The smallest volume division on the 50ml glass-measuring cylinder was 1ml. All other experiments used the experiment procedures of Chapter 2 sections 2.2, 2.6, 2.7 and 2.8.

[xiii] See chapter 2, section 2.7.3, step 31 and step 35, section 2.7.4, chapter 2.

[xiv] An accuracy of 3ml is used as it allows for small inaccuracies caused by evaporation, spillages and wetting of surfaces above the meniscus in measuring cylinders.

[xv] The PTFE coil used with the syringe driver had a volume of 95.9ml, a 1.5875mm bore, a length of approximately 48.5m and a β-value range of 0.816 to 0.845.

The dead volume was determined by two different methods: the first was the traditional manner by measuring the various lengths of tubing that make up the dead volume and then calculating the total volume of this tubing, see step 1 from sections 2.7.3 and 2.7.4 Chapter 2 and the second method used is described in section 4.3.1[xvi] of this chapter. The volume of stationary phase in the coil was calculated using equation 4.3.1.9. The percentage of stationary phase retention (S_f) was then calculated using equation 4.3.1.5. S_f was then plotted against the square root of the mobile phase flow rate to produce graphs similar to figure 4.5.1.3[xvii].

4.4.2 Retention Studies

Chapter 2 contains the experimental procedures used for both normal and reverse phase mode retention studies. The phase systems flow rates and rotational speeds used are listed below.

Burettes were used to measure the volume of displaced stationary phase rather than measuring cylinders because burettes have a greater volumetric resolution and therefore greater accuracy than measurements taken using measuring cylinders.

4.4.2.1 Three Stainless Steel Coils

These coils were used to study the effect of bore on retention. Three helical stainless steel coils each with different bores have been wound. For clarity these coils will be known as the IMI (EPSRC - Innovative Manufacturing Initiative) coils, which acknowledges the funding sources of these coils. Each IMI coil has been made from the same length of tubing (5.656m) and has been wound at the same β-value 0.82 with the same helical pitch 11.5mm (same helical pitch angle) that gives each coil 10 loops. The bore of the first coil is 3.73mm, the second is 5.33mm and the third is 7.73mm. This means that the volume of each coil is different. The first coil has a measured volume of 59.1ml, the second 120.5ml and the third 259.5ml.

The retention tests were conducted at rotational speeds of 600, 800, 1000 and 1200rpm using the 4A phase systems. For details of the composition phase systems see table 2.2.1 Chapter 2. These experiments show the effect of bore on retention.

[xvi] Microsoft Excel was used to plot the results for dead volume, fit linear trend lines and determine the equations of the fitted trend lines.

[xvii] Microsoft Excel was used to plot the results for retention, fit linear trend lines and determine the equations of the fitted trend lines.

The following flow rates were used for each coil: 3.73mm bore coil 5, 10, 20, 40 and 50ml/min; 5.33mm bore coil 10, 20, 40, 60 and 80ml/min and 7.73mm bore coil 20, 50, 80, 110 and 140ml/min. These flow rates were used to produce a straight Du characteristic. At higher flow rates the Du characteristic is no longer straight. The stationary phase retention reduces much more quickly at high flow rates than at low flow rates.

The Du style retention characteristics were produced using an accurate dead volume determined for each test. The system dead volume was estimated from flying lead volumes and other associated tubing and then confirmed accurately by volume measurement of displaced stationary phase see section 4.3.1. The test data for estimating the dead volume is obtained during the retention tests, see Chapter 2, for the retention test procedures for both normal and reverse phase modes.

The 3.73mm bore coil had the normal phase mode retention test repeated four times to determine the repeatable accuracy (precision) of the retention test at 1200rpm.

4.4.2.2 PTFE Coil

These coils were used to establish if the ratios of Du gradients for normal and reverse phase mode are as indicated in equation 4.3.2.13 and the second hypothesis "*that the pressure drop across a coil is independent of whether the coil is being operated in normal of reverse phase mode*". Normal and reverse phase mode retention studies were performed using a PTFE coil that had a volume of 99.9ml, a 1.5875mm bore, a length of approximately 50.5m and a β-value range of 0.816 to 0.845. This coil is known as a PTFE coil throughout this thesis. Five flow rates are to be used were: 1.0, 2.0, 3.0, 4.0 and 5.0ml/min. The retention tests were conducted at rotational speeds of 800, 1000 and 1200rpm using the 4A phase system.

4.5 Results

The raw data for the results from this chapter are shown in Appendix 4. The dead volume for each set of tests was different due to different lengths of tubing being used and different bores of the flying leads used for each set of tests. The dead volume for each set of tests is recorded in the appropriate results section.

4.5.1 Dead Volume Results using a Syringe and Syringe driver

The dead volume determined in the traditional manner by measuring the lengths of the flying leads and the calculating the volume from the cross-sectional area was 6.4ml. The results are recorded in table 4.5.1.1. These results were used to plot displaced volume against the square root of mobile phase flow (figure 4.5.1.1) in order to calculate the true dead volume from the intercept. This value of dead volume was used to correct stationary phase retention and plot the Du and V_s plots of figures 4.5.1.2 and 4.5.1.4 for comparison with figure 4.5.1.3, which just uses the dead volume of the inlet outlet leads.

Mobile phase flow rate (ml/min)	Square root of Mobile phase flow rate $(ml/min)^{0.5}$	Volume of displaced Stationary phase (ml)
0.455	0.675	13.3
0.902	0.950	15.8
1.979	1.407	19.5
2.714	1.647	22.0
4.250	2.062	25.5

Table 4.5.1.1 shows the mobile phase flow rate and displaced volumes of stationary phase (V_E) for the test using a Syringe driver and Syringe to pump the mobile phase of the 4A phase system in reverse phase mode in the 95.9ml coil.

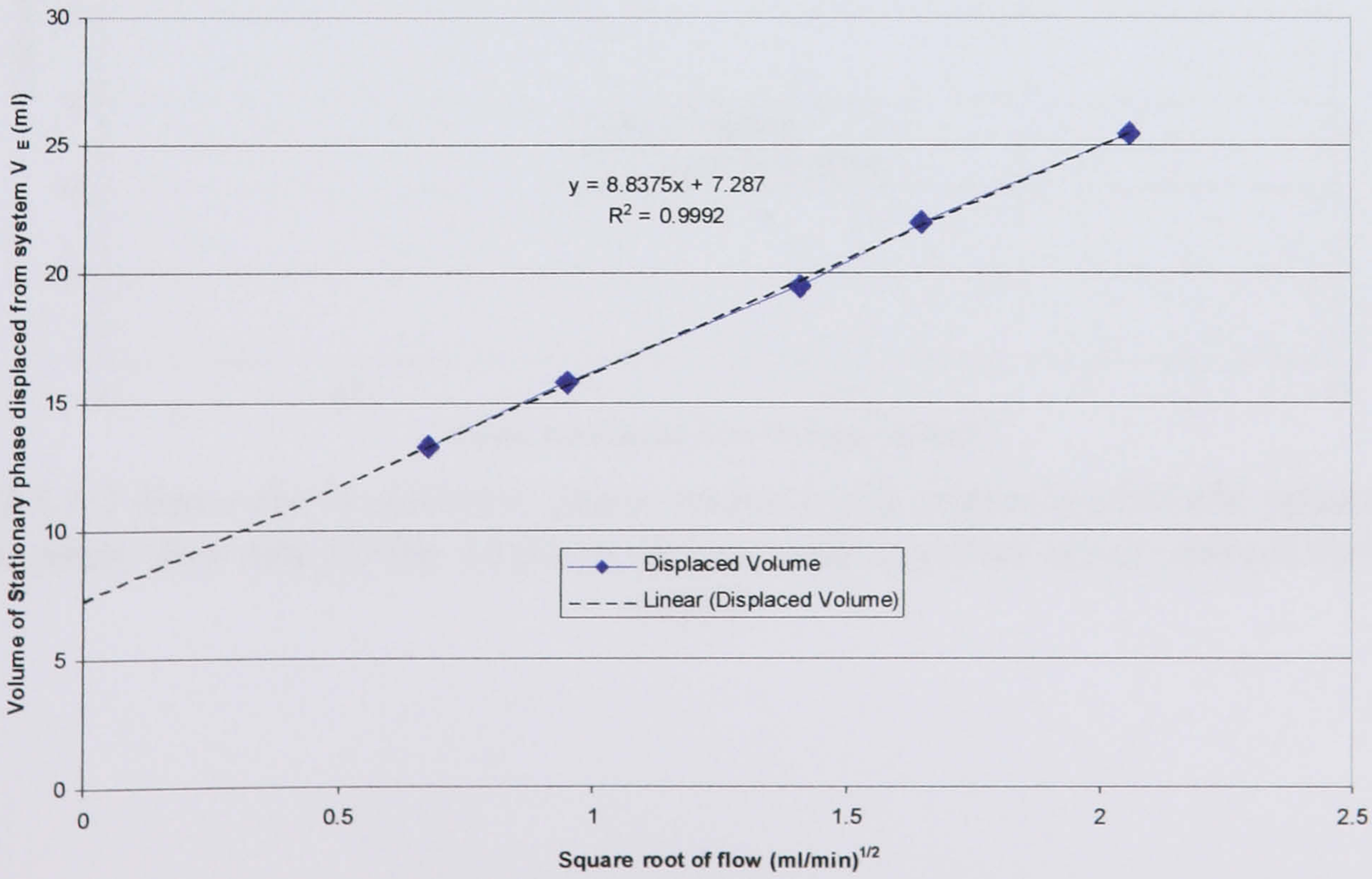

Figure 4.5.1.1 shows the displaced volume of stationary phase plotted against the square root of mobile phase flow rate for the 4A phase system using a syringe driver in reverse phase mode

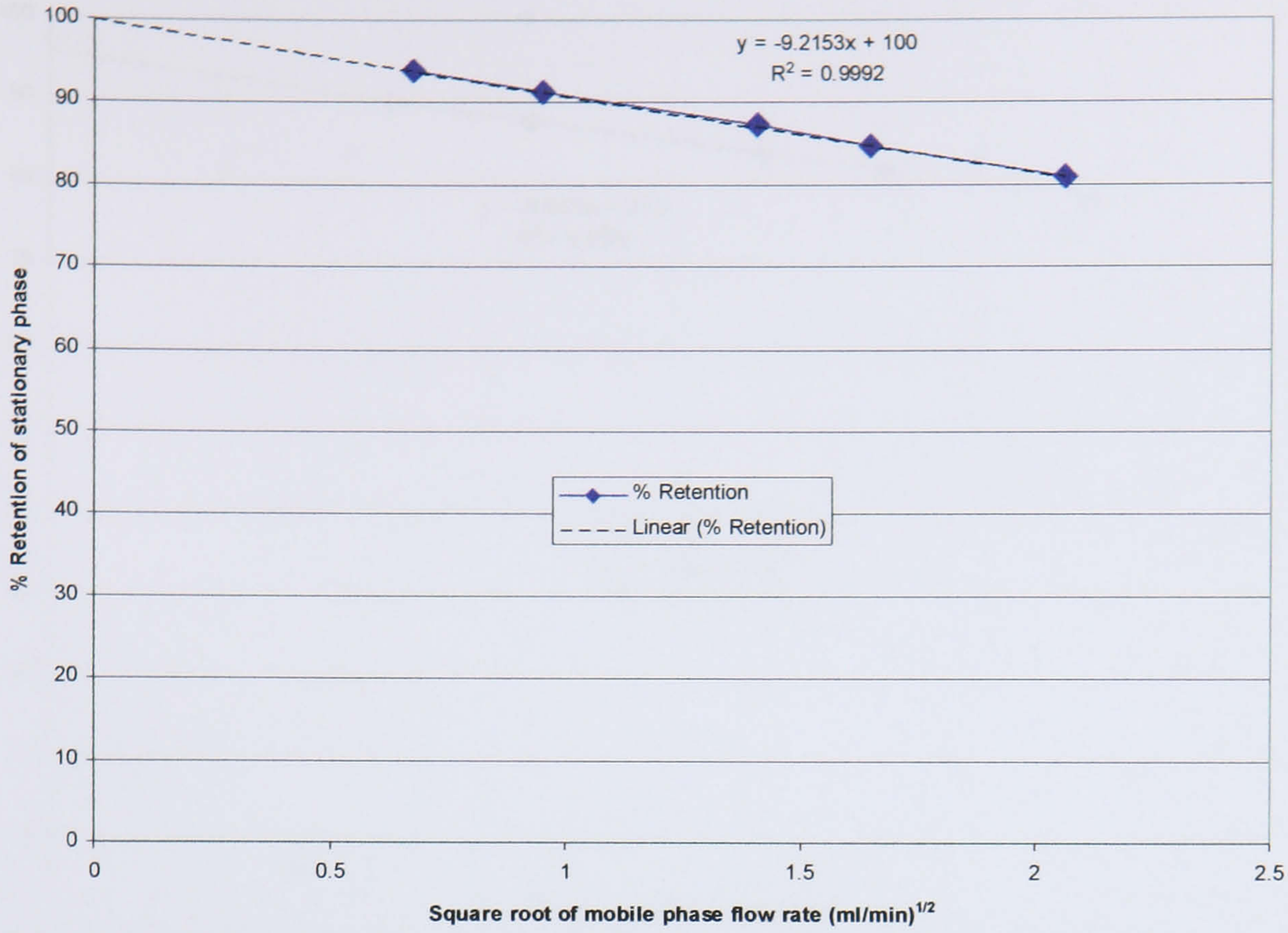

Figure 4.5.1.2 shows the % stationary phase retention (S_f) plotted against the square root of mobile phase flow rate for the 4A phase system using a syringe driver and a dead volume of 7.287ml

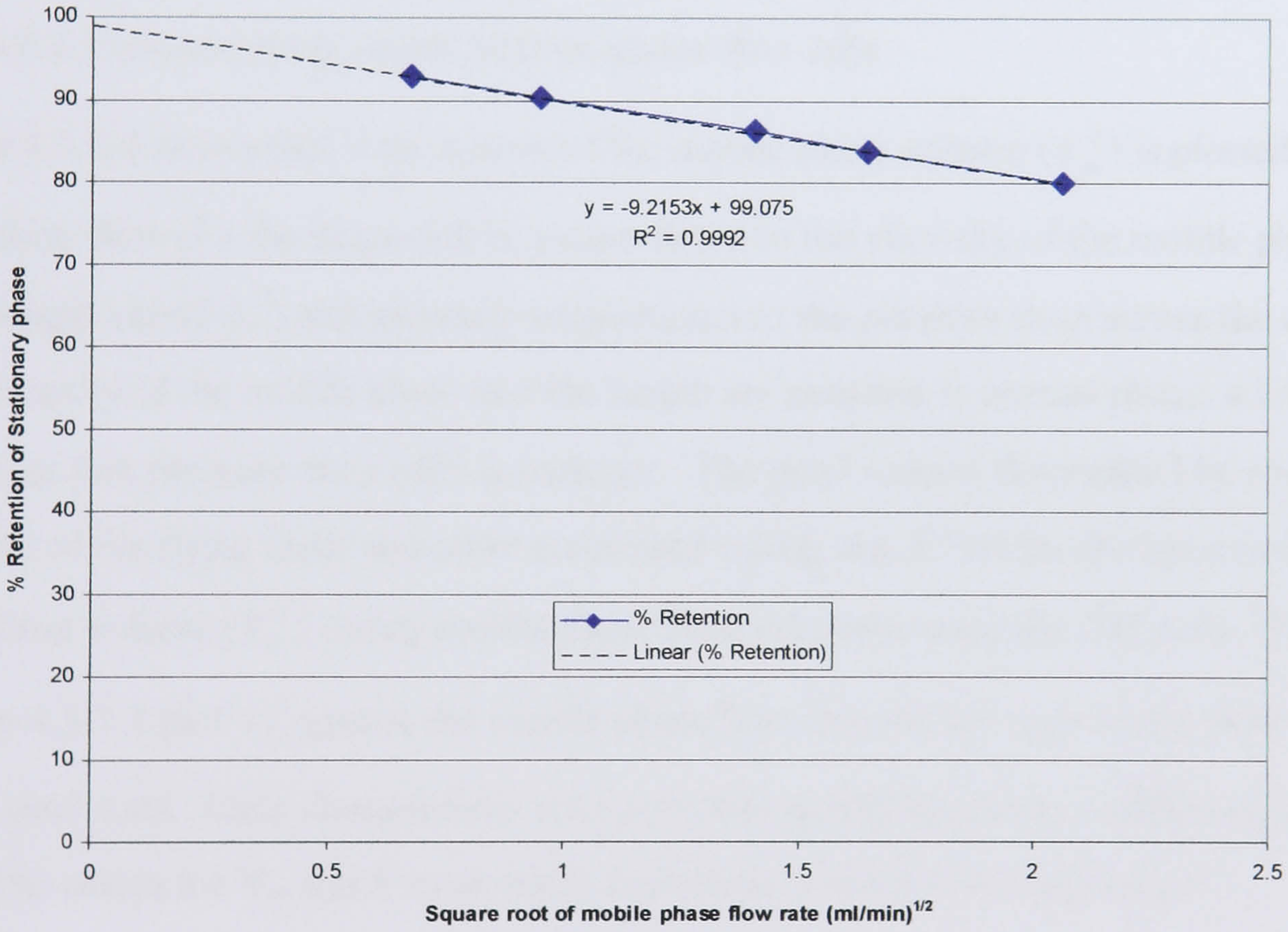

Figure 4.5.1.3 shows the % stationary phase retention (S_f) plotted against the square root of mobile phase flow rate for the 4A phase system using a syringe driver and a 6.4ml dead volume

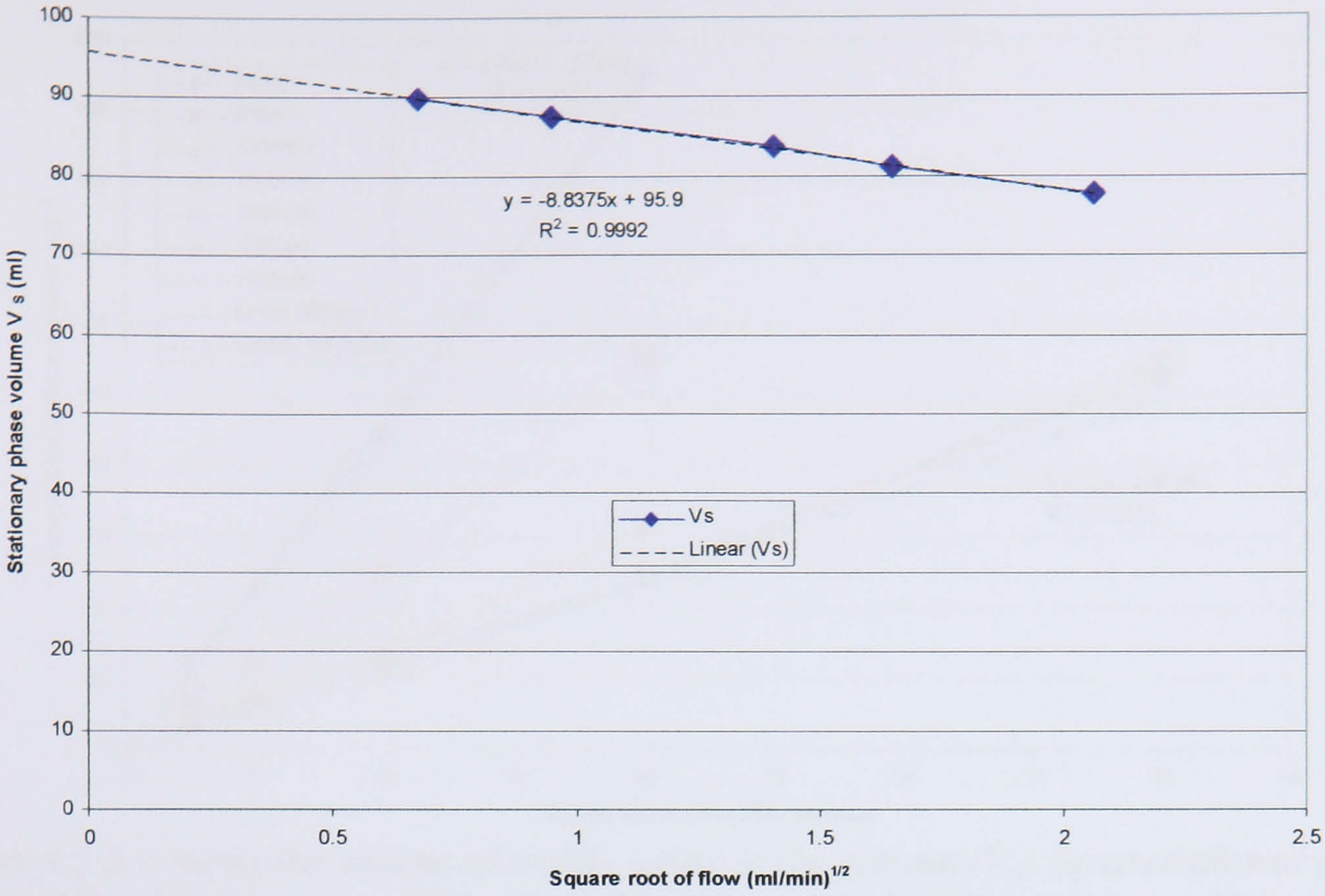

Figure 4.5.1.4 shows the volume of stationary phase plotted against the square root of mobile phase flow rate for the 4A phase system using a syringe driver

Figures 4.5.1.1 to 4.5.1.4 were produced using the data contained in table 4.5.1.1.

4.5.2 Pressure drop verses Mobile phase flow rate

Equation 4.3.2.4 shows that if the square of the mobile phase volume (V_m^2) is plotted against mobile phase flow (F): the slope will be proportional to the viscosity of the mobile phase (μ_m), the coil length cubed (L^3) and inversely proportional to the pressure drop across the coil (ΔP). As the viscosity of the mobile phase and the length are constant in normal phase, a linear result will indicate that pressure drop (ΔP) is constant. The dead volume determined by measuring the lengths of the flying leads and other associated tubing was 8.5ml for the square of the mobile phase volume (V_m^2) verses mobile phase flow rate tests using the IMI coils. Figures 4.5.2.1 to 4.5.2.3 plot V_m^2 against the mobile phase flow rate (F) for each of the three IMI stainless steel coils. Each characteristic on a particular graph represents a different rotational speed. The values for V_m and F were taken from table A.4.1.2 from Appendix 4.

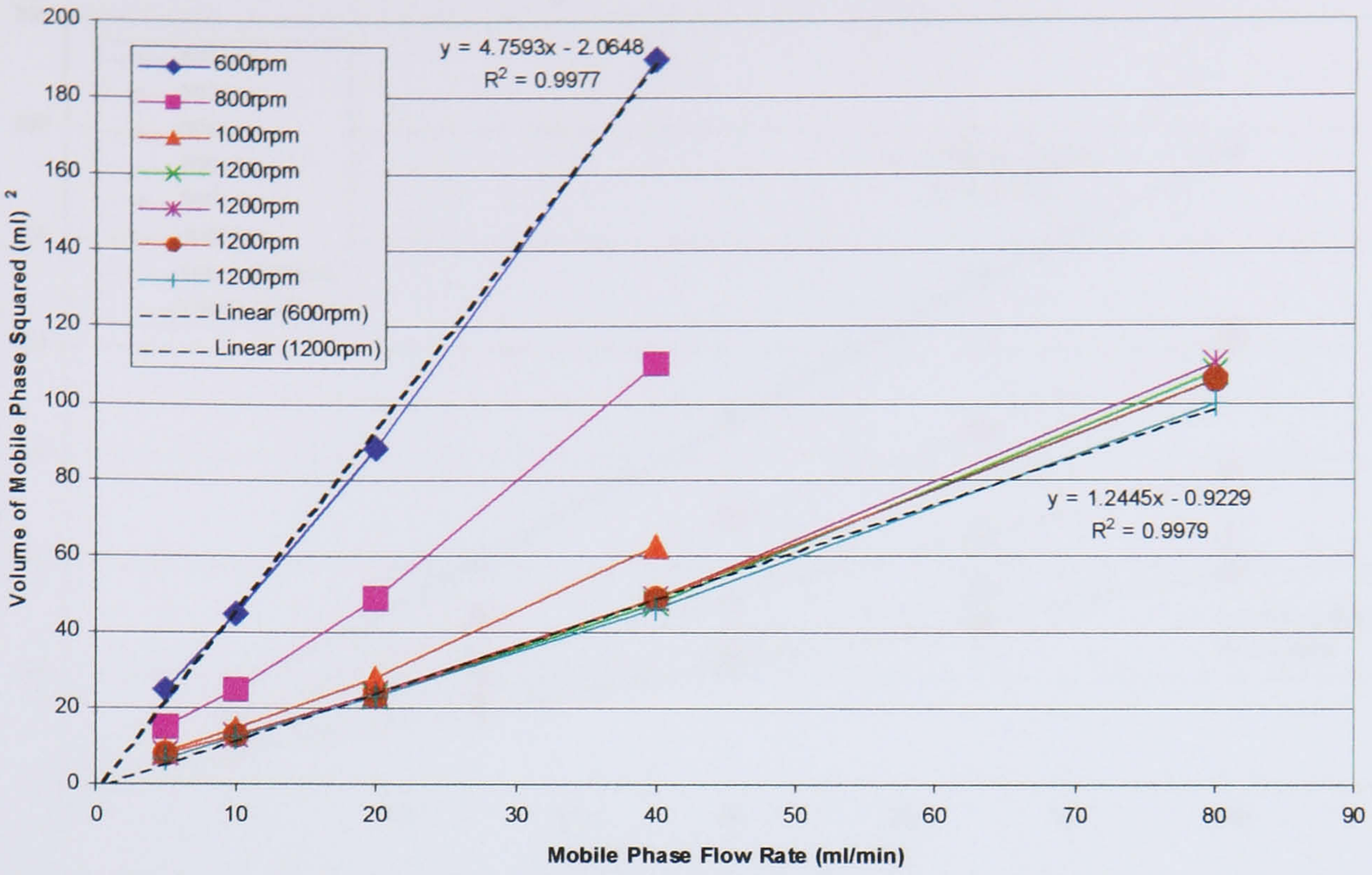

Figure 4.5.2.1 shows the volume of mobile phase in the column (V_m) squared plotted against the mobile phase flow rate (F) for the 3.73mm bore (60ml) IMI stainless steel helical coil

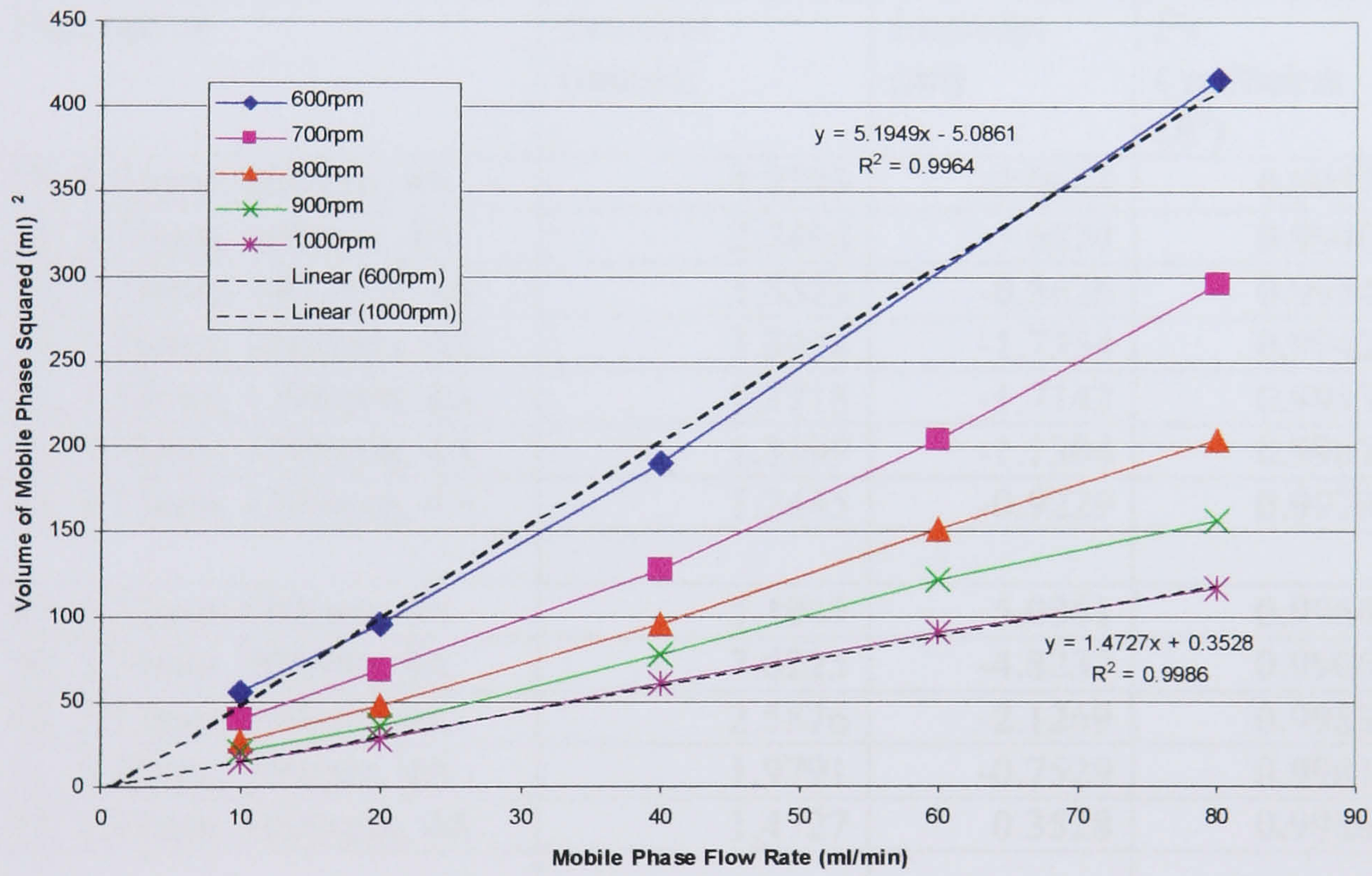

Figure 4.5.2.2 shows the volume of mobile phase in the column (V_m) squared plotted against the mobile phase flow rate (F) for the 5.33mm bore (120ml) IMI stainless steel helical coil

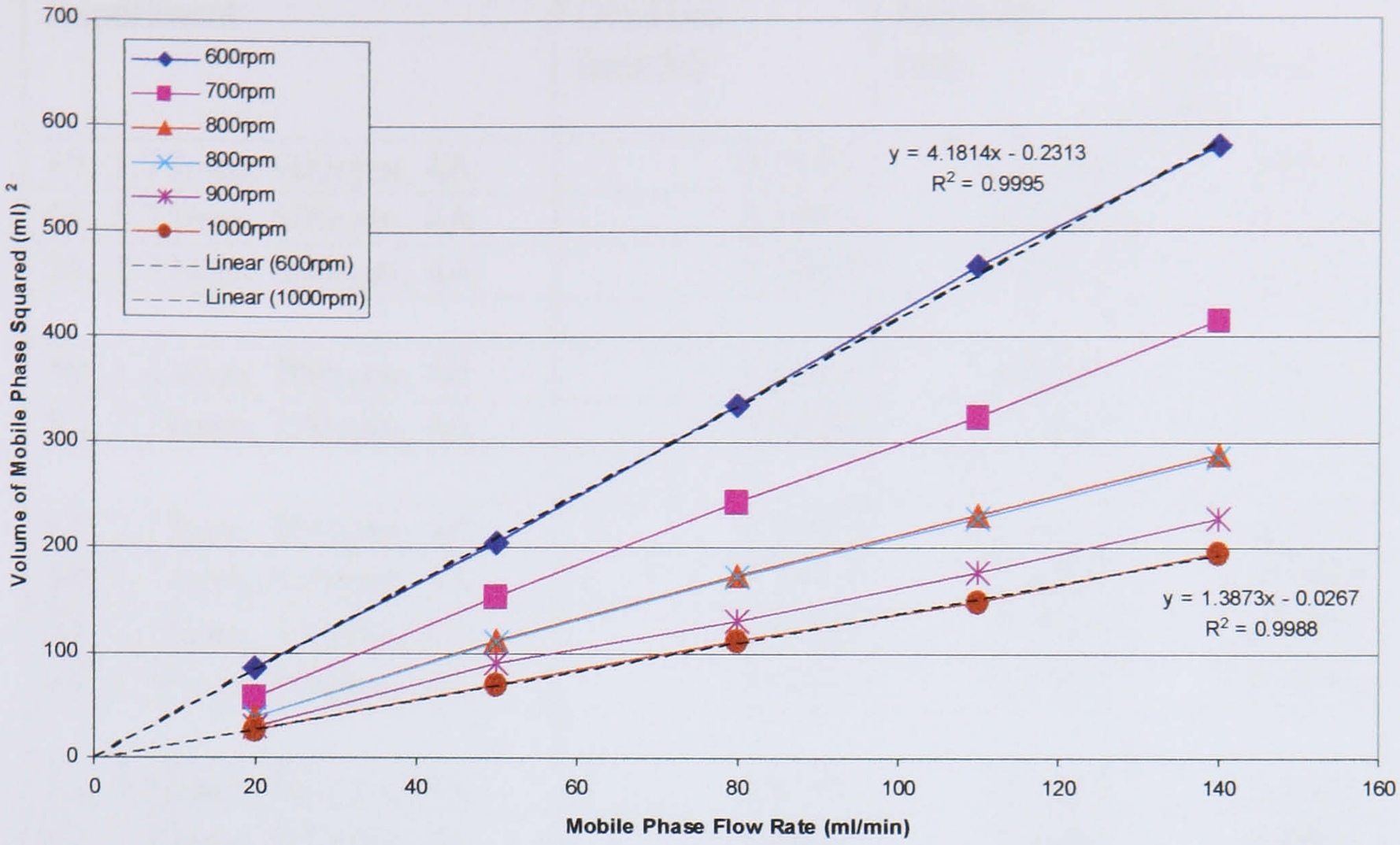

Figure 4.5.2.3 shows the volume of mobile phase in the column (V_m) squared plotted against the mobile phase flow rate (F) for the 7.73mm bore (260ml) IMI stainless steel helical coil

Experiment	Gradient (mlmin)	Intercept (ml)	Fit Coefficient (R^2)
39, 3.73mm, 600rpm, 4A	4.7593	-2.0648	0.9977
41, 3.73mm, 800rpm, 4A	2.7495	-1.6874	0.9940
42, 3.73mm, 1000rpm, 4A	1.5573	-0.8626	0.9954
33, 3.73mm, 1200rpm, 4A	1.3438	-1.7354	0.9942
34, 3.73mm, 1200rpm, 4A	1.3718	-1.7142	0.9953
35, 3.73mm, 1200rpm, 4A	1.3199	-1.1304	0.9967
44, 3.73mm, 1200rpm, 4A	1.2445	-0.9229	0.9979
47, 5.33mm, 600rpm, 4A	5.1949	-5.0861	0.9964
50, 5.33mm, 700rpm, 4A	3.6225	-4.8237	0.9906
48, 5.33mm, 800rpm, 4A	2.5576	-2.1269	0.9983
51, 5.33mm, 900rpm, 4A	1.9791	-0.7529	0.9981
49, 5.33mm, 1000rpm, 4A	1.4727	0.3528	0.9986
56, 7.73mm, 600rpm, 4A	4.1814	-0.2313	0.9995
55, 7.73mm, 700rpm, 4A	2.9568	2.4640	0.9992
57, 7.73mm, 800rpm, 4A	2.0660	3.7360	0.9970
54, 7.73mm, 800rpm, 4A	2.0403	3.5573	0.9950
52, 7.73mm, 900rpm, 4A	1.6072	2.4960	0.9965
53, 7.73mm, 1000rpm, 4A	1.3873	-0.0267	0.9988

Table 4.5.2.1 shows the gradients, intercepts and fit coefficients of the fitted straight-line characteristics for figures 4.5.2.1 to 4.5.2.3

The first column of table 4.5.2.1 contains: the experiment number, the bore of the coil tubing, the rotational speed and the phase system used.

Experiment	Gradient (mlmin)	Intercept (ml)	Fit Coefficient (R^2)
39, 3.73mm, 600rpm, 4A	4.7593	-2.0648	0.9977
47, 5.33mm, 600rpm, 4A	5.1949	-5.0861	0.9964
56, 7.73mm, 600rpm, 4A	4.1814	-0.2313	0.9995
50, 5.33mm, 700rpm, 4A	3.6225	-4.8237	0.9906
55, 7.73mm, 700rpm, 4A	2.9568	2.4640	0.9992
41, 3.73mm, 800rpm, 4A	2.7495	-1.6874	0.9940
48, 5.33mm, 800rpm, 4A	2.5576	-2.1269	0.9983
57, 7.73mm, 800rpm, 4A	2.0660	3.7360	0.9970
54, 7.73mm, 800rpm, 4A	2.0403	3.5573	0.9950
51, 5.33mm, 900rpm, 4A	1.9791	-0.7529	0.9981
52, 7.73mm, 900rpm, 4A	1.6072	2.4960	0.9965
42, 3.73mm, 1000rpm, 4A	1.5573	-0.8626	0.9954
49, 5.33mm, 1000rpm, 4A	1.4727	0.3528	0.9986
53, 7.73mm, 1000rpm, 4A	1.3873	-0.0267	0.9988
33, 3.73mm, 1200rpm, 4A	1.3438	-1.7354	0.9942
34, 3.73mm, 1200rpm, 4A	1.3718	-1.7142	0.9953
35, 3.73mm, 1200rpm, 4A	1.3199	-1.1304	0.9967
44, 3.73mm, 1200rpm, 4A	1.2445	-0.9229	0.9979

Table 4.5.2.2 shows the results of table 4.5.2.1 rearranged in terms of rotational speed

In table 4.5.2.2 the 1200rpm values from the 3.73mm bore coil give an indication of the experimental error for the other results.

Flow Rate (ml/min) Experiment	5	10	20	40	50	60	80	110	140
33, 3.73mm, 1200rpm	2.8	3.6	4.8	6.9			10.4		
34, 3.73mm, 1200rpm	2.8	3.6	4.9	7.0			10.5		
35, 3.73mm, 1200rpm	2.8	3.6	4.8	7.0			10.3		
44, 3.73mm, 1200rpm	2.6	3.5	4.8	6.8			10.0		
39, 3.73mm, 600rpm	5.0	6.7	9.4	13.8					
47, 5.33mm, 600rpm		7.5	9.8	13.8			20.4		
56, 7.73mm, 600rpm			9.2		14.3		18.3	21.6	24.1
50, 5.33mm, 700rpm		6.3	8.3	11.3		14.3	17.2		
55, 7.73mm, 700rpm			7.6		12.4		15.6	18.0	20.4
41, 3.73mm, 800rpm	3.9	5.0	7.0	10.5					
48, 5.33mm, 800rpm		5.2	6.9	9.8		12.3	14.3		
57, 7.73mm, 800rpm			6.2		10.6		13.2	15.2	17.0
54, 7.73mm, 800rpm			6.2		10.5		13.1	15.1	16.9
51, 5.33mm, 900rpm		4.6	6.0	8.8		11.0	12.5		
52, 7.73mm, 900rpm			5.5		9.4		11.4	13.3	15.1
42, 3.73mm, 1000rpm	2.9	3.8	5.3	7.9					
49, 5.33mm, 1000rpm		3.9	5.3	7.8		9.5	10.8		
53, 7.73mm, 1000rpm			5.2		8.4		10.6	12.2	14.0

Table 4.5.2.3 shows the displaced volumes of mobile phase (V_m) for the 4A phase system in normal phase for each IMI stainless steel coil

The table 4.5.2.3 is table A.4.1.2 from Appendix 4 rearranged to show the volume of mobile phase (V_m) in each IMI coil for the same rotational speed. The first four rows show the same experiment repeated four times on the same coil at the same rotational speed. The figures shown in blue indicate approximately equal volumes displaced from different IMI coils at the same rotational speed and flow rate.

4.5.3 Retention verse Bore for IMI Stainless Steel Coils

The dead volume determined by measuring the lengths of the flying leads and other associated tubing was 8.5ml for both normal and reverse phase mode retention studies using the IMI coils. For normal phase mode (NM) the first column of table 4.5.3.1 contains: the experiment number, the bore of the coil tubing, the rotational speed and the phase system used. The second column contains dead volume data determined as in section 4.3.1. The values in the third column are calculated using raw data from tables A.4.1.1 and A.4.1.3 Appendix 4. The fit coefficients shown in the fifth column are for the trend lines fitted to both the dead volume figures and the Du retention characteristics, which are identical for the same experiment. The analysis of the pressure drops associated with these retention characteristics is conducted in Chapter 5.

Experiment	Dead Vol. (ml) $F^{0.5}$	Pump out Vol. – largest Displaced Vol. (ml)	Du Gradient $(min/ml)^{0.5}$	Fit Coefficient (R^2)
39, 3.73mm, 600rpm, 4A	7.7738	1.4	3.6573	0.9970
41, 3.73mm, 800rpm, 4A	8.2064	-0.6	2.7556	0.9917
42, 3.73mm, 1000rpm, 4A	8.6958	-1.3	2.0809	0.9941
33, 3.73mm, 1200rpm, 4A	8.3911	-0.8	1.9212	0.9924
34, 3.73mm, 1200rpm, 4A	8.4693	0.0	1.9488	0.9940
35, 3.73mm, 1200rpm, 4A	8.4372	-1.0	1.9057	0.9946
44, 3.73mm, 1200rpm, 4A	8.9983	-0.8	1.8650	0.9976
47, 5.33mm, 600rpm, 4A	6.9008	0.2	1.8659	0.9950
50, 5.33mm, 700rpm, 4A	7.4967	-0.7	1.5817	0.9973
48, 5.33mm, 800rpm, 4A	8.1579	0.5	1.3189	0.9976
51, 5.33mm, 900rpm, 4A	8.4708	0.0	1.1655	0.9971
49, 5.33mm, 1000rpm, 4A	8.8049	0.4	1.0093	0.9986
56, 7.73mm, 600rpm, 4A	7.5927	-0.7	0.7880	0.9996
55, 7.73mm, 700rpm, 4A	7.8261	-0.2	0.6650	0.9991
57, 7.73mm, 800rpm, 4A	8.6726	-2.2	0.5612	0.9961
54, 7.73mm, 800rpm, 4A	8.2971	0.8	0.5565	0.9969
52, 7.73mm, 900rpm, 4A	8.3837	0.0	0.4931	0.9965
53, 7.73mm, 1000rpm, 4A	8.2685	0.7	0.4551	0.9991

Table 4.5.3.1 shows the retention results for the 4A phase system in normal phase for the three IMI stainless steel coils

Figure 4.5.3.1 uses results from table 4.5.3.1 and plots the Du gradient against $1/d_C^2$ for normal phase operation at three different rotational speeds. The coil tubing bore d_C being measured in cm.

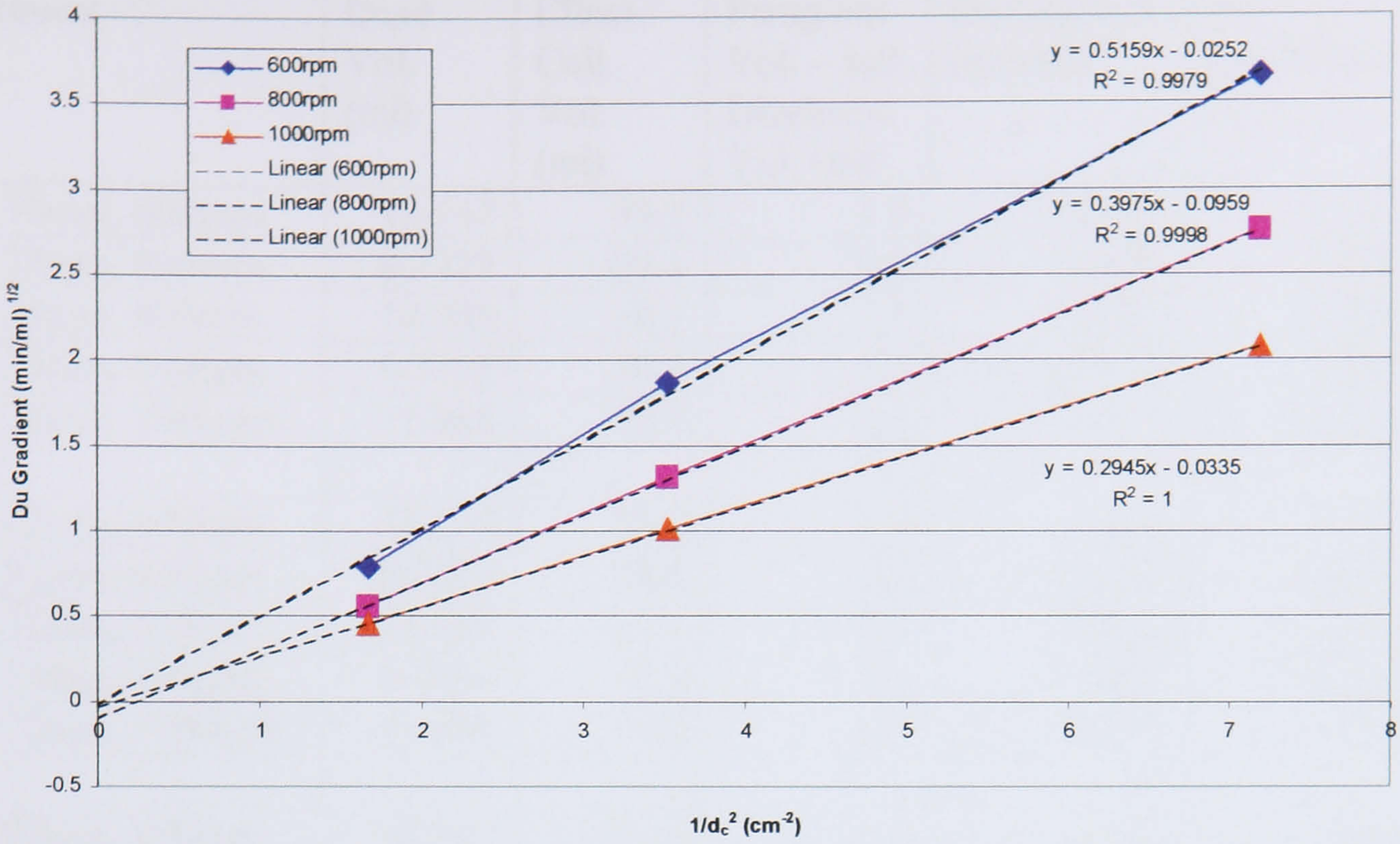

Figure 4.5.3.1 show how the Du gradient varies with $1/d_C^2$ for the 4A phase system in normal phase mode in the three IMI stainless steel coils

For reverse phase mode (RM) the first column, of table 4.5.3.2, contains the experiment number, the bore of the coil tubing, the rotational speed and the phase system used. The values in the fourth column are calculated using values from tables A.4.2.1 and A.4.2.2 in Appendix 4. The fit coefficients shown in the sixth column are for the trend lines fitted to both the dead volume figures and the Du retention characteristics, which are identical for the same experiment.

Experiment	Dead Vol. (ml)	Effect. Coil Vol. (ml)	Pump out Vol. – last Displaced Vol. (ml)	Du Gradient $(min/ml)^{0.5}$	Fit Coefficient (R^2)
61, 3.73mm, 600rpm	12.147	59.1	1.4	3.2345	0.9984
58, 3.73mm, 800rpm	8.7722	59.1	6.6	2.3519	0.9928
59, 3.73mm, 800rpm	14.006	59.1	3.6	2.0828	0.9942
60, 3.73mm, 800rpm	9.7508	59.1	5.6	2.3356	0.9967
62, 3.73mm, 1000rpm	11.808	59.1	2.1	1.9975	0.9982
61, 3.73mm, 600rpm	12.147	55.5	1.4	3.4472	0.9984
58, 3.73mm, 800rpm	8.7722	58.8	6.6	2.3628	0.9928
59, 3.73mm, 800rpm	14.006	53.6	3.6	2.2968	0.9942
60, 3.73mm, 800rpm	9.7508	57.8	5.6	2.3861	0.9967
62, 3.73mm, 1000rpm	11.808	55.8	2.1	2.1159	0.9982
64, 7.73mm, 600rpm	49.829	218.2	14.5	1.0473	0.9996
63, 7.73mm, 1000rpm	38.109	229.9	11.1	1.0377	0.9953

Table 4.5.3.2 shows the retention results for the 4A phase system in reverse phase mode for two of the IMI stainless steel coils

The raw data for the results shown in the table above are given in table A.4.2.1 Appendix 4. The Dead Volume for the 4A phase system in reverse phase mode for the IMI coils calculated from cross-sectional areas and lengths of tubing and was 8.5ml. The dead volumes in the second column of the table above were determined as described in section 4.3.1. The effective coil volume results shown in the third column were determined using equation 4.3.1.1 rearranged to give:

$$\text{Effective Coil Volume} = V_C = V_{SYS} - V_d \qquad (4.5.3.1)$$

For the 3.73mm bore coil the system volume (V_{SYS}) was determined by adding the theoretical coil volume of 59.1ml and the 8.5ml Dead Volume to give V_{SYS} = 67.6ml. A similar procedure was used for the 7.73mm bore tubing giving a V_{SYS} = 268ml. The retention gradient shown in the first five rows were calculated using the 8.5ml dead volume and a coil volume of 59.1ml for 3.73mm bore coil. The results in the remaining rows were calculated using the dead volumes in the second column and adjusting the coil volume (V_C) as per equation 4.5.3.1. V_m was determined using equation 4.3.1.7 and the stationary phase retention (S_f) was determined using the following equation:

$$S_f = 100\left(\frac{V_C - V_m}{V_C}\right) \qquad (4.5.3.2)$$

The fit coefficients shown in the sixth column, of the table 4.5.3.2, are for the trend lines fitted to both the dead volume figures and the Du retention characteristics, which are identical for the same experiment.

4.5.4 Reynolds Numbers verses Bore for IMI Stainless Steel Coils

Flow Rate (ml/min) Experiment	5	10	20	40	50	60	80	110	140
39, 3.73mm, 600rpm	184	318	537	886					
41, 3.73mm, 800rpm	209	369	623	1018					
42, 3.73mm, 1000rpm	242	423	716	1172					
33, 3.73mm, 1200rpm	246	434	752	1254			2043		
34, 3.73mm, 1200rpm	245	432	742	1243			2032		
35, 3.73mm, 1200rpm	249	437	755	1249			2057		
44, 3.73mm, 1200rpm	255	440	752	1264			2085		
47, 5.33mm, 600rpm		301	527	888			1460		
50, 5.33mm, 700rpm		328	572	960		1285	1590		
48, 5.33mm, 800rpm		360	626	1051		1408	1741		
51, 5.33mm, 900rpm		383	671	1110		1489	1863		
49, 5.33mm, 1000rpm		418	716	1181		1605	2007		
56, 7.73mm, 600rpm			550		1103		1560	1974	2378
55, 7.73mm, 700rpm			606		1186		1691	2164	2587
57, 7.73mm, 800rpm			668		1279		1834	2351	2830
54, 7.73mm, 800rpm			670		1287		1843	2361	2840
52, 7.73mm, 900rpm			710		1359		1975	2514	3003
53, 7.73mm, 1000rpm			729		1436		2046	2623	3117

Table 4.5.4.1 shows the Reynolds number for the upper phase mobile (normal phase mode) for the 4A phase system in the three IMI stainless steel coils

The values in table 4.5.4.1 were calculated using equation A.5.5 from Appendix 5, density and viscosity data for the upper phase was taken from table 2.2.2 of Chapter 2 and data from table A.4.1.2 from Appendix 4. The data from table 4.5.4.1 has been regrouped by speed in table 4.5.4.2.

Flow Rate (ml/min) Experiment	5	10	20	40	50	60	80	110	140
39, 3.73mm, 600rpm	184	318	537	886					
47, 5.33mm, 600rpm		301	527	888			1460		
56, 7.73mm, 600rpm			550		1103		1560	1974	2378
50, 5.33mm, 700rpm		328	572	960		1285	1590		
55, 7.73mm, 700rpm			606		1186		1691	2164	2587
41, 3.73mm, 800rpm	209	369	623	1018					
48, 5.33mm, 800rpm		360	626	1051		1408	1741		
57, 7.73mm, 800rpm			668		1279		1834	2351	2830
54, 7.73mm, 800rpm			670		1287		1843	2361	2840
51, 5.33mm, 900rpm		383	671	1110		1489	1863		
52, 7.73mm, 900rpm			710		1359		1975	2514	3003
42, 3.73mm, 1000rpm	242	423	716	1172					
49, 5.33mm, 1000rpm		418	716	1181		1605	2007		
53, 7.73mm, 1000rpm			729		1436		2046	2623	3117
33, 3.73mm, 1200rpm	246	434	752	1254			2043		
34, 3.73mm, 1200rpm	245	432	742	1243			2032		
35, 3.73mm, 1200rpm	249	437	755	1249			2057		
44, 3.73mm, 1200rpm	255	440	752	1264			2085		

Table 4.5.4.2 shows the Reynolds number results from table 4.5.4.1 rearranged in terms of rotational speed

The values highlighted in blue indicate similar *Re* at the same rotational speed and flow rate but in different bore coils. The 1200rpm values for the 3.73mm bore coil give an indication of the experimental error for the other results.

4.5.5 Retention for Normal and Reverse phase mode for PTFE Coils

These experiments show the effect of operating in normal and reverse phase mode for the same operating conditions. The dead volume determined by measuring the lengths of the flying leads and other associated tubing was 5.8ml for both normal and reverse phase mode retention studies using the PTFE coils.

The first column of table 4.5.5.1 contains: the experiment number and whether the coil was operated in normal (NM) or reverse phase mode (RM) and the phase system used. The second column contains the dead volume data taken from table A.4.3.1 and processed as described in section 4.3.1. The values in the third column are calculated using raw data from tables A.4.3.1 and A.4.3.3 Appendix 4. The fit coefficients shown in the fifth column are for the trend lines fitted to both the dead volume figures and the Du retention characteristics, which are identical for the same experiment. The analysis of the pressure drops associated with these retention characteristics is conducted in Chapter 5.

Run (Coil Vol. = 99.9ml, bore = 1.5875mm & length = 50.5m)	Dead Volume (ml)	Pump out Vol. – last Displaced Vol. (ml)	Du Gradient $(min/ml)^{0.5}$	Fit Coefficient (R^2)	Temperature Range (°C)
67, 800rpm, RM, 4A	3.9836	0.1	9.9095	0.9859	30.0 to 30.1
70, 800rpm, NM, 4A	5.4850	-3.3	5.0840	0.9759	30.0 to 30.1
68, 1000rpm, RM, 4A	6.1193	-0.1	7.1177	0.9972	30.9 to 32.4
71, 1000rpm, NM, 4A	5.1995	-2.0	3.8097	0.9838	30.5 to 31.7
69, 1200rpm, RM, 4A	7.1313	-0.3	5.4268	0.9991	33.7 to 37.1
72, 1200rpm, NM, 4A	5.3472	-2.1	3.3036	0.9654	33.3 to 37.5

Table 4.5.5.1 shows the results for the 1.58mm bore PTFE coil for normal and reverse phase mode for the 4A phase system

The following table predicts the normal Du gradient from the measured reverse phase Du gradients contained in table 4.5.5.1 using equation 4.3.2.13 and viscosity data taken from table 2.2.2 Chapter 2 for the 4A phase system.

Experiment (Coil Vol. = 99.9ml, bore = 1.5875mm & length = 50.5m)	Predicted Du Gradient $(min/ml)^{0.5}$
800rpm	5.0984
1000rpm	3.6620
1200rpm	2.7921

Table 4.5.5.2 shows the predicted normal phase mode Du gradients for the 1.58mm bore PTFE coil and the 4A phase system

Figures 4.5.5.1, 4.5.5.2 and 4.5.5.3 are Du plots of the measured normal and reverse phase mode results contained in table 4.5.5.1. The predicted normal phase Du retention characteristics shown in table 4.5.5.2 are plotted in figures 4.5.5.1, 4.5.5.2 and 4.5.5.3, to be compared with the measured normal phase mode retention characteristics.

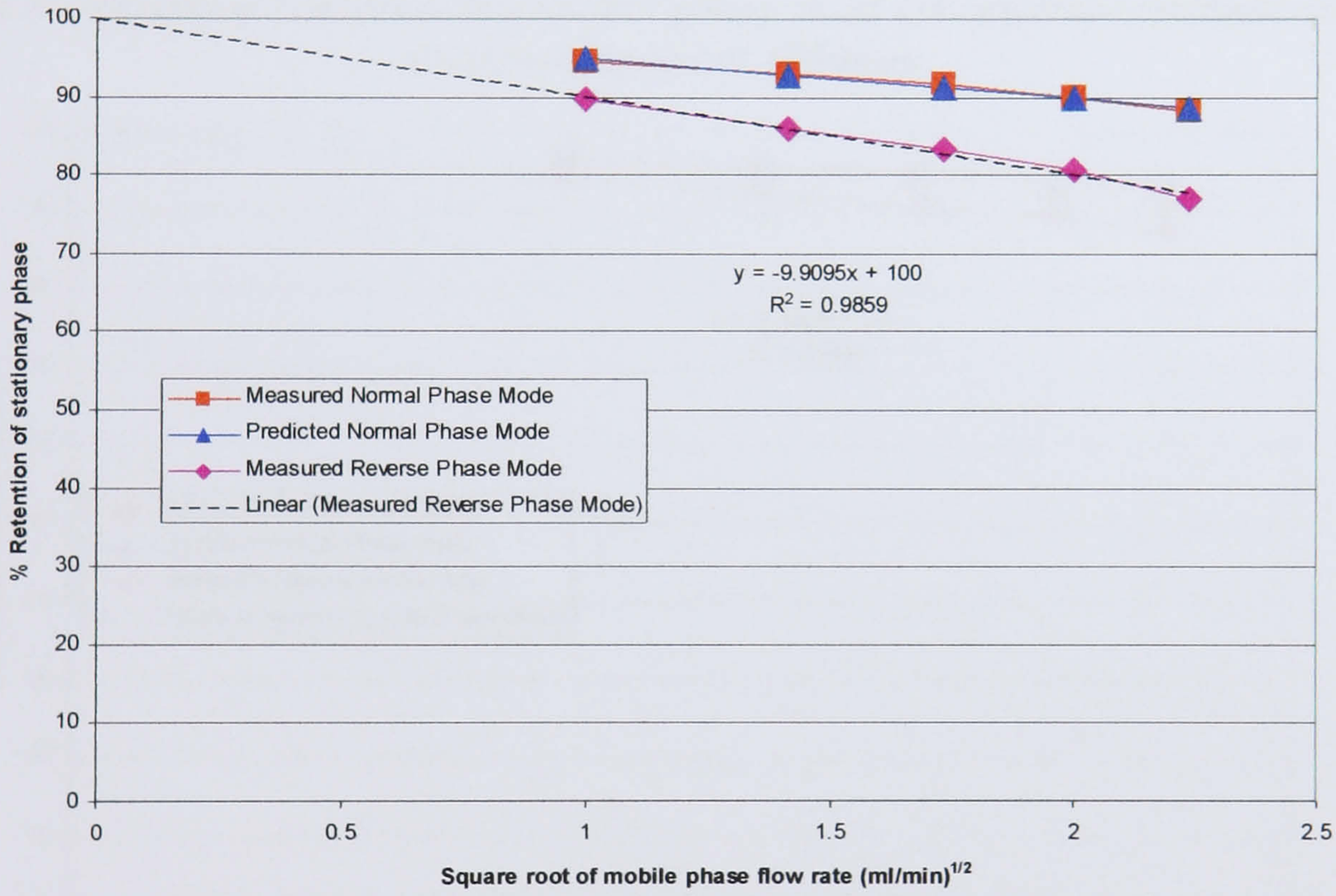

Figure 4.5.5.1 shows the measured reverse phase mode Du retention characteristic and compares the measured and predicted normal phase mode Du retention characteristics for a rotational speed of 800rpm

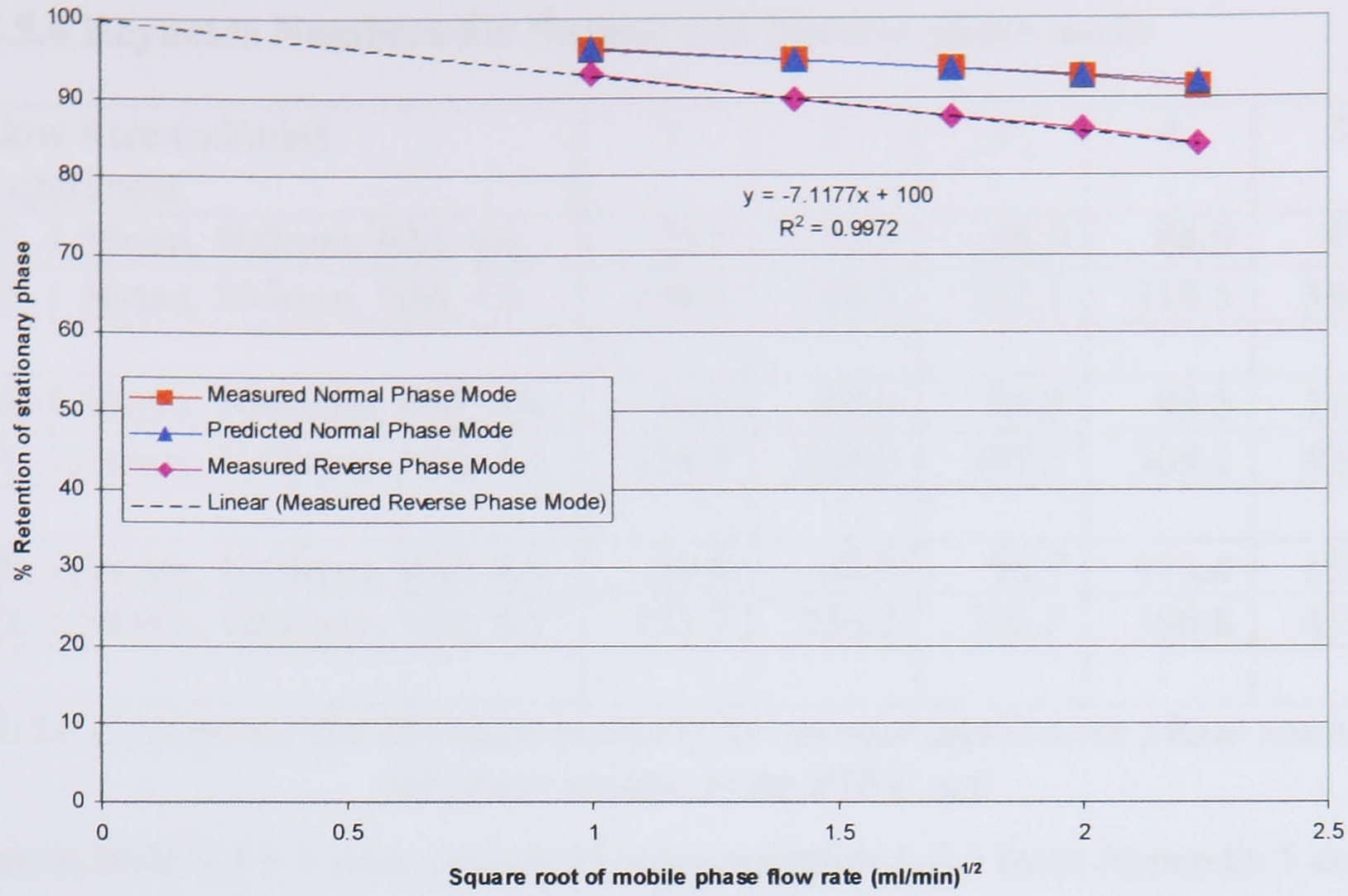

Figure 4.5.5.2 shows the measured reverse phase mode Du retention characteristic and compares the measured and predicted normal phase mode Du retention characteristics for a rotational speed of 1000rpm

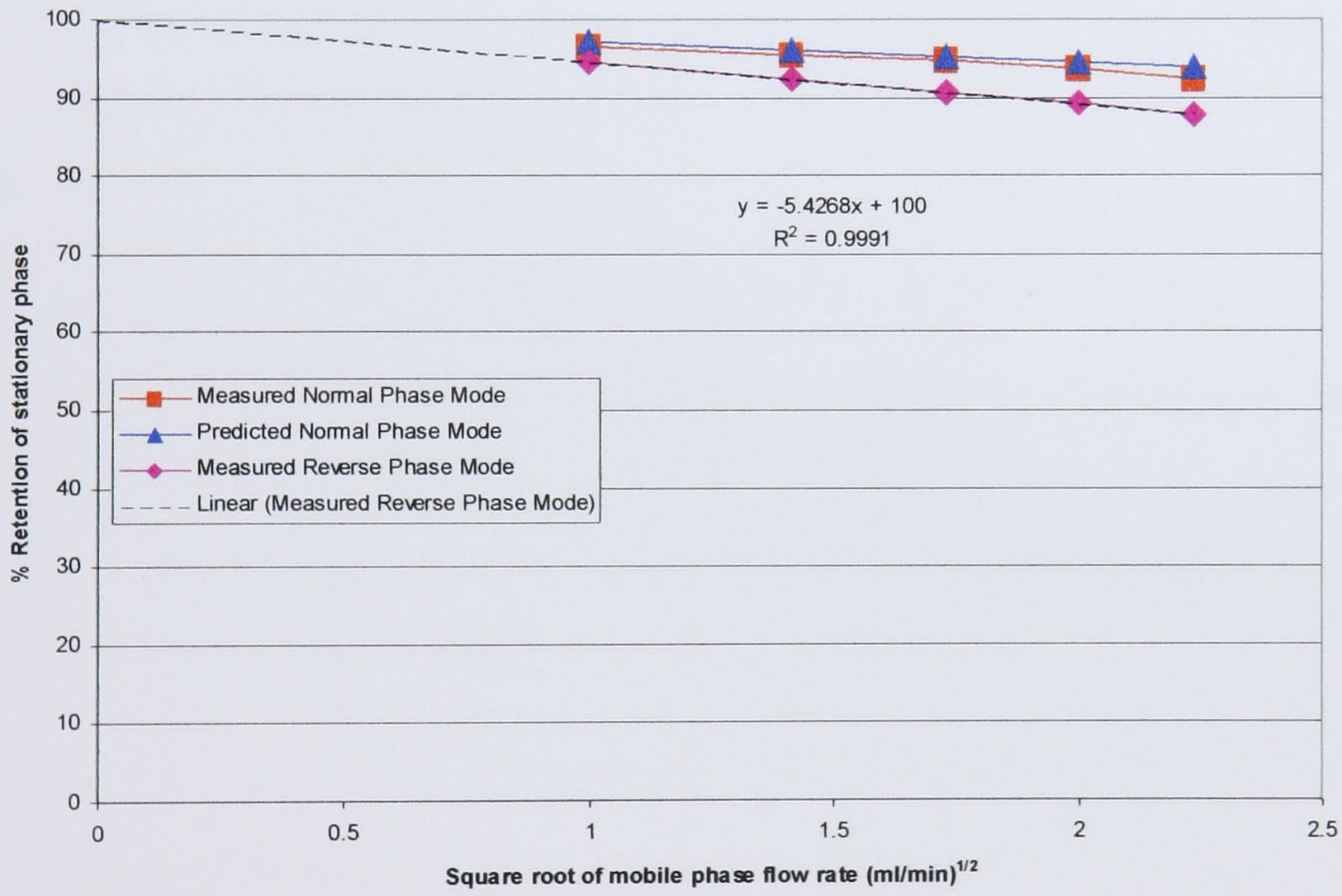

Figure 4.5.5.3 shows the measured reverse phase mode Du retention characteristic and compares the measured and predicted normal phase mode Du retention characteristics for a rotational speed of 1200rpm

4.5.6 Reynolds Numbers for Normal and Reverse phase mode

Flow Rate (ml/min) Experiment	1	2	3	4	5
67, 1.58mm, 800rpm, RM, 4A	29.1	49.7	68.5	84.9	97.2
70, 1.58mm, 800rpm, NM, 4A	108.3	190.3	262.1	318.5	366.6
68, 1.58mm, 1000rpm, RM, 4A	35.2	58.0	79.3	99.5	116.4
71, 1.58mm, 1000rpm, NM, 4A	126.0	218.9	301.2	368.1	424.7
69, 1.58mm, 1200rpm, RM, 4A	39.8	67.3	90.7	113.4	133.3
72, 1.58mm, 1200rpm, NM, 4A	133.7	236.2	326.8	396.8	452.5

Table 4.5.6.1 compares the Reynolds numbers for normal and reverse phase modes for the 4A phase system in the PTFE coil

The values in table 4.5.6.1 were calculated using equation A.5.5 from Appendix 5 and data from table A.4.3.2 from Appendix 4. In the first column RM means reverse phase mode and NM means normal phase mode.

4.6 Discussion

4.6.1 Dead Volume

4.6.1.1 Dead Volume using a Syringe and Syringe driver

The dead volume determined in the traditional manner by measuring the lengths of the flying leads and the calculating the volume from the cross-sectional area was 6.4ml. Figure 4.5.1.1 shows the displaced volume of stationary phase plotted against the square root of mobile phase flow. The equation of the fitted linear relationship is:

$$V_E = 8.8375\sqrt{F} + 7.287$$

and the coefficient of linear regression is 0.9992. Therefore the dead volume determined by the above equation is 7.287ml that is approximately 0.9ml greater than the volume of the flying leads measured in the traditional way. The 0.9ml is due to the combination of dead volume in the delivery tubes, the switching valve used to switch between stationary and mobile phases and the dead volume in the pressure transducer. Figure 4.5.1.2 is the Du plot from the same run using the 7.287ml dead volume. The equation of the fitted linear relationship from figure 4.5.1.2 is:

$$\%\ \text{Retention of stationary phase} = -9.2153\sqrt{F} + 100$$

and the coefficient of linear regression is also 0.9992. The above equation shows that the retention will be 100% when there is no mobile phase flow.

Figure 4.5.1.3 is the Du graph from the same run using the 6.4ml flying lead volume. The equation of the fitted linear relationship from figure 4.5.1.3 is:

$$\%\ \text{Retention of stationary phase} = -9.2153\sqrt{F} + 99.075$$

and the coefficient of linear regression is also 0.9992. The gradients of the fitted linear relationships of figures 4.5.1.2 and 4.5.1.3 are identical. However for figure 4.5.1.3 the intercept on the y-axis is not 100% but is 99.075%. This means that all calculated retentions would be approximately 1% lower than the actual retentions leading to errors in predicting resolution and elution points.

Equation 4.3.1.11 shows that the magnitude of the gradient of figure 4.5.1.1 equals the magnitude of the gradient of figure 4.5.1.2 multiplied by the coil volume (95.9ml) and divided by 100 ie:

$$\text{Magnitude of Gradient figure 4.5.1.1} = \text{Magnitude of Gradient figure 4.5.1.2 x } \frac{V_C}{100}$$

$$8.8375 = \frac{9.2153 \times 95.9}{100} = 8.8375$$

If the Du graph was modified so that the actual volume of stationary phase (V_S) was plotted against the square root of mobile phase flow rate as described by equation 4.3.1.6 and shown in figure 4.5.1.4 the magnitudes of the gradients would be equal. The equation of the fitted linear relationship from figure 4.5.1.4 is:

$$V_S = -8.8375\sqrt{F} + 95.9$$

and the coefficient of linear regression is also 0.9992. The above relationship shows that the intercept on the vertical axis for zero flow of mobile phase is the coil volume ie 95.9ml.

These results confirm the derivation of equation 4.3.1.10 and the assumption that the stationary phase retention is 100% when the mobile phase flow rate is zero. This new method of determining the dead volume for a J-type centrifuge was found to be more accurate than calculating the dead volume from the length of the flying leads, since the intercept on the y-axis passes through the 100% retention mark or the coil volume see figures 4.5.1.2 and 4.5.1.4. The linear regressions of all fitted linear relationships depend upon experimental accuracy.

It would be interesting to apply this method of determining dead volume to Du et al's results [1999] to see if the characteristics would pass through the 100% retention point on the vertical axis. However this cannot be done as the published data only contains volumes for V_S and no data for V_E. Also no data is given for the dead volume. Plotting V_S against the square root of mobile phase flow rate will only determine the possible error in the dead volume. Most of Du et al's retention characteristics pass through the vertical axis close to the 100% mark except one for Ethyl Acetate - Water (1:1) that passes through at 132.59% see figure 1.4.2.6.8 section 1.4.2.6 Chapter 1. Although this suggests that the actual dead volume was larger than that used to calculate the retention. Figures 4.5.1.2 and 4.5.1.3 show that using an accurate dead volume moves the retention characteristic so that it will pass through the 100% retention mark at zero flow of the mobile phase without changing the gradient of the characteristic. This means that for the Ethyl Acetate – Water characteristic 32.59% should be subtracted from each

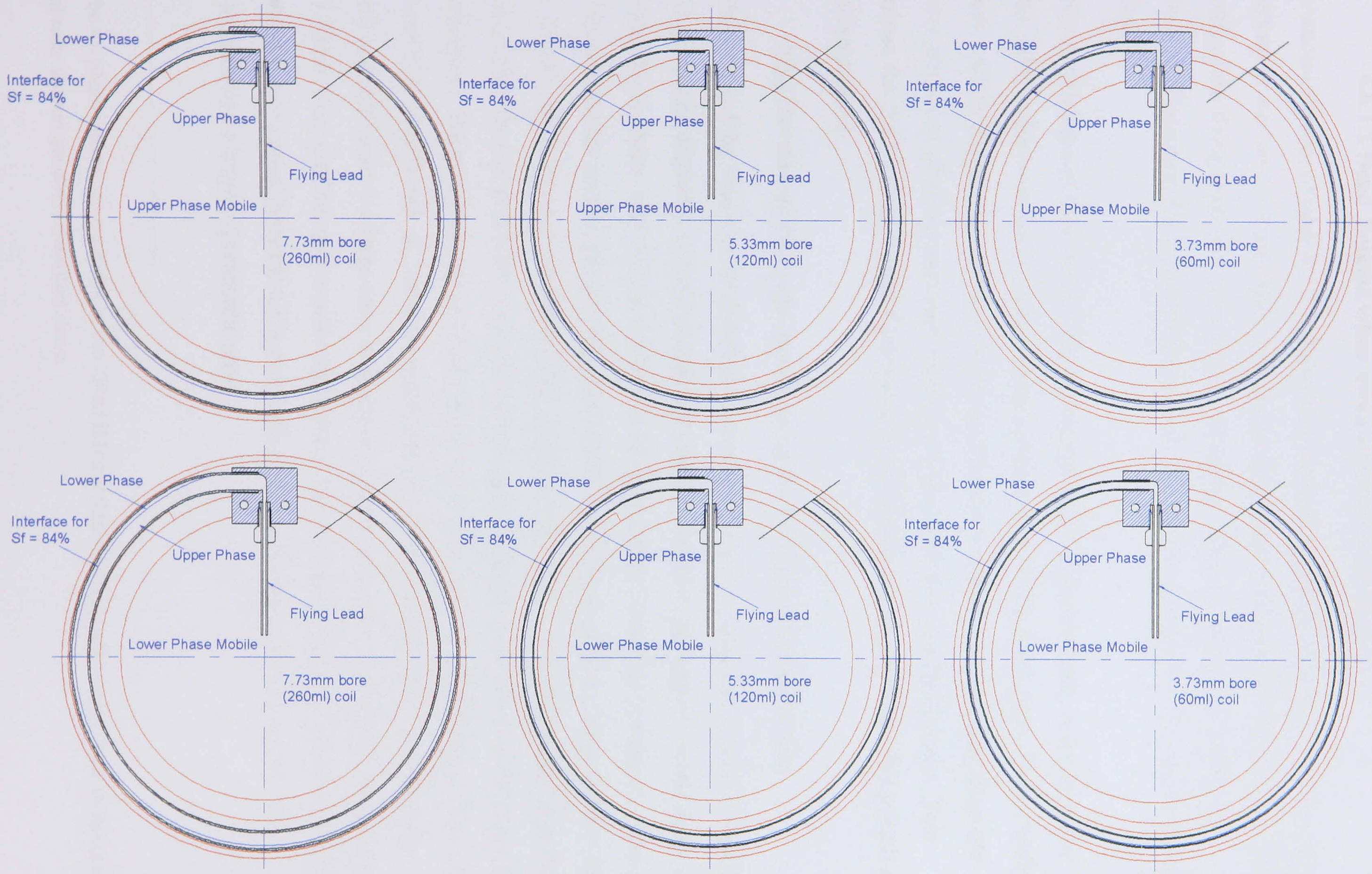

Figure 4.6.2.1 shows a comparison of the normal and reverse phase mode for the three IMI stainless steel helical coils

retention result for each given mobile phase flow rate. However this would mean that for the 3.0 and 3.6ml/min flow rates the retention of stationary phase would be –1.09% and –9.99% respectively, negative retentions are impossible. This shows that there are gross experimental errors for this phase system as discussed in section 1.4.2.6 of Chapter 1.

4.6.1.2 Dead Volume when using a Dynamax SD-1 pump

The second column of table 4.5.3.1 shows that the dead volumes determined by the method described in section 4.3.1 are close to the 8.5ml dead volume determined by measuring the lengths of the flying leads and other associated tubing. These results also confirm the derivation of equation 4.3.1.10 and the method proposed in section 4.3.1 for determining dead volume.

Closer examination of table 4.5.3.1 shows that the dead volume increases with rotational speed. This is due to stationary phase being retained in the flying leads at the lower rotational speeds. At the higher rotational speeds the accelerations subjected to the flying leads are greater and cause all of the stationary phase to be displaced from the flying leads. This increases the dead volume to that determined by measuring the lengths of the flying leads and associated tubing.

4.6.2 Reverse phase mode results using the Stainless Steel IMI Coils

Examination of the values in the fourth column of table 4.5.3.2, pump out volume of mobile phase minus the displaced volume of stationary phase (V_E) form the highest mobile flow rate, indicate errors greater than the maximum 3ml allowed as part of the test procedure. These errors occurred for reverse phase mode experiments using the 4A phase system in the 3.73mm bore (60ml) and 7.73mm bore (260ml) IMI stainless steel coils[xviii]. If errors larger than 3ml are encounter the test procedure calls for the test to be repeated until errors smaller than 3ml are obtained. These tests were repeated a number of times, such as the 800rpm results for the 3.73mm bore (60ml) coil. A 3ml error represents 5% of the volume of the 3.73mm bore (60ml) coil and hence is a large error in retention data for this coil. It was hoped that using the 7.73mm bore (260ml) coil would reduce these errors to approximately 1% however the results obtained varied between 4.3% and 5.6% of the coil volume and the dead volume results indicated a large experimental error.

[xviii] The 4A phase system was not tested in the 120ml IMI stainless steel coil as the results from the 60ml and 260ml coils showed the errors described above.

The dead volume results shown in table 4.5.3.2 for the 7.73mm bore coil indicate that much more stationary phase was displaced than that contained in the dead volume. Such large dead volumes indicate that there is something unusual happening when operating the IMI coils in reverse phase mode, as the dead volumes for normal phase mode were correct. Figure 4.6.2.1 shows a possible explanation of this usual behaviour in reverse phase mode for the IMI coils. In reverse phase mode, the mobile phase is the lower phase, when entering the coil from the flying lead this phase must pass through a layer of stationary upper phase in the radial direction before it can form a layer radially outside of the upper phase and pass through the coil. When leaving the coil the lower mobile phase must again pass through a layer of upper stationary phase. Each time the mobile passes through the layer of stationary phase it causes a loss of retention and may even cause each end of the coil to flood with mobile phase. The problem is not caused in normal phase mode as the mobile phase is the upper phase and hence does not pass through a layer of lower stationary phase on entering or leaving the coil.

The dead volume values in table 4.5.3.2 for the 3.73mm bore coil are approximately correct but are not as accurate as those for the normal phase mode shown in table 4.5.3.2. These lower errors in dead volume for the reverse phase mode of the 3.73mm bore coil than the 7.73mm bore coil can be attributed to a shallower depth of stationary (upper) phase that has to be passed through before entering and leaving the 3.73mm bore coil. Accurate retention data can only be gained for normal phase mode in the IMI helical stainless steel coils and do not operate correctly in reverse phase mode due to design details of coil inlets and outlets that favour normal phase operation. Therefore the design of coil inlets and outlets is important for the correct operation of a coil.

4.6.3 Normal phase mode retention using the three stainless steel IMI coils

Table 4.5.2.1 shows that the (R^2) fit coefficient varies from 0.9906 to 0.9995 indicating that a straight-line characteristic is applicable when the volume of mobile phase in the coil squared $\left(V_m^2\right)$ is plotted against mobile phase flow rate (F). The intercepts on the vertical $\left(V_m^2\right)$ axis vary from –5.0861 to 3.7360 $(ml)^2$ straddling the origin and these values are small when compared to the ranges of the vertical axes of figures 4.5.2.1 to 4.5.2.3. If the hypothesis that the pressure drop across a coil is constant and independent of mobile phase flow rate (F) is correct then plotting $\left(V_m^2\right)$ against F as shown in equations 4.3.2.3 and 4.3.2.4 should produce straight-line characteristics that pass through the origin similar to figures 4.5.2.1, 4.5.2.2 and 4.5.2.3. These figures therefore indicate that the pressure drop across a

coil is constant and independent of mobile phase flow rate for a given coil, phase system and operational conditions. These results confirm the first hypothesis of section 4.3.

Table 4.5.2.2 shows that the $\frac{V_m^2}{F}$ gradient is approximately the same for each bore of coil tubing at the same rotational speed. This indicates **that the pressure drop across a coil is independent of bore of the coil tubing.**

In table 4.5.2.3 the figures shown in blue indicate approximately equal volumes displaced from different IMI coils at the same rotational speed and flow rate. Given that the volumes of the IMI coils approximately double for each increase in tubing bore these displaced volumes are remarkably similar. These volumes suggest that the mobile phase occupies the same volume in each coil for the same flow rate and rotational speed. As each of the IMI coils is the same length, the mean cross-sectional area occupied by the mobile phase must be the same in each coil. This implies that the pressure drop across each coil is identical for the same flow rate and rotational speed. **This demonstrates that the pressure drop is independent of tubing bore.**

Examination of equation 4.3.2.11 and figure 4.5.3.1 shows that the gradient of the Du plot is inversely proportional to the square of the bore of the coil tubing for coils of the same length. The gradient of figure 4.5.3.1 is:

$$\text{Gradient} = \frac{B}{1/d_C^2} = Bd_C^2 = 800\sqrt{\frac{2\mu_m L}{\pi \Delta P}} \qquad (4.6.3.1)$$

The above equation shows that the only possible variable for the gradients of each characteristic shown in figure 4.5.3.1 is the pressure drop (ΔP). As figure 4.5.3.1 produced a straight-line, constant gradient, characteristics for each rotational speed that passed through the vertical axis close to the origin implying that the **pressure drop across a coil is constant for a given rotational speed and is independent of the bore of the coil tubing provided that coils of the same length, helical pitch and β-value are used.** The relationships between pressure drop, rotational speed and coil length are investigated further in Chapter 5, in the context of which variables affect the pressure drop across the coil (ΔP).

4.6.4 Reynolds Numbers

In the past, the Hagan-Poiseuille equation for laminar flow has not been seriously considered for the analysis of flow within a coil on a J-type centrifuge because of the mixing that occurs either side of the proximal key node. Lower Reynolds numbers (*Re*) indicate laminar flow occurs at higher Reynolds numbers. Reynolds number is the ratio of the Inertia Force to the Viscous Force ie:

$$Re = \frac{\text{Inertia Force}}{\text{Net Viscous Force}} \qquad (4.6.4.1)$$

The Inertia Force = $\rho u^2 d^2$ and the Net Viscous Force = $\mu u d$ [page 290 of Massey 1989] which gives the classic equation for *Re*:

$$Re = \frac{\rho u d}{\mu} \qquad (4.6.4.2)$$

Examination of the equations for Inertia Force and Viscous Force shows that neither of these forces is directly affected by the high acceleration experienced on the coil of a J-type centrifuge. However the critical values of *Re* for transition from laminar to turbulent flow have not been studied for two phase flow on a J-type centrifuge.

The *Re* obtained for the three stainless steel IMI coils, see table 4.5.4.1, vary from 184 to 3117 for the 4A phase system in normal phase mode. Table 4.5.4.1 shows that the *Re* in the 3.73mm bore coil varies from 184 to 255 at 5ml/min. At 5ml/min it is reasonable to assume that the flow of the mobile phase is laminar. The 1200rpm results for the 3.73mm bore coil have a highest flow rate of 80ml/min when the *Re* reaches a maximum value of 2085. Figure 4.5.2.1 indicates that the pressure drop is the same as at both 80 and 5ml/min, if a transition to turbulent flow had occurred this pressure drop would have increased significantly. The *Re* for the 7.73mm bore coil varies between 550 and 729 for a flow rate of 20ml/min see table 4.5.4.1. These *Re* are blow the 2085 *Re* encountered in the 3.73mm bore coil at a flow rate of 80ml/min when the flow was laminar. Therefore it is reasonably to assume that the mobile phase flows in a laminar manner in the 7.73mm bore coil at a flow rate of 20ml/min. Figure 4.5.2.3 shows that the same pressure drops are applied across the 7.73mm bore coil at flows up to 140ml/min for each rotational speed tested. The maximum Re in the 7.73mm bore coil is 3117. This indicates that the flow of the mobile phase can still be considered as laminar at such high *Re*. As the mobile phase flow is laminar, the mixing that occurs close to the proximal key node cannot be due to turbulence. When hydrodynamic equilibrium has been achieved the mean flow rate of the stationary phase is zero and hence the mean linear velocity

is also zero therefore the *Re* is zero. Therefore turbulent flow of the stationary phase cannot be causing the mixing between the phases.

If the flow of both phases is laminar then how does the observed mixing about the proximal key node occur? A hypothesis that mixing and settling occurs due to an interfacial phenomenon called the Kelvin-Helmholtz instability criterion has been put forward by Sutherland [1986]. The author of this thesis [Wood 2001B[xix]] showed that the relative flow velocity between the mobile and stationary phase was below that required by the Kelvin-Helmholtz instability criterion to cause mixing at any position in the coil, see also Section 1.4.3.1. This paper showed how the mean flow velocity could be below the Kelvin-Helmholtz velocity required for wave formation at the distal key node and above this velocity at the proximal key node creating mixing waves. Using *Re* to indicate the nature of the flow shows that the flow is laminar at both the distal and proximal key node for the 2A and 2C phase system analysed in this paper. For the mobile lower phase at the distal key node the *Re* was 22 for the 2A phase system and 16 for the 2C phase system. At the proximal key node the *Re* had increased to 115 for the 2A phase system and 72 for the 2C phase system[xx]. The *Re* for the stationary upper phase was less than 1 for both phase systems at both the distal and proximal key nodes. Wave mixing at the proximal key node is therefore an interfacial phenomenon and occurs when both phases are flowing in a laminar manner. Gardner and Kubie [1975] showed that wave formation and wave growth (instability) could occur when both phases are flowing in a laminar manner. Considering all of the above, mixing is not caused by turbulent flow of the mobile phase.

Table 4.5.4.2 shows that similar Reynolds numbers are obtained in each IMI coil at the same rotational speed and flow rate. This shows that the ***Re* is independent of the coil-tubing bore.** This also indicates that the flow of the mobile phase is similar in each of these coils for the same rotational speed and flow rate as implied in table 4.5.2.3. These observations are discussed further in Chapter 5.

[xix] 90% of the work in reference [Wood 2001B] was that of the author of this thesis and 10% was Professor Ian Sutherland's.

[xx] These Reynolds number were calculated for a rotor radius of 100mm, a rotational speed of 800rpm, a β-value of 0.615, a tubing bore of 3.175mm and a mobile phase flow rate of 2ml/min. The calculated stationary phase retention of the 2A phase system was 95% and the 2C had a calculated retention of 91%.

Reynolds number has only been used to study the mean flow of the mobile phase through a coil to determine if it is laminar or turbulent. A Reynolds number analysis has not been applied to the experimental results combined with a possible interfacial movement as conducted in [Wood 2001B] because such an analysis would relay upon too many unproven assumptions to be reliable. For instance, in [Wood 2001B] an initial value of the interfacial distance was assumed at the distal key node and the calculated value of the retention was accepted. However the modelled retention would have to match the measured retention, which would require a number of empirical tries with different initial values of the interfacial distance at the distal key node. The modelling of the interfacial movement does not include the flow rate of the mobile phase. In [Wood 2001B] the mobile phase flow rate used in conjunction with the interfacial movement was 2ml/min and it was assumed that such a low flow rate would not significantly change the position of the interface. However the flow rates used in the experiments varied from 5 to 140ml/min. At such high flow rates it is assumed that the position of the interface will be significantly different to those predicted by the modelling described in [Wood 2001A].

4.6.5 Normal and Reverse phase mode Du retention gradients

The second hypothesis *"that the pressure drop across a coil is independent of whether the coil is being used in normal or reverse phase mode for the same operational parameters"* is confirmed in figures 4.5.5.1, 4.5.5.2 and 4.5.5.3. It must be remembered that in normal phase mode the upper mobile phase, as regarding the 4A phase system, was pumped from tail-periphery to head-centre in the PTFE coil as recommended by Sutherland et al [2000A]. In reverse phase mode the lower mobile phase, as regarding the 4A phase system was pumped through the coil from head-centre to tail periphery also as recommended by Sutherland et al [2000A]. Pumping each mobile phase as described above ensures that the same pressure drop occurs across the coil. Under these conditions the only variables to change between normal and reverse phase mode are the viscosities of the stationary and mobile phases. Equation 4.3.2.8 shows and the results shown in figures 4.5.5.1 to 4.5.5.3 show that the **viscosity of the mobile phase is an important variable that affects the retention of the stationary phase.** Equation 4.3.2.8 shows that the stationary phase retention decreases as the square root of the mobile phase dynamic viscosity increases. **This equation also indicates that the viscosity of the stationary phase does not significantly affect <u>stationary</u> phase retention.** This is not surprising given that the stationary phase movement inside the coil is localised [Wood 2001A] and that generally the stationary phase occupies a greater proportion of the cross-section area of the tubing.

The results from figures 4.5.5.1, 4.5.5.2 and 4.5.5.3 show that, for the 4A phase system, the stationary phase retention is greater for normal phase mode, where the viscosity of the mobile phase is lower than for reverse phase mode, for all the flow rates tested. This means that in normal phase mode, for the 4A phase system, for a given flow rate the upper mobile occupies less cross-sectional area of the tubing than in reverse phase mode. Therefore, for the 4A phase system, in **normal phase mode the mobile phase has a higher mean flow velocity than in reverse phase mode.** This indicates that the *Re* in normal phase mode should be greater than for reverse phase mode, this is confirmed in table 4.5.6.1. **The higher *Re* in normal phase mode may indicate that flow of the mobile phase is less stable than in reverse phase mode.** This also means for a given coil there is less time for mass transfer that in turn could lead to lower resolution, if the changes to distribution constants are ignored. Equation 4.3.2.8 combined with the finding that the pressure drop across a coil is the same in both normal and reverse phase mode shows that the viscosity is an important parameter in determining the stability of the flow of the mobile phase.

Sutherland et al recommended in [2000A] that:

1. Spiral or multi-layer coils should be rotated in the direction that orientates the coil head-centre, tail-periphery.
2. The denser phase when mobile (often reverse phase mode) should be pumped from head-centre to tail-periphery.
3. The less dense phase when mobile (often normal phase mode) should be pumped from tail-periphery to head-centre.

The PTFE coil used for the normal and reverse phase mode retention tests is a multi-layer coil and was operated in accordance with these three recommendations. Following these recommendations for spiral and multi-layer coils means that the best retention will be achieved for each mode of operation because the hydrostatic pressure head and the Archimedean pumping effect are added together to create the maximum pressure drop across a coil. If these recommendations are not followed the hydrostatic pressure head and the Archimedean pumping effect are subtracted from each other reducing the pressure drop across the coil and hence the retention of the stationary phase see equation 4.3.2.10. Following these recommendations means that when the upper (less dense) phase is the mobile phase the inlet is at the periphery of the coil and when the lower (denser) phase is the mobile phase the inlet is at the centre of the coil. If the coil is operated in both normal and reverse phase modes with the same inlet then to achieve retention in both modes the direction of rotation must to be

changed when switching from one mode to the other. This means that the pressure drop across the coil will be different in each mode and equation 4.3.2.13 cannot be applied. Equation 4.3.2.12 could be applied if it is known how the pressure drop changes between operational modes if the recommendations of Sutherland et al [2000 A] are not followed.

Fedotov [1998] pumped the aqueous lower mobile phase from head to tail in a spiral coil but no mention was made of whether the head was placed at the centre or the periphery. Fedotov's experimental data from the spiral coil was used to support the derivation of an equation that predicts stationary phase retention [Fedotov 1996]. This derivation states, "*the inertia, density and adhesion forces in these systems are negligibly small in comparison with the Archimedean forces*". The systems considered are hydrophobic phase systems. In helical coils this statement is probably correct, however the hydrostatic pressure generated in a spiral coil is based upon the densities of the phases and is not negligible. Also the relative significance of hydrostatic pressure (density forces) and Archimedean (pumping effect) forces in a spiral coil as used by Fedotov [1996] cannot be evaluated unless the orientation of the coil is known. In private communications between the author of this thesis and both Fedotov [2001 B] and Thiebaut [2001] the authors of Fedotov et al [1998] it has become apparent that the orientation of the coil tested was not recorded and hence will never be known. This means that the conclusion drawn by Fedotov et al [1998] must be considered carefully. This is not a criticism of Fedotov's or Thiebaut's work as it predates Sutherland et al's [2000 A] but highlights the importance of the orientation of a coil for future publications and anyone trying to reproduce the results presented in this chapter.

4.6.6 Experimental Accuracy

The experimental approach used for the retention studies has been to use the IMI coils and PTFE coils, a total of five coils, at a number of rotational speeds to test the hypothesis and theories contained in sections 4.3.1 and 4.3.2. These tests have also been conducted to provide experimental data to determine if and how the pressure drop, see Chapter 5, varies with parameters such as mobile phase viscosity, phase system, tubing bore, rotational speed and normal or reverse phase operation. This chapter presents results from 27 retention tests that cover these parameters. A traditional approach to determine experimental accuracy would be to repeat each test a minimum of three times. This would have required three times as much testing hence three times as much experimental time or a reduction in the number of parameters tested. A reduction in the parameters tested would have reduced the thoroughness of the testing of the hypothesis and theories contained in sections 4.3.1 and 4.3.2. Previous

normal and reverse phase mode retention studies by Sutherland et al [2001C] have shown the importance of accuracy and the author realised that the procedures then in use would not produce the required accuracy. The procedures given in Chapter 2 were written to systematically produce accurate results and be self-checking to detect random errors. Thirty-one retention tests were conducted while developing the test procedures. The improvements to increase accuracy are described in the following paragraphs.

Stationary phase collectors were designed for both normal and reverse phase modes. These collectors stop the systematic errors in measuring the volume of stationary phase collected each time the flow from the J-type centrifuge is switched from a full measuring cylinder to an empty measuring cylinder, see Experimental Retention Tests [Sutherland et al 2001B]. These errors would increase at the higher flow rates used in the tests described in this chapter. The design of the stationary phase collectors is also based upon 100ml burrettes. The smallest volume division on a 100ml burrette is 0.2ml allowing the smallest measurable reading to be 0.1ml compared to 0.5ml on a 100ml measuring cylinder, thus increasing the accuracy of the volume measurement by a factor of five.

The stationary phase collectors are designed to trap the stationary phase as it is displaced from the coil and flying leads and allow the mobile phase to flow through the collector. One stationary phase collector is used when the lower phase is the stationary phase and a different one when the upper phase is the stationary phase. When the lower phase is the stationary phase, the stationary phase collector is as shown in figure 2.7.2.1 Chapter 2. The output from the coil flows into the top of the stationary phase collector. The stationary phase sinks to the bottom while the mobile phase flows out of the top of the collector. The stationary phase collector for when the upper phase is the stationary phase is shown in figure 2.7.4.1 Chapter 2. The flow from the coil enters the bottom of the stationary phase collector. The stationary (upper) phase floats to the top of the collector where it is trapped while the mobile (lower) phase flows out of the bottom of the collector. Both stationary phase collectors rely upon the acceleration due to gravity to separate the mobile and stationary phases.

The Dynamax SD-1 pump used to pump the mobile phase in these retention studies produces an accurate steady non-pulsatile flow at all flow rates [Rainin 1982]. The Dynamax SD-1 pump is combined with a 1.7bar backpressure valve placed downstream of the coils to ensure accurate operation of the pump's non-return values and to stop siphoning of either phase through the coil. These measures ensure that the actual flow rate is the same as the one set.

The Syringe and Syringe driver used in the dead volume study also produced a steady flow of mobile phase. A steady flow of the mobile phase appears to be necessary to obtain the Du retention characteristic in normal phase mode when the flow of mobile phase is less stable than in reverse phase mode [Sutherland 2001A]. This is confirmed by work conducted by Berthod [2000] using a heptane-methanol-water phase system in normal phase mode with the upper phase mobile. Berthod used a Shimadzu LC10-AS pump, these Shimadzu pumps are known for pulse-free constant flow delivery [Shimadzu] unlike the pulsitile flow produced by the Gilson 302 HPLC pump used by Sutherland [2001C]. For heptane-methanol-water phase systems the upper phase is less viscous than the lower phase see table 2.2.2 Chapter 2. The 4A phase system referenced throughout this chapter is a mixture of heptane, methanol and water, see table 2.2.2 Chapter 2. Without the use of the pulse-free Dynamax SD-1 pump the results produced in this chapter would have had significant errors similar to those shown by Sutherland [2001C].

The mobile and stationary phase reservoirs were placed above the Dynamax SD-1 and Gilson pumps, see figures 2.7.2.1and 2.7.4.1 Chapter 2, to gravity feed the pumps to ensure that bubbles did not form between the reservoirs and the pumps during the filling stroke of a one of the pistons belonging to either pump. Bubbles in the feed lines to the pumps can cause the actual flow rate of the pumps to be lower than that set because the pump's cylinder is not completely filled during the filling stroke. The fed line between the mobile phase reservoir and the Dynamax pump had a 4.7625mm (3/16 inch) bore to stop the air bubbles forming at the high mobile phase flow rates used. The phase systems were also degassed before use, see section 2.2.2 Chapter 2. The use of the 1.7bar backpressure valve also minimises the formation of bubbles between the pumps and the backpressure valve, see figures 2.7.2.1 and 2.7.4.1 in Chapter 2, ie in the coil and flying leads. The formation of bubbles in this region can cause errors in volume measurements of the mobile and stationary phase and the flow rate of the mobile phase.

The Brunel CCC machine is temperature controlled. The mobile and stationary phase reservoirs are also temperature controlled, being placed in a water bath see figures 2.7.2.1and 2.7.4.1 Chapter 2. The operating temperature of the Brunel CCC machine and the water bath was set at 30°C. This ensures that the physical properties of the phase system while under test are the same as those listed in table 2.2.2 Chapter 2. The physical properties as listed in table 2.2.2 were determined as described in sections 2.3, 2.4 and 2.5 of Chapter 2. Retention test results were rejected if the temperature varied more than ± 1°C ie outside of the range of 29 to 31°C. For example of the eight results rejected for the three IMI stainless steel coils, from a

total of twenty-six normal phase retention tests, four were for temperatures outside of the 29 to 31°C range. If results are presented with temperatures outside of this range the temperatures have been shown.

One result from the IMI coils was rejected as the fit coefficients (R^2) was lower than 0.98, which indicates random errors or misreading the volumes of stationary phase (V_E) displaced from the coil and flying leads for each flow rate. Misreading the volume V_E leads to errors in determining the dead volume as described in section 4.3.1 and the Du gradient.

The comparison of the total volume of stationary phase displaced from the system volume[xxi] and the volume of mobile phase collected during pump out detects random errors in the data collected. The procedures for normal and reverse phase mode retention tests, section 2.7 of Chapter 2, call for the data to be rejected and the test repeated if these volumes differ by more than 3ml. For example of the eight retention tests rejected for the three IMI stainless steel coils in normal phase three were for a volume discrepancy greater than 3ml. Some results are presented that have volume discrepancies greater than the 3ml limit such as the reverse phase results from the three IMI coils which helped to indicate that something was fundamentally wrong with these coils when operating in reverse phase mode. The volume discrepancy for the 7.73mm bore coil were 11.1ml and 14.5ml see table 4.5.3.2.

The rejection of eight of the twenty-six normal phase retention tests leaves the eighteen presented in this chapter.

An analysis of the four 1200rpm normal phase retention tests for the 3.73mm (59.1ml) IMI stainless steel coil shows that the Du gradients are within ±2.5% of the mean of these four gradients. At 1200rpm the Du gradient is going to be the lowest as this is the highest rotational speed at which a retention test was performed. This means that the volume of stationary phase displaced from the coil will be the smallest and hence any errors in the volume measurement will be proportionally the greatest. The results from table 4.5.2.3 show that the same volumes of stationary phase are displaced from each of the IMI coils at identical rotational speeds[xxii]. This means that the retention in the largest bore coil will be the best due to the largest bore coil having the greatest volume. It also means that the coil will have the lowest Du gradient. However the error in the Du gradient for the 7.73mm bore IMI coil at

---

[xxi] The system volume (V_{SYS}) is the addition of coil volume (V_C) and the dead volume (V_d).

[xxii] The stationary phase is displaced from a coil by the mobile phase; therefore the volume of mobile phase in a coil (V_m) equals the volume of stationary phase displaced from a coil.

1200rpm would still be within ±2.5%. This is demonstrated by the following example. Assume that one of the IMI coils has a volume of 10ml and that another IMI coil has a volume of 100ml. Both have retention tests performed at 1200rpm and that 5ml of stationary phase are displaced at a flow rate of 25ml/min. The retention in the 10ml coil at this flow rate will be 50% and the Du gradient will be 10 $(min/ml)^{0.5}$. The retention in the 100ml coil will be 95% and the Du gradient will be $1(min/ml)^{0.5}$. Now assume that the possible error in the volume of displaced stationary phase is +1ml. The retention in the 10ml coil would be 40% and the Du gradient would be $12(min/ml)^{0.5}$, giving an error in the Du gradient of +20%. Assuming the same error for the 100ml coil, the retention would be 94% and the Du gradient would be 1.2 $(min/ml)^{0.5}$, also giving an error in the Du gradient of +20%. Therefore the % errors in the Du gradient for each coil will be the similar at the same rotational speed.

If the 100ml coil was rotated at 600rpm and assuming that twice as much stationary phase was displaced from the coil ie 10ml at a flow rate of 25ml/min. Then the retention would be 90% and the Du gradient would be $2(min/ml)^{0.5}$. Again assuming a possible +1ml reading error in the volume of displaced stationary phase the volume of displaced stationary would be 11ml. The retention would be 89% and the Du gradient would be $2.2(min/ml)^{0.5}$, giving a possible 10% error in the Du gradient. This means that the % errors in the Du gradients reduce as rotational speed is reduced and the errors in the Du gradients for rotational speeds below 1200rpm are better than ±2.5% for the IMI coils. As the same experimental set up and procedures were used for the FEP and PTFE coils similar magnitudes of error are likely ie within ±2.5% for the measured Du gradients.

4.6.7 Derivation of the retention equation

Equation 4.3.2.8 can be compared to the Du retention characteristic, $S_f = A - B\sqrt{F}$ equation 1.4.2.6.4 from Chapter 1. The 100% value for constant A was determined without using the assumption that "*the intercept on the vertical axis of a Du plot is 100% retention of the stationary phase when the mobile phase flow rate is zero*". Hence the derivation of equation 4.3.2.8 supports this assumption and the subsequent derivation of the equation 4.3.1.10 that is used to determine the dead volume.

4.7 Concluding Remarks

The dead volume results confirm the assumption that the intercept on the vertical axis, when the mobile phase flow rate is zero, is the dead volume when the displaced volume of stationary phase is plotted against the square root of the mobile phase flow rate.

These results also confirm the assumption that the Du retention characteristic will pass through the 100% retention mark on the vertical axis of a Du plot when the mobile phase flow rate is zero see equation 4.3.1.4 provided the dead volume was determined as in section 4.3.1.

The Reynolds number results confirm that the flow of mobile phase is laminar and that the use of the Hagan-Poiseuille equation is justified when deriving an expression for the retention of stationary phase. As the flow of the mobile phase is laminar and does not directly cause mixing either side of the proximal key node. The mixing near the proximal key node is caused by an interfacial instability between the mobile and stationary phases at the interface.

Reynolds numbers for the mobile phase flow are independent of coil-tubing bore. For a given phase system the *Re* for the lower viscosity mobile phase are higher than those for the higher viscosity mobile phase.

The pressure drop across a coil is independent of the mobile phase flow rate and remains constant for a given: coil, phase system and rotational speed. The pressure drop is the same in both normal and reverse phase modes for a given: coil, phase system and rotational speed provided the recommendations of Sutherland et al [2000A] are followed. The pressure drop is independent of the coil tubing bore provided coils of the same length are used.

To complete the prediction of the stationary phase retention an equation of the pressure drop needs to be developed. The derivation of the constant pressure drop equation occurs in Chapter 5.

Chapter 5 Pressure Drop across a Coil

5.1 Summary

This chapter derives an empirical equation for the pressure drop (ΔP) across a coil. This pressure drop equation further develops the retention equation of Chapter 4:

$$S_f = 100 - \frac{800}{d_C^2}\sqrt{\frac{2\mu_m L}{\pi \Delta P}}\sqrt{F}$$

This derivation of the ΔP term builds upon the retention results of Chapter 4, dimensional analysis and Du et al's [1998] research into the effects of coil length, which showed that retention is independent of coil length. These results showed the ΔP term to be independent of tubing bore, proportional to coil length and proportional to the centripetal acceleration ($R\omega^2$). The results of Sutherland et al [2001B] are also used to show that the ΔP term is proportional to the density difference between the upper and lower phases. The combination of these results is the following equation that predicts the retention of stationary phase for a coil mounted on a J-type centrifuge given details of the coil, centrifuge, phase system and operating conditions.

$$S_f = 100 - \frac{24000}{N d_C^2}\sqrt{\frac{2\mu_m}{K\pi^3 \Delta\rho R}}\sqrt{F}$$

A conclusion is that the constant K in the above equation is a property of the coil and centrifuge configuration and is independent of the: phase system, the rotational speed (N rpm) and operation in normal or reverse phase. It is argued that once the value of K is determined for a coil-centrifuge configuration, from one retention test, that retention of other phase systems at different speeds in both normal and reverse phase can be predicted using the above equation.

5.2 Introduction

In Chapter 4 an equation for the gradient of the Du plot was derived. This equation contained some of the properties of the coil and the mobile phase, however other properties and operational parameters were not included. These properties and operational parameters are contained in the pressure drop or ΔP term of the Du gradient. Determining the retention of a phase system operating in either normal or reverse phase mode requires a formula for the ΔP term. The ΔP term represents the total pressure drop across a coil, the pressure drop term being the sum of the pressure drop provided by the external HPLC pump and the Archimedean pumping effect of the coil. This derivation is partially based upon the retention results of Chapter 4, where some results have shown how retention varies with rotational speed and the pressure drop is independent of tubing bore. These results are processed to show how the ΔP term varies with rotational speed and tubing bore.

A transducer has been used to measure gauge pressure between the HPLC pump and the input to the coil. This measures the pressure required to pump the mobile phase into the coil by the HPLC pump. Experiments were conducted using a Brunel CCC outer PTFE coil at 800rpm with the 4A phase system in reverse phase mode. The bore of the PTFE tubing in the outer coil is 1.5875mm. Calculations using the Hagen-Poiseuille equation for laminar flow showed that the pressure drop across the coil needed to be 8.3bar in order to pump the mobile phase through the coil given that the stationary phase is occluding the majority of the cross-sectional area of the coil's tubing. The peak pressure measured was only 4.7bar at a flow rate of 11.5ml/min. It should be noted that the external HPLC pump, pumps the mobile phase through the coil by the in the same direction that the coil pumps the mobile phase. Hence, at a flow of 11.5ml/min, the coil is contributing 3.6bar (8.3bar minus 4.7bar). The experimental problem is that the pumping effort of the coil is very difficult to measure directly since the coil pumping pressure is both generated and dissipated within the coil.

5.3 Theory

5.3.1 Calculation of Pressure drop

There are two methods of determining the pressure drop from retention information. The first is to rearrange equation 4.3.2.11 from Chapter 4 in terms of ΔP as follows:

$$B = \frac{800}{d_C^2}\sqrt{\frac{2\mu_m L}{\pi \Delta P}} \qquad (4.3.2.11)$$

$$\left(\frac{d_C^2 B}{800}\right)^2 = \frac{2\mu_m L}{\pi \Delta P}$$

$$\Delta P = \frac{2\mu_m L}{\pi}\left(\frac{800}{d_C^2 B}\right)^2$$

$$\Delta P = \frac{1{,}280{,}000\mu_m L}{\pi d_C^4 B^2} \qquad (5.3.1.1)$$

To calculate the pressure drop in N/m^2 using equation 5.3.1.1 the coil tubing bore (d_C) must be in metres, the coil length L must be in metres and the viscosity must be in Ns/m^2. The gradient term B must be in $(s/m^3)^{0.5}$ ie determined from a Du retention plot, where the S_f was plotted against the square root of mobile phase flow rate where the mobile phase flow rate was quantified in m^3/s.

Equation 5.3.1.1 can be modified to give the pressure drop in units of bar as follows since 1bar = 100,000 N/m^2:

$$\Delta P = \frac{12.8\mu_m L}{\pi d_C^4 B^2} \qquad (5.3.1.2)$$

The second method is to use equation 4.3.2.3 from Chapter 4 as follows:

$$\Delta P = \frac{8\pi\mu_m L^3 F}{V_m^2} \qquad (4.3.2.3)$$

To calculate the pressure drop in N/m^2 using equation 4.3.2.3 the mobile volume in the coil (V_m) must be in m^3, the coil length L must be in metres, the viscosity must be in Ns/m^2 and the mobile phase flow rate must be measured in m^3/s.

Equation 4.3.2.3 can be modified to give the pressure drop in units of bar as follows since 1bar = 100,000 N/m^2:

$$\Delta P = \frac{8\times10^{-5}\pi\mu_m L^3 F}{V_m^2} \qquad (5.3.1.3)$$

5.3.2 Pressure Drop and Coil length

Du [1998] has shown that the retention of stationary phase is independent of coil length providing that sample volumes and sample concentrations do not effect the properties of phase system see table 1.4.2.7.1 Chapter 1. Du measured the retention of stationary phase in one coil and then connected it in series with another identical coil and measured the retention in these two combined coils operating under the same conditions as the single coil. The same experiment was repeated for three and four identical coils connected in series and found that under the same operating conditions the retention of stationary phase did not change regardless of the number of coils. This means that the retention in each coil is identical and is the same as the overall retention if the coils connected in series are viewed as one coil. This also shows that the gradient of the Du retention characteristic does not change with the number of coils connected in series. Equation 4.3.2.8 from Chapter 4 is the gradient term of the Du retention characteristic:

$$B = \frac{100}{V_C}\sqrt{\frac{8\pi\mu_m L^3}{\Delta P}} \qquad (4.3.2.8)$$

As the gradient is constant regardless of the number of coils connected in series then $B_1 = B_2 = B_3 = B_4$ where B_1 is the gradient for 1 coil and B_2 is the gradient for 2 coils connected in series and so on. For 1 coil let the volume be V_C and the coil length be L then:

$$B_1 = \frac{100}{V_C}\sqrt{\frac{8\pi\mu_m L^3}{\Delta P_1}}$$

Now for 2 coils connected in series the volume is $2V_C$ and the length is 2L and the gradient is B_2 therefore:

$$B_2 = \frac{100}{2V_C}\sqrt{\frac{8\pi\mu_m (2L)^3}{\Delta P_2}} = \frac{100}{2V_C}\sqrt{\frac{8\pi\mu_m 8L^3}{\Delta P_2}}$$

$$B_2 = \frac{100}{V_C}\sqrt{\frac{8\pi\mu_m 2L^3}{\Delta P_2}}$$

Now for $B_1 = B_2$, $\Delta P_2 = 2\Delta P_1$:

$$B_2 = \frac{100}{V_C}\sqrt{\frac{8\pi\mu_m 2L^3}{2\Delta P_1}} = \frac{100}{V_C}\sqrt{\frac{8\pi\mu_m L^3}{\Delta P_1}}$$

Similar analyses can be conducted for 3 and 4 coils connected in series giving $\Delta P_3 = 3\Delta P_1$ and $\Delta P_4 = 4\Delta P_1$ hence it can be seen that ΔP is proportional to the coil length L.

5.3.3 Basic Pressure Drop term

The derivation of the basic pressure drop equation assumes that the coil is wound and rotated so that the coil is orientated head-centre, tail-periphery as recommended in [Sutherland 2000A].

Using dimensional analysis shows that the fundamental dimensions of pressure and pressure drop to be $[ML^{-1}T^{-2}]$, all fundamental magnitudes used are taken from pages 584 to 589 of [Massey 1989]. Density and acceleration have the fundamental magnitudes of $[ML^{-3}]$ and $[LT^{-2}]$ respectively. A finding of Chapter 4 was that the pressure drop was proportional to the square of the rotational speed, which suggests that the pressure drop is proportional to the centripetal acceleration $R\omega^2$. Multiplying density by acceleration gives $[ML^{-2}T^{-2}]$ which only needs to be multiplied by a [L] term to have the same fundamental magnitudes as pressure drop. In the previous section pressure drop was shown to be proportional to coil length hence pressure drop has the same fundamental magnitudes as the multiplication of length, density and acceleration. Density difference has the same fundamental magnitudes as density hence pressure drop could be the multiplication of coil length, density difference and acceleration. The normal and reverse phase retention study on the PTFE coil shown in Chapter 4 indicates that the pressure drop is independent of the density of either phase and must therefore depend upon the density difference between the phases ($\Delta\rho$). The acceleration on a J-type centrifuge is proportional to $R\omega^2$ hence the basic pressure drop equation could be:

$$\Delta P \propto L\Delta\rho R\omega^2$$

and using a constant K

$$\Delta P = KL\Delta\rho R\omega^2 \qquad (5.3.3.1)$$

This equation ignores β-value, as no β-value results are currently available.

5.3.4 Stationary Phase Retention, rotational speed and tubing bore

Equation 4.3.2.10 Chapter 4 is as follows:

$$B = \frac{800}{d_C^2}\sqrt{\frac{2\mu_m L}{\pi\Delta P}} \qquad (4.3.2.10)$$

Substituting equation 5.3.3.1 into equation 4.3.2.10 gives:

$$B = \frac{800}{d_C^2}\sqrt{\frac{2\mu_m L}{\pi KL\Delta\rho R\omega^2}}$$

$$B = \frac{800}{d_C^2}\sqrt{\frac{2\mu_m}{K\pi\Delta\rho R\omega^2}}$$

$$B = \frac{800}{d_C^2\omega}\sqrt{\frac{2\mu_m}{K\pi\Delta\rho R}} \qquad (5.3.4.1)$$

The equation above shows that the gradient of a Du retention characteristic is independent of the length of coil. Equation 5.3.4.1 also shows that the gradient of the Du retention characteristic is inversely proportional to the square of the tubing bore and is also inversely proportional to the rotational speed.

The angular velocity ω, radians/s, is related to the rotational speed N, rpm, by the following equation:

$$\omega = \frac{2\pi N}{60} = \frac{\pi N}{30} \qquad (5.3.4.2)$$

Substituting for ω from the above equation in equation 5.3.4.1 gives:

$$B = \frac{24000}{Nd_C^2}\sqrt{\frac{2\mu_m}{K\pi^3\Delta\rho R}} \qquad (5.3.4.3)$$

The full equation for the Du retention characteristic can now be written as follows:

$$S_f = 100 - \frac{24000}{Nd_C^2}\sqrt{\frac{2\mu_m}{K\pi^3\Delta\rho R}}\sqrt{F} \qquad (5.3.4.4)$$

5.4 Methods and Materials

The pressure sensor was calibrated for each phase system used as described in section 2.6 of Chapter 2. During the retention studies described in Chapter 4 the upstream or input pressure to the coil under test was measured as described in section 2.7 of Chapter 2. The upstream pressure is determined by subtracting the calibration pressure, the pressure drop across the flying leads and non-return valve, from the measured pressure across the coil, flying leads and non-return valve. The result of this subtraction is the measured input pressure to only the coil.

5.5 Results

The results presented in this section are based upon the retention studies presented in Chapter 4. The raw data for the measure pressure calibration and pressure measurements are contained in Appendix 6.

5.5.1 Measured Pressure Drop results for IMI Stainless Steel coils

The pressure drop data given in table 5.5.1.1 below was calculated by subtracting the calibration data in table A.6.2 Appendix 6 from the measured data in table A.6.1 Appendix 6 where the same flow rates were used. If a pressure drop was taken at a flow rate for which a calibration pressure was not available in table A.6.2 then the equation from figure A.6.1 Appendix 6 was used to determine the calibration pressure, which was subtracted from the data in table A.6.1 to give the result in the table 5.5.1.1 below.

Flow Rate (ml/min) Experiment	5	10	20	40	50	60	80	110	140	Du
Rows 3.73mm										
39, 600rpm	0.60	0.55	0.45	0.50						0.06
41, 800rpm	0.80	0.70	0.50	0.50						0.10
42, 1000rpm	0.85	0.80	0.60	0.50						0.18
33, 1200rpm	1.40	1.00	0.70	0.40			0.35			0.21
34, 1200rpm	1.15	1.00	0.70	0.40			0.20			0.21
35, 1200rpm	1.15	0.95	0.70	0.50			0.40			0.22
44, 1200rpm	1.15	1.00	0.60	0.50			0.40			0.23
Rows 5.33mm										
47, 600rpm		0.60	0.60	0.60			0.60			0.05
50, 700rpm		0.70	0.65	0.65		0.65	0.70			0.08
48, 800rpm		0.70	0.60	0.65		0.60	0.55			0.11
51, 900rpm		0.70	0.60	0.60		0.55	0.55			0.14
49, 1000rpm		0.80	0.70	0.65		0.55	0.55			0.18
Rows 7.73mm										
56, 600rpm			0.60		0.63		0.55	0.56	0.47	0.07
55, 700rpm			0.60		0.53		0.50	0.51	0.52	0.09
57, 800rpm			0.60		0.53		0.60	0.57	0.52	0.13
54, 800rpm			0.55		0.58		0.50	0.51	0.52	0.13
52, 900rpm			0.55		0.53		0.45	0.46	0.42	0.17
53, 1000rpm			0.65		0.63		0.60	0.51	0.52	0.20

Table 5.5.1.1 shows the corrected pressure drop (bar) across the coil for the 4A phase system in normal phase for the three IMI stainless steel coils

The data in the right hand column represents the pressure drop obtained from the gradient of the Du characteristic using equation 5.3.1.2 and is called the Du pressure drop.

Flow Rate (ml/min) Experiment	5	10	20	40	50	60	80	110	140
Rows 3.73mm									
39, 600rpm	0.05	0.05	0.06	0.05					
41, 800rpm	0.08	0.10	0.10	0.09					
42, 1000rpm	0.15	0.17	0.18	0.16					
33, 1200rpm	0.16	0.19	0.21	0.21			0.18		
34, 1200rpm	0.16	0.19	0.20	0.20			0.18		
35, 1200rpm	0.16	0.20	0.22	0.21			0.19		
44, 1200rpm	0.18	0.20	0.22	0.21			0.20		
Rows 5.33mm									
47, 600rpm		0.04	0.05	0.05			0.05		
50, 700rpm		0.06	0.07	0.07		0.07	0.07		
48, 800rpm		0.09	0.10	0.10		0.10	0.10		
51, 900rpm		0.12	0.14	0.13		0.12	0.13		
49, 1000rpm		0.16	0.18	0.16		0.17	0.17		
Rows 7.73mm									
56, 600rpm			0.06		0.06		0.06	0.06	0.06
55, 700rpm			0.09		0.09		0.09	0.09	0.09
57, 800rpm			0.13		0.12		0.12	0.12	0.13
54, 800rpm			0.14		0.12		0.12	0.13	0.13
52, 900rpm			0.17		0.15		0.16	0.16	0.16
53, 1000rpm			0.19		0.18		0.18	0.19	0.19

Table 5.5.1.2 shows the Hagan-Poiseuille pressure drop (bar) across the coil for the 4A phase system in normal phase for the three IMI stainless steel coils

The pressure drop values given in table 5.5.1.2 were calculated using equation 5.3.1.3 knowing the length of the coils used, the volume of mobile phase in the coil (V_m), see table A.4.1.2 Appendix 4, the viscosity of the mobile phase, see table 2.2.2 Chapter 2, the mobile phase flow rate. These results represent the pressure drop across a coil for each flow rate.

5.5.2 Pressure drop in Normal and Reverse phase modes in the PTFE Coils

These experiments have shown the effect of operating in normal and reverse phase mode for the same operating conditions.

Run (Coil Vol. = 99.9ml, bore = 1.5875mm & length = 50.5m)	Dead Volume (ml)	Du Gradient $(min/ml)^{0.5}$	Fit Coefficient (R^2)	Pressure Drop (bar)	Temperature Range (°C)
67, 800rpm, RM, 4A	3.9836	9.9095	0.9859	7.5	30.0 to 30.1
70, 800rpm, NM, 4A	5.4850	5.0840	0.9759	7.5	30.0 to 30.1
68, 1000rpm, RM, 4A	6.1193	7.1177	0.9972	14.5	30.9 to 32.4
71, 1000rpm, NM, 4A	5.1995	3.8097	0.9838	13.4	30.5 to 31.7
69, 1200rpm, RM, 4A	7.1313	5.4268	0.9991	24.9	33.7 to 37.1
72, 1200rpm, NM, 4A	5.3472	3.3036	0.9654	17.8	33.3 to 37.5

Table 5.5.2.1 compares the pressure drop results for the 1.6mm bore PTFE coil for normal and reverse phase mode for the 4A phase system

In table 5.5.2.1 the Dead Volume, Du Gradient and Fit Coefficient data are taken from table 4.5.5.1 Chapter 4. The Pressure drop data in the fifth column was determined using equation 5.3.1.2 and the Du gradient data in the third column assuming 30°C viscosities. The temperature range data in the sixth column shows the increase in temperature the start of the experimental run to the finish.

5.5.3 Pressure drop and tubing bore

Experiment	Dead Vol. (ml) $F^{0.5}$	Pump out Vol. – last Displaced Vol. (ml)	Du Gradient $(min/ml)^{0.5}$	Fit Coefficient (R^2)	Pressure Drop (N/m^2)
33, 3.73mm, 1200rpm	8.3911	-0.8	1.9212	0.9924	21164
34, 3.73mm, 1200rpm	8.4693	0	1.9488	0.9940	20569
35, 3.73mm, 1200rpm	8.4372	-1	1.9057	0.9946	21509
44, 3.73mm, 1200rpm	8.9983	-0.8	1.8650	0.9976	22460
39, 3.73mm, 600rpm	7.7738	1.4	3.6573	0.9970	5840
47, 5.33mm, 600rpm	6.9008	0.2	1.8659	0.9950	5397
56, 7.73mm, 600rpm	7.5927	-0.7	0.7880	0.9996	6525
50, 5.33mm, 700rpm	7.4967	-0.7	1.5817	0.9973	7511
55, 7.73mm, 700rpm	7.8261	-0.2	0.6650	0.9991	9163
41, 3.73mm, 800rpm	8.2064	-0.6	2.7556	0.9917	10288
48, 5.33mm, 800rpm	8.1579	0.5	1.3189	0.9976	10802
57, 7.73mm, 800rpm	8.6726	-2.2	0.5612	0.9961	12867
54, 7.73mm, 800rpm	8.2971	0.8	0.5565	0.9969	13085
51, 5.33mm, 900rpm	8.4708	0	1.1655	0.9971	13832
52, 7.73mm, 900rpm	8.3837	0	0.4931	0.9965	16661
42, 3.73mm, 1000rpm	8.6958	-1.3	2.0809	0.9941	18041
49, 5.33mm, 1000rpm	8.8049	0.4	1.0093	0.9986	18446
53, 7.73mm, 1000rpm	8.2685	0.7	0.4551	0.9991	19561

Table 5.5.3.1 shows the retention results from table 4.5.3.1 rearranged for rotational speed, these results were for the 4A phase system in normal phase for the three IMI stainless steel coils

Table 5.5.3.1 also has the right hand column added for the Du pressure drop determined using equation 5.3.1.1.

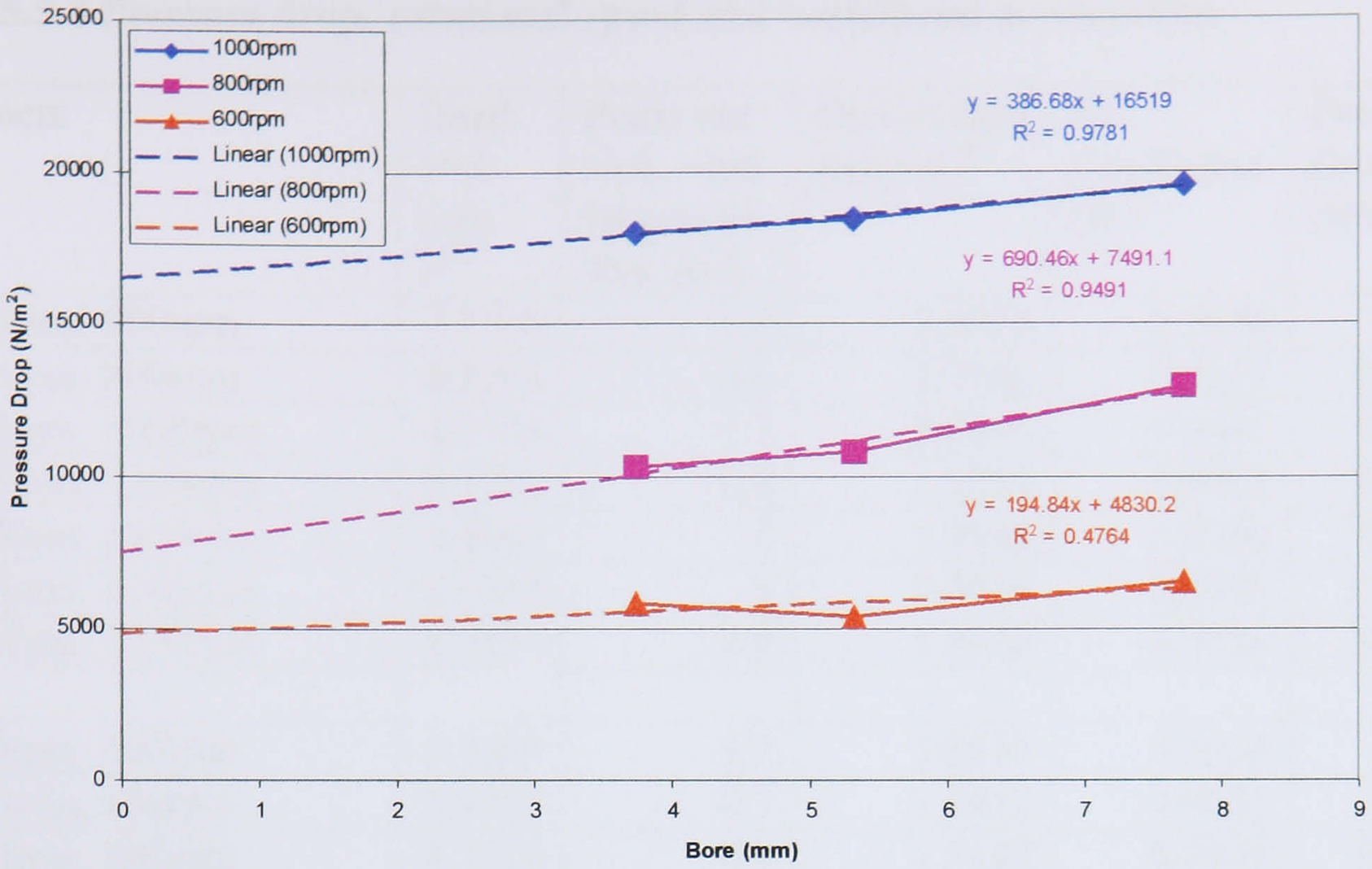

Figure 5.5.3.1 shows Pressure drop across the three IMI coils for the 4A phase system in normal phase mode

Figure 5.5.3.1 plots the pressure drop against bore using results from table 5.5.3.1.

5.5.4 Pressure drop, rotational speed and centripetal acceleration

Experiment	Dead Vol. (ml) $F^{0.5}$	Pump out Vol. – last Displaced Vol. (ml)	Du Gradient $(min/ml)^{0.5}$	Fit Coefficient (R^2)	Pressure Drop (N/m^2)
39, 3.73mm, 600rpm	7.7738	1.4	3.6573	0.9970	5840
41, 3.73mm, 800rpm	8.2064	-0.6	2.7556	0.9917	10288
42, 3.73mm, 1000rpm	8.6958	-1.3	2.0809	0.9941	18041
33, 3.73mm, 1200rpm	8.3911	-0.8	1.9212	0.9924	21164
34, 3.73mm, 1200rpm	8.4693	0	1.9488	0.9940	20569
35, 3.73mm, 1200rpm	8.4372	-1	1.9057	0.9946	21509
44, 3.73mm, 1200rpm	8.9983	-0.8	1.8650	0.9976	22460
47, 5.33mm, 600rpm	6.9008	0.2	1.8659	0.9950	5397
50, 5.33mm, 700rpm	7.4967	-0.7	1.5817	0.9973	7511
48, 5.33mm, 800rpm	8.1579	0.5	1.3189	0.9976	10802
51, 5.33mm, 900rpm	8.4708	0	1.1655	0.9971	13832
49, 5.33mm, 1000rpm	8.8049	0.4	1.0093	0.9986	18446
56, 7.73mm, 600rpm	7.5927	-0.7	0.7880	0.9996	6525
55, 7.73mm, 700rpm	7.8261	-0.2	0.6650	0.9991	9163
57, 7.73mm, 800rpm	8.6726	-2.2	0.5612	0.9961	12867
54, 7.73mm, 800rpm	8.2971	0.8	0.5565	0.9969	13085
52, 7.73mm, 900rpm	8.3837	0	0.4931	0.9965	16661
53, 7.73mm, 1000rpm	8.2685	0.7	0.4551	0.9991	19561

Table 5.5.4.1 shows the retention pressure drop results from table 5.5.3.1 rearranged for tubing bore, these results were for the 4A phase system in normal phase for the three IMI stainless steel coils

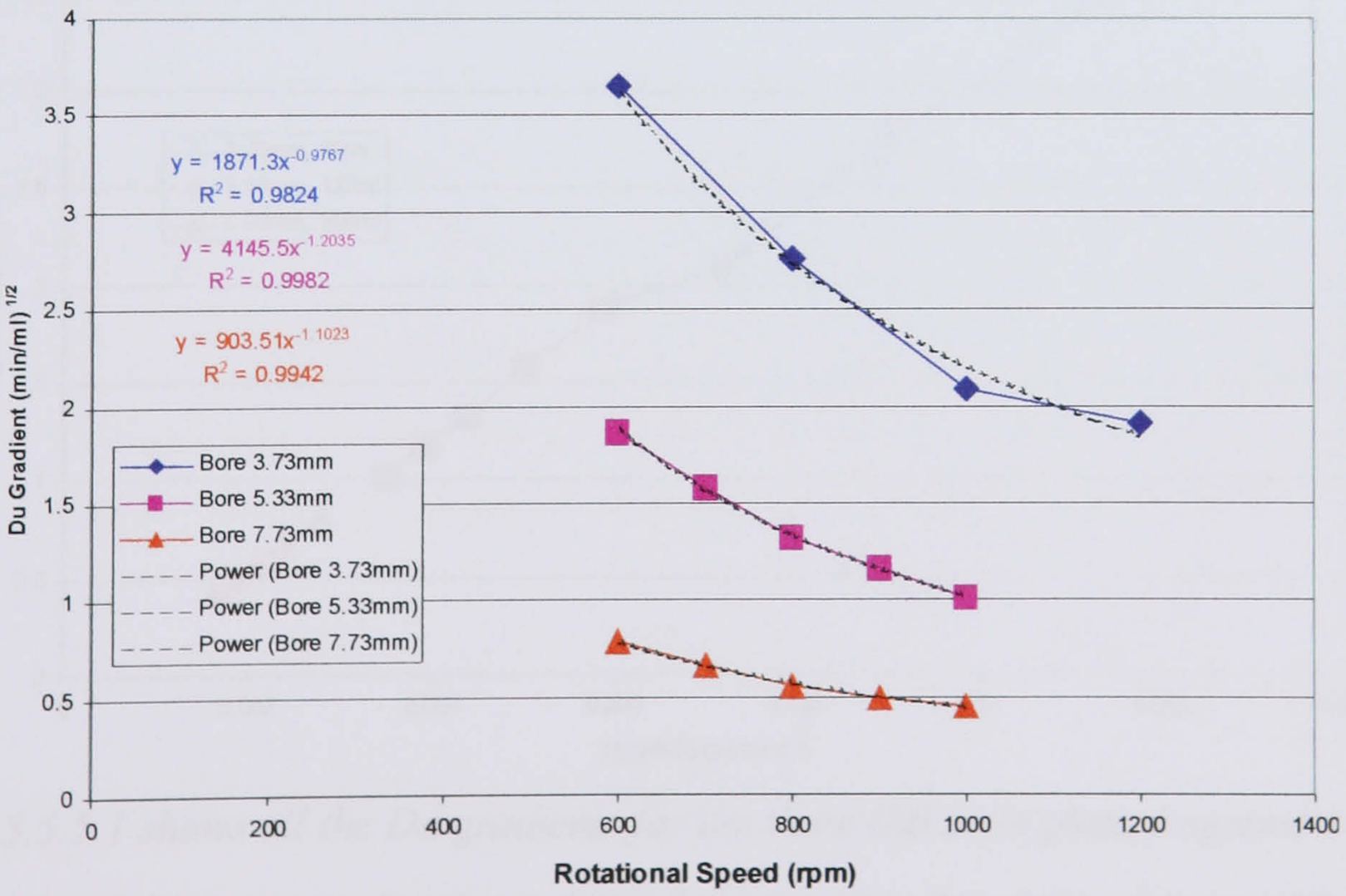

Figure 5.5.4.1 show how the Du gradient varies with rotational speed for the 4A phase system in normal phase mode in the three IMI stainless steel coils

Figure 5.5.4.1 was plotted using values taken from table 5.5.4.1. The 1200rpm point for the 3.73mm bore coil was the average of four results.

Figure 5.5.4.2 plots the centripetal acceleration $R\omega^2$ against pressure drop using data from table 5.5.4.1 for a rotor radius (R) of 0.11m.

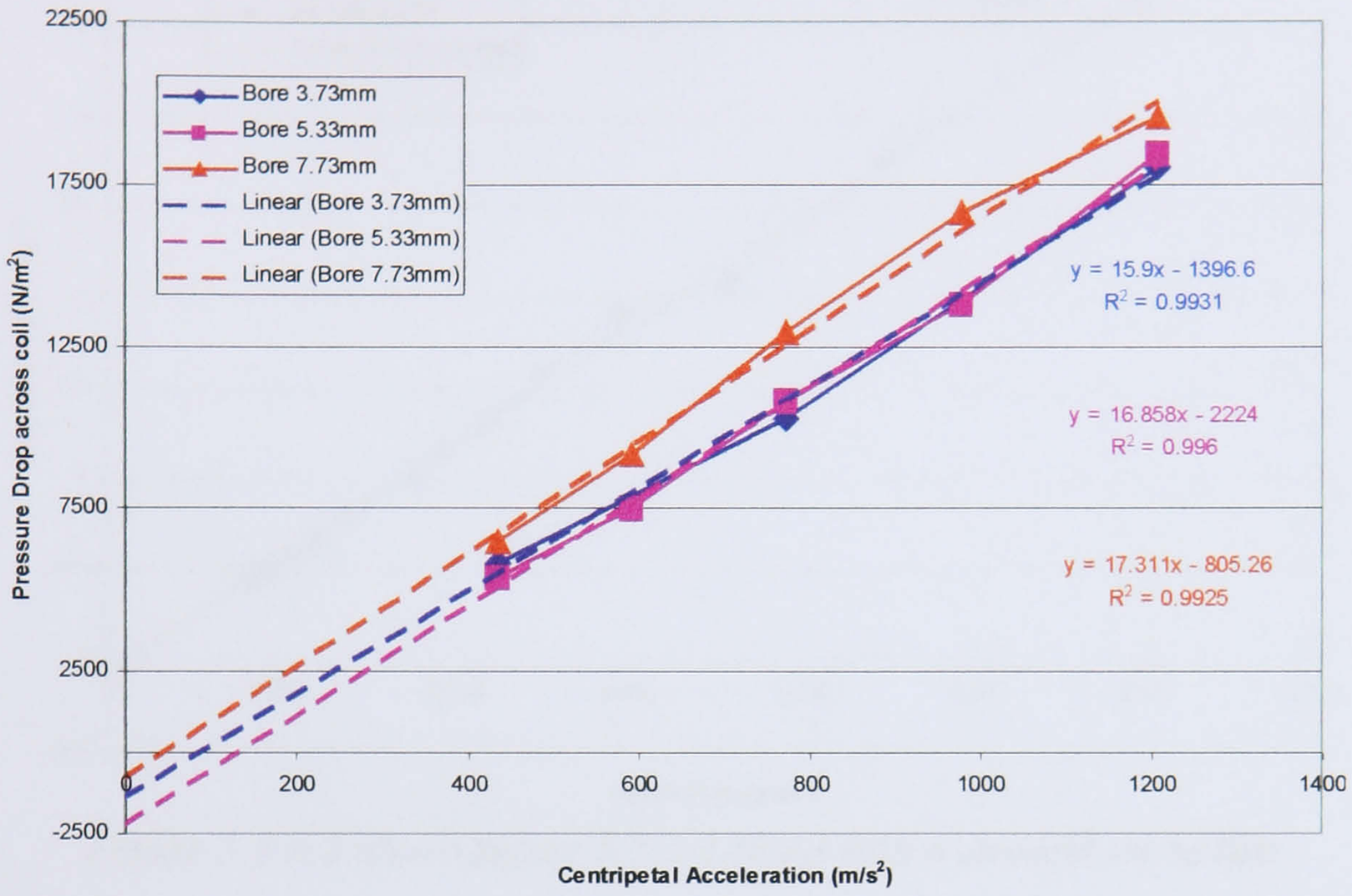

Figure 5.5.4.2 shows the pressure drop verses centripetal acceleration for the 4A phase system in normal phase mode in the three IMI stainless steel coils

5.5.5 All Du gradients for IMI coils plotted on one characteristic

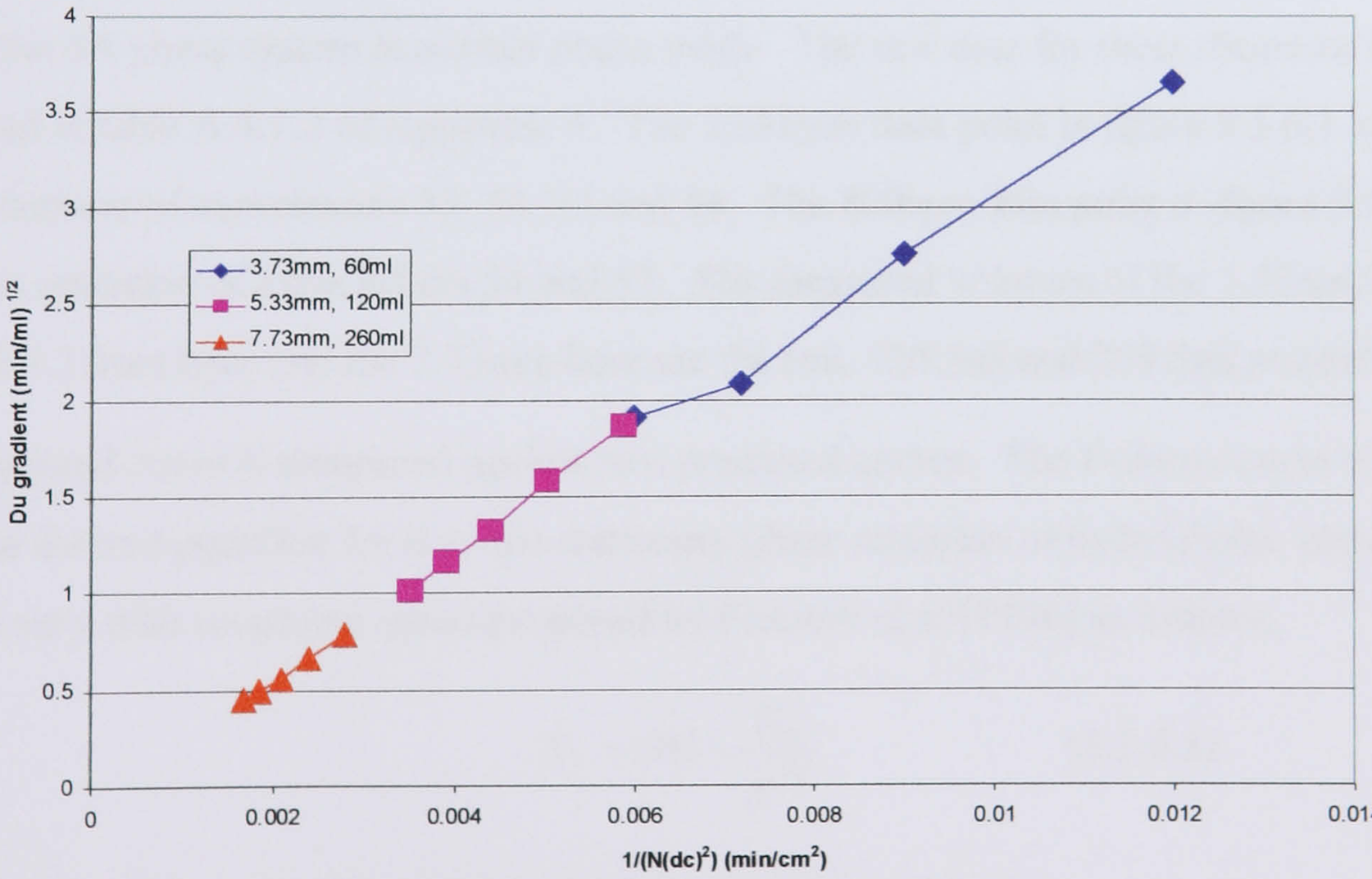

Figure 5.5.5.1 shows all the Du gradients for the three IMI coils plotted against $1/(Nd_C^2)$

The major variables were rotational speed (N) and bore (d_C). Viscosity, density difference and interfacial tension were kept constant by operating in normal phase mode with the same phase

system. All the elements in the square root term of equation 5.3.4.3 are therefore constant with the possible exception of K, however if K is constant B will be proportional to $1/(Nd_C^2)$. Figures 5.5.5.1 and 5.5.5.2 plot all data from table 5.5.4.1 in this format.

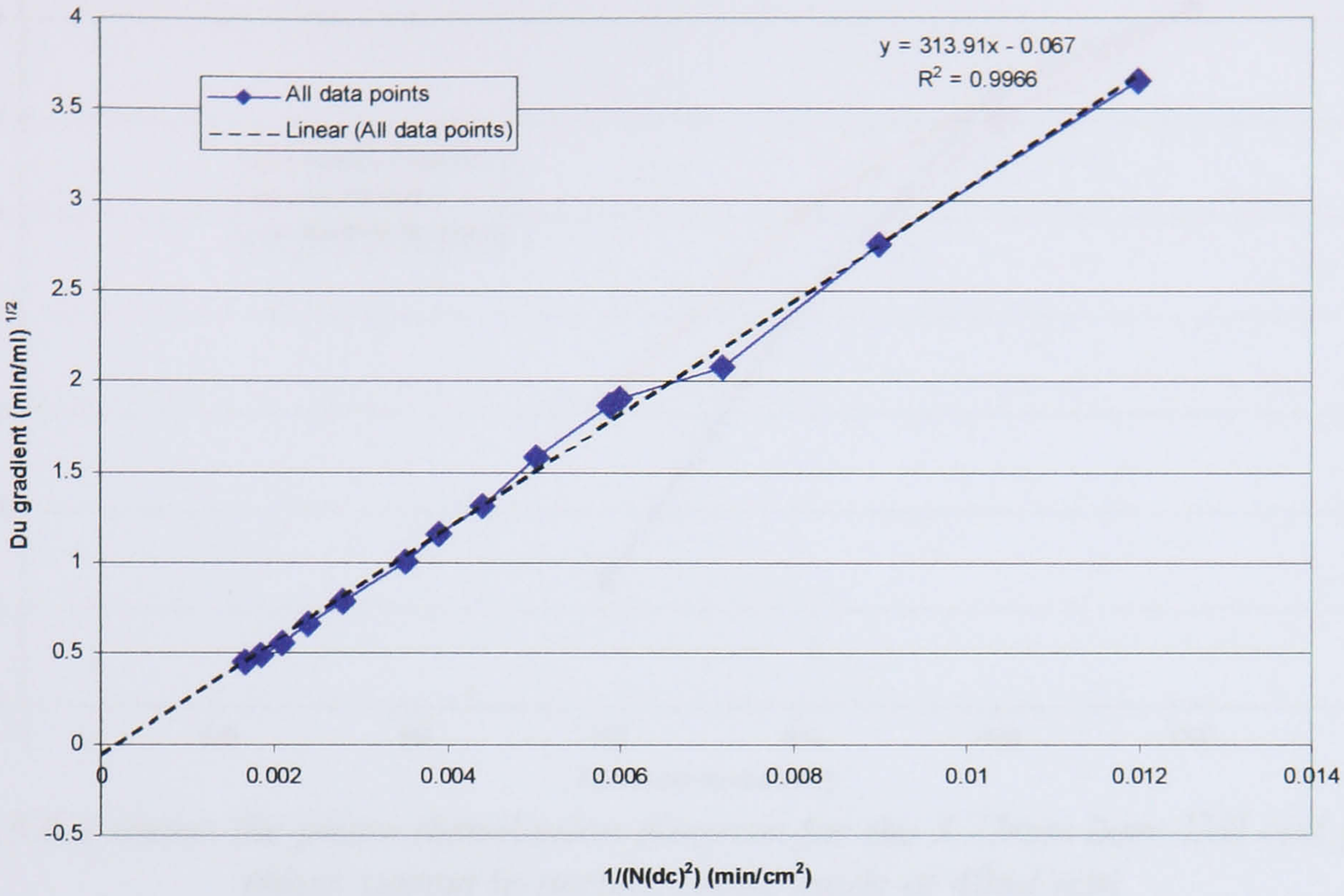

Figure 5.5.5.2 shows figure 5.5.5.1 fitted with a straight trend line

5.5.6 Phase Distribution Diagrams

The following phase distribution diagrams show the retention of the stationary phase in the three IMI coils for constant mobile phase flow rate but varying rotational speed. These results are for the 4A phase system in normal phase mode. The raw data for these diagrams is contained in table A.4.1.2 of Appendix 4. The 1200rpm data point in figure 5.5.6.1 is the mean retention of experiments 33, 34, 35 and 44. The 800rpm data point in figure 5.5.6.3 is the mean retention of experiments 54 and 57. The measured volumes of the 3.73mm bore coil, the 5.33mm bore and the 7.73mm bore are 59.1ml, 120.5ml and 259.5ml respectively.

The measured curve is compared against two predicted curves. The Fedotov curve is based upon the derived equation for how the stationary phase retention of hydrophobic phase systems vary with rotational speed proposed by Fedotov et al [1996] as follows:

$$S_f = 100 - \frac{K_F}{N^{3/4}} \qquad (5.5.6.1)$$

The 1/N curve is based upon equation 5.3.4.4 simplified as follows:

$$S_f = 100 - \frac{K_N}{N} \qquad (5.5.6.2)$$

The constants K_F and K_N are determined from the measured retention point at the highest rotational speed for each phase distribution diagram.

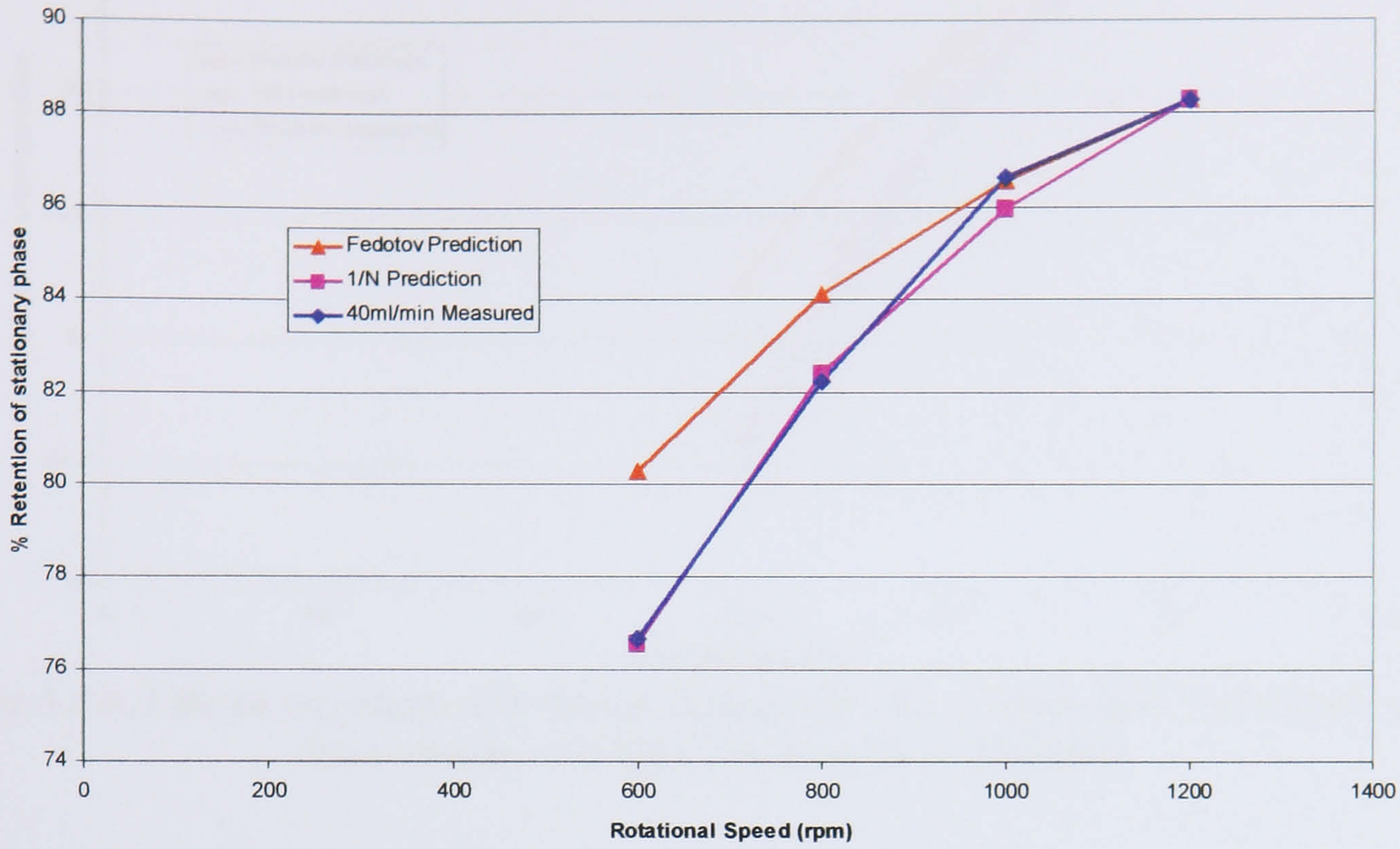

Figure 5.5.6.1 shows the phase distribution diagram for the 3.73mm bore IMI coil for the 4A phase system in normal phase mode at 40ml/min

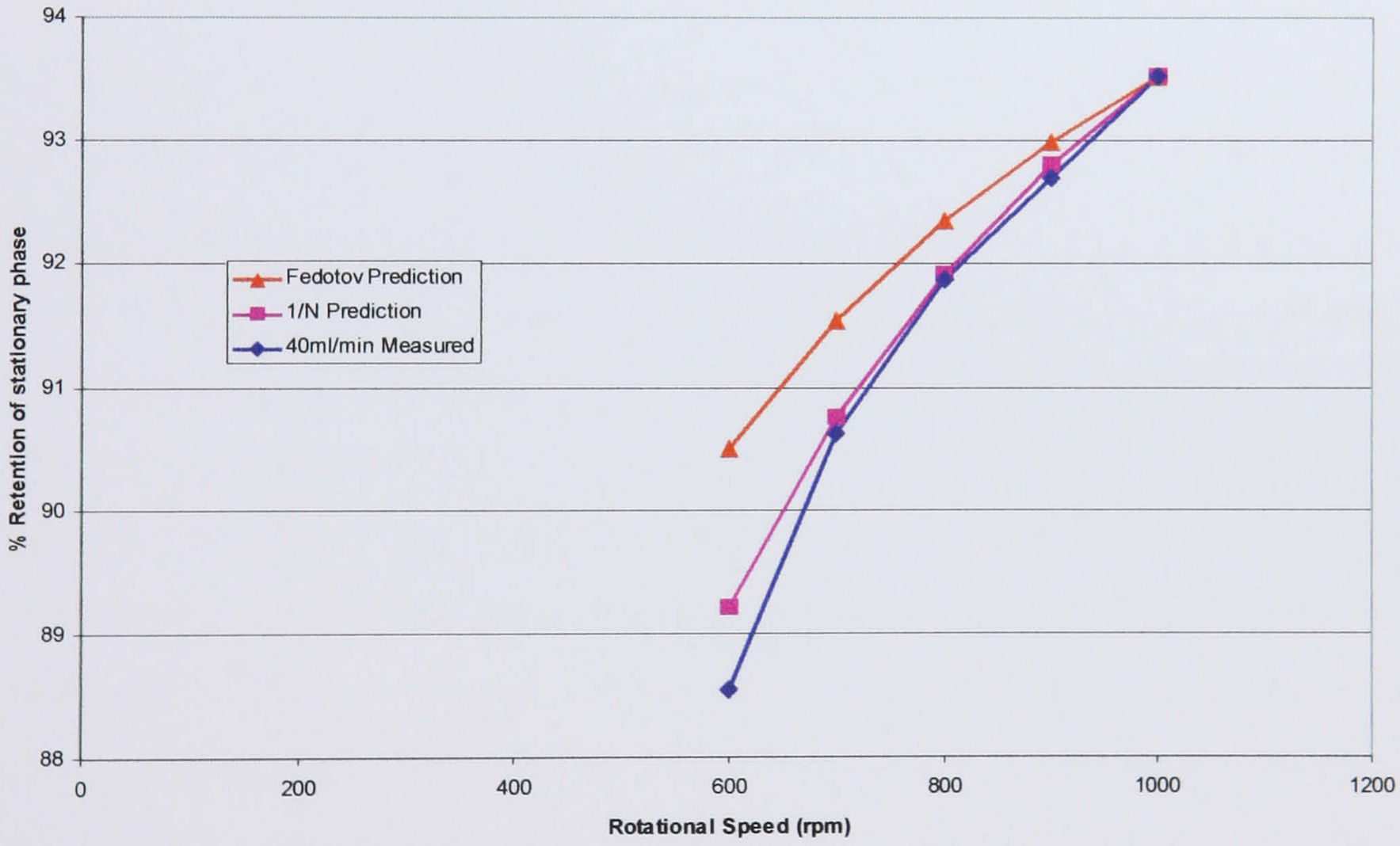

Figure 5.5.6.2 shows the phase distribution diagram for the 5.33mm bore IMI coil for the 4A phase system in normal phase mode at 40ml/min

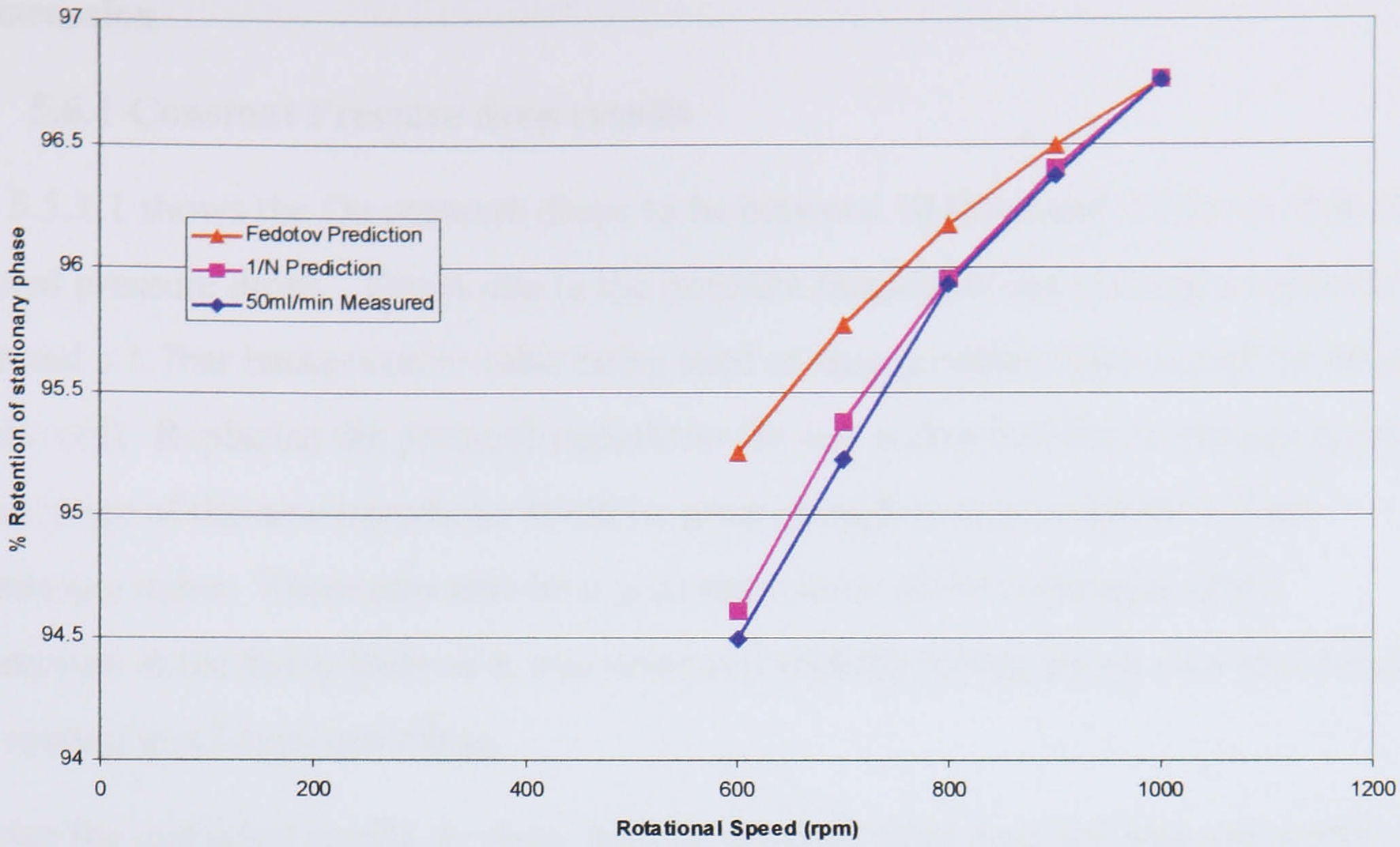

Figure 5.5.6.3 shows the phase distribution diagram for the 7.73mm bore IMI coil for the 4A phase system in normal phase mode at 50ml/min

5.6 Discussion

5.6.1 Constant Pressure drop results

Table 5.5.1.1 shows the Du pressure drops to be between 10 times and 2.5 lower than the corrected pressure drops. This is due to the pressure transducer used having a resolution of 0.1bar and a 1.7bar backpressure valve being used to stop possible siphoning of the phase from the coil. Replacing the pressure transducer for one with a 0.01bar resolution is possible and the range of the new transducer could be great enough to cope with the 1.7 bar backpressure valve. There may also be a systematic error in the calibration of the backpressure in the flying leads as it was measured with the tubing laying on a bench and not being rotated in a J-type centrifuge.

However the corrected results do show that the pressure drop does not increase significantly with flow in fact these results show that the pressure decreases with increasing flow. This suggests that as the flow rate increases the HPLC pump is required to perform less work because the amount of work being performed by the centrifuge is increasing to keep the total pressure drop across the coil constant.

The hypothesis from Chapter 4 states that total pressure drop across a coil is independent of mobile phase flow rate. The pressure drop across a coil is constant because the mobile flow rate proportionally increases the effective across-sectional area occupied by the mobile phase. The total pressure drop across a coil is the addition of the contribution of the external pump and the Archimedean pumping effect of the coil. A coil rotating in planetary motion can be viewed as a pump, as experiments conducted using closed spiral wound coils have shown that the upper and lower phases will distribute or pump to opposite ends of the coil (upper to the head and lower to the tail) with no externally pumped mobile phase flow [Sutherland 2000 A, Wood 2001 A] and Chapter 3 for helically wound coils. The pressure drops shown in table 5.5.1.2 are approximately constant while increasing the flow rate of the mobile phase. The slight differences in pressure drop can be accounted for as experimental error. **These pressure drop results add further support evidence to the constant pressure drop hypothesis given in Chapter 4.**

5.6.2 Comparison of normal and reverse phase mode pressure drop

Table 5.5.2.1 shows that the pressure drop across the coil is the same in normal or reverse phase mode for 800 and 1000rpm. The 7.1bar discrepancy between the normal and reverse phase pressure drop results for the 1200rpm results can be attributed to poor temperature

control during the tests. The temperature increases during the experiment would continuously reduce the viscosity of the mobile phase. As the test progressed the mobile phase would displace less stationary phase than if the mobile phase viscosity had remained constant. This will increase the retention of the stationary phase reducing the gradient of the Du retention characteristic and hence introduce experimental errors.

5.6.3 Pressure Drop and Tubing bore

Figure 5.5.3.1 shows that the pressure drop does not vary significantly with the tubing bore. The gradient term of the fitted linear trend line is small compared to the intercept on the vertical axis. The figure also shows the greater the rotational speed the greater the pressure drop. **This confirms the finding of Chapter 4 that the pressure drop across a coil is independent of the tubing bore.** The pressure drop for the 600rpm characteristic varies about 0.06bar, the 800rpm characteristic varies between 0.10 and 0.14bar and the 1000rpm characteristic varies between 0.17 and 0.20bar for the three IMI coils. The combination of the small magnitudes of these pressure drops and the ±2.5% experimental errors, see section 4.6.6 Chapter 4, in the Du gradients from which these pressure drops are determined make these slope of these characteristics appear significant. However if the magnitudes of the pressure drops were much greater the slopes of the three characteristics would be much less significant.

5.6.4 Pressure drop verses Centripetal Acceleration

Examination of table 5.5.4.1 shows that the Du gradient reduces as the rotational speed increases. In equation 4.3.2.11 Chapter 4 the only parameter that can vary with rotational speed is the pressure drop therefore pressure drop must change with rotational speed. Figure 5.5.4.1 shows the Du gradient plotted against the rotational speed for each of the IMI coils. The fitted trend lines on figure 5.5.4.1 show **that the Du gradient is inversely proportional to the rotational speed.** Combining this observation with equation 4.3.2.11 suggests that **the pressure drop increases with the square of the rotational speed or the centripetal acceleration.**

Figure 5.5.3.1 suggests that the pressure drop is related to rotational speed and equation 5.3.3.1 based upon dimensional analysis shows that pressure drop is proportional to the square of rotational speed and therefore centripetal acceleration. Figure 5.5.4.2 shows three linear relationships that intercept the vertical axis close to the origin. **This confirms that the pressure drop is directly proportional to the centripetal acceleration and validates equations 5.3.3.1 and 5.3.4.4.** The gradients of the fitted tread lines are similar again suggesting that the pressure drop is independent of the tubing bore.

Equation 5.3.3.1 is $\Delta P = KL\Delta\rho R\omega^2$ where K is a dimensionless constant. The gradient of each straight-line characteristics in figure 5.5.4.2 is:

$$\frac{\Delta P}{R\omega^2} = KL\Delta\rho$$

Therefore $$K = \frac{Gradient}{L\Delta\rho} \qquad (5.6.4.1)$$

This allows a value for the constant K to be determined for the three IMI stainless steel coils from the mean gradient of the three fitted tread lines of figure 5.5.4.2. The mean gradient is 16.6897kg/m^2. For the 4A phase system $\Delta\rho$ is 268kg/m^3, see table 2.2.2 Chapter 2, and the coil length L was 5.656m.

Hence $$K = \frac{16.6897}{268\times 5.656} = 0.011$$

Therefore equation 5.3.4.3 becomes:

$$B = \frac{24000}{Nd_C^2}\sqrt{\frac{2\mu_m}{0.011\pi^3\Delta\rho R}}$$

$$B = \frac{58117}{Nd_C^2}\sqrt{\frac{\mu_m}{\Delta\rho R}} \qquad (5.6.4.2)$$

for the three IMI stainless steel coils using the 4A phase system.

Figures 5.5.5.1 and 5.5.5.2 show that the retention data for the 4A phase system in Normal phase mode for all three IMI coils can be plotted on one straight-line characteristic. The straight-line characteristic has a fit coefficient (R^2) of 0.9966, which is high for 14 data points and passes through the vertical axis close to the origin. **This shows that the Du gradient is directly proportional to $\frac{1}{Nd_C^2}$ and partially validates equations 5.3.4.3 and 5.3.4.4.** The straight-line characteristic could be used to predict the retention of other helical coils with the same β-value, the same helical pitch but different bores operating at different rotational speeds.

The gradient of the straight-line characteristic is:

$$Gradient = 24000\sqrt{\frac{2\mu_m}{K\pi^3\Delta\rho R}} \qquad (5.6.4.3)$$

The gradient from figure 5.5.5.2 is 313.91$(cm/min)^{0.5}$. If standard international units (SI units) are to be used to determine a value for K the gradient must be modified to have SI units of $(m/s)^{0.5}$. This is achieved by converting the units of the Du gradients from $(min/ml)^{0.5}$ to $(s/m^3)^{0.5}$ by multiplying by the square root of 60,000,000 ie 7745.9, for the vertical axis, and converting the cm^2 to m^2 by dividing by 10,000, for the horizontal axis. The combination of these conversions is to multiply the gradient by 0.77459 to get $243.15(s/m^3)^{0.5}$. Equation 5.6.5.1 can now be modified to give:

$$243.15 = 24000\sqrt{\frac{2\mu_m}{K\pi^3\Delta\rho R}} \qquad (5.6.4.4)$$

where for the 4A phase system $\Delta\rho$ is $268kg/m^3$, see table 2.2.2 Chapter 2, $\mu_m = 0.00036Ns/m^2$ (upper mobile) and R = 0.11m. Substituting these values in equation 5.6.5.2 and rearranging for K gives:

$$K = \frac{2\times 0.00036}{\pi^3\times 268\times 0.11}\left(\frac{24000}{243.15}\right)^2 = 0.008$$

The value for K is close to the value determined earlier in this section of 0.011. The difference between these values for K (0.003) can be attributed to experimental errors in the gradients of the fitted trend lines in figures 5.5.4.2 and 5.5.5.2 and that the fitted trend lines do not pass through the origin of either figure. However both methods of determining a value for K show that **K is independent of tubing bore and rotational speed.** Therefore a value for K once determined for a coil could be used in equation 5.3.3.1 to determine the pressure drop for that coil for a range of rotational speeds. **The same value of K can also be used to predict the retention in similar coils, with the same β-value and the same helical pitch fitted on a rotor with the same radius, but with different tubing bores.** If the inlet and outlet details on the coils are designed correctly unlike the IMI coils see section 4.6.2 Chapter 4, then the value for K can be used for prediction of retention in both normal and reverse phase modes, the pressure drop being the same in both normal and reverse phase modes.

Figures 5.5.6.1 to 5.5.6.3 compare actual retention results for each IMI coil with predicted results based upon equations 5.5.6.1 and 5.5.6.2. These figures show that the stationary phase retention at a constant flow decreases with the rotational speed and not the rotational speed raised to the power of three quarters. Eleven other results were plotted for constant flow and varying rotational speed in a similar manner to figures 5.5.6.1 to 5.5.6.2. These other results also confirmed the finding that the retention varies with the rotational speed and not the rotational speed raised to the power three quarters as proposed by Fedotov et al in [1996].

Fedotov et al's equation, see equation 5.5.6.1, was developed for hydrophobic phase systems before Du et al's retention paper [1999] and the head and tail studies by Sutherland et al [2000A] and is remarkably similar to equation 5.5.6.2 which has been developed since the dissemination of experimental findings of Du's and Sutherland's groups. Fedotov et al stated that the prediction given using equation 5.5.6.1 matched experimental results although the experimental and the predicted results are presented on different graphs. Fedotov has extended his theories given in [1996] to hydrophilic phase systems and were presented in [2001A]. This paper does not reference the head and tail study work of Sutherland et al [2000A] that stressed the importance of rotating the coil in the same direction as it is wound so that the head is at the centre and the tail is at the periphery. A coil rotated in this manner will have the Archimedean and hydrostatic pumping effects working together and in this condition the head and tail preferences of hydrophobic and hydrophilic phase systems are the same for tubing bores of 3.2mm. Fedotov does reference [Mandava 1988] retention studies performed by Ito on hydrophobic and hydrophilic phase systems first published four years previously [Ito 1984]. The hydrophilic phase systems used in Ito's retention studies used Butanol and secondary-Butanol as the organic phase. Butanol and secondary-Butanol are very viscous liquids with a density close to that of water see the viscosities of the 2C and 3C phase systems listed in tables 2.2.1 and 2.2.2 of Chapter 2. For the hydrodynamics this means that a low pressure drop across the coil will be generated because of the low density difference between the upper and lower phases. This low pressure drop will need to redistribute the viscous phases to each end of the coil. The 3C phase system is the Butanol-Acetic Acid-Water (4:1:5) phase systems used by both Sutherland and Ito. In the head and tail study conducted by Sutherland et al [2000A] the 3C phase system showed the same head and tail preferences as the hydrophobic and intermediate phase systems tested ie the upper phase goes to the head and the lower phase goes to the tail when the coil is rotated in the same direction that it is wound. In the retention study conducted by Ito [1984] the 3C phase system showed the opposite behaviour to hydrophobic and intermediate phase systems tested. The retention behaviour of the 3C phase system suggests that the upper phase would redistribute to the tail and the lower phase to the head in a head and tail study contradicting the findings of Sutherland et al. Reviewing both sets of published results shows that Ito used 1.6mm and 2.6mm bore tubing in his spiral coils and that Sutherland used 3.175mm bore tubing while the rotor radius, β-value and rotational speeds remained approximately equal. Therefore the difference in the behaviour of the 3C phase system can only be attributed to the different tubing bores used. In Chapter 4 it was shown that the mobile phase flows in a laminar fashion

in both normal and reverse phase and that the Hagen-Poiseuille formula can be applied to the hydrodynamics in the coils of a J-type centrifuge. During a head and tail study the upper and lower phases must flow past each other in order to redistribute to opposite ends of a coil. In a coil that is made from small bore tubing there will be only a small cross-sectional area for each phase to flow past the other. In larger bore coils the area for each phase to pass the other is greater and hence it is easier for the phases redistribute. If it is assumed that during a head and tail redistribution both phases flow in a laminar manner then the resistance to flow is proportional to the bore of the tubing raised to the fourth power. This means that its is 2.2 times easier for the 3C phase system to redistribute in 3.175mm bore tubing than in 2.6mm bore tubing and may explain the difference in Ito's and Sutherland et al's results. If Ito's results for the 3C phase system in the 1.6mm and 2.6mm spiral coils are compared it can be seen that the 2.6mm results show a better correlation to Sutherland et al's results than the 1.6mm results. Fedotov et al [2001A] have ascribed the behaviour of the hydrophilic phase systems to the properties of hydrophilic phase systems. However it appears that the behaviour of hydrophilic phase systems is a combination of the phase system properties and the coil used. For the hydrophilic phase systems the main determining factor for head and tail behaviour may be the bore of the coil used and if the bore is large enough the head and tail preferences of the upper and lower phases will be the same as hydrophobic phase systems.

The 4C hydrophilic phase system used in the head and tail study of Chapter 3, physical properties also listed in table 2.2.2 of Chapter 2 has the same head and tail preference as the 4A hydrophobic phase system and the 4B intermediate phase system. The FEP coils used in Chapter 3 had a bore of 3.175mm, which indicates that the head and tail preferences of the upper and lower phases for hydrophilic phase systems are the same as the other types of phase systems provided the coil tubing bore is large enough.

5.6.5 Pressure Drop and Density Difference

Sutherland et al [2001B] have shown that the pressure drop across a coil is directly proportional to the density difference ($\Delta\rho$) and is also directly proportional to the acceleration ($R\omega^2$), confirming the results presented above. The paper plots the retention data for the 4A, 4B and 4C phase systems on the same straight-line characteristic that passes through the origin of figure 6 [Sutherland 2001B]. The gradient of this characteristic was assumed to be a dimensionless number called (S_u) and has the following equation, see equation 11 [Sutherland 2001B]:

$$S_u = \frac{u_m^2 \mu_m}{F \Delta\rho R \omega^2} \qquad (5.6.5.1)$$

where $\Delta\rho = \rho_L - \rho_U$

$$u_m = \frac{F}{A_m} = \frac{FL}{V_m} \qquad (5.6.5.2)$$

From equation 4.3.2.5 from Chapter 4:

$$V_m = \sqrt{\frac{8\pi\mu_m L^3}{\Delta P}}\sqrt{F} \qquad (4.3.2.5)$$

Substituting equation 4.3.2.5 into equation 5.6.5.2 gives:

$$u_m = FL\sqrt{\frac{\Delta P}{8\pi\mu_m L^3 F}} = \sqrt{\frac{\Delta P F}{8\pi\mu_m L}} \qquad (5.6.5.3)$$

Therefore $$u_m^2 = \frac{\Delta P F}{8\pi\mu_m L} \qquad (5.6.5.4)$$

Substitute equation 5.6.5.3 into equation 5.6.5.1 gives:

$$S_u = \frac{\Delta P F}{8\pi\mu_m L}\frac{\mu_m}{F\Delta\rho R\omega^2} = \frac{\Delta P}{8\pi L \Delta\rho R\omega^2} \qquad (5.6.5.5)$$

Substituting equation 5.3.3.1 for the pressure drop in equation 5.6.5.5 gives:

$$S_u = \frac{KL\Delta\rho R\omega^2}{8\pi L\Delta\rho R\omega^2} = \frac{K}{8\pi} \qquad (5.6.5.6)$$

Therefore the derived equation for the dimensionless number S_u is the pressure drop divided by the pressure drop and is not a dimensionless number but a dimensionless constant. However the value of S_u can be used to calculate the value of K. The value of S_u from figure 6 of [Sutherland 2001B] was 0.002, which gives a value of 0.050 for K[xxiii]. This value is between 4.55 and 6.25 times larger than the K values determined for the three IMI stainless steel coils, see section 5.6.5. The difference in the value of K cannot be attributed to the pulsitile and steady flow HPLC pumps used respectively with the PTFE and IMI coils. This is because the Du gradients from which the K values for the PTFE coil were determined would

---

[xxiii] It must be remembered that for equation $S_u = K/8\pi$ to be valid both the values for K and S_u must be determined from same units for all the parameters used to determine both S_u and K. SI units (Standard International units) were used for determining the values of K and S_u shown in this section.

need to **increase** by a factor between 2.13 and 2.5, the square roots of 4.55 and 6.25, when a steady flow pump was used. This would mean that steady flow of the mobile phase improves retention when compared to using a pulsitile flow, experience has shown the converse to be true. Section 5.6.3 showed that the value for **K is independent of tubing bore**; pressure drop being independent of tubing bore. Section 5.6.4 has shown that pressure drop is directly proportional to ($R\omega^2$), provided the same rotor radius (R) is used, hence **K must be independent of ($R\omega^2$) for the same rotor radius.** Further research is needed to determine if K is independent of the rotor radius (R). Figure 6 from [Sutherland 2001B], combined with equation $S_u=K/8\pi$, shows that **K is independent of the density difference.** Section 5.3.2 shows that the pressure drop across a coil is proportion to coil length and therefore **K is independent of coil length.** Therefore K must vary with either or both β-value and helical pitch. The PTFE coil used by Sutherland et al [2001B] had a β-value range of 0.87 to 0.90 being a two layer multi-layer coil and had a helical pitch of 3.175mm (1/8 inch). The IMI stainless steel coils had a β-value of 0.82 being helical coils with a helical pitch of 11.5mm. The difference in the β-values, 0.05 to 0.08 or 5.5 to 8.8mm, of these coils cannot account for the differences in the K values alone. The hydrostatic head generated will be small in the PTFE coil due to the small β-value range described listed above. The hydrostatic head, although small, will aid the Archimedean pumping, as described by Sutherland et al [2000A], since the coil was orientated head-centre to tail-periphery. The helical pitch of the IMI coils is approximately 3.6 times that of the PTFE coil used by Sutherland et al [2001B] and may account for the lower K value of the IMI coils. It appears from these results that as helical pitch increases the K-value decreases making the coils less effective at pumping. If a coil is less effective at pumping its retention of stationary phase will be lower. The effect of helical pitch on retention needs to be studied, as this appears to be significant. Also the influence of β-value on retention needs to be studied to produce a complete understanding of how pressure drop is generated in a coil of a J-type centrifuge.

Given that the equation 14 from [Sutherland 2001B] for the Du gradient (B) given below:

$$B = \frac{1}{A_C \omega}\sqrt{\frac{\mu_m}{S_u \Delta\rho R}} \qquad (5.6.5.7)$$

where $\Delta\rho = \rho_L - \rho_U$. The S_u term has been shown to be a constant then equation 5.6.5.7 can be used to derive equation 5.3.4.1. Substituting in equation 5.6.5.7 for A_C and S_u gives:

$$B = \frac{4}{\pi d_C^2 \omega}\sqrt{\frac{8\pi\mu_m}{K\Delta\rho R}} = \frac{8}{d_C^2 \omega}\sqrt{\frac{2\mu_m}{K\pi\Delta\rho R}}$$

(5.6.5.8)

Equation 14 from [Sutherland 2001B] was derived for stationary phase retention expressed as a fraction and equation 5.3.4.1 was derived for stationary phase retention expressed as a percentage. Therefore equation 5.6.5.8 must be multiplied by 100 to be identical to equation 5.3.4.1. Equation 14 was derived using the results contained within [Sutherland 2001B] and as shown above the results also support the derivation of equation 5.3.4.1 and the research work presented in section 5.6.4 of this chapter.

The dimensionless constant K is independent of the phase system properties, rotational speed and normal or reverse phase mode operation. Therefore K appears to be a property of the coil and centrifuge. The helical pitch and β-value of the coil appear to influence the value of K. These two variables combine to pitch, or blade angle, which is the actual parameter to be studied in future work. The centrifuge parameter that may affect K is the rotor radius (R) that will require further research to determine its influence.

5.7 Concluding Remarks

The value for K can be used in equation 5.3.4.4 to predict the stationary phase retention in the coil of a J-type centrifuge:

$$S_f = 100 - \frac{24000}{Nd_C^2}\sqrt{\frac{2\mu_m}{K\pi^3\Delta\rho R}}\sqrt{F} \qquad (5.3.4.4)$$

Currently a value for the dimensionless constant K can be determined from one accurate retention test. Then retention predictions for other phase systems operating in either normal or reverse phase mode, at different rotational speeds, in coils with different tubing bores can be made, provided that the same helical pitch, β-value and rotor radius are used.

It is not yet known how the value of K will change with rotor radius (R), β-value, spiral pitch and helical pitch and hence further research is required.

Chapter 6 General Discussion

6.1 Summary

This chapter discusses the research achievements made by the author and shows how the following aims and objectives from Chapter 1 were met. The aims and objectives as listed in section 1.2 of Chapter 1 are:

1. To determine which phase, upper or lower, is pumped to the head end of a helical coil and compare with the results for spiral coils.
2. To qualitivily understand head and tail distribution of the upper and lower phases in helical coils when there is no external pumping of a mobile phase.
3. To understand and mathematically model the retention of stationary phase in the coil when an externally pumped mobile phase is present. This mathematical model will be developed for both normal and reverse phase modes.

The chapter then discusses further research that is required to fully complete the mathematical modelling of stationary phase retention to allow the retention to be predicted for any J-type centrifuge without needing to perform a single retention test. This will allow the performance of production scale J-type centrifuges to be predicted before being built, thus reducing the technical and financial risks involved.

6.2 Introduction

There are a number of ways for considering a J-type centrifuge. The primary consideration is to view the device for performing liquid-liquid chromatograph or liquid-liquid extraction. The more formal view is to consider the process as a multi-stage liquid-liquid extraction process that has such a vast number of mixing and settling stages that sample components with very slightly different distribution constants can be separated. This view is applicable to understanding the chemical processes that occur during the operation of the device but not much help in understanding how the stationary phase is retained in the coil while the mobile phase is pumped through the coil or in understanding how the mixing and settling zones occur [Conway 1990]. The second view is to consider the device as a centrifuge as its name suggests. Sutherland et al [1987] took this view and used the Kelvin-Helmholtz stability criterion to qualitatively explain the mixing and settling zones. The third view to be taken is that the J-type centrifuge is a pump or more formerly a piece of rotodynamic machinery. Head and Tail studies conducted by Sutherland et al [2000A] on a spiral coil and a similar study performed on helical coils, described in Chapter 3, shows that the upper phase is always pumped to the head end and consequently the lower phase is displaced to the tail end of a coil in a J-type centrifuge. These head and tail studies confirm that the J-type centrifuge acts as a pump. From this concept the refined view that the J-type centrifuge is a constant pressure drop pump has grown, as described in Chapters 4 and 5.

6.3 The author's contribution to the science and technology of the hydrodynamics of CCC

In 1991, how the stationary phase was retained in a coil, against the flow of a mobile phase, was not understood. Ito [1992] published a speculative discussion on how the stationary phase was retained in the coil of a J-type centrifuge, based on hydophobicity/hydrophilicity. He proposed that for hydrophobic phase systems the heavy phase moved to the tail end of the coil. For Hydrophilic phase systems, he maintained the opposite was true, with the heavy phase moving to the head. In between, for intermediate phases, there was confusion. In general, it was known that the retention of stationary phase decreased as the flow rate of the mobile phase increased. It was also known that the retention increased as the rotational speed increased, as shown by phase distribution diagrams [Ito 1984 and Manadava 1988], and that the retention varied with different phase systems [Du 1999]. Two groups of scientists had plotted retention against the flow rate of mobile phase [Bousquet 1991 and Menet 1992]. Du et al [1999] proposed plotting retention against the square root of flow and replotting Bousquet and Menet results in this fashion improved the R^2 fit coefficients of the straight-line characteristic and moved the intercept on the vertical axis closer to the 100% retention mark for a zero flow rate of mobile phase, see section 1.4.2.6 Chapter 1. The first theory of how the stationary phase is retained in a coil was proposed by Fedotov in 1996 and has been built upon with subsequent papers published in 1998, 2000 and 2001 [A]. His theory was produced in response to phase distribution diagrams and has not yet been adapted for Du plots. This theory appears to be inaccurate as regard to the effect of rotational speed, see section 5.6.4 Chapter 5 and also differs slightly for hydrophobic and hydrophilic phase systems.

The following advances in the understanding of the hydrodynamics of CCC have been made:

1) ***Understanding that the coil planet centrifuge acts like a constant pressure pump.*** The constant pressure drop theory proposed in section 4.3.2 of Chapter 4 was developed in response to Du plots.

2) ***Devising a method of accurately determining the dead volume.*** Du et al's [1999] original results had characteristics that passed either side of the 100% retention mark for zero flow rate of mobile phase, strongly suggesting that all characteristics should pass through the 100% if a coil is first completely filled with stationary phase. This led to the method of determining the dead volume, described in section 4.3.1 of Chapter 4, where the volume of stationary phase displaced from the coil and flying leads (V_E) is plotted against the square root of mobile phase flow rate, the dead volume being the

intercept on the displaced volume axis. Results see section 4.6.1 Chapter 4, have shown that the predicted dead volume is very close to the calculated dead volume based upon the cross-sectional area and length of flying leads. The use of the predicted dead volume also ensures that the characteristic on a Du plot passes through the 100% mark at a zero flow rate of mobile phase, see section 4.6.1 Chapter 4. The value of dead volume used does not change the gradient of the Du characteristic, compare figures 4.5.1.2 and 4.5.1.3 Chapter 4.

3) ***Modelling the movement of the interface between the upper and lower phases and suggesting that this movement aids the mixing observed [Conway 1990] at the proximal key node [Wood 2001B].*** This satisfies the second objective.

4) ***Showing that for Helical coils the upper phase distributes to the head end the coil and the lower phase distributes to the tail end of a the coil during a head and tail study.*** This distribution is the same as that for spiral wound coils orientated head-centre to tail-periphery, this satisfies the first objective. Chapter 3 also gives a simple explanation of how this distribution occurs based upon a pressure gradient generated in the coil by the wound tubing acting as the blades in a rotary pump.

5) ***Combining the constant pressure drop hypothesis with the Hagan-Poiseuille equation for laminar flow to produce a theoretical basis for the Du plot, see section 4.3.2 Chapter 4.*** The results discussed in section 4.6.3 Chapter 4 show that the pressure drop across a coil is constant and independent of the mobile phase flow rate. The *Re* results discussed in section 4.6.4 of Chapter 4 show that the flow of mobile phase is laminar validating the use of the Hagan-Poiseuille equation in developing a theory of retention that fits the Du plot and can be used to produce phase distribution diagrams, see section 5.6.4 Chapter 5.

6) ***Showing that this pressure drop is the same in both normal and reverse for the same phase system, coil and rotational speed provided that the recommendations of Sutherland et al [2000A] are followed, see section 4.6.5.*** This allows the retention in normal phase mode to be predicted from reverse phase mode measurements and establishes a relationship between normal and reverse phase mode retention characteristics. **This allows the same retention model to be applied to both normal and reverse phase modes.** The *Re* results of section 4.6.4 Chapter 4 have also shown that the flow of mobile phase is identical at the same flow rate in different bore coils at the same rotational speed provided each coil has the same helical pitch. Table 4.5.2.3

of Chapter 4 shows the mobile phase occupies the same volume at the same flow rate in each helical coil of a different bore provided that the same rotational speed is used and each coil has the same helical pitch and β-value. Given that each of the IMI coils was wound from the same length of tubing the mean cross-section area occupied by the mobile phase is the same in each coil. This means that the proportion of stationary phase retained is primarily based upon the bore of the tubing from which a coil is wound.

7) ***Improving the accuracy of retention tests for both normal and reverse phase modes at high flow rates.*** This allowed the constant pressure drop hypothesis, the hypothesis that the pressure drop is the same in both normal and reverse phase modes and the determination of dead volume as described in section 4.3.1 of Chapter 4 to be tested. The main improvement was making the measurement of the volume of displaced stationary phase (V_E) easier and more accurate, this was achieved by designing and using stationary phase collectors for both normal and reverse phase mode retention tests. The design of these collectors is based on 100ml burrettes improving the measurement accuracy from 0.5ml (measuring cylinder) to 0.1ml, see section 4.6.6 Experimental Accuracy, Chapter 4.

8) ***Predicting the retention once a value for the constant K has been determined from equation 5.3.4.4 of Chapter 5 using properties of the phase system, the coil geometry, the rotor radius (R) and rotational speed.*** The constant K appears to be a property of the J-type centrifuge and its coil and is independent of the phase system, operation in normal or reverse phase mode and the rotational speed, see section 5.6.5 of Chapter 5. Therefore it is possible to determine the value of K for a coil and centrifuge by performing one retention test for one phase system, in one mode of operation, normal or reverse, at one rotational speed and use this value to predict the retention of other phase systems in normal or reverse phase mode at all rotational speeds. **This shows that retention of stationary phase has been understood and modelled mathematically achieving the third aim/objective of the research work contained in this thesis.** Further work is required to find a way of predicting the value of K for production scale machines, which may complete the prediction of retention. It is not yet fully known how K varies with β-value, helical pitch and spiral pitch.

9) ***Showing that for helical coils the helix angle is an important variable for determining the value of K and hence the retention of stationary phase.***

6.4 Future Research and Recommendations

6.4.1 Helix angle and β-value

The discussion in section 5.6.5 of Chapter 5 showed that the dimensionless constant K in equation 5.3.4.4 was independent of the phase system used, the rotational speed, coil tubing bore and whether the coil was operated in normal or reverse phase mode. However the value of constant K differed significantly for the PTFE coil with a helical pitch of 3.175mm and the IMI coils that have a 11.5mm pitch at approximately the same β-values. Both the PTFE and IMI coils were mounted on the rotor of a Brunel CCC J-type centrifuge. This implies that the helical pitch is significant in determining the retention in a given coil. Chapter 3 also indicated that the coiled tubing acts in a similar way to the blades in radial or axial pumps. It is known that for rotodynamic machines, pumps and turbines, that the blade angle is an important factor in determining the machines performance [Massey 1989]. It is such an important parameter that complex mechanisms are often used to vary the blade angle to keep the operating efficiency of the pump or turbine high across a wide range of operating speeds. The blade angle for a helical coil is the helix angle, which is defined by the mean radius of the coil and the helical pitch. The mean radius (r) of the coil is the β-value multiplied by the rotor radius (R). Hence it can be seen that the helical pitch and the β-value are two closely related variables. If the helix angle is measured in radians, the angle is dimensionless, a radian angle being an arc length divided by a radius. Therefore the relationship between K and helix angle will be dimensionless. This means that the dimensional analysis of the basic pressure drop equation 5.3.3.1 will still be valid, see section 5.3.3 of Chapter 5.

The FEP coils used in the head and tail studies contained within Chapter 3 both have the same helix angle (1.09°) because the helical pitch was increased in proportion to the β-value. A third FEP coil also exists with the same helix angle but with a β-value of 0.382. Hence the complete set of FEP coils has β-values of 0.382, 0.615 and 0.864 and pitches of 5.0mm, 8.1mm and 11.3mm respectively. These coils also have identical tubing bore and approximately the same tubing length and hence roughly the same coil volume. A retention study using the same phase system and rotational speeds would determine the relationship between the constant K and the helix angle. If the constant K were the same for each FEP coil then the relationship between the constant K, helical pitch and β-value would be understood. It is generally known that retention increases with β-value [Baalen 1997], however the coils

from such studies used the external diameter of the tubing to define the helical pitch. The lowest β-value coil has the highest helix angle and the highest β-value coil has the lowest helix angle. A coil with a β-value of 0.9 has half the helix angle of a coil with a β-value of 0.45 if the helical pitch is the same for both coils. The results discussed in section 5.6.5 showed that high helix angles give significantly lower values for K and poorer retention, hence the lower retention may not be due to purely the lower β-value but the higher helix angle. It must also be remembered that the tangential acceleration does not vary with β-value, see equation 1.4.1.2.3.2 Chapter 1. The acceleration along the axis of the coil tubing is the tangential acceleration multiplied by the cosine of the helix angle. If the same helix angle is used at all β-values then the acceleration along the axis of the tubing will be the same at all β-values. This constant acceleration along the axis of the tubing at all β-values may cause the value of constant K to be the same at all β-values. If the same value for constant K is obtained at a lower β-value the retention will be the same at the low β-value as at higher β-values. The radial acceleration increases with β-value see equation 1.4.1.2.3.1 Chapter 1. The Kelvin-Helmholtz stability criterion, see equations 1.4.3.1.1 and 1.4.3.1.3, shows that, as the radial acceleration increases, the relative flow velocity between the phases needs to increase in order for instability and wave formation to occur. If the retention and mobile phase flow rate is the same at all β-values then the relative flow velocity will be the same at all β-values, however at the higher β-values the radial acceleration is greater and hence the amount of instability and wave mixing will reduce. This will reduce the column efficiency, or mass transfer, at high β-values causing the peak widths to increase. If the retention is the same for all β-values the distance/time between peak elution will be the same for coils of high and low β-values, all other considerations being the same. However the peaks widths from the high β-value coils will be wider reducing the resolution obtained. A design aim for a coil should be to maximise the value of constant K for a coil so that the rotational speed can be minimised but still produce high retention of stationary phase and increase column efficiency to maximise resolution. There is also a need to use the FEP coils to investigate the changes in column efficiency with β-value for the same rotational speed and the same retention. This investigation would determine if the column efficiency changes significantly with β-value. A similar study would also use a coil at different rotational speeds while keeping the retention the same so that column efficiency can be measured against rotational speed.

If the values of the constant K differ for the three FEP coils, then a different relationship between K, β-value and helical pitch exists. This alternative relationship may be based on the

radial acceleration that increases with β-value, see equation 1.4.1.2.3.1 Chapter 1. Hence the value of constant K may increase with β-value even though the helix angle does not change with β-value. This alternative relationship will still enable the value of K to be predicted from the β-value. New coils with a the same β-value but different helix angles will then be required to determine now the value of constant K varies with helix angle. As β-value is dimensionless the dimensional analysis of equation 5.3.3.1 will still be valid for this alternative relationship.

6.4.2 Mathematical Modelling

The helical nature of the coiled tubing should be accounted for in any future modelling of the interfacial movement. A model constructed in this manner would show how the head to tail pressure gradient distributes the upper and lower phases in a coil during a head and tail study. This model combined with a mobile phase flow rate, although rather complex, may show how mixing occurs at the proximal key node for both normal and reverse phase modes. The stationary phase retention in such a model may also change with the square root of the mobile phase flow rate and indicate the magnitude of the pressure drop across the coil.

6.4.3 Retention at low speed

Phase distribution diagrams and stroboscopic photographs [Sutherland 1999] have shown that retention of the stationary phase suddenly stops at a critical rotational speed below which little or no retention is obtained. At speeds above the critical rotational speed, retention is obtained, and at lower speeds, no retention is obtained. This critical rotational speed also increases as the mobile phase flow rate increases. A dimensionless number with a critical value may predict the critical rotational speed. The Russian scientists [Fedotov 1996, 1998, 2000, 2001A; Maryutina 1998; Ignatova 2001] have shown that this critical rotational speed is related to density difference, viscosity, interfacial tension and tubing material for tubing bores up to 1.5mm. A review of the Russian scientists published work and raw data may be sufficient to determine the appropriate dimensionless number to use and the critical value of this dimensionless number.

6.4.4 Dynamic similarity

There is a need to study the use of Dynamic Similarity ie using dimensionless numbers such as Reynolds number, Froude number and Weber number to the scaling up of the process from small radius to large radius machines. A high capacity pump is said to be dynamically similar to a low capacity pump when each relevant dimensionless number is the same for both pumps. For Dynamic Similarity to work it must be known which are the relevant dimensionless

numbers to use. Comparing the performance of the existing Brunel CCC (R = 110mm) machines with Milli (the new Brunel analytical prototype R = 50mm), the new IMI prototype (R = 300mm) that is yet to be built will establish which are the relevant dimensionless numbers to be used. Once it is known which dimensionless numbers to use the design and performance of the larger radius machines can be predicted using Dynamic Similarity.

6.4.5 Sample volume and concentration

Du et al [1998] studied the effect of increasing: sample concentration, sample volume and the combined effect of increasing both sample volume and sample concentration on the retention of the stationary phase. Du et al concluded that the sample volume and sample concentration both change the physical properties of the mobile and stationary phase once the sample was injected into a coil. The results presented by Du for four coils connected in series show for high sample concentrations and high sample volumes the retention in the first coil after the injection valve was significantly reduced. The retention in the second coil was reduced less significantly and the retention in the third coil was only slightly reduced while the retention in the fourth coil was unchanged from before the sample injection. This suggests that as the sample is separated into its constituent components, that travel through the coils at different speeds, thus diluting the effects on the physical properties of the mobile and stationary phases to such an extent that the retention in the fourth coil is unchanged. It is possible to repeat Du et al experiment, connect four coils in series and inject a large volume high concentration sample but stop the experiment just before the elution of the solvent front. The physical properties of the mobile and stationary phases from each coil can then compared to those for unused mobile and stationary phase. Given the understanding of stationary phase retention presented in Chapters 4 and 5 of this thesis it would be possible to increase the basic understanding of how sample volume and concentration effects retention of the stationary phase. In turn this would allow the selection of sample volume and concentration to be determined for the best performance of a production scale J-type centrifuge. This study could also be extended to include the frequency or how often a sample of a given volume and concentration can be injected before retention is significantly reduced.

6.4.6 Column efficiency

Conway's method of predicting when peaks elute depended upon knowing the retention of the stationary phase for the specific operating conditions used. The retention theory presented in Chapters 4 and 5 combined with Conway's peak elution theory allows the elution times for peaks to be predicted once the value of the constant K for a coil is known. This means that

the time separating two adjacent peaks can also be predicted however the peak width cannot yet be predicted for all operating conditions. However section 1.4.2.8 of Chapter 1 showed that the width of a peak is proportional to the square root of the peak elution time, see equation 1.4.2.8.7. This equation also showed the effect of retention on the peak width. The constant C in this equation is the column efficiency or mass transfer coefficient. Equation 1.4.2.8.13 uses the constant C to predict the resolution of a separation, the constant B in this equation is the Du gradient and can now be predicted see equation 5.3.4.1 of Chapter 5. For a given set of operating conditions the column efficiency (C) is the same for each peak [Sutherland 2002A and B] however it is not known how the separation efficiency changes with stationary phase retention, mobile phase flow rate, rotational speed, phase system properties, coil geometry and operation in normal or reverse phase mode. Further study is required to determine the parameters that control the column efficiency. Once a value for the column efficiency can be predicted the resolution would also be predictable using equation 1.4.2.8.13. The prediction of resolution greatly reduces the technical risks involved in designing and building production scale J-type centrifuges as the size of machine required can be more accurately matched to the technical and economic requirements. The economic performance of a production scale machine will be accessible during the design stage and a financial justification for such a machine will be more accurate.

6.5 Concluding Remarks

The aims and objectives listed in section 1.2 of Chapter 1 have been met by the research work described in this thesis.

The mathematical modelling of retention developed in Chapters 4 and 5 is a major advance toward being able to predict the resolution of a separation and that future research needs to be targeted at the controlling parameters for column efficiency and mass transfer with the aim to complete the modelling of the CCC process.

Appendix 1 Derivation of the Radial and Tangential Acceleration equations for J-type centrifuges

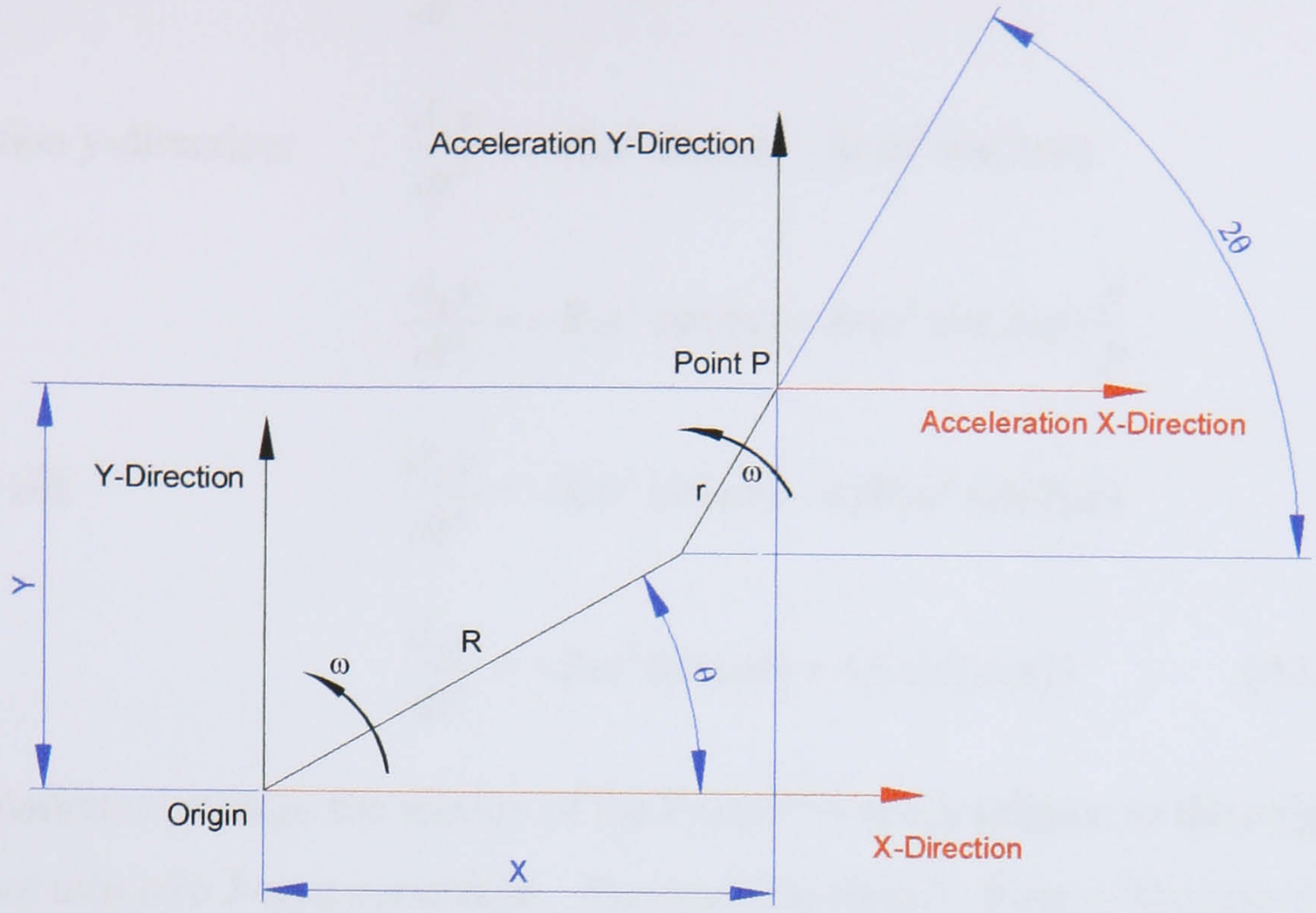

Figure A1.1 shows the free-body diagram for a J-type centrifuge

From figure A1.1 resolve for the displacement of the Point P in the x-direction taking the centre of rotation as the origin. Then differentiate to obtain formulas for velocity and acceleration in the x-direction remembering that $\theta = \omega t$.

Displacement x-direction: $$x = R\cos(\omega t) + r\cos(2\omega t) \qquad \text{(A1.1)}$$

Velocity x-direction: $$\frac{dx}{dt} = -R\omega\sin(\omega t) - 2r\omega\sin(2\omega t) \qquad \text{(A1.2)}$$

Acceleration x-direction: $$\frac{d_2x}{dt^2} = -R\omega^2\cos(\omega t) - 4r\omega^2\cos(2\omega t)$$

$$\frac{d_2x}{dt^2} = -R\omega^2\cos(\omega t) - 4r\omega^2\cos(2\omega t)\frac{R}{R}$$

Now $\beta = r/R$ $$\frac{d_2x}{dt^2} = -R\omega^2\cos(\omega t) - 4\beta R\omega^2\cos(2\omega t)$$

$$\frac{d_2x}{dt^2} = -R\omega^2\left(\cos(\omega t) + 4\beta\cos(2\omega t)\right) \qquad \text{(A1.3)}$$

From figure A1.1 resolve for the displacement of the Point P in the y-direction taking the centre of rotation as the origin. Then differentiate to obtain formulas for velocity and acceleration in the y-direction.

Displacement y-direction: $$y = R\sin(\omega t) + r\sin(2\omega t) \quad \text{(A1.4)}$$

Velocity y-direction: $$\frac{dy}{dt} = R\omega\cos(\omega t) + 2r\omega\cos(2\omega t) \quad \text{(A1.5)}$$

Acceleration y-direction: $$\frac{d_2y}{dt^2} = -R\omega^2\sin(\omega t) - 4r\omega^2\sin(2\omega t)$$

$$\frac{d_2y}{dt^2} = -R\omega^2\sin(\omega t) - 4r\omega^2\sin(2\omega t)\frac{R}{R}$$

Now $\beta = r/R$ $$\frac{d_2y}{dt^2} = -R\omega^2\sin(\omega t) - 4\beta R\omega^2\sin(2\omega t)$$

$$\frac{d_2y}{dt^2} = -R\omega^2\left(\sin(\omega t) + 4\beta\sin(2\omega t)\right) \quad \text{(A1.6)}$$

These equations represent the motion of the Point P in space relative to the origin, which is the main rotary axis of a J-type centrifuge. The negative signs in front of the above equations mean that the directions of the vector quantities are in the opposite direction to that shown in figure A1.1.

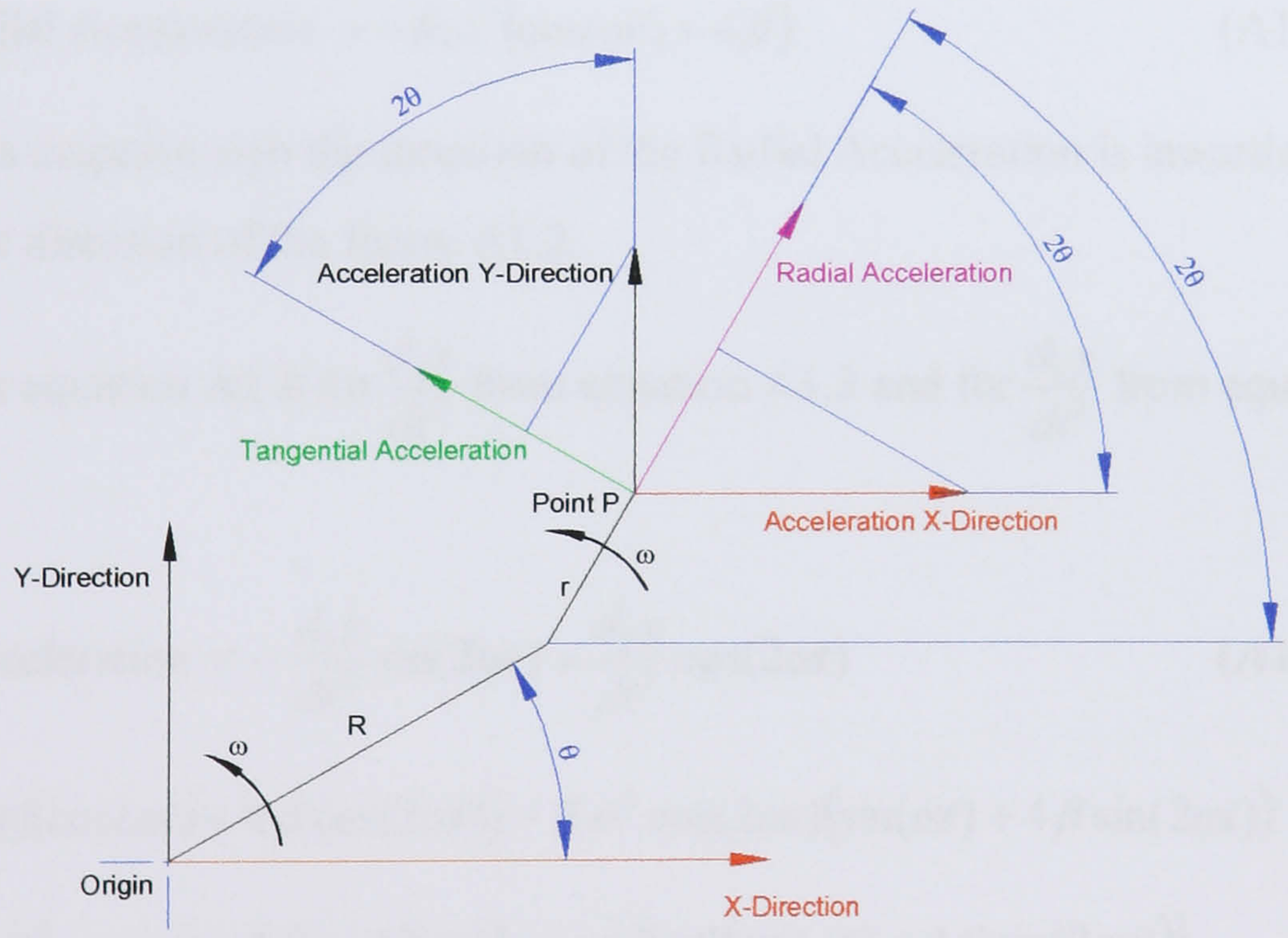

Figure A1.2 shows the free-body diagram of a J-type centrifuge with the radial and tangential acceleration vectors added

From figure A1.2 resolving in the Radial and Tangential directions.

Radial Acceleration = $$\frac{d_2x}{dt^2}\cos(2\omega t) + \frac{d_2y}{dt^2}\sin(2\omega t) \quad \text{(A1.7)}$$

Tangential Acceleration = $-\frac{d_2x}{dt^2}\sin(2\omega t)+\frac{d_2y}{dt^2}\cos(2\omega t)$ (A1.8)

Substituting in equation A1.7 for $\frac{d_2x}{dt^2}$ from equation A1.3 and for $\frac{d_2y}{dt^2}$ from equation A1.6 gives:

Radial Acceleration =

$$=-R\omega^2\cos(2\omega t)\left(\cos(\omega t)+4\beta\cos(2\omega t)\right)-R\omega^2\sin(2\omega t)\left(\sin(\omega t)+4\beta\sin(2\omega t)\right)$$

$$=-R\omega^2\left[\cos(2\omega t)\left(\cos(\omega t)+4\beta\cos(2\omega t)\right)+\sin(2\omega t)\left(\sin(\omega t)+4\beta\sin(2\omega t)\right)\right]$$

$$=-R\omega^2\left[\cos(2\omega t)\cos(\omega t)+4\beta\cos^2(2\omega t)+\sin(2\omega t)\sin(\omega t)+4\beta\sin^2(2\omega t)\right]$$

But $\cos^2(2\omega t)+\sin^2(2\omega t)=1$ therefore:

$$=-R\omega^2\left[\cos(2\omega t)\cos(\omega t)+\sin(2\omega t)\sin(\omega t)+4\beta\right]$$

Using $\cos(A-B)=\cos(A)\cos(B)+\sin(A)\sin(B)$ where A = 2ωt and B = ωt

Therefore $\cos(\omega t)=\cos(2\omega t)\cos(\omega t)+\sin(2\omega t)\sin(\omega t)$

Therefore Radial Acceleration $=-R\omega^2\left(\cos(\omega t)+4\beta\right)$ (A1.9)

Since there is a negative sign the direction of the Radial Acceleration is inwards due to being in the opposite direction of the figure A1.2.

Substituting in equation A1.8 for $\frac{d_2x}{dt^2}$ from equation A1.3 and for $\frac{d_2y}{dt^2}$ from equation A1.6 gives:

Tangential Acceleration = $-\frac{d_2x}{dt^2}\sin(2\omega t)+\frac{d_2y}{dt^2}\cos(2\omega t)$ (A1.8)

$$=R\omega^2\sin(2\omega t)\left(\cos(\omega t)+4\beta\cos(2\omega t)\right)-R\omega^2\cos(2\omega t)\left(\sin(\omega t)+4\beta\sin(2\omega t)\right)$$

$$=R\omega^2\left[\sin(2\omega t)\left(\cos(\omega t)+4\beta\cos(2\omega t)\right)-\cos(2\omega t)\left(\sin(\omega t)+4\beta\sin(2\omega t)\right)\right]$$

$$=R\omega^2\left[\sin(2\omega t)\cos(\omega t)+4\beta\cos(2\omega t)\sin(2\omega t)-\cos(2\omega t)\sin(\omega t)-4\beta\cos(2\omega t)\sin(2\omega t)\right]$$

$$=R\omega^2\left[\sin(2\omega t)\cos(\omega t)-\cos(2\omega t)\sin(\omega t)\right]$$

Using $\sin(A-B)=\sin(A)\cos(B)-\cos(A)\sin(B)$ where A = 2ωt and B = ωt

Therefore $\sin(\omega t)=\sin(2\omega t)\cos(\omega t)-\cos(2\omega t)\sin(\omega t)$

Therefore Tangential Acceleration $= R\omega^2 \sin(\omega t)$ (A1.10)

Since there is no negative sign the direction of the Tangential Acceleration is anti-clockwise due to being in the same direction of the figure A1.2.

Appendix 2 Derivation of the Radial and Tangential Acceleration equations for I-type centrifuges

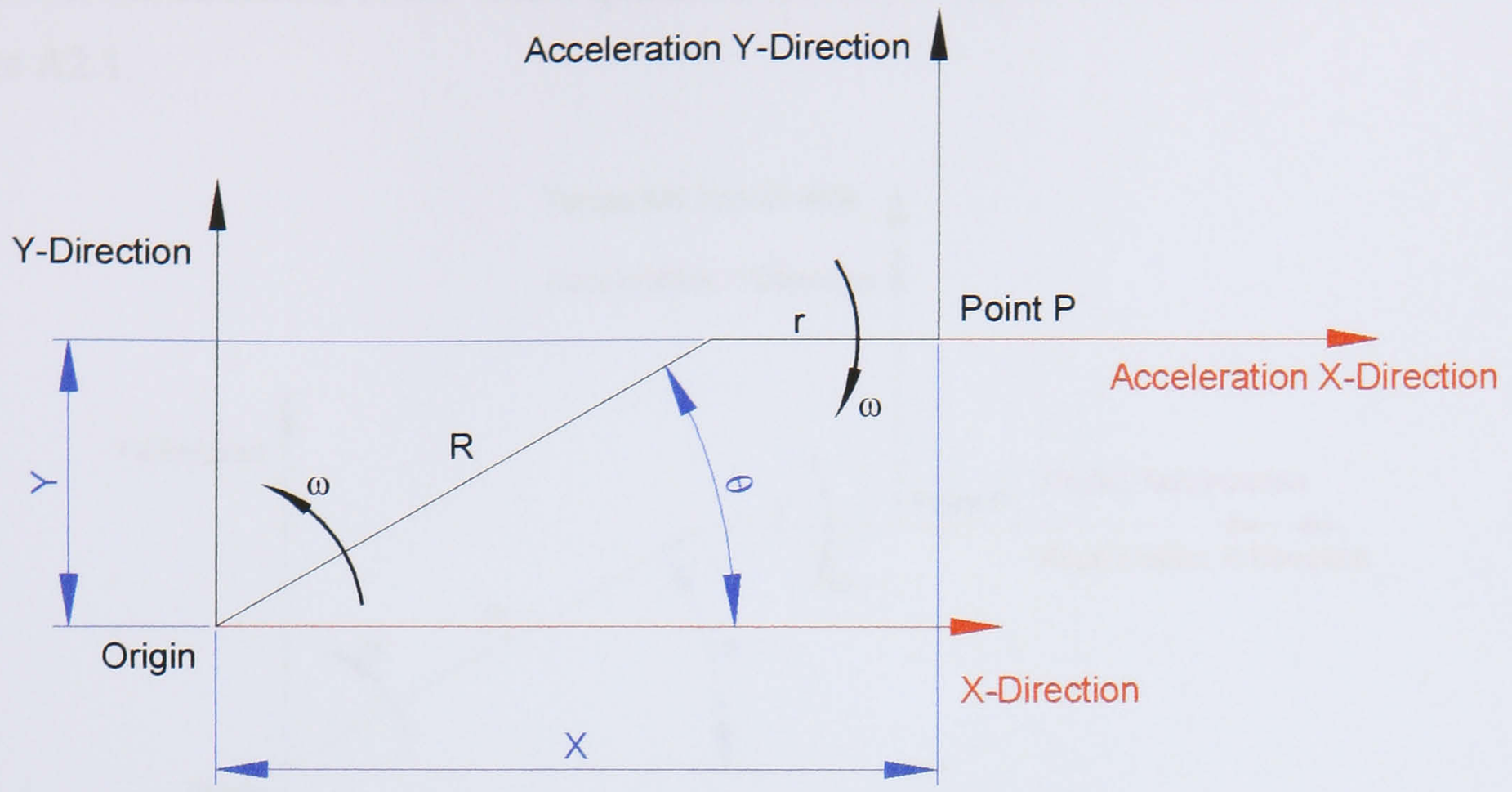

Figure A2.1 shows the free-body diagram for a I-type centrifuge

From figure A2.1 resolve for the displacement of the Point P in the x-direction taking the centre of rotation as the origin. Then differentiate to obtain formula for velocity and acceleration in the x-direction given that $\theta = \omega t$.

Displacement x-direction: $$x = R\cos(\omega t) + r \quad \text{(A2.1)}$$

Velocity x-direction: $$\frac{dx}{dt} = -R\omega\sin(\omega t) \quad \text{(A2.2)}$$

Acceleration x-direction: $$\frac{d_2x}{dt^2} = -R\omega^2\cos(\omega t) \quad \text{(A2.3)}$$

From figure A2.1 resolve for the displacement of the Point P in the y-direction taking the centre of rotation as the origin. Then differentiate to obtain formula for velocity and acceleration in the y-direction given that $\theta = \omega t$.

Displacement y-direction: $$y = R\sin(\omega t) \quad \text{(A2.4)}$$

Velocity y-direction: $$\frac{dy}{dt} = R\omega\cos(\omega t) \quad \text{(A2.5)}$$

Acceleration y-direction: $$\frac{d_2y}{dt^2} = -R\omega^2\sin(\omega t) \quad \text{(A2.6)}$$

These equations represent the motion of the Point P in space relative to the origin, which is the main rotary axis of an I-type centrifuge. The negative signs in front of the above equations mean that the directions of the vector quantities are in the opposite direction to that shown in figure A2.1.

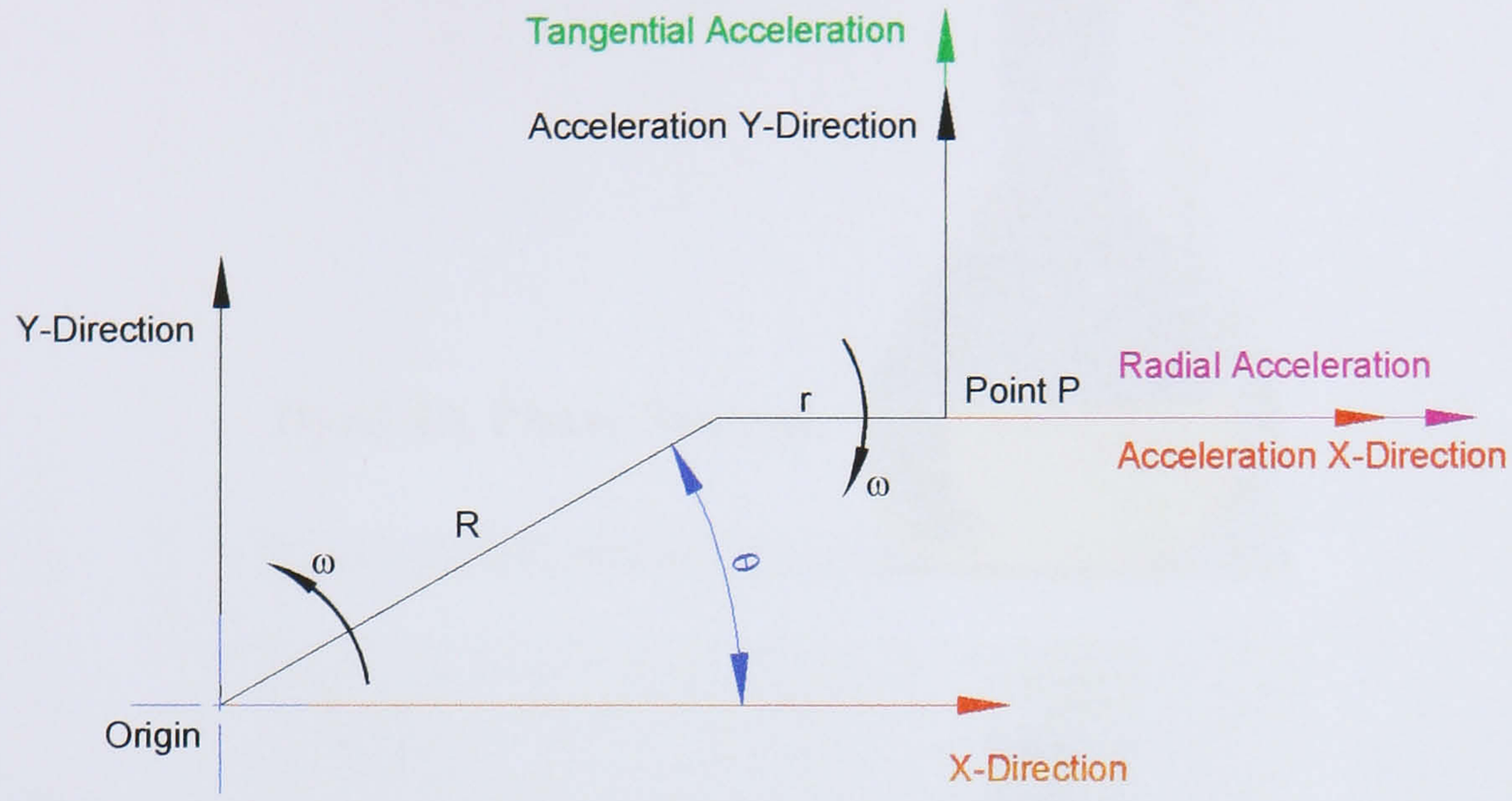

Figure A2.2 shows the free-body diagram of an I-type centrifuge with the radial and tangential acceleration vectors added

From figure A2.2 resolving in the Radial and Tangential directions and using equations A2.3 and A2.6.

$$\text{Radial Acceleration} = \text{Acceleration x-direction} = -R\omega^2\cos(\omega t) \qquad \text{(A2.7)}$$

$$\text{Tangential Acceleration} = \text{Acceleration y-direction} = -R\omega^2\sin(\omega t) \qquad \text{(A2.8)}$$

The negative signs indicate that the both the Radial and Tangential accelerations are in the opposite directions to those shown in figure A2.2.

Appendix 3 Head and Tail Study Results

Dyed 4A Phase System.

Dyed 4B Phase System.

Dyed 4C Phase System.

Figure A.3.1 shows the dyed 4A, 4B and 4C phase systems dyed with Sudan Blue for the upper organic phase and Procion Brilliant Yellow for the lower aqueous phase

BEFORE Forward Direction of Rotation
4A Phase System at 763rpm in FEP
Run for 5 minutes

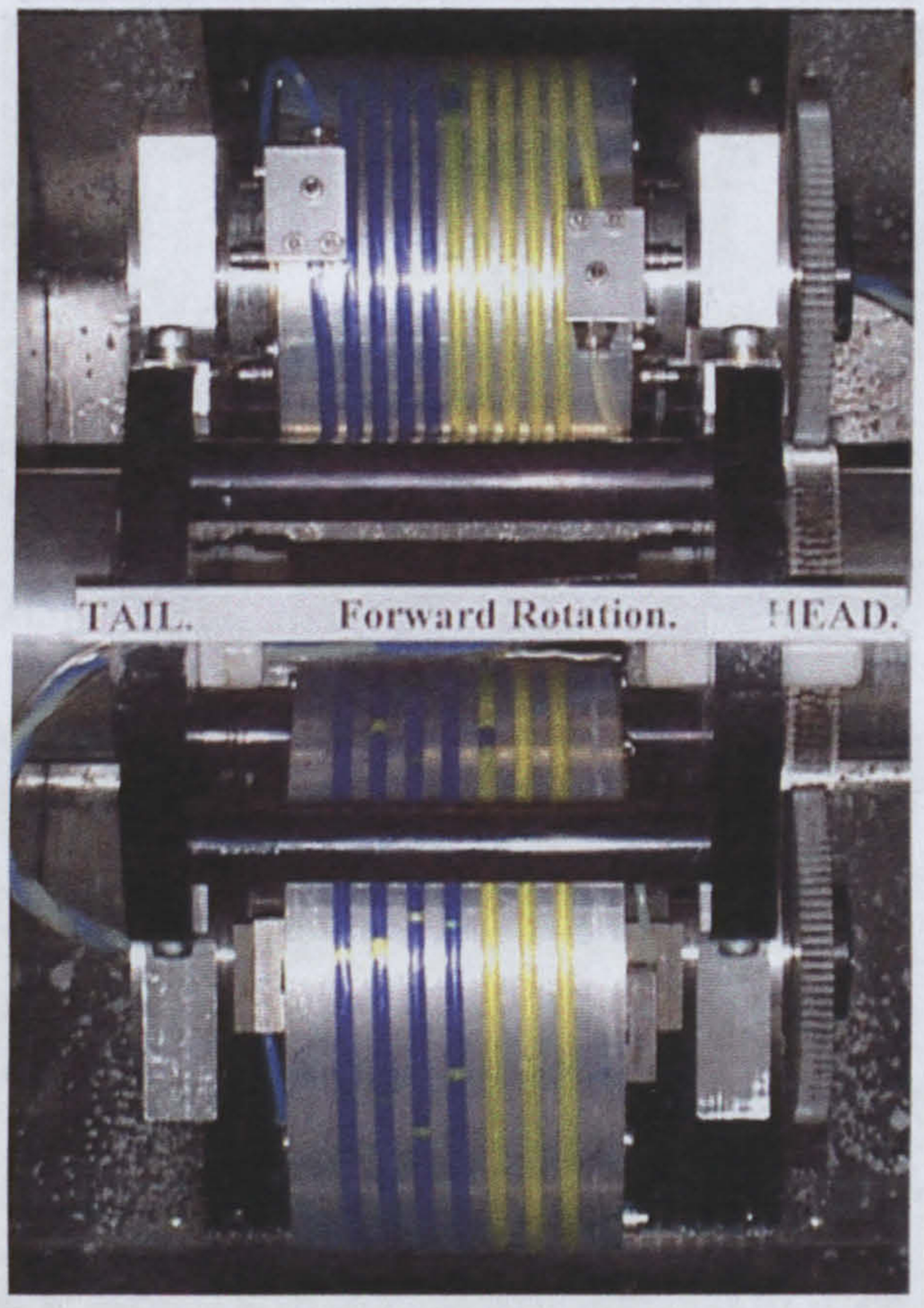

AFTER Forward Direction of Rotation
4A Phase System at 763rpm in FEP
Run for 5 minutes

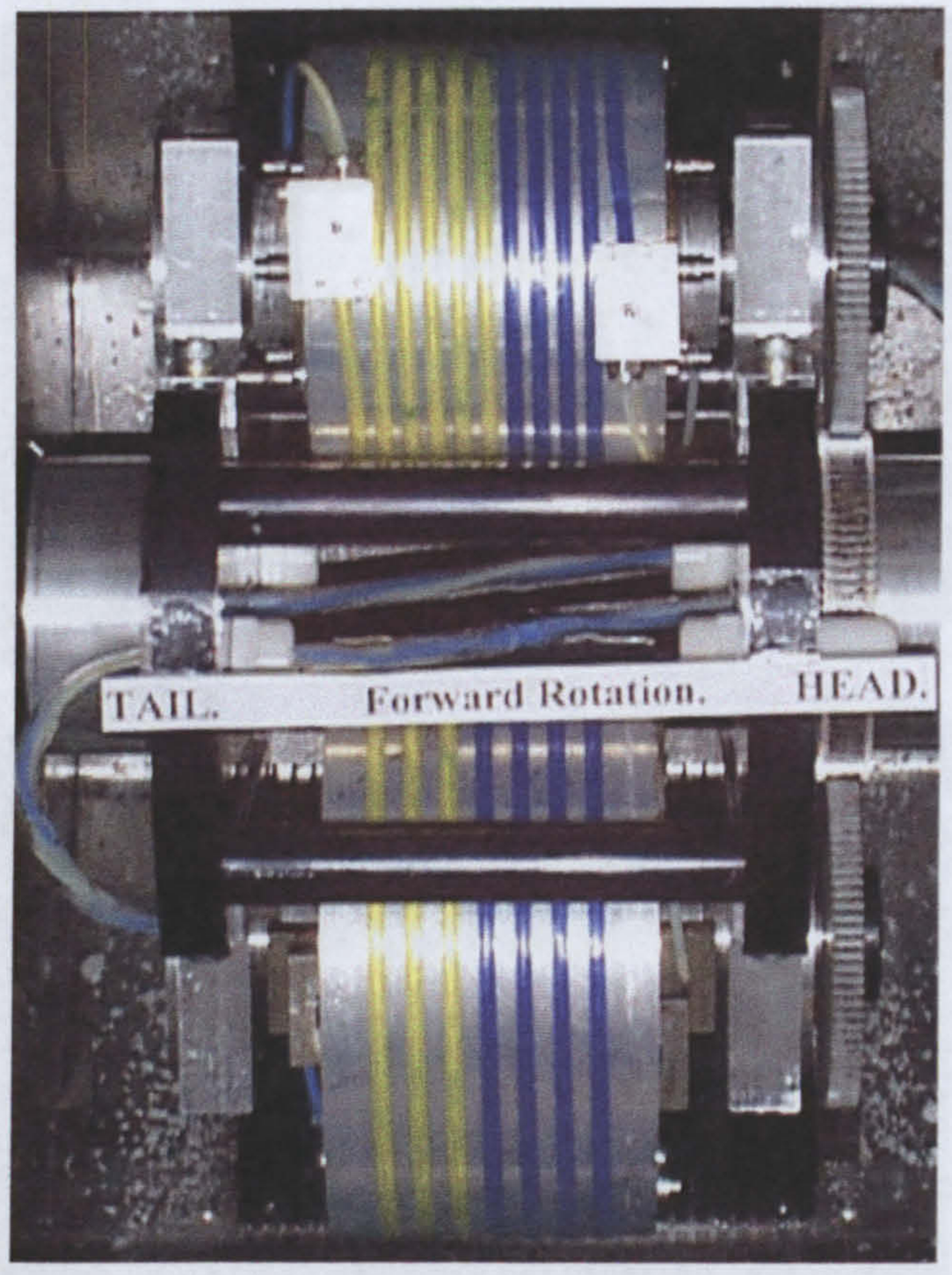

Figure A.3.2 shows the Head and Tail distribution of the 4A phase system for before and after rotation in the forward direction

BEFORE Reverse Direction of Rotation
4A Phase System at 763rpm in FEP
Run for 5 minutes

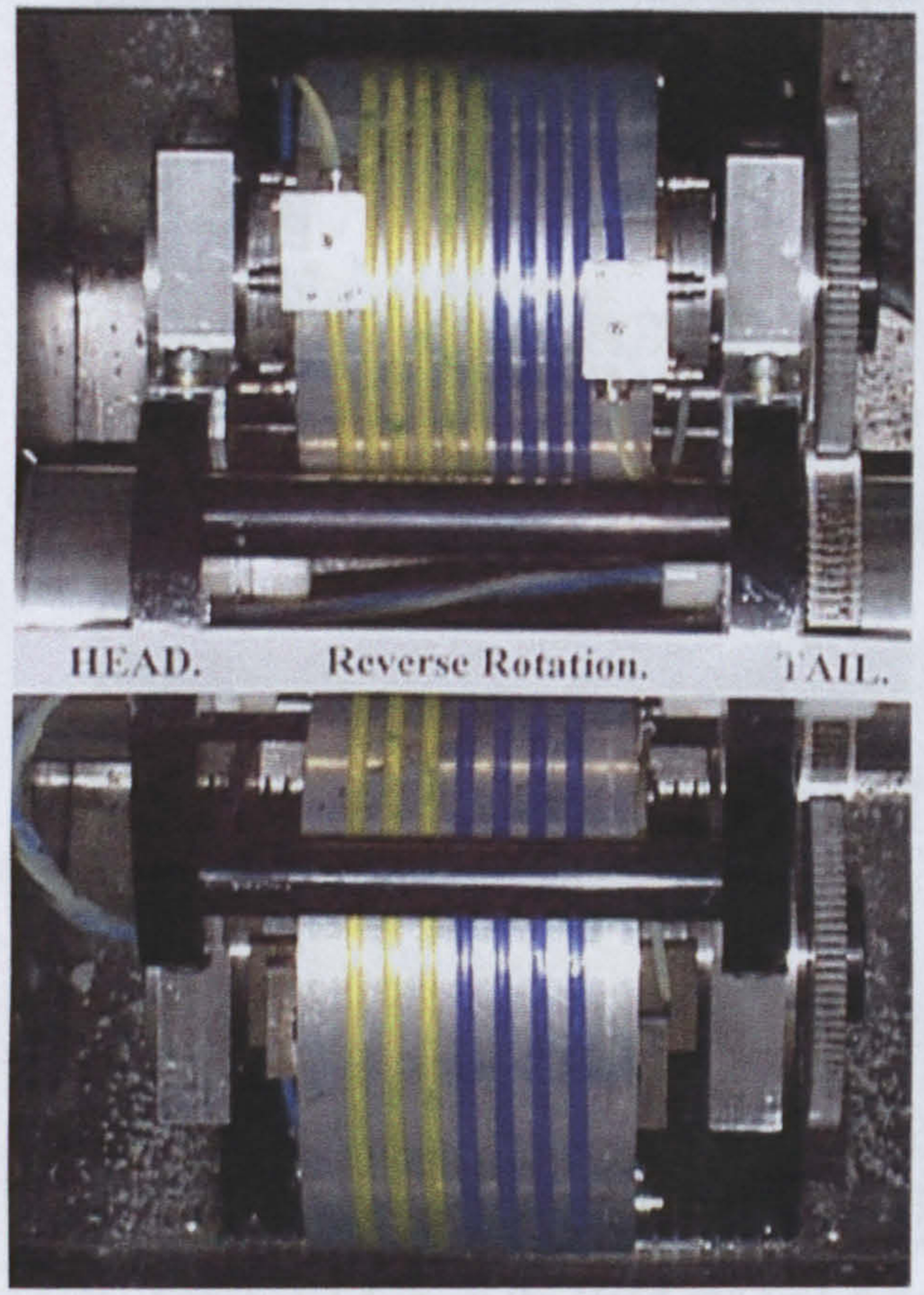

AFTER Reverse Direction of Rotation
4A Phase System at 763rpm in FEP
Run for 5 minutes

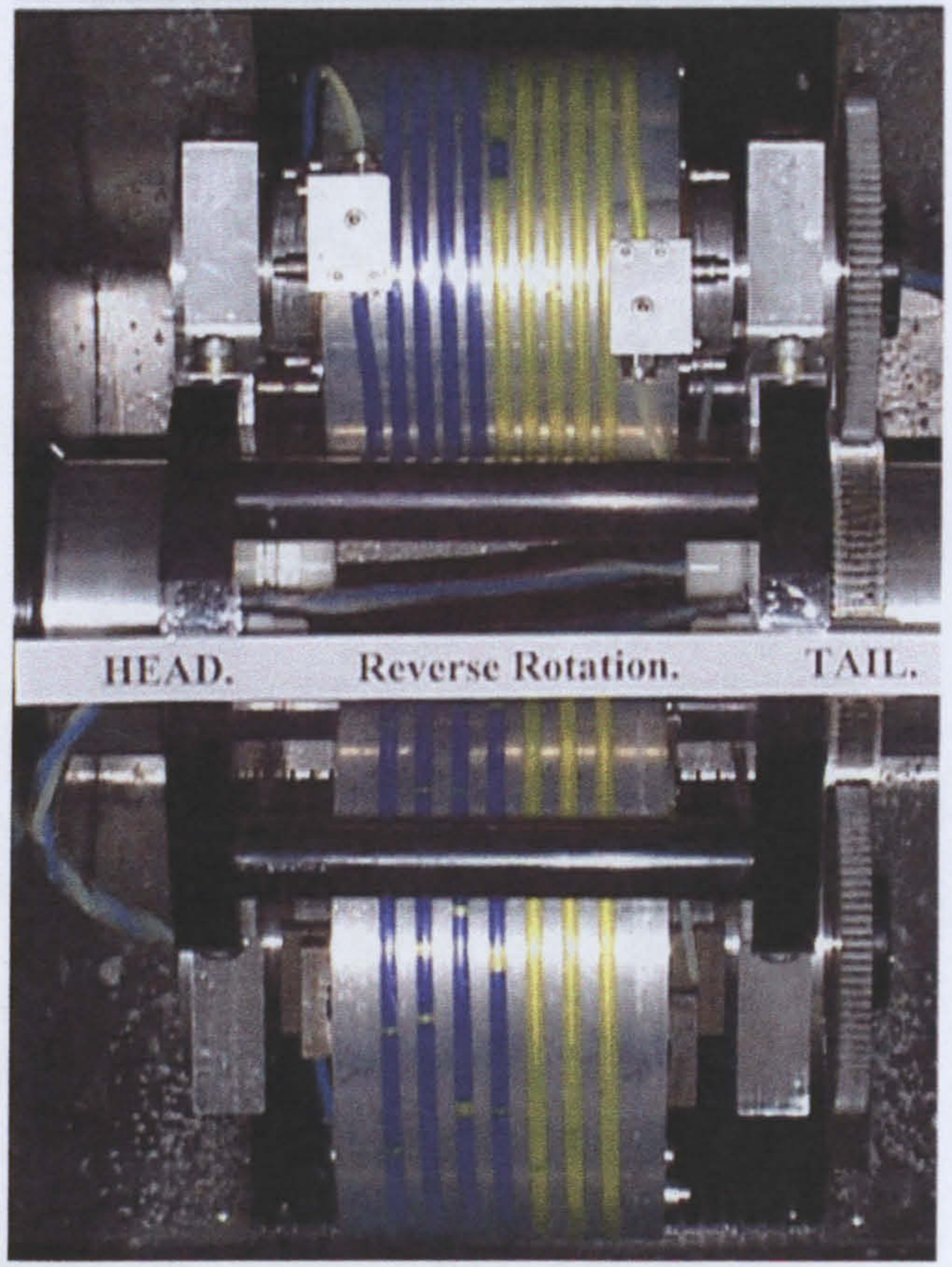

Figure A.3.3 shows the Head and Tail distribution of the 4A phase system for before and after rotation in the reverse direction

BEFORE Forward Direction of Rotation
4B Phase System at 763rpm in FEP
Run for 5 minutes

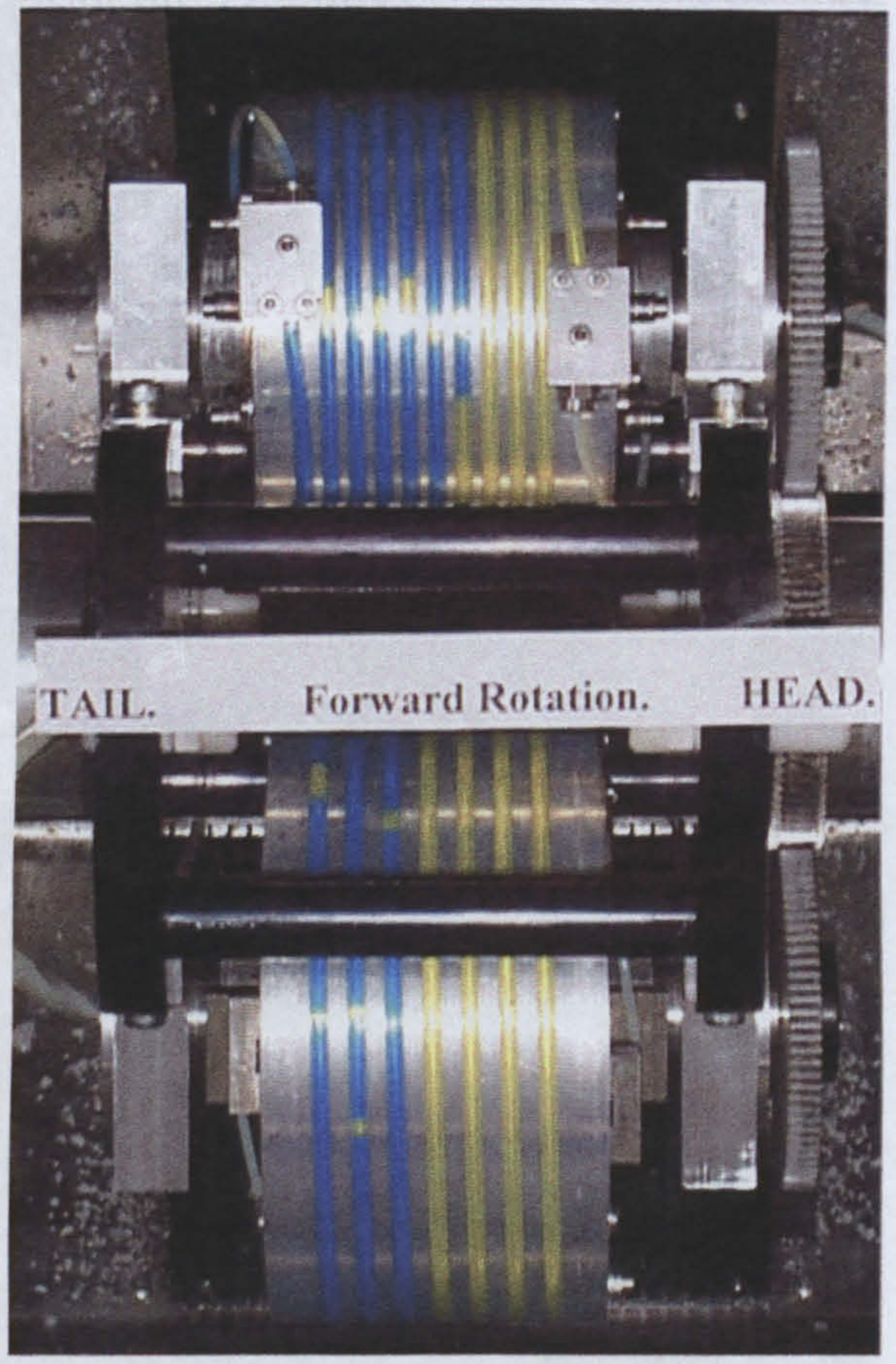

AFTER Forward Direction of Rotation
4B Phase System at 763rpm in FEP
Run for 5 minutes

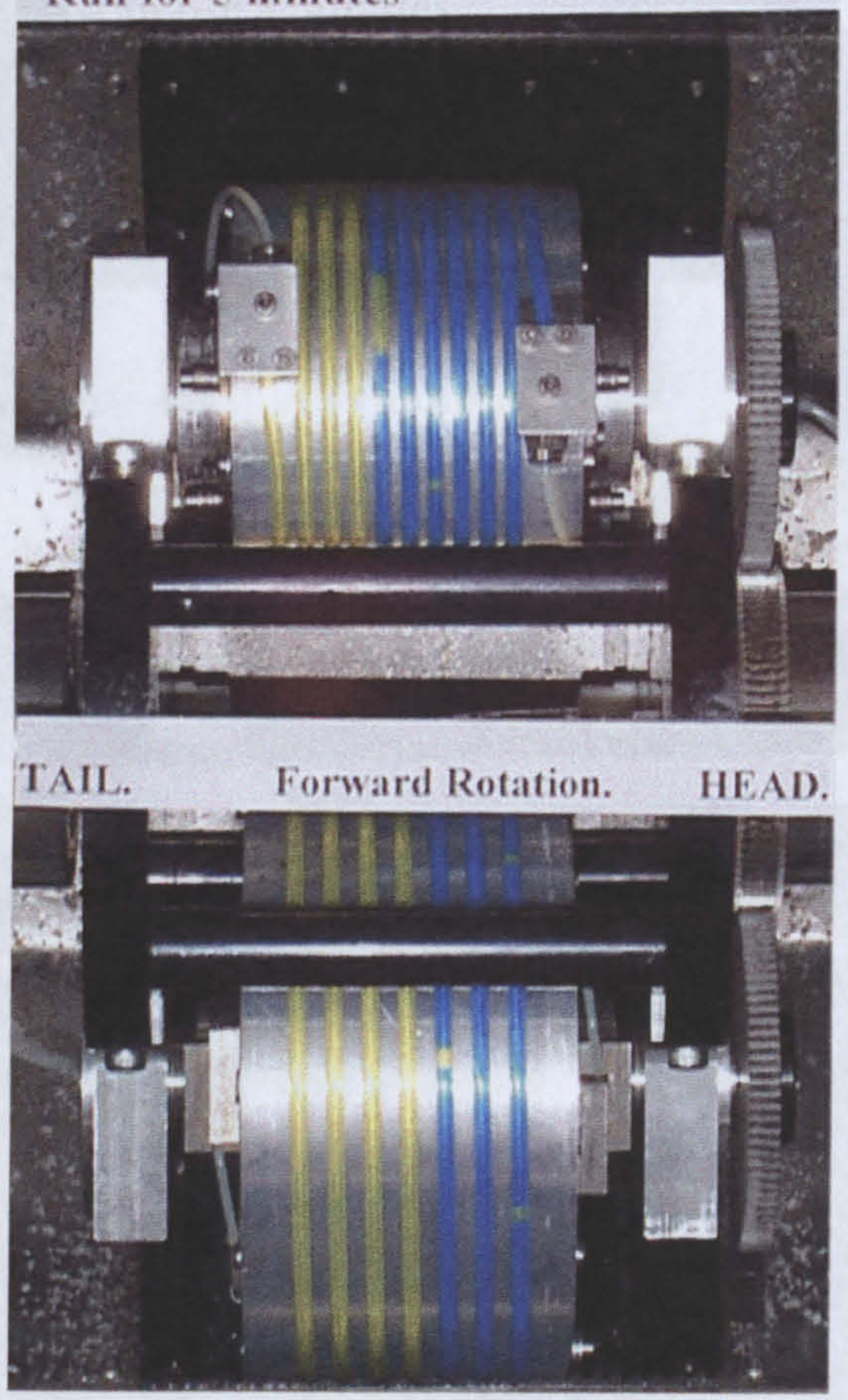

Figure A.3.4 shows the Head and Tail distribution of the 4B phase system for before and after rotation in the forward direction

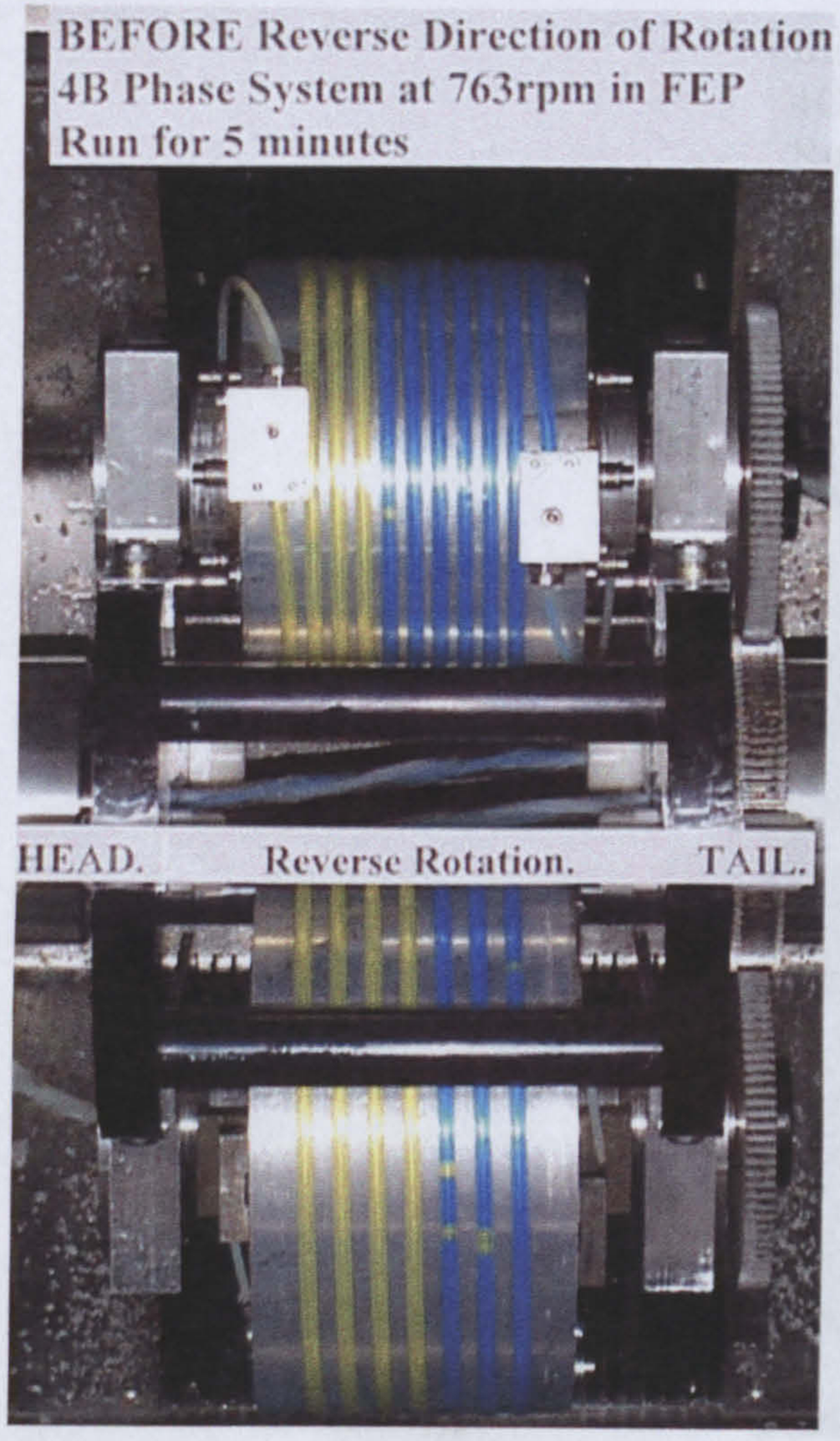

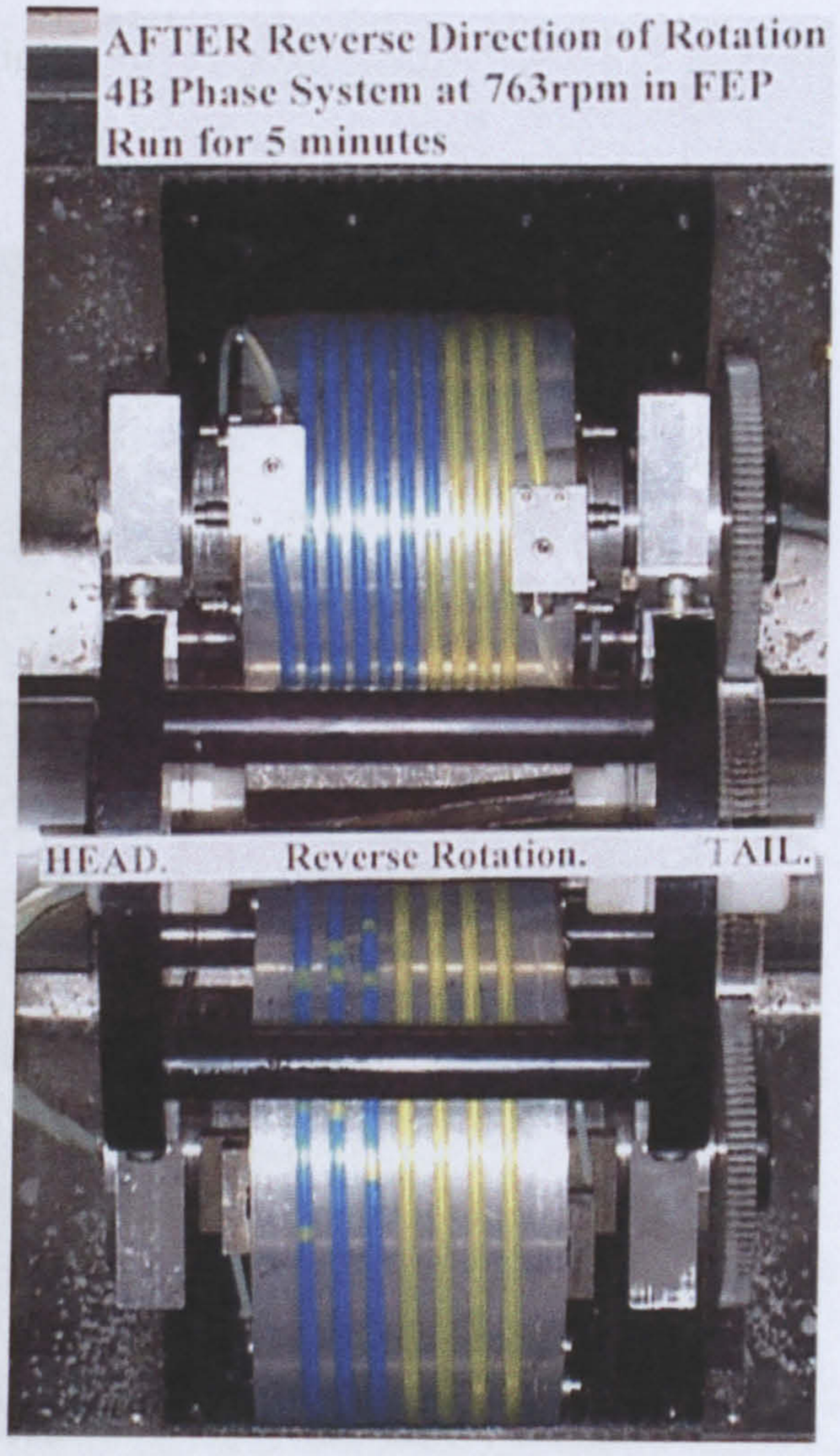

Figure A.3.5 shows the Head and Tail distribution of the 4B phase system for before and after rotation in the reverse direction

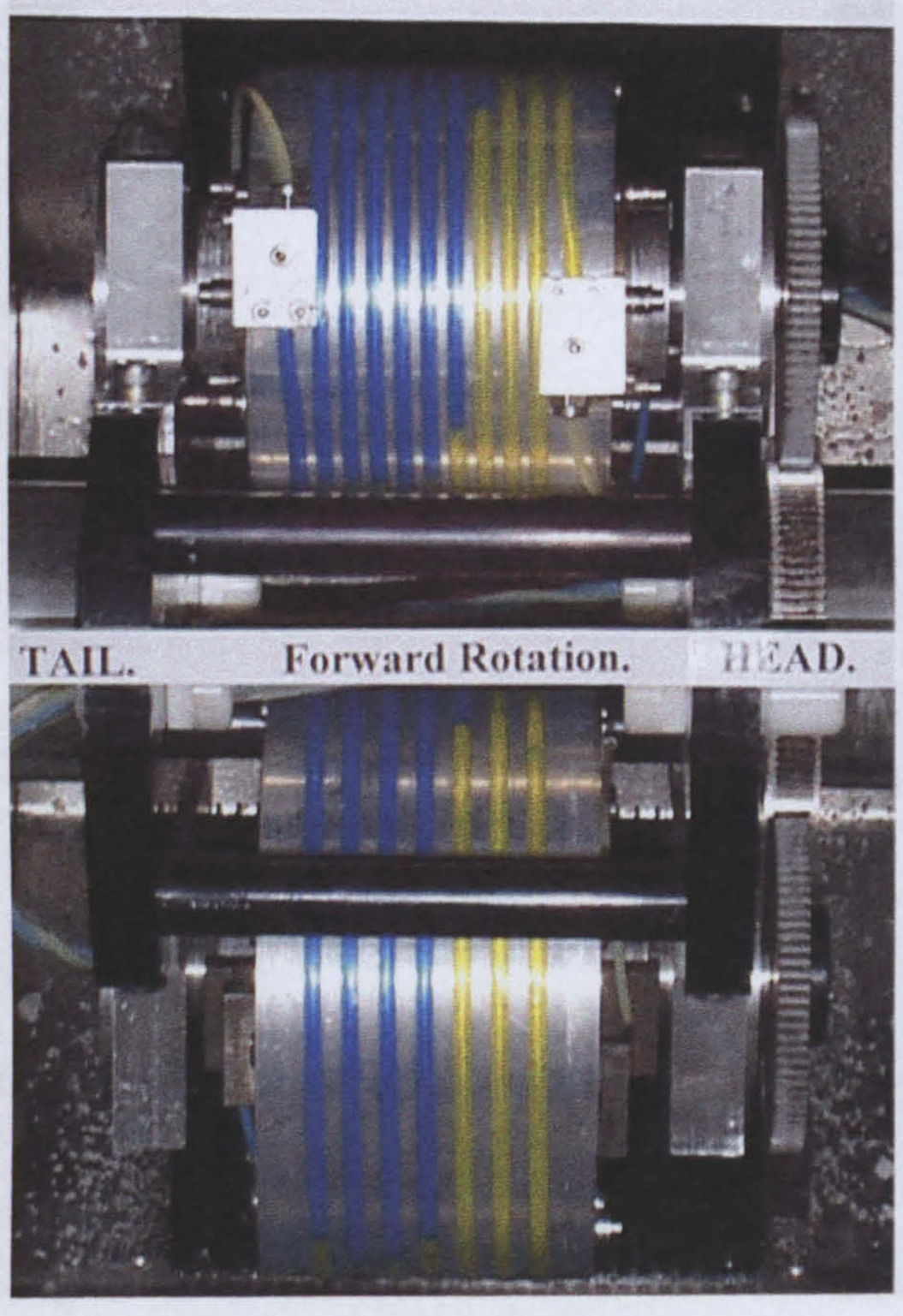

Figure A.3.6 shows the Head and Tail distribution of the 4C phase system before rotation in the forward direction

AFTER Forward Direction of Rotation
4C Phase System at 763rpm in FEP
Run for 5 minutes

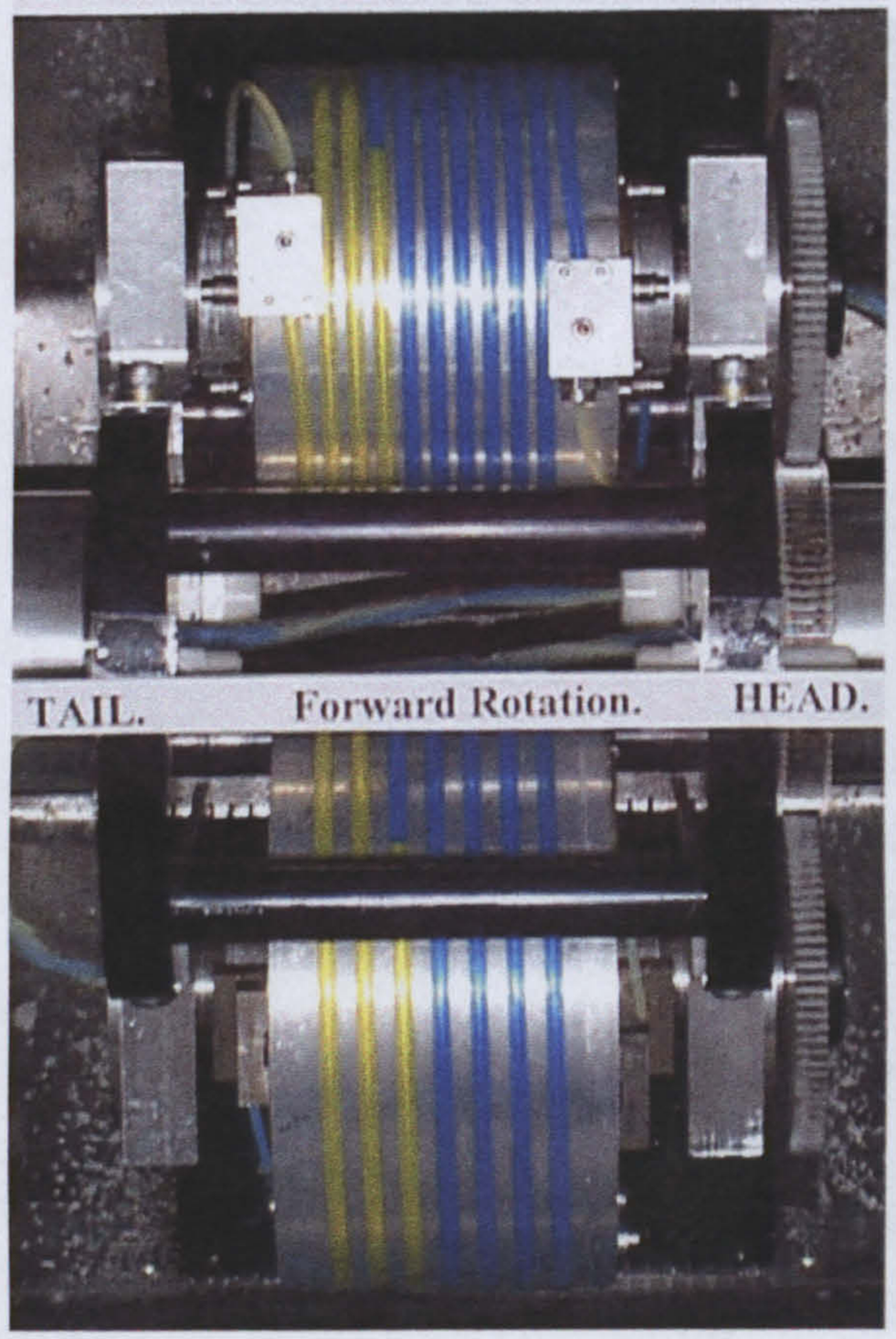

AFTER Forward Direction of Rotation
4C Phase System at 763rpm in FEP
Run for 5 minutes

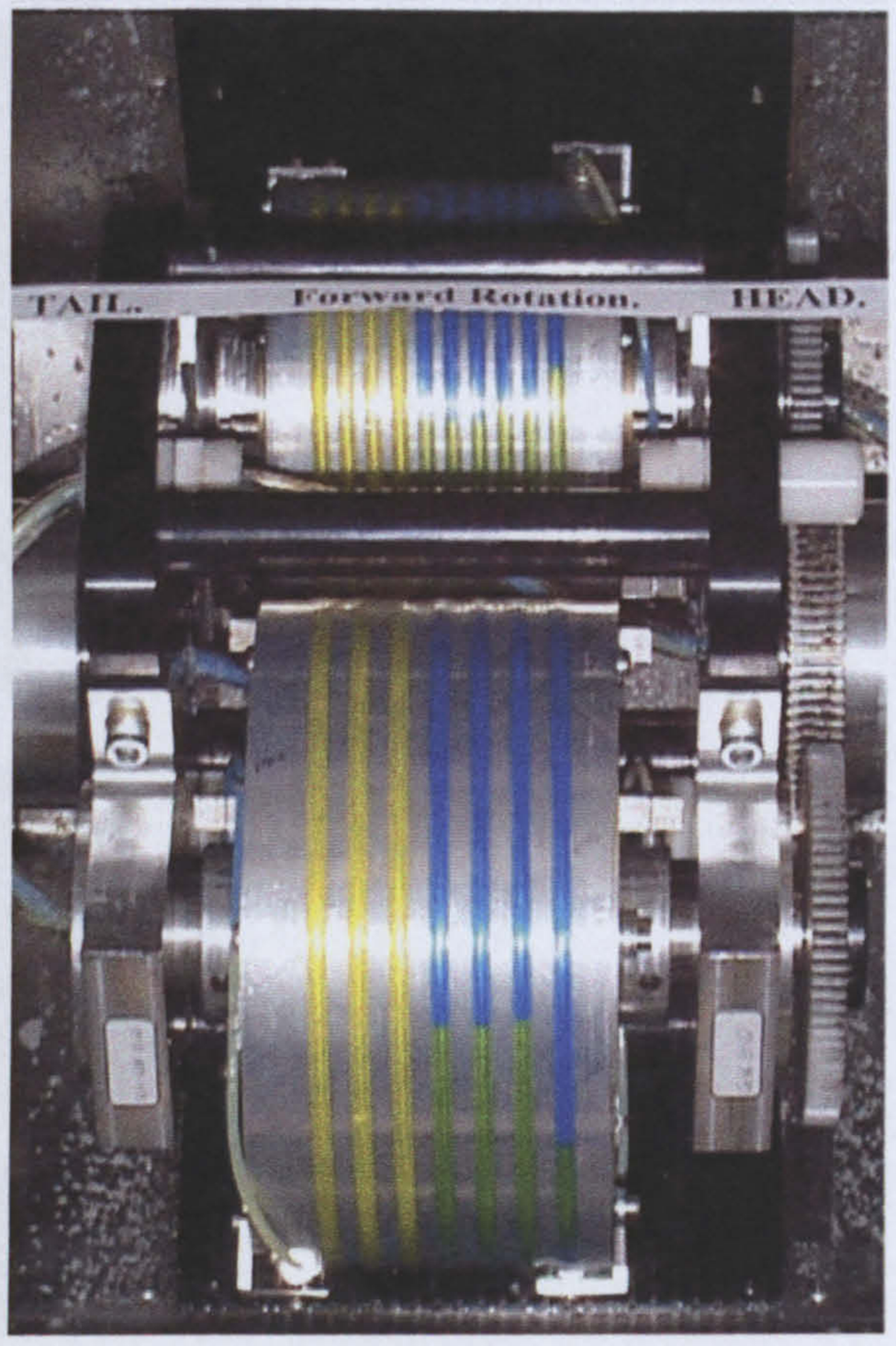

Figure A.3.7 shows the Head and Tail distribution of the 4C phase system after rotation in the forward direction

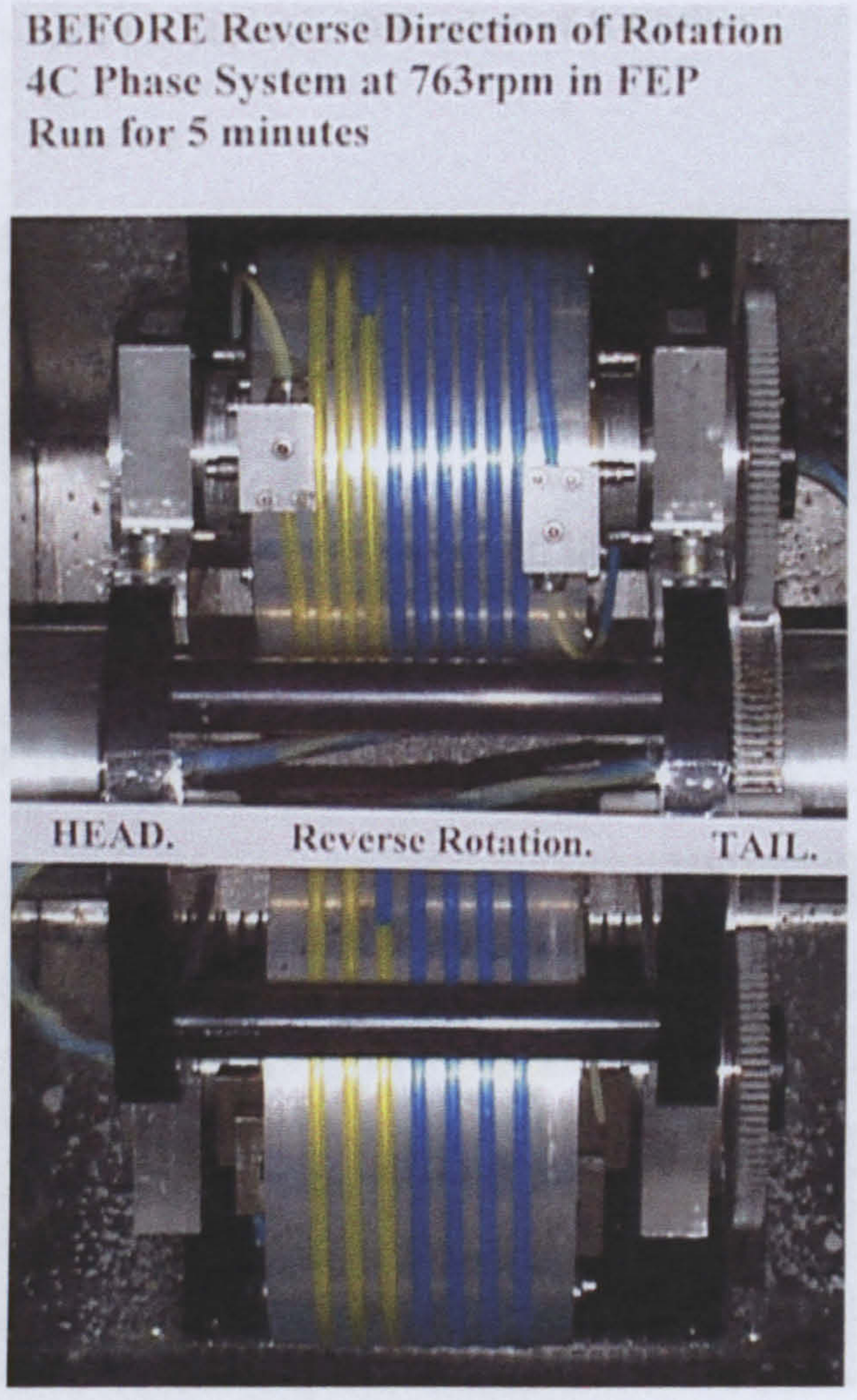

Figure A.3.8 shows the Head and Tail distribution of the 4B phase before rotation in the reverse direction

AFTER Reverse Direction of Rotation
4C Phase System at 763rpm in FEP
Run for 5 minutes

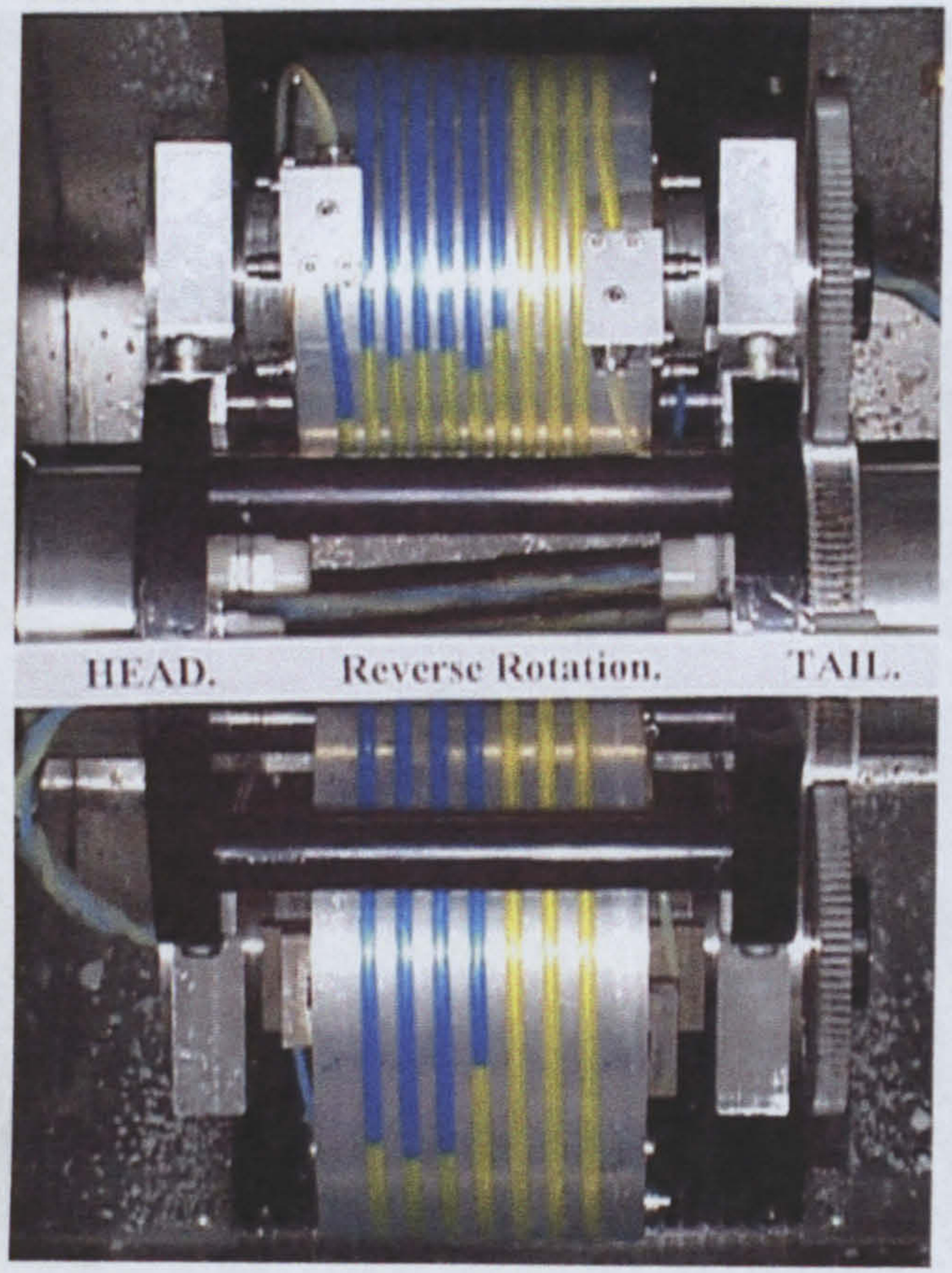

Figure A.3.9 shows the Head and Tail distribution of the 4C phase system for after 5 minutes of rotation in the reverse direction

AFTER Reverse Direction of Rotation
4C Phase System at 763rpm in FEP
Run for 10 minutes

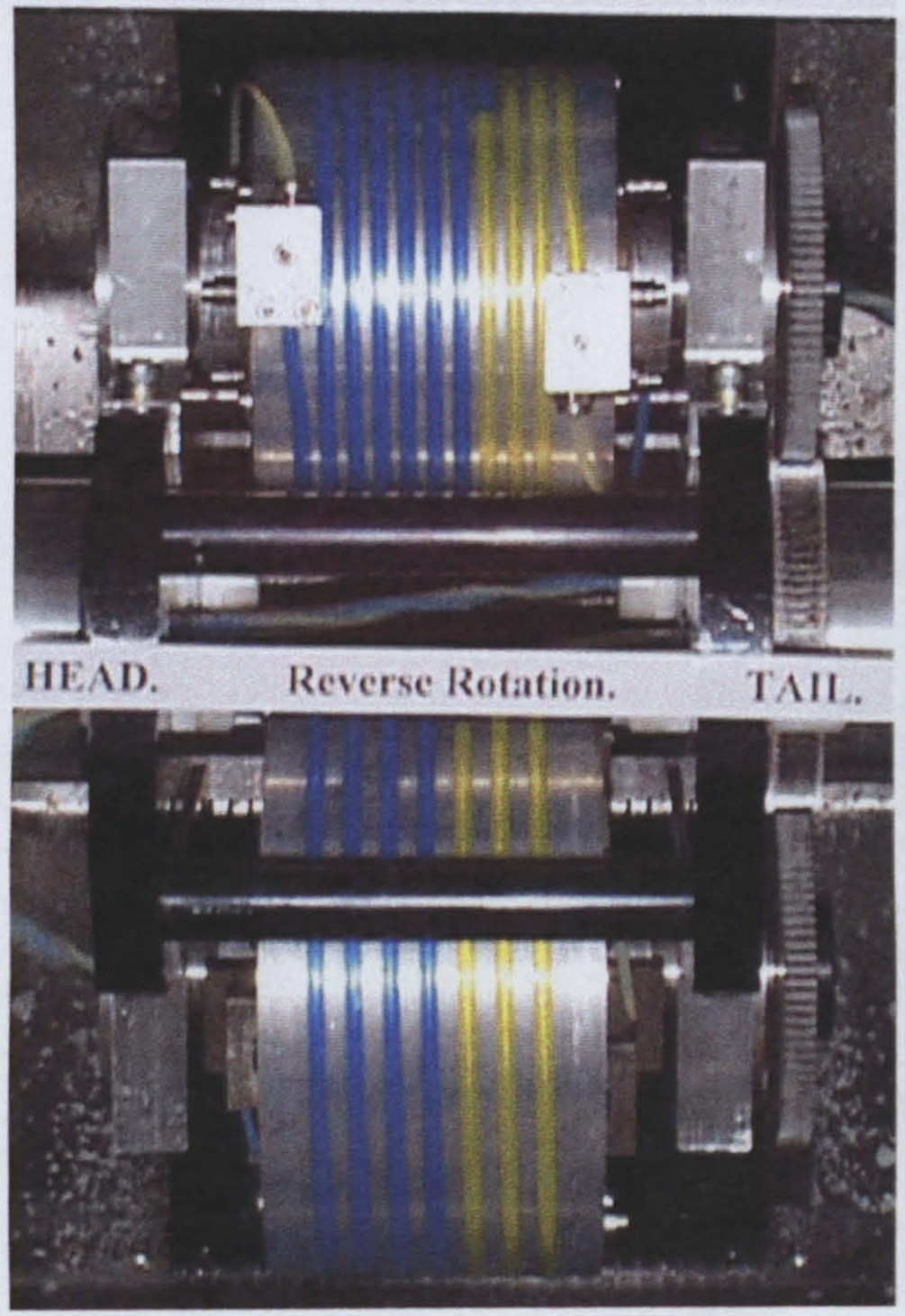

AFTER Reverse Direction of Rotation
4C Phase System at 763rpm in FEP
Run for 30 minutes

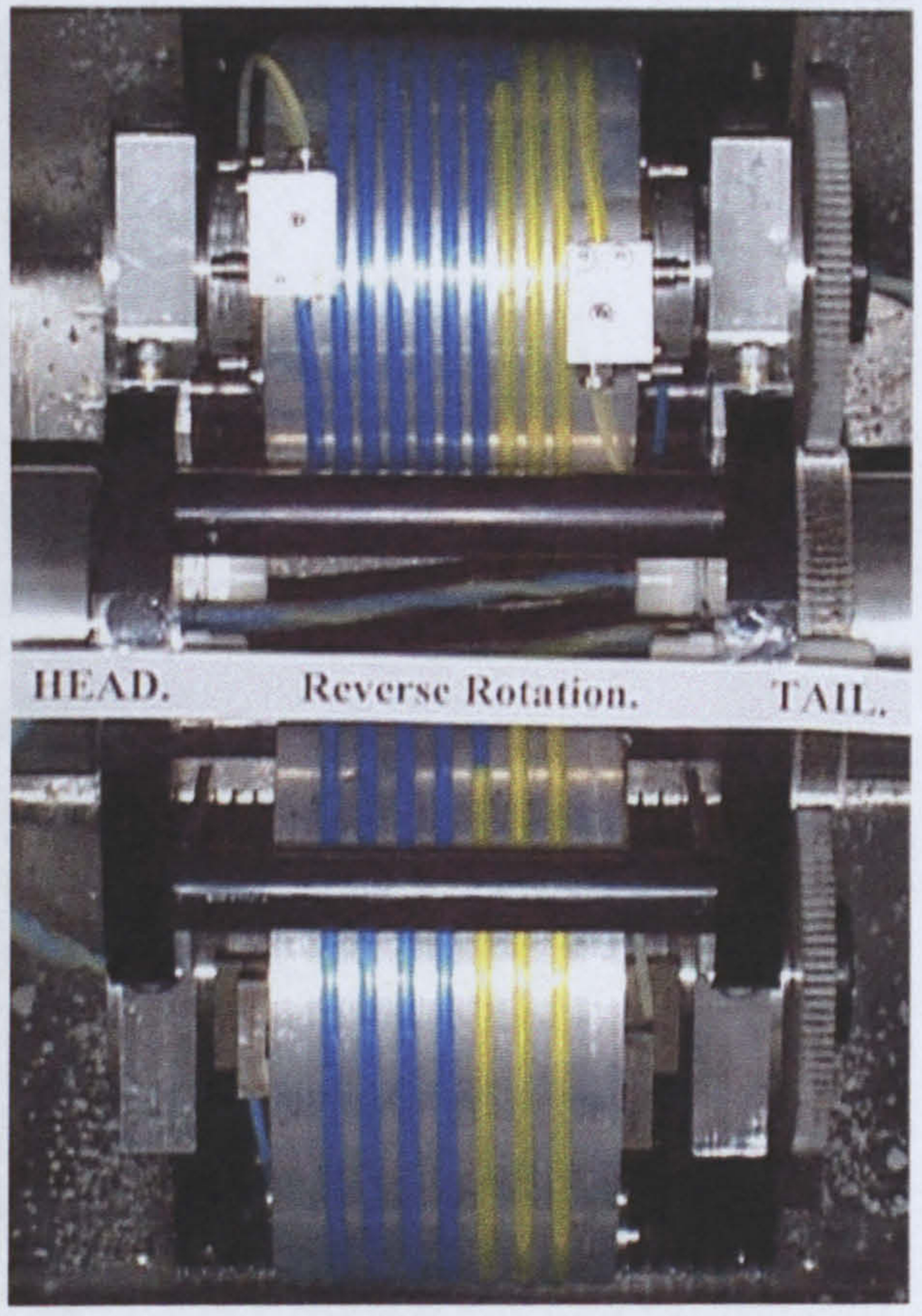

Figure A.3.10 shows the Head and Tail distribution of the 4C phase system for after 10 and 30 minutes of rotation in the reverse direction

AFTER Reverse Direction of Rotation
4C Phase System at 763rpm in FEP
Run for 60 minutes

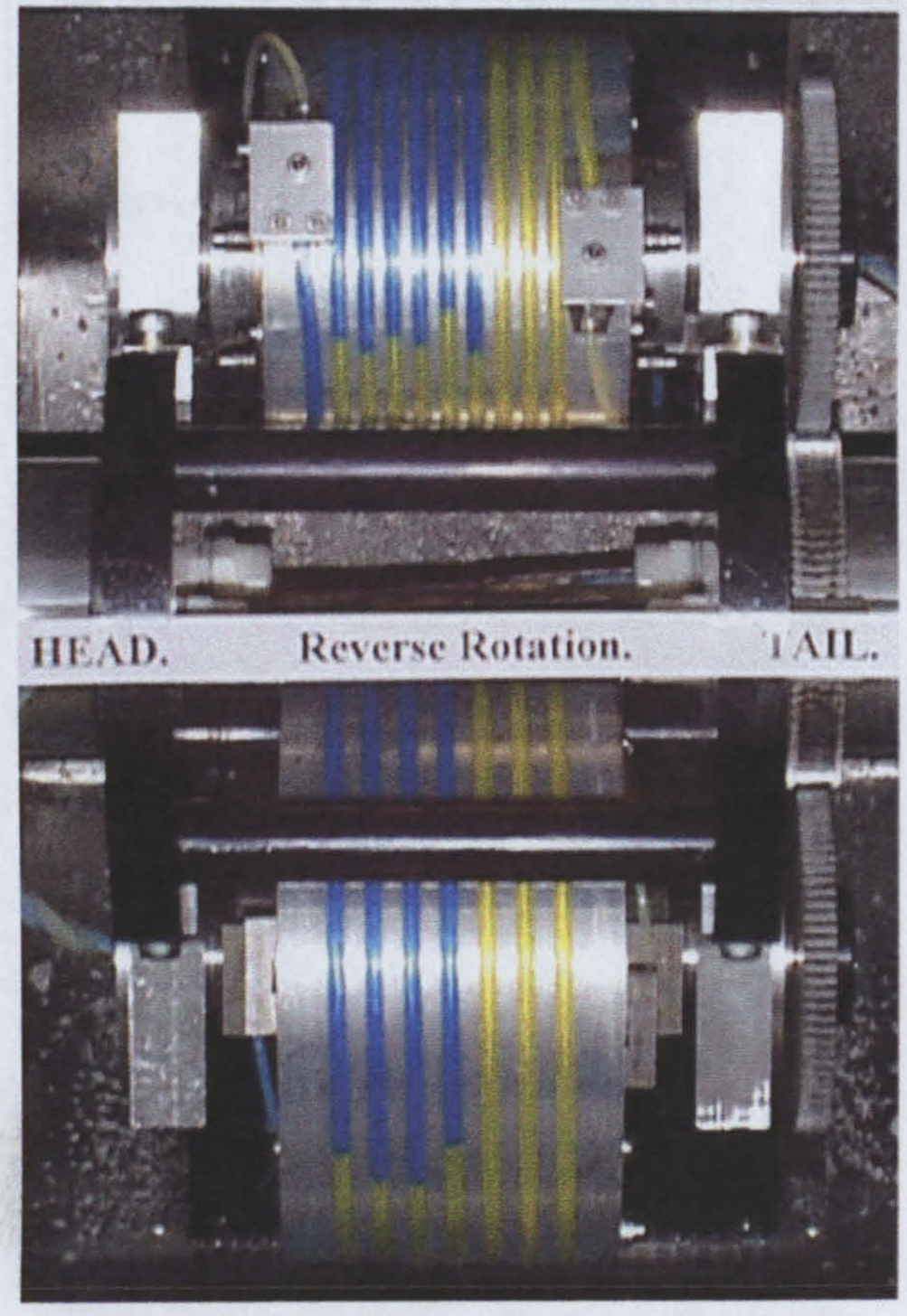

Figure A.3.11 shows the Head and Tail distribution of the 4C phase system for after 60 minutes of rotation in the reverse direction

Appendix 4 Experimental Raw Data from Retention Measurements

A.4.1 Dead Volume and Retention Raw Data for the 4A phase system in normal phase mode

The first number in the left hand column is the number of the experiment from which the results were taken. The second number is the coil tubing bore and the third number is the nominal rotational speed.

Flow Rate (ml/min) Experiment	5	10	20	40	50	60	80	110	160
39, 3.73mm, 600rpm	12.8	14.5	17.2	21.6					64.6
41, 3.73mm, 800rpm	12.1	13.2	15.2	18.7					35.6
42, 3.73mm, 1000rpm	11.6	12.5	14.0	16.6					29.8
33, 3.73mm, 1200rpm	11.2	12.0	13.2	15.3			18.8		25.8
34, 3.73mm, 1200rpm	11.3	12.1	13.4	15.5			19.0		26.0
35, 3.73mm, 1200rpm	11.2	12.0	13.2	15.4			18.7		26.0
44, 3.73mm, 1200rpm	11.6	12.5	13.8	15.8			19.0		25.8
Flow Rate (ml/min)	5	10	20	40	50	60	80	110	160
47, 5.33mm, 600rpm		14.4	16.7	20.7			27.3		38.9
50, 5.33mm, 700rpm		13.8	15.8	19.3		22.3	24.7		
48, 5.33mm, 800rpm		13.4	15.1	18.0		20.5	22.5		
51, 5.33mm, 900rpm		13.1	14.5	17.3		19.5	21.0		
49, 5.33mm, 1000rpm		12.7	14.1	16.6		18.3	19.6		
Flow Rate (ml/min)	5	10	20	40	50	60	80	110	140
56, 7.73mm, 600rpm			16.8		21.9		25.9	29.2	31.7
55, 7.73mm, 700rpm			15.4		20.2		23.4	25.8	28.2
57, 7.73mm, 800rpm			14.9		19.3		21.9	23.9	25.7
54, 7.73mm, 800rpm			14.5		18.8		21.4	23.4	25.2
52, 7.73mm, 900rpm			13.9		17.8		19.8	21.7	23.5
53, 7.73mm, 1000rpm			13.5		16.7		18.9	20.5	22.3

Table A.4.1.1 shows the total volume (ml) of displaced stationary phase (V_E) from the system (raw data) for the 4A phase system in normal phase mode for the three IMI stainless steel coils

The volumes shown in the above table are the total volumes of stationary phase collected in the stationary phase collector. These volumes are the displaced volumes of stationary phase from the coil and dead volume ie V_E. The values shown in blue are values that were used for the comparison of pump out volumes of mobile phase and displaced volume of stationary phase from the coil and flying leads. However these values were not used to plot the dead volume figure or the Du plot as these values were obtained at high flow rates where the Du relationship no longer produces a straight line characteristic.

Flow Rate (ml/min) Experiment	5	10	20	40	50	60	80	110	140
39, 3.73mm, 600rpm	5.0	6.7	9.4	13.8					
41, 3.73mm, 800rpm	3.9	5.0	7.0	10.5					
42, 3.73mm, 1000rpm	2.9	3.8	5.3	7.9					
33, 3.73mm, 1200rpm	2.8	3.6	4.8	6.9			10.4		
34, 3.73mm, 1200rpm	2.8	3.6	4.9	7.0			10.5		
35, 3.73mm, 1200rpm	2.8	3.6	4.8	7.0			10.3		
44, 3.73mm, 1200rpm	2.6	3.5	4.8	6.8			10.0		
47, 5.33mm, 600rpm		7.5	9.8	13.8			20.4		
50, 5.33mm, 700rpm		6.3	8.3	11.3		14.3	17.2		
48, 5.33mm, 800rpm		5.2	6.9	9.8		12.3	14.3		
51, 5.33mm, 900rpm		4.6	6.0	8.8		11.0	12.5		
49, 5.33mm, 1000rpm		3.9	5.3	7.8		9.5	10.8		
56, 7.73mm, 600rpm			9.2		14.3		18.3	21.6	24.1
55, 7.73mm, 700rpm			7.6		12.4		15.6	18.0	20.4
57, 7.73mm, 800rpm			6.2		10.6		13.2	15.2	17.0
54, 7.73mm, 800rpm			6.2		10.5		13.1	15.1	16.9
52, 7.73mm, 900rpm			5.5		9.4		11.4	13.3	15.1
53, 7.73mm, 1000rpm			5.2		8.4		10.6	12.2	14.0

Table A.4.1.2 shows the displaced volumes (ml) of stationary phase from each coil for the 4A phase system in normal phase mode for the three IMI stainless steel coils

The volumes shown in table A.4.1.2 are the volumes of stationary phase displaced from the coil only, having subtracted the dead volume (V_d) from the values listed in Table A.4.1.1. The volume of stationary phase displaced from the coil equals the volume of mobile phase in the coil (V_m). Equation 4.3.1.7 from Chapter 4 was used to determine V_m from the volumes of stationary phase collected in the stationary phase collector (V_E) contained in table A.4.1.1 and the dead volumes (V_d) shown in table 4.5.3.1.

Experiment	Pump out Volume of mobile phase (ml)
39, 3.73mm, 600rpm, 4A	66.0
41, 3.73mm, 800rpm, 4A	35.0
42, 3.73mm, 1000rpm, 4A	28.5
33, 3.73mm, 1200rpm, 4A	25.0
34, 3.73mm, 1200rpm, 4A	26.0
35, 3.73mm, 1200rpm, 4A	25.0
44, 3.73mm, 1200rpm, 4A	25.0
47, 5.33mm, 600rpm, 4A	39.0
50, 5.33mm, 700rpm, 4A	24.0
48, 5.33mm, 800rpm, 4A	23.0
51, 5.33mm, 900rpm, 4A	21.0
49, 5.33mm, 1000rpm, 4A	20.0
56, 7.73mm, 600rpm, 4A	31.0
55, 7.73mm, 700rpm, 4A	28.0
57, 7.73mm, 800rpm, 4A	23.5
54, 7.73mm, 800rpm, 4A	26.0
52, 7.73mm, 900rpm, 4A	23.5
53, 7.73mm, 1000rpm, 4A	23.0

Table A.4.1.3 shows the Pump Out Volumes of mobile phase for the Retention studies for the 4A phase system in normal phase mode for the three IMI stainless steel coils

After pumping out or emptying the coil as described in section 2.7.3 Chapter 2 the amount of mobile phase collected should theoretically equal the total amount of stationary phase displaced from system (V_E) during the retention test. For the 4A phase system in normal phase mode the amount of mobile phase collected during pump out is the volume of the upper phase in the measuring cylinder used during pump out. This volume of upper (mobile) phase should equal the volume of lower (stationary) phase in the stationary phase collector within the defined limits of the test procedure in section 2.7.3.

A.4.2 Reverse phase mode Raw Data for the 4A phase system

Flow Rate (ml/min) Experiment	5	10	20	40	50	60	80	110	140
61, 3.73mm, 600rpm	16.4	18.4	20.5	24.1		27.1			
58, 3.73mm, 800rpm	11.6	13.3	15.3	17.6	18.4				
59, 3.73mm, 800rpm	16.5	18.0	19.8	21.8		23.4			
60, 3.73mm, 800rpm	12.6	14.3	16.1	18.4		20.4			
62, 3.73mm, 1000rpm	14.3	15.7	17.1	19.3		20.9			
64, 7.73mm, 600rpm			60.0		66.1		70.2		73.5
63, 7.73mm, 1000rpm			48.6		55.4		59.2		59.9

Table A.4.2.1 shows the total volume (ml) displaced stationary phase (V_E) from the system (raw data) for the 4A phase system in reverse phase mode for two of the IMI stainless steel coils

The volumes shown in the above table are the volumes of stationary phase collected in the stationary phase collector. These volumes are the displaced volumes of Stationary phase from the coil and dead volume ie V_E. The values shown in blue are values that were used for the comparison of pump out volumes of mobile phase and displaced volume of stationary phase from the coil and flying leads. However these values were not used to plot the dead volume figure or the Du plot as these values were obtained at high flow rates where the Du relationship no longer produces a straight line characteristic.

Experiment	Pump out Volume of mobile phase (ml)
61, 3.73mm, 600rpm	28.5
58, 3.73mm, 800rpm	25.0
59, 3.73mm, 800rpm	27.0
60, 3.73mm, 800rpm	26.0
62, 3.73mm, 1000rpm	23.0
64, 7.73mm, 600rpm	88.0
63, 7.73mm, 1000rpm	71.0

Table A.4.2.2 shows the Pump Out Volumes of mobile phase for the Retention studies for the 4A phase system in reverse phase mode for two of the IMI stainless steel coils

After pumping out or emptying the coil as described in section 2.7.4 Chapter 2 the amount of mobile phase collected should theoretically equal the total amount of stationary phase displaced from system (V_E) during the retention test, in the same way as for normal phase. For the 4A phase system in reverse phase mode the amount of mobile phase collected during pump out is the volume of the lower phase in the measuring cylinder used during pump out. This volume of lower (mobile) phase should equal the volume of upper (stationary) phase in the stationary phase collector within the defined limits of the test procedure in section 2.7.4.

A.4.3 Normal and Reverse phase mode retention data for the 4A phase system using the PTFE coil

Flow Rate (ml/min) Experiment	1	2	3	4	5
67, 1.58mm, 800rpm, RM, 4A	14.2	18.0	20.6	23.2	26.9
68, 1.58mm, 1000rpm, RM, 4A	13.1	16.4	18.5	20.1	22.1
69, 1.58mm, 1200rpm, RM, 4A	12.6	14.7	16.6	17.9	19.3
70, 1.58mm, 800rpm, NM, 4A	10.9	12.5	13.8	15.5	17.3
71, 1.58mm, 1000rpm, NM, 4A	9.2	10.5	11.5	12.7	14.0
72, 1.58mm, 1200rpm, NM, 4A	8.9	9.9	10.7	11.8	13.1

Table A.4.3.1 shows the total volume (ml) displaced stationary phase (V_E) from the system (raw data) for the 4A phase system in normal and reverse phase mode for the PTFE coil

The volumes shown in the above table are the total volumes of stationary phase collected in the stationary phase collectors. These volumes are the displaced volumes of stationary phase from the coil and dead volume ie V_E.

Flow Rate (ml/min) Experiment	1	2	3	4	5
67, 1.58mm, 800rpm, RM, 4A	10.2	14.0	16.6	19.2	22.9
68, 1.58mm, 1000rpm, RM, 4A	7.0	10.3	12.4	14.0	16.0
69, 1.58mm, 1200rpm, RM, 4A	5.5	7.6	9.5	10.8	12.2
70, 1.58mm, 800rpm, NM, 4A	5.4	7.0	8.3	10.1	11.8
71, 1.58mm, 1000rpm, NM, 4A	4.0	5.3	6.3	7.5	8.8
72, 1.58mm, 1200rpm, NM, 4A	3.6	4.6	5.4	6.5	7.8

Table A.4.3.2 shows the displaced volumes of stationary phase in ml from each coil for the 4A phase system in normal and reverse phase modes for the PTFE coil

The volumes shown in table A.4.3.2 are the volumes of stationary phase displaced from the coil. The volume of stationary phase displaced from the coil equals the volume of mobile phase in the coil (V_m). Equation 4.3.1.7 from Chapter 4 was used to determine V_m from the volumes of stationary phase collected in the stationary phase collector (V_E) contained in table A.4.3.1 and the dead volumes (V_d) shown in table 4.5.5.1.

Experiment	Pump out Volume of mobile phase (ml)
67, 1.58mm, 800rpm, RM, 4A	27
68, 1.58mm, 1000rpm, RM, 4A	22
69, 1.58mm, 1200rpm, RM, 4A	19
70, 1.58mm, 800rpm, NM, 4A	14
71, 1.58mm, 1000rpm, NM, 4A	12
72, 1.58mm, 1200rpm, NM, 4A	11

Table A.4.3.3 shows the Pump Out Volumes of mobile phase for the Retention studies for the 4A phase system in normal and reverse phase modes for the PTFE coil

After pumping out or emptying the coil as described in sections 2.7.3 and 2.7.4 Chapter 2 the amount of mobile phase collected should theoretically equal the total amount of stationary phase displaced from system (V_E) during the retention test. The volume of mobile phase in the measuring cylinder used during pump out should equal the volume of stationary phase in a stationary phase collector within the defined limits of the test procedures in sections 2.7.3 and 2.7.4.

Appendix 5 Reynolds Numbers

The equation for Reynolds number (*Re*) for the mobile phase is as follows:

$$Re = \frac{\rho_m d_m u_m}{\mu_m} \qquad \text{(Reynolds Number)}$$

where ρ_m = density of the mobile phase
d_m = characteristic dimension of the mobile phase
u_m = mean linear velocity of the mobile phase
μ_m = viscosity of the mobile phase

d_m is calculated assuming that the across sectional area of the mobile phase is a circle as follows:

$$V_m = \frac{L\pi d_m^2}{4} \qquad \text{(A.5.1)}$$

and by the same token given that d is the bore diameter of the coil tubing.

$$V_C = \frac{L\pi d_C^2}{4} \qquad \text{(A.5.2)}$$

Rearranging equation 4.3.1.8 from section 4.3.1 of chapter 4 for V_m gives:

$$V_m = V_C - V_S$$

Multiplying by $\frac{100}{V_C}$ gives: $\frac{100V_m}{V_C} = 100 - \frac{100V_S}{V_C}$

Equation 4.3.1.5 from section 4.3.1 of chapter 4 shows that $S_f = \frac{100V_S}{V_C}$

Therefore $\frac{100V_m}{V_C} = 100 - S_f$

$$V_m = V_C \frac{(100 - S_f)}{100}$$

Substituting from equations A.5.1 and A.5.2 into the above equation gives:

$$\frac{L\pi d_m^2}{4} = \frac{L\pi d_C^2}{4} \frac{(100 - S_f)}{100}$$

$$d_m^2 = \frac{d_C^2(100 - S_f)}{100}$$

$$d_m = \frac{d_C}{10}\sqrt{100 - S_f} \qquad \text{(A.5.3)}$$

The mean linear velocity of the mobile phase is given by the following equation:

$$u_m = \frac{F}{A_m} \text{ where } A_m = \frac{\pi d_m^2}{4}$$

Hence

$$u_m = \frac{4F}{\pi d_m^2}$$

Substituting for d_m from equation A.5.3 gives:

$$u_m = \frac{400F}{\pi d_C^2\left(100 - S_f\right)} \qquad \text{(A.5.4)}$$

Substituting into the *Re* equation for d_m from equation A.5.3 and for u_m from equation A.5.4 gives:

$$Re = \frac{\rho_m}{\mu_m}\frac{d_C\sqrt{100 - S_f}}{10}\frac{400F}{\pi d_C^2\left(100 - S_f\right)}$$

$$Re = \frac{\rho_m}{\mu_m}\frac{40F}{\pi d_C\sqrt{100 - S_f}} \qquad \text{(A.5.5)}$$

To obtain *Re* of the correct magnitude the mobile phase density must be in kg/m^3, the coil tubing bore diameter d must be in metres, the viscosity must be in Ns/m^2 and the mobile phase flow rate must be measured in m^3/s.

Appendix 6 Pressure Drop Results

Flow Rate (ml/min) Experiment	5	10	20	40	50	60	80	110	140
39, 3.73mm, 600rpm	2.15	2.20	2.20	2.35					
41, 3.73mm, 800rpm	2.35	2.35	2.25	2.35					
42, 3.73mm, 1000rpm	2.40	2.45	2.35	2.35					
33, 3.73mm, 1200rpm	2.95	2.65	2.45	2.25			2.50		
34, 3.73mm, 1200rpm	2.70	2.65	2.45	2.25			2.35		
35, 3.73mm, 1200rpm	2.70	2.60	2.45	2.35			2.55		
44, 3.73mm, 1200rpm	2.70	2.65	2.35	2.35			2.55		
47, 5.33mm, 600rpm		2.25	2.35	2.45			2.75		
50, 5.33mm, 700rpm		2.35	2.40	2.50		2.65	2.75		
48, 5.33mm, 800rpm		2.35	2.35	2.50		2.60	2.70		
51, 5.33mm, 900rpm		2.35	2.35	2.45		2.55	2.70		
49, 5.33mm, 1000rpm		2.45	2.45	2.50		2.55	2.70		
56, 7.73mm, 600rpm			2.35		2.55		2.70	2.95	3.10
55, 7.73mm, 700rpm			2.35		2.45		2.65	2.90	3.15
57, 7.73mm, 800rpm			2.35		2.45		2.75	2.95	3.15
54, 7.73mm, 800rpm			2.30		2.50		2.65	2.90	3.15
52, 7.73mm, 900rpm			2.30		2.45		2.60	2.85	3.05
53, 7.73mm, 1000rpm			2.40		2.55		2.75	2.90	3.15

Table A.6.1 shows the directly measured raw pressure drop (bar) results from each coil for the 4A phase system in normal phase for the three IMI stainless steel coils

Flow rate (ml/min)	Pressure Readings (bar)	Mean of Pressure Reading (bar)
5	1.5 to1.6	1.55
10	1.6 to 1.7	1.65
20	1.7 to 1.8	1.75
40	1.8 to 1.9	1.85
80	2.1 to 2.2	2.15
160	2.7 to 2.9	2.80

Table A.6.2 shows the pressure calibration data for the 4A phase system in normal phase mode for the IMI stainless steel coils

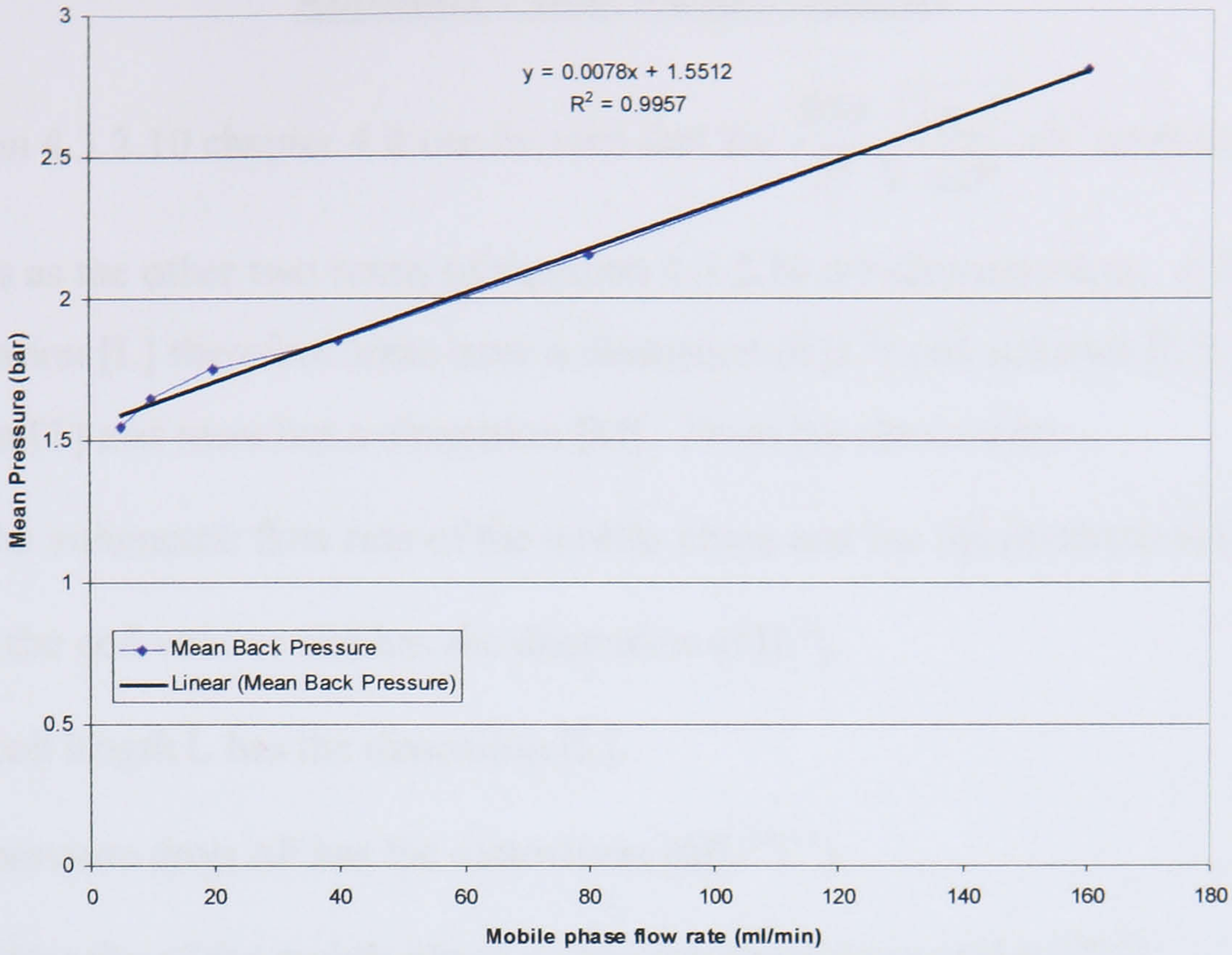

Figure A.6.1 shows the pressure calibration characteristic of the 1/16 inch bore flying leads for the 4A phase system in normal phase mode in the IMI stainless steel coils

Appendix 7 Dimensional Analysis

From equation 4.3.2.10 chapter 4 it can be seen that the $\frac{800}{d_C^2}\sqrt{\frac{2\mu_m L}{\pi\Delta P}}\sqrt{F}$ term should be dimensionless as the other two terms of equation 4.3.2.10 are dimensionless. A linear distance has the dimension [L] therefore areas have a dimension of [L^2] and volumes [L^3]. Time has the dimension [T] and mass has a dimension [M]. From the above term:

1. F is the volumetric flow rate of the mobile phase and has the dimensions [L^3T^{-1}].
2. V_C is the coil volume and has the dimension of [L^3].
3. The coil length L has the dimension [L].
4. The pressure drop ΔP has the dimensions [$ML^{-1}T^{-2}$].
5. The viscosity of the mobile phase μ_m has the dimensions of [$ML^{-1}T^{-1}$].

Substituting these 5 dimensional groups into the $\frac{800}{d_C^2}\sqrt{\frac{2\mu_m L}{\pi\Delta P}}\sqrt{F}$ term and ignoring dimensionless constants gives:

$$\left[\frac{1}{L^2}\right]\left[\frac{ML^{-1}T^{-1}L}{ML^{-1}T^{-2}}\right]^{0.5}\ [L^3T^{-1}]^{0.5} = [L^{-2}][TL]^{0.5}\ [L^3T^{-1}]^{0.5} = [L^{-2}][\ TLL^3T^{-1}]^{0.5} = [L^{-2}][\ L^4]^{0.5}$$

$$[L^{-2}L^2] = [1] = \text{Dimensionless}$$

therefore the gradient term has the correct dimensions. By the same process the equation 4.3.2.11 has the following dimensions:

$$\text{Dimensional analysis of B} = \left[\frac{1}{L^2}\right]\left[\frac{ML^{-1}T^{-1}L}{ML^{-1}T^{-2}}\right]^{0.5} = [L^{-2}][TL]^{0.5} = [L^{-4}TL]^{0.5} = [TL^{-3}]^{0.5}$$

Substituting the Dimensional analysis terms for B in the $\frac{BV_C}{100}\sqrt{F}$ term of equation 4.3.1.11 from section 4.3.1 in chapter 4 gives, $[L^3][TL^{-3}]^{0.5}\ [L^3T^{-1}]^{0.5} = [L^3]$ which is a volume and is dimensionally correct.

Appendix 8 Glossary

"Solar axis" the main axis or rotor axes of a J-type centrifuge.

"Planetary axis" the main axis of both the coil and bobbin that rotates about the solar axis.

"Coil" a length of tubing wound around a common axis; in chromatographic terms a coil is a column.

"Bobbin" is the structure upon which a coil or coils are mounted and to which one or more flying leads are attached.

"Rotor" the structure upon which one or more bobbins are mounted.

"Flying lead" the lengths of tubing connected to each end of a coil and clamped to the bobbin and routed through the rotor to stop twisting during rotation and finally clamped to a stationary object outside of the centrifuge. Flying leads allow fluids to be pumped through a coil while the centrifuge assembly is rotating.

"Loop" a single winding of coiled tubing.

"Distal key node" the closest point of a single loop to the solar axis.

"Proximal key node" the furthest point of a single loop from the solar axis.

"Head" the end of the tubing to which a bubble or bead would move under the action of Archimedean screw action.

"Tail" the opposite end of the tubing to the "Head".

"Periphery" the outside of the coil of tubing with the highest β-value.

"Centre" the inside of the coil of tubing with the lowest β-value.

"Mobile phase" is the solvent phase that is pumped through the coil during an experiment.

"Stationary phase" is the solvent that is retained in the coil during an experiment.

"Normal phase mode" is when the organic solvent is the mobile phase and the aqueous solvent is the stationary phase.

"Reverse phase mode" is when the aqueous solvent is the mobile phase and the organic solvent is the stationary phase.

"Lower Phase," if two settled phases are present in a test tube the densest phase occupies the lower portion and hence is called the lower phase

"Upper Phase," if two settled phases are present in a test tube the least dense phase occupies the upper portion and hence is called the upper phase

Appendix 9 References

Armstrong, D., W., Bertrand, G., L., Berthod, A., *Study of the Origin and Mechanism of Band Broadening and Pressure drop in Centrifugal Countercurrent Chromatography,* Anal. Chem. 60, 2513-2519, **1988**

Baalen van, M. and Helden van, E., *Countercurrent Chromatography; the effects of different variables on the process*, Brunel University internal publication, **1997**

Berthod, A, Schmitt, N., *Water-Organic solvent systems in Countercurrent Chromatography: Liquid Stationary Phase Retention and Solvent Polarity,* Talanta Vol. 15, No. 10, 1489-1498, **1993**

Berthod, A., Billardello, B., *Test to evaluate countercurrent chromatographs Liquid stationary phase retention and chromatographic resolution,* J. of Chromatography A, 902, 323-335, **2000**

Berthod, A., private communication to Wood, P. regarding the Berthod, A., Billardello, B., *Test to evaluate countercurrent chromatographs Liquid stationary phase retention and chromatographic resolution,* J. of Chromatography A, 902, 323-335, 2000 paper dated 25th July **2001**

Bousquet, O., Foucault, A., P., Le Goffic, F., *Efficiency and Resolution in Countercurrent Chromatography,* J. Liquid Chromatography, 14 (18), 3343-3363, **1991**

Conway, W., D., Ito, Y., *Resolution in Countercurent Chromatography,* J. Liquid Chromatography, 8 (12), 2195-2207, **1985**

Conway, W., D., *Countercurrent Chromatography Apparatus: Theory and Applications*, VCH Publishers (UK) Ltd, ISBN 0-89573-331-5, **1990**

Craik, A. D. D., *Wave Interactions and Fluid Flows,* Cambridge University Press, ISBN 0-521-26740-4 **1982**

Du, Q., Z., Ke, C., Q., Ito, Y., *Separation of Epigallocatechin Gallate and Gallocatechin Gallate using multiple instruments connected in series,* J. Liq. Chrom. & Rel. Technol., 21(1&2), 203-208, **1998**

Du, Q., Wu, C., Qian, G., Wu, P., Ito, Y., *Relationship between the flow-rate of the mobile phase and retention of the stationary phase in countercurrent chromatography,* J. of Chromatography A, 835, 231-235, **1999**

Fedotov, P.S., Kronrod, V., A., Maryutina, T.A., Spivakov, B.Ya., *On the mechanism of Stationary phase retention in rotating coil columns,* J. Liq. Chrom. & Rel. Technol., 19(20), 3237-3254, **1996**

Fedotov, P., S., Thiebaut, D., *Retention of the Stationary phase in a coil planet centrifuge: Effects of interfacial Tension, density difference, and viscosities of liquid phases,* J. Liq. Chrom. & Rel. Technol., 21(1&2), 39-51, **1998**

Fedotov, P., S., Khachaturov, R., V., *A New approach to describing the regularities of Stationary phase retention in Countercurrent Chromatography,* J. Liq. Chrom. & Rel. Technol., 23(5), 655-667, **2000**

Fedotov, P.S., Kronrod, V., A., *Modeling of the Hydrodynamic behaviour of two non-miscible liquid phases in a rotating coiled column,* J. Liq. Chrom. & Rel. Technol., 24(11&12), 1685-1697, **2001 A**

Fedotov, P., S., private communication to Wood, P. regarding the Fedotov, P., S., Thiebaut, D., *Retention of the Stationary phase in a coil planet centrifuge: Effects of interfacial*

Tension, density difference, and viscosities of liquid phases, J. Liq. Chrom. & Rel. Technol., 21(1&2), 39-51, 1998 paper dated December **2001 B**

Folter, J., de, *Countercurrent Chromatography Practical and Theoretical models.* Brunel University internal publish, **1998**

Foucault, A., P., *Centrifugal Partition Chromatography,* by Marcel Dekker, Inc. ISBN: 0-8247-9257-2

Gardner, G. C., Kubie, J., *Flow of Two Liquids in Sloping Tubes: An Analogue of High Pressure Steam and Water*, Int. J. Multi-phase Flow, vol. 2, pp 435-451. Pergamon/Elsevier. **1975**

Giddings, J., C., *Dynamics of Chromatography: Principles and Theory,* ChromatographyScience Series Vol. 1, M.Dekker, N. Y., **1965**

Helmholtz, H., Über discontinuierliche Flüssigkeitsbewegungen, Monatsber. Dtsch. Akad. Wiss. Berlin, pp. 215-228, **1868**

Ignatova, S., N., Maryutina, T., A., Spivakov. B., Ya., *Effect of Physiochemical Properties of Two-phase liquid systems on the retention of Stationary phase in a CCC column.* J. Liq. Chrom. & Rel. Technol., 24 (11 & 12), 1655-1668, **2001**

Ito, Y., Weinstein, M., A., Aoki, I., Harada, R., Kimura, E., Nunogaki, K., *The coil planet centrifuge,* Nature, 212, 985-987, **1966**

Ito, Y., Bowman, R., L., *Horizontal flow-through coil planet centrifuge without rotating seals,* Anal. Biochem., 82, 63-68, **1977 A**

Ito, Y., Bowman, R., L., *Preparative Countercurrent Chromatography with a slowly rotating helical tube,* Anal. Biochem., 78, 506-512, **1977 B**

Ito, Y., Bowman, R., L., *Preparative countercurrent chromatography with horizontal flow-through coil planet centrifuge,* J. Chromatography, 147, 221-231, **1978**

Ito, Y., *Experimental Observations of the Hydrodynamic behaviour of solvent systems in High-Speed Countercurrent Chromatography, part II Phase Distribution diagrams for Helical and spiral Columns,* J. of Chromatography, 301, 387-403, **1984**

Ito, Y., Oka, H. and Slemp, J., L., *Improved High-Speed Counter-Current Chromatography with three multilayer coils connected in series. I. Design of the apparatus and performance of semipreparative columns in 2,4-dinitrophenyl amino acid separation, J. of Chromatography*, 475, 219-227, **1989**

Ito, Y, *Speculation on the Mechanism of Unilaterial Hydrodynamic Distribution of Two Immiscible Solvent Phases in the Rotating Coil*, J. Liquid Chromatography, 15 (15 & 16), 2639-2675, **1992**

Karger, B., L., Snyder, L., R., Horvath, C., *An Introduction to Separation Science*, J. Wiley & Sons, New York, **1973**

Kelvin, Lord, Phyl. Mag. 4, ser 42, **1871**

Khun, R., Winterstein, A., Lederer, E., Hoppe-Seyler's Z. Physical Chem., 197, 141, **1931**

Levich, V., G., *Physicochemical Hydrodynamics,* Prentice-Hall **1962**

Mandava, N., B., and Ito, Y., *Countercurrent Chromatography. Theory and Practice,* Marcel Dekker Inc., New York, (Chromatographic science series volume 44), **1988**

Martin, A., J., P., Synge, R., L., M., *Countercurrent Distribution,* J. Biochem 35, 1358, **1941**

Marston, A., Hostettmann, K., Counter-current chromatography as a preparative tool - applications and perspectives, J. Chromatography A, 658, 315-341, **1994**

Maryutina, T.A., Ignatova, S.N., Fedotov, P.S., Spivakov, B.Ya., Thiébaut, D., *Influence of composition and some physico-chemical properties of two-phase liquid systems on the stationary phase retention in a coil planet centrifuge*, J. Liq. Chrom. & Rel. Technol., 21(1&2), 19-37, **1998**

Massey, B., S., *Mechanics of Fluids,* 6th Edition, Chapman & Hall, ISBN 0-412-34280-4, **1989**

Menet, J., M., Rolet,M., C., Thiebaut, D., Rosset, R., and Ito, Y., *Fundamental Chromatographic parameters in Countercurrent Chromatography: Influence of the volume of stationary phase and the flow rate,* J. Liq Chromatography, 15 (15 & 16), 2883-2908, **1992**

Precisa Balances Ltd., *Precisa Operating Instructions,* Bucks pp 34-36

Prins, M., *Countercurrent Chromatography, Research on the Physical Properties,* internal Brunel University publication, **1998**

Rainin Instrument Co., Inc. sales catalogue PB-96 R1 for the Dynamax SD-1 HPLC pump **1982**

Shimadzu catalogue CA197-920J, *LC-6A System Liquid Chromatograph*

Sutherland, I., A., Jones, S., and Heywood-Waddington, D., *A Preliminary Study of the Hydrodynamics of a Range of Solvent Systems in a Single Layer Coil Planet Centrifuge*, Preparative Countercurrent Chromatography, No. 1045. Proceedings of the Pittsburgh Conference, Atlantic City, New Jersey, March **1986**

Sutherland, I., A., Heywood-Waddington, D. and Ito, Y., *Counter-Current Chromatography, Applications to the separation of biopolymers, organelles and cells using either aqueous-organic or aqueous-aqueous phase systems*, J. of Chromatography, 384, 197-207, **1987**

Sutherland et al, *Countercurrent Chromatography (CCC) and its versatile application as an industrial purification and production process*, J. Liq. Chrom. & Rel. Technol., 21(3), 279-298, **1998**

Sutherland, I., A., Wood, P., *A New Perspective on the mechanism of Mixing and Settling in Countercurrent Chromatography using a J-type coil planet centrifuge,* Proceedings of Pittsburgh Conference CCC Session, Orlando, Florida, March 10th **1999**

Sutherland, I., A., Muytjens, J., Prins, M., Wood, P., *A New Hypothesis on the phase distribution in Countercurrent Chromatography,* J. Liq. Chrom. & Rel. Technol., 23 (15), 2259-2276, **2000 A**

Sutherland, I., A., *Relationship between retention, linear velocity and flow for countercurrent chromatography,* J. of Chromatography A, 886, 283-287, **2000 B**

Sutherland et al, *Industrial Scale-up of Countercurrent Chromatography,* J. Liq. Chrom. & Rel. Technol., 24 (11&12), 1533-1553, **2001 A**

Sutherland, I., A., Du, Q., Z., and Wood, P., *The relationship between retention, linear flow and density difference in Countercurrent Chromatography*, J. Liq. Chrom. & Rel. Technol., 24 (11&12), 1669-1683, **2001 B**

Sutherland, I., A., Kidwell, H., and Wood, P., *Comparing Normal and Reverse CCC: The importance of the viscosity of the mobile phase,* Proceedings of the Pittsburgh Conference New Orleans 4th to 9th March **2001 C**

Sutherland, I., A., *Liquid Stationary Phase Retention and Resolution in Hydrodynamic CCC,* Countercurrent Chromatography, The Support Free Liquid Stationary Phase (Editor Berthod, A.) Comprehensive Analytical Chemistry, Elsevier, Amsterdam, Vol XX, Chapter 6. *in press* **2002 A**

Sutherland, I., A., De Folter, J., and Wood, P., *Modelling Countercurrent Chromatography using an Eluting Countercurrent Distribution Model,* J. Liq. Chrom., *in preparation,* **2002 B**

Thiebaut, D., private communication to Wood, P. regarding the Fedotov, P., S., Thiebaut, D., *Retention of the Stationary phase in a coil planet centrifuge: Effects of interfacial Tension, density difference, and viscosities of liquid phases,* J. Liq. Chrom. & Rel. Technol., 21(1&2), 39-51, 1998. December **2001**

Thorpe, S. A., *A Method of producing a shear flow in a stratified fluid,* J. Fluid Mech., vol. 32, part 4, pp 693-704, **1968**

Thorpe, S. A., *Experiments on the instability of stratified shear flows: immiscible fluids,* J. Fluid Mech., vol. 39, part 1, pp 25-48, **1969 A**

Thorpe, S. A., *Experiments on the stability of stratified shear flows,* Radio Science, vol. 4, No. 12, pp 1327-1331, **1969 B**

Thorpe, S. A., *Experiments on the instability of stratified shear flows: miscible fluids,* J. Fluid Mech., vol. 46, part 2, pp 299-319, **1971**

Timmers, T., *Countercurrent Chromatography, Research on Phase Systems and Analytical CCC,* internal Brunel University publication, **2001**

Tswett, M., S., Proc. Warsaw Soc. Nat. Sci., Biol. Soc. 14, No. 6 (1903): Ber. Deut. Bot., 24, 234, 316, 384, **1906**

Wee, R., Tee, *Countercurrent Chromatography, Stationary phase retention, Contact Angle, Interfacial Tension,* Brunel University internal publish, **1998**

Wood, P., and Sutherland, I., A., *Brunel CCC Countercurrent Chromatography Instruction Manual, revision 0, 18th December 2000,* Brunel University publication, **2000**

Wood, P., Jaber, B., and Sutherland, I., A., *A New Hypothesis on the Hydrodynamic Distribution of the Upper and Lower phase in CCC,* J. Liq. Chrom. & Rel. Technol., 24 (11 & 12), 1629-1654, **2001 A**

Wood, P., and Sutherland, I., A., *Mixing, Settling and the movement of the Interface between the mobile and Stationary phases in CCC,* J. Liq. Chrom. & Rel. Technol., 24 (11 & 12), 1699-1710, **2001 B**